

# Development and Characterisation of an Immunocompetent Human *in vitro* Model of the Small Airways

Written by

Abigail Martin

November 2021

Submitted to the University of Hertfordshire in partial fulfilment of the requirements of the  
degree of PhD

## Abstract

Lung diseases such as asthma and chronic obstructive pulmonary disease (COPD) increase the global health burden affecting hundreds of millions of people worldwide. The development of novel inhaled therapies is hindered by the lack of understanding of alveolar macrophages to inhaled particulate medicines. In animal models, there is increasing evidence that inhaled medicines are taken up by alveolar macrophages resident within the lung resulting in poorly understood perturbations.

*In vitro* alveolar models are frequently employed to investigate the biological roles of alveolar macrophages in human health and disease and for inhaled drug discovery research. To generate translational data, it is crucial that such cell systems respond similarly to cells *in situ*. Cell culture lung models are available, but few are representative of alveolar drug delivery response, and, additionally, most exclude macrophages.

*In vitro* cell culture models provide an ideal platform for assessing cell response to exposure of compounds in a high throughput manner and investigating the mechanisms involved that support undefined macrophage phenotype responses. To generate such platforms, it is first necessary to identify an appropriate, well-characterized cell line to develop a robust *in vitro* human model. To date, no human alveolar macrophage cell line is readily available. As such, current models rely on lung and blood-derived monocyte cell lines, which are differentiated using various stimuli to generate a mature monocyte/macrophage-like cell line that can be exposed to aerosols or particulate matter of interest. However, the methodologies available to differentiate and validate these cell lines are poorly defined, especially for U937 cells,

whereby differentiation protocols vary significantly from the use of different stimuli, incubation and resting times.

This research aimed to investigate if varying the differentiation protocols for U937 impacted the resulting cell characteristics and, with them, construct two co-culture models incorporating alveolar type I or type II epithelial cells to determine changes in alveolar like macrophage phenotypes in the presence of cationic amphiphilic drug amiodarone commonly used to generate a 'foamy' macrophage phenotype.

Our results suggested that the concentration of PMA U937 cells are exposed to has a more significant impact on cell characteristics (differentiation markers and functionality) than the length of incubation. A differentiation protocol was adopted, and co-culture models were characterized regarding their morphology and barrier properties, with permeability assays and cytokine interactions. High content image analysis assessed macrophage responses when exposed to drug concentrations of amiodarone. Morphological changes induced by amiodarone could be compared rather than determined cell death for vacuolated "foamy" macrophage assessments.

In summary, these models were characterised regarding their morphology and viability properties, with functional assays showing applicability for evaluating macrophage cell response and cell-cell communication. Cocultivation allows a more physiologically relevant representation of the lower airway, and immunocompetent *in vitro* models can be applied as a valuable tool to evaluate new formulations intended for pulmonary delivery

## Acknowledgements

Throughout the writing of this dissertation, I have received a great deal of support and assistance. I would like to express my deep gratitude to my primary supervisor Dr Victoria Hutter, for her enthusiastic encouragement and support throughout the years. I look forward to many more years of working together! To my supervisory team, I would like to thank Dr David Chau for his innovative experiments and his 'think outside the box' solutions and Professor Darragh Murnane for helping me unlock my full potential.

I would also like to thank Dr Ewelina Hoffman for her advice and assistance in designing and troubleshooting experiments (and feeding my cells occasionally). My grateful thanks are also extended to Dr Liam McAuley and Dr Stewart Kirton in the Centre for Research in Topical Drug Delivery and Toxicology for their help when I have needed it. I want to thank the senior technical team in the science building and Lee Rixon thank you for managing our cell culture lab so well.

To Pro-Vice-Chancellor Julie Newlan, thank you for championing me and supporting me into the next chapter of my career. Thank you to the business development team, particularly Dr Kate Byford and Dr Peter Gooden, for your expertise and business support. Thank you for your motivational pep talks and all the 'on the spot' presentations you had me do in the enterprise team, Steve Robinson.

In addition, I would like to thank my family for their wise counsel and moral support. I am grateful to my dad Andrew for helping me get to this point in my life. To my Mum Liz, Nan, Jonathan and Kathryn. You are always there for me.

Thank you, Kennedy, for keep calm and smash it approach, particularly in these final months; I appreciate you. Finally, my friends and colleagues at UH were of great support in deliberating over our problems and findings, as well as providing a happy distraction to rest my mind outside of my research. To Katie, Giorgia, Rhamiya and Dan, thank you.

# Contents

<b>Abstract .....</b>	<b>I</b>
<b>Acknowledgements.....</b>	<b>III</b>
<b>Contents .....</b>	<b>IV</b>
<b>List of Tables.....</b>	<b>VII</b>
<b>List of Figures.....</b>	<b>VIII</b>
<b>Abbreviations.....</b>	<b>X</b>
<b>1. Introduction to The Lung .....</b>	<b>1</b>
1.1. Drug delivery to the lungs.....	1
1.1.1 Challenges for drug delivery to the lungs.....	3
1.2. The lung .....	4
1.2.1 Structure and function of the lungs .....	4
1.2.2 The Alveolus.....	6
1.2.3 The fate of inhaled particles in the airways .....	8
1.2.4 Macrophages.....	9
1.2.5 Alveolar macrophages .....	10
1.3. AM mechanisms of response to inhaled pharmaceuticals.....	12
1.3.1 Classification of AMs responses .....	15
1.4. Current <i>in vitro</i> AM models of the alveoli for inhaled pharmaceutical response .....	15
1.4.1 Primary macrophages .....	17
1.4.2 Alveolar macrophage cell lines .....	18
1.4.3 Alveolar epithelial culture models .....	20
1.4.4 <i>In vitro</i> co-culture models of the lung.....	22
1.4.5 <i>In vivo</i> models.....	25
1.4.6 <i>Ex vivo</i> models .....	26
1.4.7 In silico models .....	27
1.5. Model selection for inhaled pharmaceutical response .....	28
1.5.1 Selection of human representative models .....	28
1.6. Summary .....	29
1.7. Thesis Aims.....	31
<b>2. Materials and Methods .....</b>	<b>34</b>
2.1. Materials.....	34
2.1.1 Equipment.....	34
2.1.2 General reagents.....	35
2.1.3 Cell culture reagents .....	35
2.1.4 Immuno-chemicals .....	35
2.1.5 Compounds .....	36
2.1.6 Morphology and staining chemicals.....	36

2.2.	Methods.....	38
2.2.1	Cell culture.....	38
2.2.2	Human primary alveolar macrophages.....	39
2.2.3	Human alveolar epithelial cell lines.....	40
2.2.4	Co-culture cultivation and assembly.....	41
2.2.5	Cell revival.....	42
2.2.6	Cryopreservation.....	42
2.2.7	Viability assays.....	42
2.2.8	Morphological characterisation.....	43
2.2.9	Immunofluorescent staining.....	45
2.2.10	Transepithelial electrical resistance (TEER).....	49
2.2.11	Transport studies.....	50
2.2.12	Proteome Profiler Human Cytokine Array.....	50
2.2.13	General data management and statistical analysis.....	53
<b>3.</b>	<b>Validation of human monocytic lymphoma cell line-U937 as alveolar like macrophages .....</b>	<b>54</b>
3.1.	Introduction.....	54
3.2.	Aims.....	60
3.3.	Results.....	61
3.3.1	Biomarker Identification of PMA treated U937 cells.....	61
3.3.2	CD Marker expression profile.....	64
3.3.3	Phagocytic activity of PMA treated U937 cells.....	69
3.3.4	Morphology of differentiated U937 cells and primary AMs.....	72
3.3.5	Cell Health.....	75
3.4.	Discussion.....	86
3.4.1	Differentiation of AMs.....	86
3.4.2	Biomarker identification in PMA naive and PMA treated U937 cells ...	87
3.4.3	CD biomarker differentiation profiles.....	90
3.4.4	Phagocytosis activity.....	93
3.4.5	Cell viability and physiology.....	93
3.5.	Conclusion.....	95
3.6.	Appendix I.....	96
<b>4.</b>	<b>Development &amp; characterisation of human immunocompetent alveolar co-culture models .....</b>	<b>97</b>
4.1.	Introduction.....	97
4.2.	Aims.....	100
4.3.	Results.....	101
4.3.1	Optimisation of co-culture conditions.....	101
4.3.2	Construction of immunocompetent alveolar co-culture systems .....	116
4.3.3	Characterisation of immunocompetent alveolar co-culture systems .	118
4.4.	Discussion.....	132
4.4.1	Optimising the in vitro co-culture systems.....	132
4.4.2	Characterisation of co-culture model.....	137
4.5.	Conclusion.....	139

---

<b>5. U937 cell phenotypes in mono- and co-culture systems using a high content image analysis approach .....</b>	<b>140</b>
5.1. Introduction.....	140
5.2. Aims.....	143
5.3. Results.....	144
5.3.1 Effect of amiodarone on cell viability and functionality in mono- and co-culture U937 models. ....	144
5.3.2 Adaptation of high content image analysis for co-culture system.....	147
5.3.3 Quantitative High Content Analysis .....	151
5.4. Discussion .....	165
5.4.1 High content image analysis as a tool to assess macrophage responses.....	165
5.4.2 Impact of co-culture on PMA-differentiated U937 morphology .....	169
5.4.3 Interpretation of data .....	171
5.4.4 Conclusion .....	172
<b>6. General discussion .....</b>	<b>173</b>
6.1. Respiratory diseases.....	173
6.2. Immunocompetent alveolar <i>in vitro</i> cell culture models .....	173
6.3. Limitations of Current <i>in vitro</i> Inhalation Testing .....	174
6.4. Overcoming limitations: Advanced tools, the immunocompetent <i>in vitro</i> model	176
6.5. Concluding thoughts and deliverables of this PhD .....	180
6.6. Future perspectives.....	181
<b>7. References .....</b>	<b>184</b>

## List of Tables

Table 1.1 Alveolar macrophage responses in rats.....	15
Table 1.2 Morphometric parameters of cells in the alveolar region of rat, dog, baboon and human lungs. ....	28
Table 2.1. Properties of immuno-chemicals used in this thesis.....	37
Table 3.1 Current PMA differentiation protocols for U937 cells.....	58
Table 3.2 CD Microarray table of surface biomarkers measured. ....	96
Table 4.1 List of cell behaviours that can be examined in co-culture models.....	99
Table 4.2 Human cytokine profile of lower airway of monoculture and co-culture models in LPS.....	131
Table 5.1 Phenotype classification of PMA-differentiated U937 cells exposed to amiodarone.....	163



## List of Figures

Figure 1.1 Diagram of the lung's branching airways. ....	5
Figure 1.2 Deposition mechanisms of inhaled particles in the respiratory tract. ....	8
Figure 1.3 Process of particle engulfment through phagocytosis by alveolar macrophages. ....	13
Figure 1.4 Illustration of a hierarchy of complexity of systems prior to clinical assessments of inhaled compounds. ....	16
Figure 3.1 Biomarkers identified in PMA treated U937 cells at passage 5 number (A) or a passage 25 (B). ....	63
Figure 3.2 Effects of DMSO on U937 cells and PMA treated U937 cells for surface markers. ....	65
Figure 3.3 Expression profile comparison of selected CD markers in PMA treated U937 cells and primary alveolar macrophages. ....	67
Figure 3.4 Determining the phagocytic ability of U937 cells following incubation with PMA. ....	70
Figure 3.5 Comparison of Phagocytic activity of PMA treated U937 cells. ....	71
Figure 3.6 Morphology of U937 cells with exposure to PMA. ....	74
Figure 3.7 Assessment of cell viability for U937 cells cultured in PMA. ....	76
Figure 3.8 Long-term proliferation profile of PMA treated U937 cells. ....	78
Figure 3.9 Effect of PMA on U937 cell mitochondrial activity determined by MTS assay. ....	81
Figure 3.10 Effect of PMA on U937 cell mitochondrial activity determined by flow cytometry. ....	82
Figure 3.11 Membrane Integrity of PMA treated U937 cells by Cytotox ONE assay. ....	84
Figure 3.12 Cytotoxic assessment of PMA treated U937 cells by Image It Dead. ....	85
Figure 4.1 Assessment of medium compositions the proliferation and viability of hAELVi cells. ....	102
Figure 4.2 Assessment of U937 CCM on the proliferation and viability of A549 cells. ....	104
Figure 4.3 Assessment of culture substratum on epithelial cell viability. ....	106
Figure 4.4 Assessment of seeding density on epithelial cell barrier function. ....	108
Figure 4.5 Assessment of cell seeding density on epithelial cell viability for apical and basolateral compartments. ....	110
Figure 4.6 Assessment of ALI culture on epithelial barrier function. ....	112
Figure 4.7 Assessment of paracellular permeability for hAELVi cell layers using paracellular marker fluorescein. ....	115
Figure 4.8 Generation and construct methodology for T I model. ....	116
Figure 4.9 Generation and experimental set-up for T II model. ....	117
Figure 4.10 Assessment of co-culture system on cell health. ....	119

Figure 4.11 Assessment of co-culture system on epithelial barrier function. ....	121
Figure 4.12 Assessment of LPS exposure on epithelial barrier function in the co-culture systems. ....	122
Figure 4.13 Phagocytic observations for PMA differentiated cells in monoculture and co-culture systems. ....	124
Figure 4.14 Phagocytic activity of PMA differentiated U937 cells (MØ) in monoculture and co-culture systems. ....	126
Figure 4.15 Human cytokine profile of lower airway for ALI cell models. ....	128
Figure 4.16 Expression of human cytokines/chemokines panel for monoculture and co-culture type I and II systems. ....	129
Figure 4.17 Expression of a panel of human cytokines/chemokines for monoculture and co-culture systems stimulated with LPS. ....	130
Figure 5.1 Cytotoxicity of monoculture and co-cultured PMA-differentiated U937 cells on exposure to amiodarone. ....	145
Figure 5.2 Influence of amiodarone on the phagocytic activity of PMA differentiated U937 cells in co-culture. ....	146
Figure 5.3 Multi-parameter images of PMA-differentiated U937 cells in monoculture exposed to 1µM and 10µM amiodarone. ....	148
Figure 5.4 Multi-parameter images of PMA-differentiated U937 cells in a co-culture system with type I alveolar epithelial cells exposed to 1µM and 10µM amiodarone. ....	149
Figure 5.5 Multi-parameter images of PMA-differentiated U937 cells in a co-culture system with type II alveolar epithelial cells exposed to 1µM and 10µM amiodarone. ....	150
Figure 5.6 Characterisation of PMA-differentiated U937 cell health using high content image analysis methodology. ....	153
Figure 5.7 Characterisation of PMA-differentiated U937 gross morphological features using high content image analysis methodology. ....	157
Figure 5.8 Characterisation of PMA-differentiated U937 detailed morphological features using high content image analysis methodology. ....	158
Figure 5.9 Population profiling of PMA differentiated U937 cells exposed to amiodarone. ....	161

## Abbreviations

A549	Alveolar Epithelial Cells Type II
AEC	Alveolar Epithelial Cells
AECI and AECII	Type I And Type II Alveolar Epithelial Cells
ALI	Air Liquid Interphase
AM	Alveolar Macrophages
ANOVA	Analysis Of Variance
ATII	Alveolar Epithelial Cells Type II
AU	Mean Signal Intensity
BAL	Bronchoalveolar Lavage
CAGR	Compound Annual Growth Rate
CCM	Complete Culture Medium
CD	Cluster Of Differentiation
COPD	Chronic Obstructive Pulmonary Disease
COVID-19	ARS-Cov-2 (2019-Ncov) Coronavirus
DCs	Dendritic Cells
DMSO	Dimethyl Sulfoxide
EA.hy 926	Endothelial Cells
EDTA	Ethylenediaminetetraacetic Acid
FAMs	Foamy Alveolar Macrophages
FBS	Foetal Bovine Serum
FBS	Foetal Bovine Serum

---

FC	Flow Cytometry
FCCP	Carbonyl Cyanide4-(Trifluoromethoxy) Phenylhydrazine
FDC	Follicular Dendritic Cell
FITC	Fluorescein Isothiocyanate
GM-CSF	Granulocyte Macrophage Colony Stimulating Factor
HAELVi	Human Alveolar Epithelial Lentivirus Immortalized
HAEPc	Human Alveolar Epithelial Primary Culture
HL-60	Mouse Leukemic Monocyte-Derived
HLA I	Biomarker Type
HMC-1	Virus Transfected Mouse Alveolar Macrophage
IFN- $\gamma$	A Type Of Stimulus
IL-10	Mouse Reticulum Cell Sarcoma- Derived
IL-4	Interleukin-4
J774.A1	Normal Rat Alveolar Macrophage Cells
LCC	Liquid Liquid Conditions
LDH	Lactate Dehydrogenase
LLI	Liquid-Liquid Interphase
LPS	Lipopolysaccharides
MARCO	Human Leukemic Myeloblast
MFI	Median Fluorescent Intensity
U937	Human Monocyte Lymphoma Cell Line Differentiated To Alveolar Macrophages In The Presence Of Phorbol Ester Or Vitamin D Treatment
MO	Monocyte

---

MØ	Macrophage
MARCO	Macrophage Receptor With Collagenous Structure
NC3R's	National Centre Of 3 Rs
NOEL	No Observed Effect Level
PBS	Phosphate Buffered Saline
PMA	Phorbol 12-Myristate 13-Acetate
QSAR	Quantitative Structure-Activity Relationship
RAW 264.7	Rat Alveolar Epithelial Cell Line
RCF	Relative Centrifugal Force,
SD	Standard Deviation
SEM	Standard Error Mean
SP	Surface Proteins
TEER	Transepithelial Electrical Resistance
THP-1	Blood DERIVED MACROPHAGES
TI	Type I Epithelial Culture Model
TIFF	Tagged Image File Format
TLR	Toll-Like Receptors
TSLPrec	Thymic Stromal Lymphopoietin Protein Receptor
UT	Untreated
VD3	1 $\alpha$ , 25-Dihydroxyvitamin D3
ZO-1	Zona Occuldens 1

# Introduction to The Lung

### 1.1. Drug delivery to the lungs

Inhaled drug delivery is defined as “the science of targeting drug administration to the required site of pharmacological action via inhalation” (Colbeck *et al.*, 2014). The respiratory tract has been used for over 3,500 years to deliver medical therapies into the human body. Inhaled smoke from tobacco, other plants and volatile oils have long been used by ancient civilisations for therapeutic and recreational purposes (Sanders, 2007).

The lung is a highly efficient organ with a large surface area and is considered a major route for pharmaceutical administration (Smyth *et al.*, 2011). It is a target for treating pulmonary diseases such as asthma and chronic obstructive pulmonary disease (COPD) and lung infections (Smyth *et al.*, 2011). The inhaled drug particles can quickly target the active site with a relatively low dose and avoid first-pass absorption metabolism in the stomach and intestines, passing through the liver before reaching systemic circulation, reducing systemic side effects. The lower airways of the lung (alveolus) have a large surface area in the region of 100 m<sup>2</sup> with almost 100% bioavailability to rapidly absorb therapeutic proteins such as insulin or growth hormones into the systemic circulation (Patton *et al.*, 2007). Furthermore, additional advantages of drug delivery via the lung include needle-free systemic delivery of drugs with poor oral bioavailability and pain/ needle-free delivery for drugs that require subcutaneous or intravenous injection (Laube, 2014). For this reason, the alveolar

region is a highly desirable route for local and systemic delivery of new aerosol formulations (de Souza Carvalho *et al.*, 2014).

Over the past fifteen years, significant advancements have been made in the accuracy, efficiency, and reproducibility of administered inhaled doses and improved particle characterisation (Siekmeier *et al.*, 2008). Inhaled drug delivery still faces many challenges, including the small fraction of inhaled drug that reaches the target region, risk of potential allergic reactions in the lungs and variability of drug absorption from the alveoli into the circulation (Siekmeier *et al.*, 2008). Developments in modern aerosol delivery systems now allow the manufacture of an aerosol with a defined and optimised aerosol particle. When combined with appropriate breathing manoeuvres, these improved inhaled formulations have significantly optimised the efficiency and clinical efficacy of inhaled pharmaceuticals (Siekmeier & Scheuch, 2008; Kwok & Chan, 2013) rather than medicines for conventional routes of administration (e.g., oral and parenteral) whereby the inhaled drug particles rapidly target the site of action with a relatively low dose, consequently decreasing systemic adverse effects (Kwok *et al.*, 2013).

Newer applications for inhaled delivery also include delivery of nucleic acids that result in a permanent expression of gene constructs or protein-coding sequences in a population of cells, thus reversing or preventing a disease process (gene therapy); and providing needle-free immunisation against diseases (aerosolised vaccination) (Laube, 2014). Inclusive of local and systemic delivery, all of these applications have achieved varying degrees of success in translational progress in clinical efficacy and commercialisation (Laube, 2014). These advancements further support the importance of the lung as a suitable route of administration for drug delivery.

### 1.1.1 Challenges for drug delivery to the lungs

Aerosolised particles are solid or liquid droplets encapsulated in a gas suspension and ideal for drug delivery to the lungs. Many new aerosolised pharmaceuticals are unable to reach the market because safety aspects set out in regulatory guidelines for non-clinical and clinical phases are not met (Forbes *et al.*, 2014). The most common response to aerosol drug delivery in *in vivo* studies is nasal and laryngeal irritation in rats, which has little relevance for human orally inhaled pharmaceuticals (Nielsen *et al.*, 2008). Rats are obligate nose-breathers, and the nasal tract of the rat is more complex than in humans (Nielsen *et al.*, 2008). Anatomically, the human lung is different in many aspects; for example, the rat lung has a long monopodial branching system, unlike the relatively symmetrical branching scheme of the human lung (Phalen *et al.*, 1983). Tracheal length/diameter ratios and branch shapes scale for humans being (6) is considerably shorter compared to rats (8.85), hamsters (9.23), dogs (10.63) and monkeys (10) (Phalen *et al.*, 1983). Differences in airway bifurcation and, consequently, airflow among species can contribute to variations in regional particle deposition in the lungs (Esch *et al.*, 1988). Rats are more sensitive than humans in developing alveolar epithelial hyperplasia, alveolar lipoproteinosis and tumour formation in response to inhalation of silica dust, whereas the human lung is more prone to developing high-grade fibrosis (Green *et al.*, 2007). Consequently, it is impossible to extrapolate findings directly from rat to human *in vivo* studies.

Lung irritation, observed in acute studies (e.g., changes in the epithelium at the bronchial and alveolar regions) may be considered adverse responses in short term studies resulting in discontinuation of those studies and the pharmaceutical agent (Jones *et al.*, 2012). What is not known is whether these responses to inhaled aerosols are truly adverse or a normal adaptive response, at what point is an adverse response



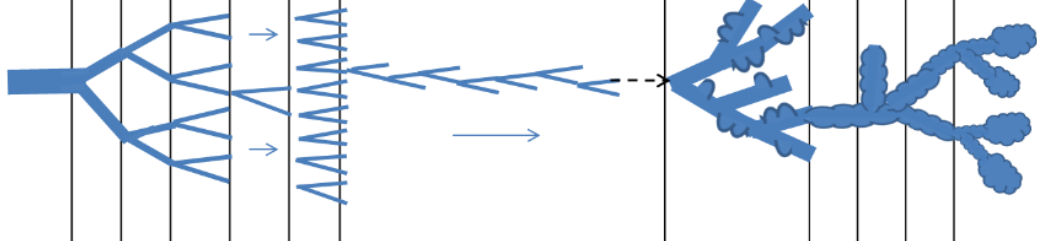
determined and at what point is the response predictive of a potentially adverse event for treated patients (Forbes *et al.*, 2014; Jones *et al.*, 2012b). In this context, *in vitro* models are valuable tools to understand the responses of alveolar cells to inhaled aerosols in monocultures and co-cultures (Nahar *et al.*, 2013).

## 1.2. The lung

### 1.2.1 Structure and function of the lungs

The respiratory system consists of nasal passages, the trachea and a pair of lungs in the thoracic cage (Ward *et al.*, 2011). The principal role of the lung is for gaseous exchange, maintaining cellular homeostasis in the body through the delivery of oxygen to tissues and removal of metabolic wastes by a process known as respiration (Ward *et al.*, 2011). In addition to respiration, the lungs act as a protective organ against gases and xenobiotics via filtration, metabolism and excretion of toxins (Davies *et al.*, 2003).

The airways of the lung divide by dichotomous branching, with approximately 23 generations of branches from the trachea to the alveoli (Weibel, 1963) (Figure 1.1). On inspiration, air passes through the nasal cavity and pharynx into the trachea, whereafter the airways subsequently bifurcate. (Weibel, 1963). The conducting airways consist of the trachea and bronchi, which function to warm, humidify and filter inspired air distributing it to and from the respiratory airways, comprising of respiratory bronchioles, alveolar ducts and alveolar sacs (Weibel, 1963). The alveolar sacs are small, round chambers roughly 300  $\mu\text{m}$  in diameter, surrounded by a wall of alveolar epithelium and a network of capillaries to allow for gaseous exchange (Davies *et al.*, 2003).

	Conducting airways										Respiratory unit						
Name	Trachea		Bronchi			Bronchioles		Terminal bronchioles			Respiratory bronchioles			Alveolar ducts		Alveolar sacs	
																	
Airways (n)	1	4						$\rightarrow 10^4$			$3 \times 10^5$			$8 \times 10^7$		$3-6 \times 10^8$	
Diameter	20mm	15 $\rightarrow$ 10mm						10 $\rightarrow$ 2mm			1mm			0.05mm		0.03 mm	
Generation	0	1	2	3	4	5	6 $\rightarrow$ 16			17	18	19	20	21	22	23	

**Figure 1.1 Diagram of the lung's branching airways.**

Division denotes the order of the conducting airways and respiratory unit via generations with trachea as zero up to alveolar sacs as 23. The airways branch 16-17 times before alveolar sacs are encountered adapted from Phalen (Phalen *et al.*, 1983).

The trachea divides into two main bronchi. The trachea and bronchi are supported by U-shaped cartilage and smooth muscle that divide to give segmental bronchi, which become narrower, shorter, and more numerous with each generation (Clancy *et al.*, 2002). Bronchioles are smaller airways embedded in lung tissue and lack cartilage in their walls. With increasing bifurcation in the bronchiolar region, the ciliated respiratory epithelial cells and mucus-secreting goblet cells become replaced by club cells. These secretory and ciliated cells work together to perform mucociliary clearance as the first line of defence against inhaled particulates in the upper conducting airways (Whittemore 2003).

The respiratory bronchioles are the first generation of the respiratory unit to have alveoli in their walls which form connected groups at the end of bronchoalveolar

ductiles. These develop into alveolar ducts and sacs, whose walls are only composed of alveoli. The alveolus wall is lined by the alveolar epithelium with underlying connective tissue and capillary networks. These networks form the septum of neighbouring alveoli with alveolar epithelium on each side (Davies *et al.*, 2003).

In adult humans, the average alveolar surface area is more than 100 m<sup>2</sup> compared to the surface area of the conducting airways, reaching only a few metres (Ward *et al.*, 2011). Due to their difference in size, rodents have a much smaller alveolar epithelial surface area than other mammals (e.g. rat: 0.4 m<sup>2</sup>, mouse: 0.05m<sup>2</sup>, dog: 52 m<sup>2</sup>) (Stone *et al.*, 1992). However, there is a strong correlation between lung size and numbers of different cell types, such as alveolar epithelial cells, when analysed using data from various mammals (Stone *et al.*, 1992).

### 1.2.2 The Alveolus

The alveolar epithelium represents 99% of the surface area of the lung (Guillot *et al.*, 2013) and comprises type I and type II alveolar epithelial cells (AECI and AECII) that occupy 95% and 5% respectively of the alveolar surface (Figure 1.2) (Guillot *et al.*, 2013). AECI cells are flat, membranous cells that form the air-blood barrier component and are found in close apposition to capillary endothelial cells to facilitate efficient gas exchange (Whitsett *et al.*, 2015). Both AECI and AECII are strongly associated with the innate immune response. AECI are understood to be involved in pro-inflammatory response through their extensive surface contact with resident alveolar macrophages in the alveolar space (Guillot *et al.*, 2013). They express Toll-like receptors (TLR) and produce pro-inflammatory cytokines, such as IL-1 $\beta$ , CXCL1, CXCL2, CXCL5 and CCL20 in response to stimuli (Yamamoto *et al.*, 2012). AECI are derived from AECII

cells through a trans-differentiation process, but the progenitor mechanism and function in the normal lung is not yet fully understood (Fehrenbach, 2001; Herzog *et al.*, 2008).

AECII are known as the “defenders of the alveolus” because of their multitude of functions related to inflammation, cell repair and synthesis of surface-active agents for alveolar protection. (Fehrenbach, 2001). They are large cuboidal cells with high plasticity, and one of their main functions is the synthesis and secretion of surfactants (Fehrenbach, 2001). Alveolar surfactant is composed mainly of lipids and a low concentration of specific surfactant proteins produced by AECII cell-lamellar bodies and secreted into the airspace (Guillot *et al.*, 2013). Alveolar surfactant plays a major role in alveolar homeostasis during breathing as it lowers the surface tension at the air-blood barrier (Fehrenbach, 2001). It is also necessary for alveolar fluid balance and a host-defence/ physical barrier. The alveolar fluid balance disruption leads to biophysical challenges (Whitsett *et al.*, 2015).

Surfactant proteins (SP) provide structure, regulation, function, and intrinsic host-defence properties to the alveoli (Whitsett *et al.*, 2015). SP- A and SP- D are well-conserved members of the collectin cohort and are highly expressed by AECII (Guillot *et al.*, 2013). The calcium-dependent lectins recognise pathogen-associated molecular patterns and modulate inflammatory and allergic responses, activating effector mechanisms like direct opsonisation, neutralisation, and phagocytosis by alveolar macrophages (Gupta *et al.*, 2007). SP-B and SP-C, synthesised by AECII, produce hydrophobic peptides necessary to spread and stabilise surfactant lipids (Whitsett *et al.*, 2015).

### 1.2.3 The fate of inhaled particles in the airways

Mechanisms of particle deposition in the respiratory tract include inertial impaction, gravitational sedimentation and Brownian motion (Smyth *et al.*, 2011) (Figure 1.2). Deposition by inertial impaction is the primary mechanism for large particles ( $<5\ \mu\text{m}$  diameter) with high momentum that impacts the airway walls rather than following the airstream deeper into the lungs (Smyth *et al.*, 2011). Gravitational sedimentation is a deposition mechanism for particles ( $0.5\text{--}3\ \mu\text{m}$  diameter) in the conducting airways; increased gravitational sedimentation occurs upon breath-holding (Smyth *et al.*, 2011). Brownian motion is the mechanism of deposition by diffusion of small particles ( $<0.1\ \mu\text{m}$ ) from a high to low concentration within the lower respiratory airways /alveolar region (Smyth *et al.*, 2011).

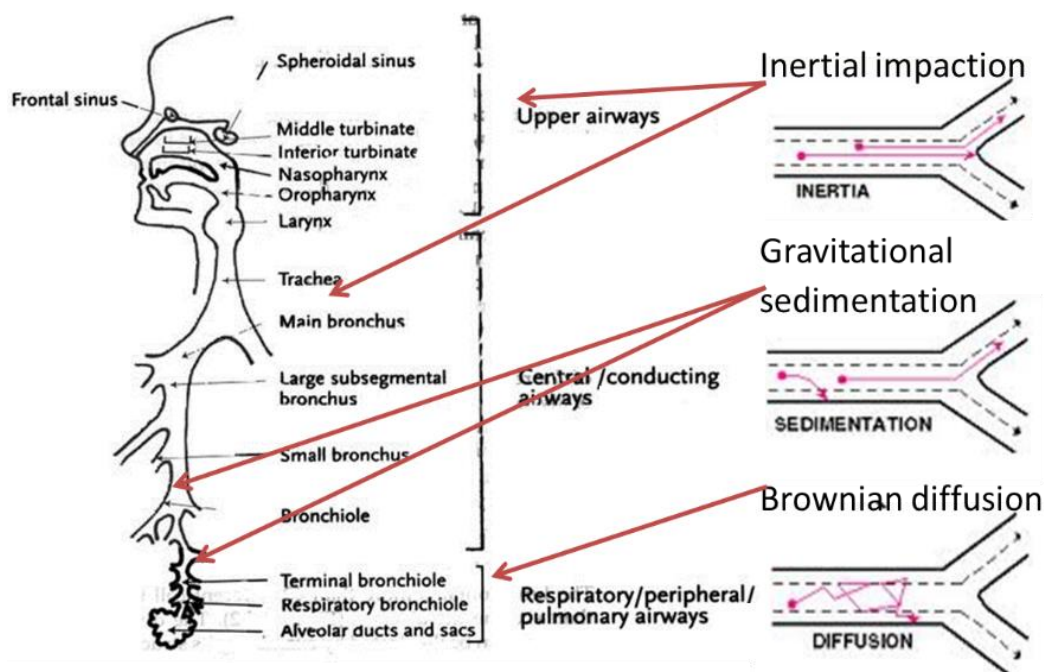


**Figure 1.2 Deposition mechanisms of inhaled particles in the respiratory tract.**

The paracellular transport pathways across the airway epithelium involve inertial impaction: large particles ( $>5\ \mu\text{m}$ ) deposit in the upper airways, gravitational sedimentation: particles ( $0.5\text{--}3\ \mu\text{m}$ ) settle in the conducting airways and Brownian motion: deposit in the small airway. Adapted from (Smyth *et al.*, 2011).

The physicochemical properties of the particles influence solubility and determine the absorption pathway across the airway epithelial barrier (Colbeck *et al.*, 2014). Paracellular transport involves molecules passing between adjacent selective cells with tight junctions and is the predominant absorption pathway for small, hydrophilic molecules and macromolecules up to 40 kDa (Colbeck *et al.*, 2014). In contrast, transcellular transport involves the partitioning of small hydrophobic molecules through the thin alveolar epithelium and capillary endothelium followed by absorption into the bloodstream and is the principal absorption pathway for most inhaled medicines. (Colbeck *et al.*, 2014). New inhaled pharmaceuticals can often be poorly soluble; thus, their resident time within the lung is increased, making them ideal for sustained drug delivery of microparticles and nanomedicines administered to treat respiratory disorders. (Loira-Pastoriza *et al.*, 2014). Particles deposited in the ciliated conducting airways are efficiently removed by mucociliary clearance mechanisms (Aulton *et al.*, 2013), whereas insoluble particles in the alveolar regions are removed by cell-specific mechanisms involving alveolar macrophages, which are discussed further in the section. Clearance mechanisms and interactions between poorly soluble or insoluble inhaled materials and alveolar macrophages is a well-established issue in the literature and poses a well-documented challenge regarding the safety of inhaled products (Forbes *et al.*, 2014).

#### **1.2.4 Macrophages**

Macrophages are essential immune effector cells with homeostatic roles that participate in host defence and survival (Mosser *et al.*, 2008). Their main functions are phagocytosis of erythrocytes and cells that have undergone cell death and rapid clearance of cellular debris generated during tissue remodelling (Mosser *et al.*, 2008).

This clearance mechanism is a vital metabolic process without which the host would not survive (Mosser *et al.*, 2008). Macrophages are present in nearly all tissues. They differentiate from circulating peripheral-blood mono-nuclear cells developed from a common myeloid progenitor cell in the bone marrow, which migrate into tissues in response to inflammation or to replenish long-lived tissue-specific macrophages of the central nervous system (microglial cells), alveoli (alveolar macrophages), bone (osteoclasts), liver (Kupffer cells), connective tissue (histocytes), gastrointestinal tract and spleen (Gordon *et al.*, 2005; Mosser *et al.*, 2008). Macrophages of the lung are anatomically located (Laskin *et al.*, 2001). Their location and phenotypic characteristics are categorised into the pulmonary surface, pleural, interstitial and alveolar macrophages (Laskin *et al.*, 2001).

### 1.2.5 Alveolar macrophages

Alveolar macrophages (AM) are resident macrophages of the lungs found in the air space of the alveoli (Laskin *et al.*, 2001). They are mononuclear phagocytes and the first line of innate cellular defence in the lower airways, in communication with AECI and AECII, where they sample microbes and particulates (Guillot *et al.*, 2013). AMs phagocytic abilities are essential for clearance of foreign pathogens and xenobiotics, efferocytosis and regulate inflammation (Murray *et al.*, 2011).

It is understood that AMs are a subset progeny of myeloid-derived circulating monocytes which enter tissues and differentiate (Gordon *et al.*, 2005). However, it is now accepted that AMs arise from embryonic progenitors that enter the organs and locally mature before and after birth (Kopf *et al.*, 2014). Foetal lungs contain two myeloid populations: F4/80<sup>hi</sup>CD11b<sup>int</sup> foetal macrophages and F4/80<sup>int</sup>CD11b<sup>hi</sup>Ly6C<sup>+</sup>

foetal monocytes derived from haematopoiesis in the yolk sac and liver, respectively. Cell surface markers on foetal lung monocytes undergo significant expression modifications during gestation via AECI extracellular signalling cross-talk (Westphalen *et al.*, 2014). AECI production of granulocyte-macrophage colony-stimulating factor (GM-CSF) induces expression of nuclear receptor PPAR- $\gamma$  until the foetal monocytes reach maturation stage; F4/80<sup>hi</sup>CD11c<sup>hi</sup>SiglecF<sup>hi</sup>CD64<sup>hi</sup>CD11b<sup>lo</sup>Ly6C<sup>+</sup> AMs (Gordon *et al.*, 2005; Guilleams *et al.*, 2013; Trapnell *et al.*, 2002).

AMs have a high level of plasticity so that they can rapidly distinguish between steady-state conditions and recognise and initiate an inflammatory response to inhaled particulates. Furthermore, they can distinguish between situations that require a tolerogenic response and those that require an anti-inflammatory response. Thus, these cells possess a multi-receptor signalling system to carry out a complex balancing act between activation and repression of signals (Hussell *et al.*, 2014).

The capability of tissue macrophages to adapt and achieve several functions has governed their broad classification as either classically activated M1 macrophages or activated M2 macrophages (Mosser *et al.*, 2008). Classification of AMs into these subgroups has proven challenging because of their intricate signalling system, resulting in functional and phenotypical differences between AMs. Tissue damage or pathophysiological conditions are known to polarise AMs towards an M2 phenotype (Cassetta *et al.*, 2011). AMs become phagocytically active following exposure to xenobiotics during respiration.



### 1.3. AM mechanisms of response to inhaled pharmaceuticals

Inflammatory responses of AMs are tightly controlled through cell-cell and soluble mediator interactions to create a well-regulated environment. Regulatory receptors play an important role in regulating AMs through their increased expression on macrophages in the lower airways compared to those in other tissues because of the enhanced availability of ligands and other immunomodulatory receptors in the alveoli or following external stimulus (Hussell *et al.*, 2014).

Reaching a desired therapeutic outcome, either to enhance or avoid AM uptake, are subject to the mechanism of phagocytosis (Patel *et al.*, 2015). Phagocytosis, by which phagocytes efficiently recognise, engulf and eliminate inhalable particulate drug carriers, are a key mechanism of action for AMs. In the respiratory airways, the removal of inhaled particles by AMs is achieved by a series of phagocytic processes. Known as opsonisation, the first of the processes is the recognition of foreign particles after their coating with soluble proteins, for example, phospholipids and surfactant proteins such as SP-A and SP-D (Aderem *et al.*, 1999; Ruge *et al.*, 2012). Dual functioning AM surface receptors such as complement and immunoglobulins bind the opsonised particles activating the receptors to initiate cytoskeletal rearrangements and formation of pseudopods by the phagocytes. Subsequently, the phagocytes engulf the particles ( $> 0.5 \mu\text{m}$ ) by internalising them through endocytosis, forming a phagosome (Greenberg *et al.*, 2002). Finally, a lysosome merges with the phagosome to form a phagolysosome. The lysosomal environment acidifies the content of the phagosome, where it is enzymatically destroyed (Figure 1.3).

Multiple mechanisms for particle recognition by phagocytes rely on receptor-specific pathways. These receptors are involved in the recognition and phagocytosis of inhaled

pharmaceuticals (Patel *et al.*, 2015). Particles detected by AMs are by specific pattern recognition receptors called scavenger receptors (Palecanda *et al.*, 1999). A group of scavenger receptors known as macrophage receptors with collagenous structure (MARCO) are involved in innate immune recognition and facilitate the elimination, alongside transporter proteins of inhaled particles (Arredouani *et al.*, 2005). Other scavenger receptors involved in particle recognition and initiation of phagocytosis in AMs include TLRs (TRL 2, TRL 4 and TRL 5), integrins (IL- 10) and mannose receptors (CD 206) (Hussell *et al.*, 2014; B. Patel *et al.*, 2015).

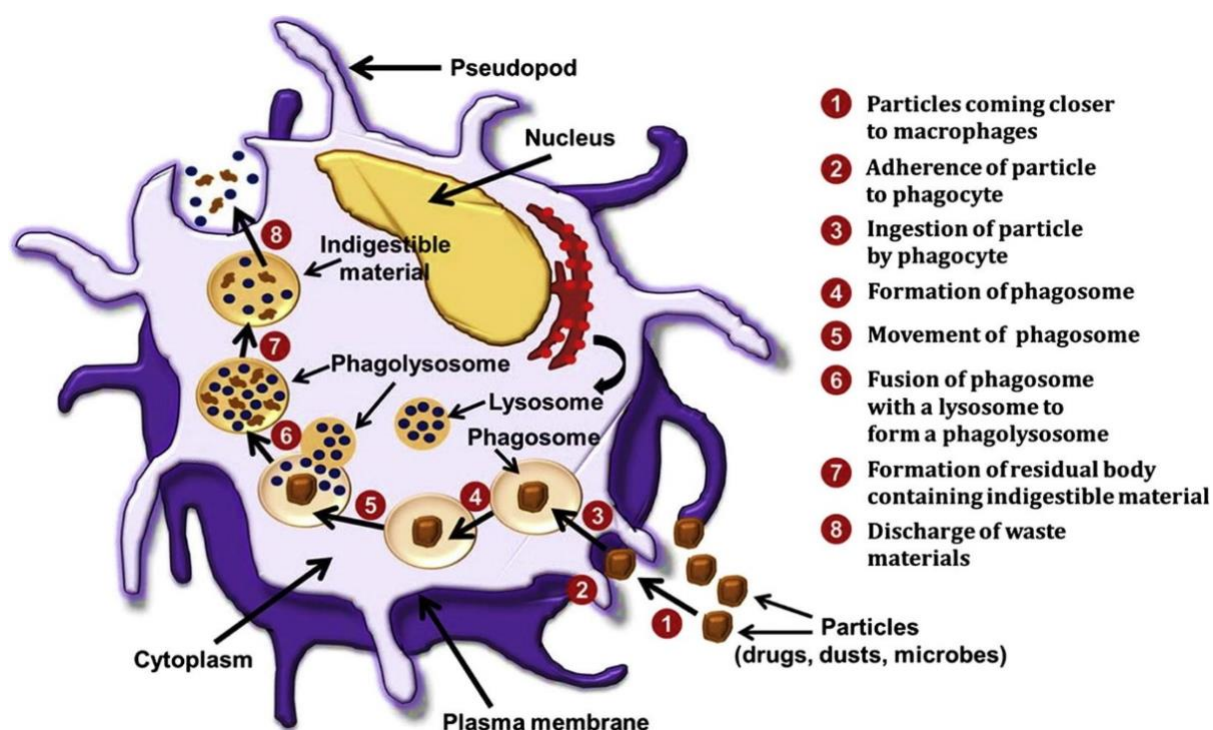


**Figure 1.3 Process of particle engulfment through phagocytosis by alveolar macrophages.**

Mechanisms of response by AMs depend on the particle's properties, such as size, shape, and physicochemical properties. With advances in inhaled drug delivery, it is possible to achieve targeted delivery specifically to the alveolar region with poorly soluble therapeutics or purpose-designed sustained-release formulations. However, whilst the increase in residence time of therapeutics in the small lung has the potential to generate medicines with reduced administration frequency and achieve superior systemic bioavailability, interactions with AMs question the safety of these strategies. (Forbes *et al.*, 2014). The image was taken from Patel *et al.* 2015.

AMs, recognise and respond by initiating particle clearance via phagocytosis of the increasing accumulation of materials. This, in turn, results in excessive macrophage stimulation and recruitment of other immune cells and inflammatory factors (*Patton et al., 2007*). During assessments of lung targeted pharmaceuticals, AMs have been reported to respond in a manner that has yet to be determined as an adaptive or adverse response (*Forbes et al., 2014*).

‘Foamy macrophage’ is a term used to describe AMs that are granular or have a vacuolated appearance under a light microscope (*Minta et al., 1985*). These foamy AMs (FAMs) are often larger in size than their phenotype due to lysosomal lamellar bodies and engulfment of insolubilised, crystalline inhaled drug materials (*Lewis et al., 2014; Patton & Byron, 2007*). The observation of a FAM phenotype likely classifies a broad spectrum of biochemical reactions, which results in a highly vacuolated phenotype. Additionally, FAM responses are highly variable depending on the pharmaceutical agent, concentration, and exposure time to the alveoli (*Lewis et al., 2014*). *Lewis et al.* proposed the classification of these AMs based on their range of responses in the rat lung (see Table 1.1)

### 1.3.1 Classification of AMs responses

**Table 1.1 Alveolar macrophage responses in rats.**

Type 1	Reversible aggregation, co-localised with hyperplastic AECII Foamy pathology Located at the bronchioloalveolar junction NOEL assigned
Type 2	Aggregation and infiltration of inflammatory cells (neutrophils/ lymphocytes) Some degradation Foamy, eosinophilic, basophilic, granular or pigmented cytoplasm Located at the bronchioloalveolar junction or diffuse
Type 3	Irreversible Granulomatous inflammation, giant cell formation and/ or fibrosis Located at the bronchioloalveolar junction or diffuse

A categorisation of AMs based on their range of responses to inhaled pharmaceuticals in the rat lung as discussed by (Lewis *et al.* 2014). NOEL: No observed effect level.

Other clinical relevant pathologies include pulmonary alveolar proteinosis and phospholipidosis (Halliwell, 1997). Pulmonary alveolar proteinosis is described as a marked accumulation of surfactant lipids, most likely related to specific exposures, e.g. silica dust (Heppleston *et al.*, 1970). Drug-induced phospholipidosis is characterised by secondary inflammatory changes and long-term fibrosis (Forbes *et al.*, 2014).

### 1.4. Current *in vitro* AM models of the alveoli for inhaled pharmaceutical response

Many viable assessment systems can be adapted to measure inhaled pharmaceutical responses. Figure 1.4 identifies how each system for preclinical and clinical outputs increases complexity. As the inhaled testing systems become more complex, from computational physicochemical measures to human studies, so do factors driving the choice of a system used. These factors include limiting the number of tested chemicals, increased expenses to run animal and human trials, and meeting ethical requirements. Each factor is carefully considered for the most appropriate and efficient output.

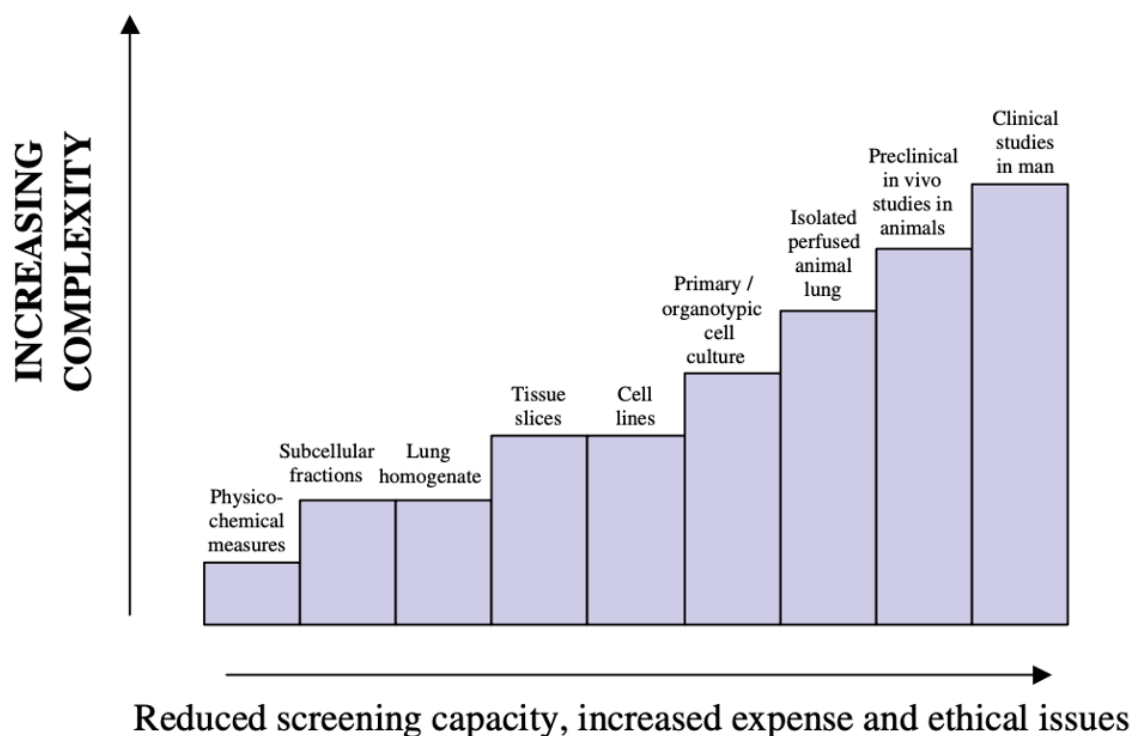


**Figure 1.4 Illustration of a hierarchy of complexity of systems prior to clinical assessments of inhaled compounds.**

Systems include *in silico*, *in vitro*, *ex vivo* and *in vivo* approaches (Ehrhardt and Forbes 2008).

*In vitro*, alveolar models predictive of the human response to inhaled medicines have been identified as valuable predictive tools to provide supplementary data for designing and interpreting inhalation toxicity in *in vivo* models and progress to the clinic (Forbes *et al.*, 2014). Furthermore, the 3R strategy (Replacement, Reduction and Refinement) recommends reducing animal usage, developing non-animal approaches, and improving scientific applications for animal welfare (Guhad, 2005). Consequently, *in vitro* models ranging from monocultures to multiple cell co-cultures and three-dimensional (3D) models of lung tissue have been developed (Alfaro-Moreno *et al.*, 2008; Braydich-Stolle *et al.*, 2010; Carterson *et al.*, 2005; Crabbé *et al.*, 2011; Klein *et al.*, 2013; Kletting, 2016; Lehmann *et al.*, 2011; Rothen-Rutishauser *et al.*, 2005).

*In vitro* human 3D alveolar cell culture models are presently in development to investigate the biological roles of AMs in human health and disease (Steimer *et al.*, 2005) and in inhaled drug discovery research (Forbes *et al.*, 2014). However, their availability is limited because of poor cell characterisations and low commercial demands. The increased need for *in vitro* AM models is due to pressure from both government industrial strategies and animal rights organisations to ban animals in testing as established in the “testing ban” 2013 for consumer products. Pharmaceutical companies struggle to prove or disprove translational inhaled test results of candidate drugs in animals and extrapolate them to physiologically relevant human response outcomes. Additionally, there are a limited number of human alveolar cell sources (macrophages and epithelial) available to develop alveolar co-culture systems.

The selection and generation of an *in vitro* model depend on the desired application; for example, bronchial cells are suitable for assessing inhaled medicines to proximal lung tissue. In order to generate translational data, it is critical that representative cell systems function similarly to cells types *in situ* (Steimer *et al.*, 2005). There are cell culture lung models available, but few represent alveolar drug delivery and response (Forbes *et al.*, 2014; Huh *et al.*, 2011; Steimer *et al.*, 2005).

#### **1.4.1 Primary macrophages**

The use of primary AM models to investigate the role of AMs in both health and disease is becoming prevalent, with most models used to investigate disease mechanisms and identify biomarkers (Lewis *et al.*, 2014). Bronchoalveolar lavage (BAL) is a commonly used technique to gain access to AMs from humans and animals but often yields low numbers and AM subpopulations among various subjects due to environmental

exposure and disease type (Hunninghake *et al.*, 1983; St-Laurent *et al.*, 2009; Taylor *et al.*, 2000). Studies have shown species sensitivity between BAL harvested AMs; human AMs were the least sensitive to effects of inhaled particles with lower phagocytic uptake of particles compared with rats and guinea pigs (Chen *et al.*, 1982; Schlesinger *et al.*, 1992). In addition to species differences discussed earlier, human AMs may be less sensitive to inhaled particulates than animal AMs because human cells are accustomed to external insults *in situ*. In contrast, housed animals are sheltered from birth, are obligate nose breathers and have narrower airway passages. These physical differences between human and rat airways mean their alveoli are exposed to different profiles of particulates (Schlesinger *et al.*, 1992).

An alternative AM model uses peripheral blood monocytes isolated from donors and differentiated with GM-CSF, resulting in a consistent cell population phenotype (Trapnell *et al.*, 2002). These macrophages display lineage qualities similar to AMs; markers, Fc gamma receptors, adhesion molecules and scavenger receptors (Redente *et al.*, 2010; Tomlinson *et al.*, 2012). Biochemically, they respond to stimulants such as cigarette smoke similarly to AMs *in vivo* and *ex vivo* via signal transduction pathways (Karimi *et al.*, 2006).

#### **1.4.2 Alveolar macrophage cell lines**

Macrophage cell lines are frequently used as models to study mechanisms of macrophage responses to xenobiotics, including inhaled pathogens, particulate materials and, to a lesser extent, pharmaceutical compounds. Continuous macrophage cell lines regular to the literature are RAW 264.7 (mouse leukemic monocyte-derived) (Jalava *et al.*, 2007; Raschke *et al.*, 1978), and MHS (virus

transfected mouse alveolar macrophage) (Saxena *et al.*, 2008), J774.A1 (mouse reticulum cell sarcoma- derived). Commonly used NR8383 (normal rat alveolar macrophage cells) cells are considered a highly suitable cell line for investigating alveolar responses as they display multiple functional characteristics similar to that of primary alveolar macrophages (Hutter *et al.*, 2014; Rojanarat *et al.*, 2012), specifically the mannose receptor, which binds and internalises soluble and particulate materials (Lane *et al.* 1998).

There are no human AM cell lines described in the literature, and primary AMs usually come from unhealthy smokers' lungs or diseased, compromised lung tissue through surgical access only. Potentially suitable AM-like cell lines are THP-1 (human leukemic monocyte derived-differentiated to monocyte-like macrophage through phorbol ester treatment) (Tsuchiya *et al.*, 1982) and HL-60 (Human leukemic myeloblast) differentiated in the presence of DMSO (Harris *et al.*, 1985).

Other prospective cell lines used for alveolar macrophage responses to stimuli include U937 (human monocyte lymphoma cell line differentiated to alveolar macrophages in the presence of phorbol ester or vitamin D treatment). U937 cells and their differentiated phenotype have been reported extensively throughout the literature and are used for measuring AM responses to environmental and pathological stimuli (Vogel *et al.*, 2012). Studies support the suitability of using differentiated U937 cells to determine alveolar macrophage responses (Braydich-Stolle *et al.*, 2010; Larrick *et al.*, 1980).

The use of a cell-line based model avoids many problems, including available cell numbers, variability, high costs and time-consuming procedures encountered while



working with primary cells (Forbes *et al.*, 2014). Monoculture cell models have improved our knowledge regarding particle interactions and nanomaterial toxicity (de Souza Carvalho *et al.*, 2014); however, the validity of any single myeloid or macrophage model system has yet to be fully verified, and challenges remain using *in vitro* systems for accurately determining their outcomes in response to inhaled particulates. There is a need for rigour in understanding macrophage models' morphological and functional characteristics to exploit these models to their full potential in inhaled drug delivery response.

### **1.4.3 Alveolar epithelial culture models**

#### **1.4.3.1. Primary cell models**

The development of an alveolar epithelium is often of primary interest when establishing responses to inhaled particulates. Primary cultures such as AECII and AEC freshly isolated from rabbit and rat alveolar epithelium, respectively, can establish a permeable barrier *in vitro*. Rabbit AECII are cultured as models for studying alveolar function in surfactant production (Finkelstein *et al.*, 1983; Kikkawa *et al.*, 1975). Rat AEC display qualities suitable for system transportation of drugs, caveolin-1 expression and presence (AECI) or lack of caveolae (AECII) and investigation of biological characteristics such as differentiation by flattening, phospholipidosis secretion and generation of trans-epithelial electrical resistance (TEER) (Borok *et al.*, 2002; Campbell *et al.*, 1999; Cheek *et al.*, 1989). Human alveolar epithelial primary culture (HAEpC), derived from human lungs, is a highly suitable approach for *in vivo* comparisons (Elbert *et al.*, 1999; Robinson *et al.*, 1984). HAEpC cells have similar characteristics to that of primary rat AEC. In addition, they exhibit tight junctions and cell-specific lectin binding (Elbert *et al.*, 1999).

Primary cultures of rat and human AECI cultures are the leading and most established alveolar epithelium *in vitro* systems presently available. A drawback remains for the use of HAEpC cells because of ethical considerations. Moreover, the material is commonly derived from tumour patients, which can lead to contamination of tumour cells and unknown patient variability's, e.g., age, smoker or non-smoker and disease hereditary. These factors limit the ability of this model and make it unsuitable for first stage high-throughput screening.

#### **1.4.3.2. Cell line models**

A number of human and non-human lung epithelial cell lines are commercially available; however, few mimic the tight barrier formed by AECI cells compared with the commercially abundant AECII cells, which have limited applications *in vitro*. A new human alveolar epithelial cell line is the hAELVi cell (human Alveolar Epithelial Lentivirus immortalised). These immortalised primary cells are reported to display AECI-like characteristics and form a polarised cell layer with functional tight junctions and epithelial electrical resistance values in line with those recorded for primary alveolar epithelial cells/native human tissues. Moreover, hAELVi cells are proposed as suitable to model the air-blood barrier of the alveolar surface (Wirth *et al.*, 2016).

For AECII type cells, the human cell line A427, derived from lung carcinoma, is suitable for measuring mucin gene expressions but not for pharmacological testing (Berger *et al.*, 2012). A549, human lung carcinoma, is a widely used and accepted *in vitro* model for pulmonary studies. The A549 cell line has many primary AECII, including synthesis of phosphatidylcholine (the major component of alveolar surfactant), possesses surfactant protein-ligand SP-A and secrete SP-B and SP-C (Rafael-Vázquez *et al.*,

2018). Furthermore, they do not form tight junctions and are thus not representative of the alveolar epithelial barrier function (Lieber *et al.*, 1976). Nevertheless, A549 cells are used as an *in vitro* tool to predict alveolar toxicity, metabolism and gene expression *in vivo* (Foster *et al.*, 1998; Hiemstra *et al.*, 2018).

Another human cell line displaying characteristics of AECII in the NCI-H441 cell line derived from human lung adenocarcinoma. Although the cell line has not been used for drug absorption studies, evidence supports that H441 cells form monolayers of polarised cells, exhibiting a significant TEER (Shlyonsky *et al.*, 2005). Alveolar epithelial cell lines from other species have also been considered in the literature and include R3/1 and L-2 (rat), MLE-12 and 15 (mouse) and RLE-6TN (rat) (ATCC, 2002). The RLE-6TN rat AECII line model has been used to measure cytokine expressions, endoplasmic reticulum stress and epithelial to mesenchymal transitions in response to xenobiotic uptake (Driscoll *et al.*; Oda *et al.*, 2011; Tanjore *et al.*, 2011). It is unknown if the rat and mouse cell lines are suitable as a model for absorption studies as, similarly to A549 cells, they do not form tight junctions but are the current models for assessing inhaled pharmaceutical responses in the alveolar region.

#### **1.4.4 *In vitro* co-culture models of the lung**

Cell culture models are becoming an acceptable alternative to animal models due to many factors, including reduced costs compared to animals, the ability to predict and simulate pharmacological and toxicological outcomes, and the potential for high throughput. The 3R strategy (Replacement, Reduction and Refinement) advocates reducing animal usage, developing non-animal methods, and improving scientific methods for animal welfare (Törnqvist *et al.*, 2014). Recent advancements in *in vitro*

models with cultured cells have been reported in several studies that aim to develop better *in vitro* and *in vivo* correlations. Thus, *in vitro* models have been developed from monocultures to multicell cell co-cultures describing simple to more lifelike three-dimensional (3D) lung tissue models. Models of interest for the current review are co-culture models that contain alveoli cells and mimic alveoli conditions.

Rothen-Rutishauser *et al.* developed a trans-epithelial network 3D model using trans-well inserts represented by human AMs and dendritic cells (DCs) derived from human blood monocytes and alveolar epithelial cells; A549. Following particle exposure, particle uptake (1  $\mu\text{m}$ ) and translocation by the three cell types were reported (Blank *et al.*, 2007; Rothen-Rutishauser *et al.*, 2005). Further work suggested higher epithelial integrity of the model following replacement of A549 cell with human alveolar epithelial primary cells whereby tight junction protein zonula occludens-1 was regularly expressed, unlike in A549 cells (Lehmann *et al.*, 2011).

Carterson *et al.* reported that a 3D culture model of A549 epithelial cells developed using a rotating-wall vessel bioreactor increased mucin-specific and cytokine markers expression compared to A549 monolayer culture. Also, 3D culture promoted tight junction formation and cell polarity similar to *in vivo* conditions (Carterson *et al.*, 2005). Crabbé and co-workers further developed Carterson's monotypic 3D model into a multicellular complex of naturally differentiated U937 macrophages and A549 cells that displayed physiologically relevant morphological characteristics (Crabbe *et al.*, 2011).

A tetra-culture composed of A549 cells, differentiated macrophage-like cells (THP-1), mast cells (HMC-1) and endothelial cells (EA.hy 926) seeded in a 3D orientation was reported to more closely resemble the *in vivo* organisation and functionality of the

alveolar region (Klein *et al.*, 2013). This system was optimised from a previous study (Alfaro-Moreno *et al.*, 2008) which, investigated the characteristics of single cultures, bi-cultures (A549 + HMC-1, THP-1 + HMC-1), tri-culture (A549 + THP-1 + HMC-1) and tetra-culture (A549 + THP-1 + HMC-1 + EA.hy926). Cytokine secretion was increased with increased complexity the systems mimicking cell-communications found in intact tissues (particularly the mast cell-macrophage crosstalk), and results generated corresponded better to report *in vivo* effects.

Several articles report the successful development of alveolar co-cultures for particulate and pathogen exposure (Braakhuis *et al.*, 2016; Grabowski *et al.*, 2016). However, the majority of these co-culture models combine epithelial cells with endothelial or goblet cells (Rayner *et al.*, 2019), and few incorporate constructs with alveolar macrophages (Evans *et al.*, 2020; Kletting, 2016; Luyts *et al.*, 2015)). The toxicity of inhaled nanoparticles to the alveoli has increased interest through the recent advancements in nanotechnology. Nanoparticles dispersed in artificial lung surfactant were exposed to differentiated U937 or THP-1 (macrophage) cells co-cultured with A549 cells (Braydich-Stolle *et al.*, 2010; Grabowski *et al.*, 2016). Increased cytokine secretion and necrosis of AMs were detected by the presence of nanoparticles (Braydich-Stolle *et al.*, 2010; Grabowski *et al.*, 2016).

Co-culture models of the rat alveolus have also been reported using the rat alveolar epithelial cell line RLE -6TN co-cultured with rat AMs via BAL (Tao *et al.*, 2002; S. J. Wang *et al.*, 2002). This model has shown sensitivity in response to environmental particulates. Reports suggest that responses to co-culture models are amplified than those of monocultures by contact-dependent interactions between epithelial cells and macrophages. Although particle uptake by macrophages did not differ between

monoculture and co-culture, particle-induced cytokine release in co-culture was significant (Tao *et al.*, 2002). Conversely, the opposite was reported for the same model when exposed to JP-8 jet fuel (Wang *et al.*, 2002). Cytokine release was reported to be higher in monocultures of both RLE-6TN and AMs than cultured together, suggesting cell signalling between cultures may provide a balance for cytokine secretion in response to stimuli.

Macrophage response is heavily dependent on the type of stimuli it is exposed to and the physiochemical properties of the stimuli. Cell-cell communications between cultures of a model have been recognised, which further highlights the need for a suitable inhaled pharmaceutical testing system for alveolar *in vivo* -*in vitro* correlations.

#### **1.4.5 *In vivo* models**

*In vivo* models are mainly used for studying the pharmacodynamics, toxicokinetics and distribution of drug formulations in various lung regions of inhaled medicines (Nahar *et al.*, 2013). Anaesthetised or conscious animals receive pharmaceutical compounds by various delivery techniques (e.g. nasal inhalation, insufflation, intratracheal instillation) with or without surgical intervention. Mice and rats have been widely used to determine the pulmonary pharmacology of large and small molecular weight drugs. The use of larger animals such as guinea pigs, rabbits, dogs, sheep, and monkeys has also been reported (Cryan *et al.*, 2007), although their use is restricted due to the high cost and standard operating procedures required to house and handle larger animals. It is crucial that variation in animal physiology is considered when exposing models to inhaled formulations. Variations in animal size, breathing patterns and lung capacity can lead to disparities in pharmacodynamic and pharmacokinetic profiles (Cheng *et al.*, 2010).

#### 1.4.6 *Ex vivo* models

Isolated perfused tissues are a well-established *ex-vivo* approach to study the mechanisms of drug transport, disposition and efficacy in the lung while retaining its structural and functional integrity. Some isolated perfused tissue models can provide a more realistic correlation with *in vivo* studies when compared to single-cell models (Nahar *et al.*, 2013).

Isolated perfused lung models have been developed for rodents such as rats (Byron *et al.*, 1986), mice and rabbits (Bleyl *et al.*, 2010). As animal models do not anatomically represent the human lung, *ex-vivo*, isolated perfused human lung models have also been developed with tissues sourced from transplantation rejection (Nahar *et al.*, 2013). However, the allocation of human lungs for research is through a closed group process, and availability is restricted to qualifying research groups who receive either whole lungs, individual lobes, airways or isolated cells for assessment of pathophysiology of acute lung injury or testing of new therapeutics (Ross *et al.*, 2019). Unfortunately, the high demand for *ex- Vivo-* lungs in research outweighs their availability and users must meet ethical requirements. Furthermore, the donor's lungs are often sourced from patients with lung injury such as pulmonary oedema or insults from smoking which questions the suitability of this model for safety and efficacy assessment of inhaled therapeutics for the small airways (Bhowmick *et al.*, 2016; Ross *et al.*, 2019). Nevertheless, *ex vivo* human lung models have gained recognition for clinical applications in gene and stem cell therapies (P. G. Chan *et al.*, 2020).

### 1.4.7 In silico models

*In silico* modelling refers to using computational methods employed for drug target validation and prediction of toxicity. *In silico* toxicology uses computational resources (i.e., methods, algorithms, software and data) intertwined with *in silico* pharmacology to model, simulate and predict the toxicity of chemicals for non-clinical and clinical outputs (Raies *et al.*, 2016). Computational methods are commonly used for transdermal and oral absorption studies and blood-brain barrier permeability pathways (C. Ehrhardt *et al.*, 2008). More recently, *in silico* approaches have been employed for inhalation toxicology studies and could help predict the toxicity of chemical compounds after inhalation exposures (Clippinger *et al.*, 2018). Inhaled compounds may be deemed “fit for purpose” through multiple assessments needs such as prioritisation, regulatory hazard identification for lethal concentration 50% (LC<sub>50</sub>) and quantitative risk assessment (Bell *et al.*, 2018). *In silico* strategies currently employed in toxicity assessment include empirical grouping approaches, quantitative structure-activity relationship (QSAR) analyses and mechanistic computational dosimetry models (Clippinger *et al.*, 2018). These approaches are based on the principle that similar compounds are expected to exhibit similar biological activities *in situ*.

Currently, computational methods aim to complement *in vitro* and *in vivo* toxicity tests to minimise the need for animal testing and reduce the cost and time of toxicity tests (Raies *et al.*, 2016). There are commercial interests in developing *in silico* methods to predict estimated ranges of LC<sub>50</sub> values. Such values could be used for better hazard classification and provide mechanistic information on how inhaled compounds cause systemic toxicity in humans, thereby leading to better Characterisation of their potential hazards than existing *in vivo* methods and in *in vitro* and *in vivo* extrapolations (Clippinger *et al.*, 2018; Koullapis *et al.*, 2019).



## 1.5. Model selection for inhaled pharmaceutical response

### 1.5.1 Selection of human representative models

Many species are available to study the disposition of drugs in the lungs. It is important to consider cells and tissue orientation in the lung whilst selecting an *in vivo* model to extrapolate the findings to humans. Anatomically, the human lung is different in many aspects, as discussed previously. The parameters of cells in the alveolar region of the lungs of rats, dogs, baboons and humans are shown in Table 1.2 (Crapo *et al.*, 1983).

**Table 1.2 Morphometric parameters of cells in the alveolar region of rat, dog, baboon and human lungs.**

	Fischer 344 Rat	Dog	Baboon	Human
Body weight, kg	0.29±0.01	16±3	29±3	79±4
Lung volume, ml	8.6±0.31	1322±64	2393±100	4341±284
Total number of cells/lung, 10 <sup>9</sup>	0.67±0.02	114±13	99±9	230±25
Total lung cells, %				
Alveolar Type I	8.1±0.3	12.5±1.7	11.8±0.6	8.3±0.6
Alveolar type II	12.1±0.7	11.8±0.06	7.7±1.0	15.9±0.8
Endothelial	51.1±1.7	45.7±0.8	36.3±2.4	30.2±2.4
Interstitial	24.4±0.7	26.6±0.7	41.8±2.7	36.1±1.0
Macrophage	4.3±1.0	3.4±0.6	2.3±0.7	9.4±2.2
Average cell surface area, µm <sup>2</sup>				
Alveolar Type I	7287±755	3794±487	4004±383	5098±659
Alveolar type II	185±56	107±15	285±85	183±14
Endothelial	1121±95	1137±127	1040±209	1353±67

Adapted from Crapo *et al.*, 1983.

Studies have reported significant interspecies differences in alveolar macrophage physiology between humans, rats, hamsters and monkeys. In addition to the human lung containing a higher percentage of macrophages than other species (Krombach *et al.*, 1997), rat and mouse alveolar macrophages have demonstrated different susceptibilities to single and repeated xenobiotic exposures (Oosting *et al.*, 1991). Furthermore, the rate and ability of AMs to phagocytose and clear particles are

dependent on the cell size of AMs, which is an inherent characteristic of the species (Krombach *et al.*, 1997).

The thickness of the pleura and the interlobular connective tissue in the human lung is also significantly greater than rats and monkeys whose interlobular connective tissue is less prevalent (Nikula *et al.* 2001). It has also been demonstrated that these species are more likely to accumulate macrophages in the interstitium in response to insoluble environmental particulates (Nikula *et al.*, 1997, 2001). Therefore, caution must be taken when extrapolating the sensitivity of an *in vivo* response to inhaled stimuli as the differences between human and animal lung anatomy and physiology are significant. Observations in *in vivo* alveolar responses to inhaled particles are not necessarily directly predictive of human responses to the same xenobiotics (Forbes *et al.*, 2014; Hoffman *et al.*, 2017). Further investigations in species-specific macrophage biology would help understand the differences in responses to inhaled pharmaceuticals.

## 1.6. Summary

The lung is a major route for the delivery of pharmaceuticals due to its accessibility. It delivers local and systemic treatment, gene therapies and vaccinations. Rat models are commonly used to assess toxicity profiles of new drug formulations, but anatomically they are not compatible and show different hypersensitivities compared with humans. Furthermore, physiological AM responses *in vivo* have been observed following inhaled treatments, and further investigation is required in defining them as adaptive or adverse events.

Several *in vitro* studies have been performed on mono-cell type cultures of monocyte/macrophage cells. These studies do not fully reflect the multicellular

complexity in *in vivo* tissues, given that; cellular interactions within the alveoli and the cellular crosstalk between the epithelial cells and macrophages are essential for innate defence. AMs work to eliminate inhaled particulates and trigger immune responses in the alveolar epithelium, such as increased immune function and cytokine production. There is also a commercial need for alveolar tissue models with 3D architecture and multicellular characterisations to consider the role of AMs and other alveolar cells (e.g., epithelial cells) in predicting the safety and efficacy of new compounds in a reliable and reproducible manner.

In order to develop a robust *in vitro* AM human lung model, a suitable, well-characterised cell model representing the human alveolar macrophage needs to be identified. This development proves challenging because no human AM cell lines are readily available. Whilst tissue and blood-derived monocyte cells (primaries and cell lines) are differentiated by various stimuli to generate mature monocytes/ macrophage, the methodologies available to differentiate and validate these cell lines are heavily variable, and the extent to how accurately these represent AM specifically is largely unreported. Validation of macrophage cells and their phenotype differ due to the lack of standardised terminology of morphological and phenotypical thresholds compared to other macrophage cell lines, highlighting the need to characterise a cell model which similarly represents human AMs.

Once this is achieved, developing a more representative immunocompetent co-culture model of the human alveolus can support chemical manufacturing companies to determine their future products without using animals safely.

## 1.7. Thesis Aims

Several *in vitro lung* models have been described and are used to evaluate the impact of inhaled substances, including chemicals, nanoparticles, microorganisms and toxins. However, most *in vitro lung* models aim to represent the upper airways and bronchiolar regions. There is a need for models of the lower airways and alveolar region that are physiologically representative with functional immune and barrier characteristics. Furthermore, many co-cultures of the lower airways currently use alveolar epithelial cells that fail to maintain suitable barrier properties and do not represent human physiology. Thus, two cell line-based co-culture models comprising alveolar epithelial type I or type II cells with differentiated monocytes to alveolar like macrophages was established.

To facilitate medium to high-throughput screening and decision making for “go” or “no-go” developments of new drug candidates based upon output readings from AMs, better understanding immunological responses by AMs mimicking healthy state conditions was addressed. Reproducible alveolus co-culture models were assessed for lower airway suitability. For this purpose, the well-established AECII cell line, A549 or newly established AECI cell line, hAELVi, was combined with the recently validated differentiated AM (U937 cell line). Suitability of epithelial function for both AECs and immunological responses of macrophages, when combined in co-culture via continued health state models, was established. In addition, immunological co-culture models should be designed to allow individual cell type assessments following exposure to drug compounds to assist in ease of translational read-across for *in vivo* and *ex vivo* correlations.

The first part of this thesis includes the differentiation and Characterisation of the U937 cell line in the presence of a range of PMA concentrations and incubation times to represent alveolar like macrophages and compare them to *ex vivo* human AMs. Characterisation was examined for cellular morphology by light microscope, cell functionality by flow cytometry (FC), cultured cell heterogony by microarray analysis and cell viability by absorbance.

The second part of this thesis includes validation of hAELVi and A549 cells cultivated at air-liquid interphase (ALI) and liquid-liquid conditions (LLC) concerning its barrier properties determined by measurement of transepithelial electrical resistance (TEER), the set-up and characterisation of the epithelial cell/ macrophage (AECI/ U937 and AECII/ U937) co-culture models with regard to the examination of cellular morphology by light microscopy, cell viability by absorbance measures, cellular interactions and cell functionality by FC for macrophages and barrier properties by TEER for epithelial cells.

The last part of this thesis includes the application of high content image staining and analysis to co-culture models AECI/ U937 and AECII/ U937 at ALI to antiarrhythmic drug amiodarone. The high content image analysis assay was developed as part of the NC3R's (National Centre FOR 3R's) funded CRACK IT inhalation challenge consortium, used to provide a detailed morphological characterisation of human alveolar-like macrophages to known and unknown drug candidates. This assay provides a basis for developing quantifiable and visual methods to predict or understand macrophage vacuolation following inhaled drug exposure. The assay was adapted to assess macrophage health from co-culture models rather than single-cell AM monocultures. In this respect, the impact of amiodarone on macrophage cell health

in co-culture with epithelial cells was determined at ALI. The system was further evaluated regarding cytotoxicity and macrophage functionality.

In summary, the overall aim of this thesis was to successfully standardise differentiation of the U937 cell line to alveolar like macrophages, establish a co-culture model of the human alveolus in the healthy state. This model should serve as a tool to categorise macrophage responses to new drug candidates and chemicals and contribute to the development of new inhaled drug formulations and products to the market.

## Materials and Methods

### 2.1. Materials

#### 2.1.1 Equipment

All fluorescent and luminescent samples were analysed using the Promega Luminometer Glomax (Southampton, UK). Assays using absorbance were read using the Multiskan Ascent plate reader (Loughborough, Leicestershire, UK) and BMG labtech CLARIOstar® (Aylesbury, Buckinghamshire, UK). Fluorescent immunocytochemistry data was collected using the Guava easyCyte™ 8HT Sampling Flow Cytometer (Watford, Herts, UK). Fluorescently stained samples were viewed using the Olympus microscope (Southend-on-Sea, Essex, UK). Images were captured using the GE Healthcare In Cell Analyser 6000 (Little Chalfont, Bucks, UK) or Nikon fluorescent microscope and EVOS FL Cell Imaging System from Thermo Fisher Scientific (Loughborough, Leicestershire UK). Immunoblots were visualised using myECL™ Imager from Thermo Scientific™. The transepithelial electrical resistance (TEER) was measured using an EVOM2 from World Precision Instruments (Stevenage, Hertfordshire, UK).

### 2.1.2 General reagents

Unless otherwise specified, general reagents were obtained from Sigma Aldrich (Poole, Dorset, UK). Water used was ultrapure distilled (dH<sub>2</sub>O) MilliQ® 700 (Watford, Hertfordshire, UK), and all cell culture reagents were purchased sterile or sterilised before use by either autoclaving at 121 °C at 1 bar for 20 min or by filtration through a 0.22 µm Whatman sterile filter. Phosphate buffered saline (PBS) was at pH 7.4 without calcium and magnesium.

### 2.1.3 Cell culture reagents

U937 and A549 cell lines were obtained from the American Type Culture Collection (Teddington, Middlesex, UK). All cell lines were cultured using foetal bovine serum (FBS) non-USA origin from Sigma (Poole, Dorset, UK). hAELVi cells were obtained from InSCREENeX GmbH (Inhoffenstr, Braunschweig, Germany). RPMI-1640 medium, phosphate-buffered saline, penicillin-streptomycin and trypsin-EDTA (ethylenediaminetetraacetic acid) from Sigma. hAELVi medium, basal supplement, coating solution and freezing medium from InSCREENeX GmbH. Culture flasks (75 cm<sup>2</sup>, 25 cm<sup>2</sup>) and polyester Transwells® 0.4 µm (CL 3470) and 3.0 µm (CLS3472) pore size, 6 well (3.48 cm<sup>2</sup>), 24 well (1.12 cm<sup>2</sup>) and 96 well (0.33 cm<sup>2</sup>) were obtained from Corning Costar (Nottingham, Nottinghamshire, UK).

### 2.1.4 Immuno-chemicals

All conjugated mouse anti-human CD (cluster of differentiation) markers and isotype controls were purchased from BD Biosciences (Oxford, Oxfordshire, UK). Details regarding fluorescent antibodies CD11a, CD11b, CD14, CD36, CD206 and isotype control IgG1 κ, IgM κ and IgG2a κ are outlined in Table 2.1.



### **2.1.5 Compounds**

Amiodarone hydrochloride, dimethyl sulfoxide (DMSO), lipopolysaccharides (LPS) and phorbol 12-myristate 13-acetate (PMA) were purchased from Sigma. All compounds used were cell culture grade.

### **2.1.6 Morphology and staining chemicals**

For cell health and morphology assessments, Cell Mask Deep Red, HCS Hoechst 33342, MitoTracker Red and Image-It Dead Green were purchased from Invitrogen (Inchinnan, Renfrewshire, UK). Shandon™ Kwik-Diff™ Stains and DAPI from ThermoFisher Scientific.

**Table 2.1. Properties of immuno-chemicals used in this thesis**

Antigen species	Raised in	Isotype/ secondary	Tag	Antibody, Isotype clone	Catalogue no. *
Human	Mouse	IgG1 κ	FITC	HI111, MOPC-21	555383, 555748
Human	Mouse	IgG1 κ	FITC	CR3, MOPC-21	562793, 555748
Human	Mouse	IgG2a κ	FITC	M5E2, G155-178	555397, 555573
Human	Mouse	IgM κ	PE	B38, G155-228	561821, 555584
Human	Mouse	IgG1 κ	APC	19.2, MOPC-21	555584, 550854
Human	Mouse	IgG1 κ	Alexa Fluor 647	5D3-F7, MOPC-21	557732, 550854

\*Immunochemicals were all purchased from BD Biosciences (Oxford, Oxfordshire, UK)

## **2.2. Methods**

### **2.2.1 Cell culture**

#### **2.2.1.1. General cell culture**

For routine cell culture, all cell types were maintained in a humidified incubator at 37 °C and 5 % v/v CO<sub>2</sub>, and medium supplemented with 1% v/v penicillin-streptomycin (10,000 units/ mL of penicillin, 10,000 µg/mL of streptomycin) antibiotic solution was replaced three times per week unless otherwise stated. Cells were passaged when confluency reached 80- 90 % of the T- 75 culture flask. FBS was heat-inactivated by incubation for 30 minutes at 56 °C in a water bath with mixing to inactivate complement. For adherent cells, cells were rinsed with 10 mL of pre-warmed PBS before incubation with 5 mL 0.25 % v/v trypsin/EDTA solution until a visual detachment of the cells occurred. Trypsin was inactivated by the addition of 7 mL of complete culture medium (CCM). The cell suspension was collected and centrifuged at 250 g for 5 min at room temperature unless otherwise stated. The supernatant was aspirated, and the resulting pellet was resuspended in CCM, and a portion of this was transferred to a new culture flask. Medium was pre-warmed to 37 °C unless stated otherwise.

#### **2.2.1.2. U937 cell culture**

Human, monocytic, U937 cells were obtained at an unknown passage number and further used for 20 subsequent passages. The cells were cultured in RPMI supplemented with 2 mM L-glutamine and 10 % v/v FBS. The suspension cells were passaged when 90% confluent using a 1: 10 split ratio.

Human alveolar epithelial cell lines A549 and hAELVi (hAELVi - human alveolar epithelial lentivirus immortalised) were cultivated onto coated T75 flasks or Polyester Transwell® membranes with a pore size either 0.4 µm, 3.0 µm in 100 µL and growth area of 0.33 cm<sup>2</sup> (Corning: 3470; 3472) to 600 µL basolateral. Cells were seeded at a density of 1 x 10<sup>5</sup> cells/ cm<sup>2</sup> in either RPMI, supplemented with 2 mM L-glutamine, and 10 % v/v FBS for A549 or small airway growth medium (hAELVi medium, basal supplement) containing 5% v/v FBS. Two days post-seeding, the seeded Transwell® filters were divided into two groups, one for culturing under liquid-liquid conditions (LCC) and the other at air-liquid interphase (ALI).

#### **2.2.1.3. U937 cell differentiation**

Cells were seeded at a density of 1.5 x 10<sup>5</sup> cells/ cm<sup>2</sup> on 96, 24 and 6 well plates. Monocytes were induced to differentiate in 5 nM or 100 nM PMA cell culture medium. After the PMA addition, cells were incubated at 37 °C and 5 % v/v CO<sub>2</sub> for up to 96 h, then further incubated with fresh CCM for 24 h (rest period).

#### **2.2.2 Human primary alveolar macrophages**

Human primary macrophages were obtained from the Helmholtz Institute for Pharmaceutical Research, Saarland University (Saarbrücken, Germany). Biopsy tissue from non-tumour lung tissue was obtained from patients undergoing surgery. Cells were isolated according to a protocol modified from Demling *et al.* (Demling *et al.* 2006). After dissection and enzymatic digestion of the lung tissue (Daum *et al.*, 2012), the crude cell suspension was transported on ice and received within 3 days from surgery. Briefly, the crude cell suspension was washed three times in buffer (137 mM NaCl, 5 mM KCl, 0.7 mM Na<sub>2</sub>HPO<sub>4</sub>, 10 mM HEPES, 5.5 mM glucose, pH 7.4) and

filtered with a cell strainer (100  $\mu\text{m}$  pore size; Becton Dickinson, Heidelberg, Germany). Alveolar macrophages from the first filtrate were incubated with RPMI medium containing 5 % FCS and 1 % v/v penicillin-streptomycin on a Petri dish for 2 h to allow the macrophages to adhere. Alveolar macrophages were rinsed with RPMI and incubated in RPMI CCM with fluorosperes (see section 2.2.5.1.2) or fixed with 3.7 % PFA by the Ehrhardt group (Biomedical Science Institute, Trinity College Dublin, Ireland) for further processing. The use of human material was approved by the Saarland State Medical Board (Saarbrücken, Germany).

### **2.2.3 Human alveolar epithelial cell lines**

Human alveolar epithelial cell lines A549 and hAELVi (hAELVi - human alveolar epithelial lentivirus immortalised) were cultivated onto coated T75 flasks or Polyester Transwell® membranes with a pore size either 0.4  $\mu\text{m}$ , 3.0  $\mu\text{m}$  as recommended by the manufacturer's guidelines and growth area of 0.33  $\text{cm}^2$  (Corning: 3470; 3472). Cells were seeded at a density of  $1 \times 10^5$  cells/  $\text{cm}^2$  in either RPMI, supplemented with 2 mM L-glutamine, and 10 % v/v FBS for A549 or small airway growth medium (hAELVi medium, basal supplement) containing 5% v/v FBS. Two days after seeding, the seeded Transwell® filters were divided into two groups, one for culturing under liquid-liquid conditions (LCC) and the other at air-liquid interphase (ALI).

After two days of cultivation, cells were raised to the ALI by the removal of media in the apical compartment. The culture of the medium was then completely aspirated, and the cells were further fed from the basolateral compartment, i.e. 600  $\mu\text{L}$  basolateral only, as described by Kletting (Kletting, 2016). The medium was changed every second day. To characterise and compare cell growth of A549 and hAELVi cells

under both LCC and ALI culture conditions. TEER measurements were performed for up to 20 days. On days 7 and 14, the cells were fixed and stained for immunocytochemistry, or transport studies were conducted.

## **2.2.4 Co-culture cultivation and assembly**

### **2.2.4.1. Cell cultivation**

Human monocytic U937 cells derived from the pleural cavity (passages 2- 20) were seeded (day 0) at  $1.5 \times 10^5$  cells/ cm<sup>2</sup> in a 24 well plate with 100 nM PMA (dissolved in DMSO; <1 % v/v) in complete RPMI medium (10% v/v FBS, 1% v/v pen-strep, 2 mM L-Glutamine). As previously validated, cells were incubated for 72 h at normal cell cultivation conditions to differentiate the cells to mature macrophages. Following PMA incubation (day 3), media was replaced with fresh CCM and incubated for a further 24 h to give the cells a rest period. After the 24 h rest phase (day 4), U937/ MØ were ready for co-culture assembly. U937/ MØ cells were prepared in line with when epithelial cells were ready (i.e. day 7 for A549 and day 12 for hAELVi cells) at ALI on 0.4 µm Transwell® membranes.

### **2.2.4.2. Model assembly**

Inserts were rinsed with RPMI prior to assembly with U937/ MØ. Model was assembled with epithelial cells on the apical Transwell® membrane and U937/ MØ on the basolateral / base of the well. Each model was incubated at normal cell cultivation conditions in RPMI for 24 h before further testing, i.e. toxicity studies.

### **2.2.5 Cell revival**

Cells were removed from liquid nitrogen storage and rapidly thawed to room temperature. Immediately, the cells (approx.  $1 \times 10^6$  cells/ mL) were transferred into a 15 mL conical centrifuge tube containing 10 mL of pre-warmed medium, centrifuged, re-suspended in 2 mL medium and transferred into a culture flask containing CCM. For adherent cells, CCM was replaced the following morning.

### **2.2.6 Cryopreservation**

Cells were removed from the culture flask as previously described for each cell type and centrifuged. The cell pellet was resuspended in a 1.5 mL 'freezing medium' comprising a complete growth medium supplemented with 10 % (v/v) DMSO for U937 and A549 or hAELVi freezing medium hAELVi cells. Approximately  $1.5 \times 10^6$  cells/ mL were transferred to cryogenic storage vials, placed in an isopropanol containing cryo-container (Mr Frosty™) and stored in a -80 °C freezer. After 24 h, vials were relocated to liquid nitrogen for long term storage.

### **2.2.7 Viability assays**

#### **2.2.7.1. Trypan blue cell viability exclusion assay**

For the trypan blue exclusion cell viability assay, a small volume (20-100  $\mu$ L) of cell suspension was added (1:1) to an equal volume of trypan blue 0.4 % w/v. The cell suspension and trypan blue were gently mixed by vortex and 10  $\mu$ L loaded onto a haemocytometer and visually examined under a microscope at low magnification (x 10). Cells were counted in three outer squares when cell count remained within a 10% range per square, and results averaged. The trypan blue-stained cells (non-viable) were excluded from the count.

### **2.2.7.2. Cytotoxicity**

Cytotoxicity was determined using the CytoTox-ONE™ Homogeneous Membrane Integrity Assay kit purchased from Promega (Southampton, UK). The assay was performed according to the manufacturer's instructions. Briefly, 50 µl of cell supernatant was incubated with 50 µl CytoTox-ONE™ reagent in the dark at room temperature for 10 min followed by 25 µl stop solution. Fluorescence (560 nm excitation and 590 nm emission wavelengths) was measured using the fluorimeter (n= 3 replicates within the same experimental system).

### **2.2.7.3. MTS assay**

The CellTiter 96® AQueous One Solution Cell Proliferation Assay (MTS) reagent was purchased from Promega. The assay was performed according to the manufacturer's instructions. Briefly, 100 µl cell suspension was incubated with 20 µl MTS reagent and incubated at 37 °C for 2 h. Absorbance was measured at 492 nm using the absorbance plate reader (n= 3 replicates within the same experimental system).

## **2.2.8 Morphological characterisation**

### **2.2.8.1. Preparation of cytology samples**

U937 cells were seeded at  $5 \times 10^5$  cells/ mL onto 8 well Permanox® Nunc® Lab-Tek® Chamber Slides and differentiated with PMA (5 nM or 100 nM for 24- 96 h) followed by a rest period of 24 h. The supernatant was removed, and the chambers were rinsed with PBS and incubated in cold 3.7 % w/v paraformaldehyde for 15 min, followed by immersion in PBS for up to 7 days. Samples were stored at 4 °C until processed.



### **2.2.8.2. Cytological staining**

PBS was removed, and chambers were extracted from slides using the manufacturer's guidelines. The slides were allowed to air dry at room temperature. Using Shandon™ Kwik-Diff™ stain kit, the samples were submerged five times, for one second each, into stain 1 (eosin), allowing the excess solution to drain after each dip and five times, for one second each, into stain 2 (methylene blue). Slides were rinsed in dH<sub>2</sub>O until the colour ran clear and mounted with glycerol and coverslip for imaging.

### **2.2.8.3. Toxicology study**

U937 cells were seeded at an optimal density of  $5 \times 10^5$  cells/cm<sup>2</sup> in 100 µl of complete cell culture medium onto bottom µclear black 96-well plates (Greiner Bio-One, Stonehouse, Gloucester, UK) or in 600 µl for 24 well plates. Cells were incubated with 100 nM PMA for 72 h followed by a 24 h rest period. Following differentiation, cells were incubated with phospholipid inducing agent- amiodarone hydrochloride (0.03–100 µM) in complete cell culture medium with 1 % v/v DMSO for 48 h alongside internal controls of either untreated cells, 1% v/v DMSO vehicle control, 200 µM carbonyl cyanide4-(trifluoromethoxy) phenylhydrazone (FCCP) mitochondrial activity positive control or 0.5% v/v Triton X-100 (TX-100) cell death control.

## **2.2.9 Immunofluorescent staining**

### **2.2.9.1. Surface marker antigens**

After the 24 h rest period, differentiated cells were detached mechanically using a pipette with 3 mL CCM and transferred to 15 mL centrifuge conical tubes. The cell suspension was centrifuged at 250 g for 5 min. Recovery (> 90 %) of adherent cells from the well plate was verified via light microscopy. The supernatant was aspirated, and cells re-suspended in 1 mL of 10 % v/v human serum (from human male AB plasma, USA origin in PBS) blocking buffer and incubated for 20 min at 37 °C. Cells were rinsed with PBS, centrifuged (250 g for 5 min) and the supernatant aspirated. Samples were incubated in 80 µl of staining buffer (5 % v/v FBS in PBS) (as recommended by the manufacturer) and either 5 µl or 20 µl (per  $1 \times 10^6$  cells) antibody specific for a receptor or with an immunoglobulin (Ig) isotype-matched control for 45 min at 4 °C. Following incubation, 100 µl of blocking buffer was added, cells were pelleted by centrifugation at 180 x g for 5 min at room temperature, and the supernatant was removed and repeated. Cells were fixed with 3.7 % w/v PFA for 15 min at room temperature, then centrifuged. Finally, the cell pellet was re-suspended in 200 µl of PBS and transferred to a 96 well plate for flow cytometry analysis.

For data analysis, each sample population was gated to only include viable cells based on their forward scatter and side scatter contours. A total of 5000 events were collected for each gated sample. Relative median fluorescent intensity (MFI) value is defined as  $[\text{Relative MFI}] = [\text{MFI value of sample}] / [\text{MFI value of isotype}]$ , where the positive signal was determined as being more fluorescent (histogram showing a shift to the right) relative to its isotype control. Raw data was analysed using Millipore Incyte software version 2.2.3.

### 2.2.9.2. Phagocytosis

Macrophages were incubated with 1.0  $\mu$ M carboxylate-modified FluoSpheres™ (ThermoFisher Scientific) for the identification of the phagocytic process *in vitro*. Carboxylate-modified FluoSpheres® beads have a high density of pendent carboxylic acids on their surface, making them suitable for covalent coupling of protein.

Differentiated cells or primary macrophages were incubated with microsphere particles (1 cell: 30 particles) for 2 h in a dark, humidified incubator at 37 °C, 5% v/v CO<sub>2</sub> in fresh CCM. Each sample was diluted with 100  $\mu$ l CCM before centrifugation, and cells were rinsed twice using 200  $\mu$ l PBS followed by incubation in 100  $\mu$ l 3.7 % w/v paraformaldehyde for 15 min. Samples were stored in the dark at 4 °C in 200  $\mu$ l PBS for a max of 7 days before imaging. Cells were imaged using the EVOS FL Cell Imaging System then resuspended by gentle pipetting for flow cytometric analysis. The engulfed fluorescent beads were detected using a fluorescence microscope measuring maxima excitation at 505 nm and emission at 515 nm.

### 2.2.9.3. Viability

Guava® ViaCount® Reagent provided precise and accurate assessments of cell suspensions allowing for quantitative analysis of cell count and viability. The ViaCount Reagent distinguished both viable and non-viable cells based on differential permeabilities of two DNA-binding dyes in the Guava ViaCount Reagent. The nuclear dye stains only nucleated cells, while the viability dye stains dying cells. The proprietary of dyes enabled the Guava ViaCount Assay to distinguish viable, apoptotic, and dead cells. Cell debris was excluded from results based on negative staining with the nuclear dye. Briefly, cells were resuspended with trypsin or by gentle pipetting.

According to the manufacturer's dilution guide, samples were diluted and stained with Guava ViaCount® Reagent in a sample tube or well plate. Accurate cell counting on the Guava system occurred at a concentration range of  $1 \times 10^4$  up to  $5 \times 10^5$  cells/ mL in the stained sample. In a 96 well plate, samples were diluted 1: 10 (cell suspension: ViaCount reagent) to ensure the appropriate concentration range for cell counting accuracy (between 10 and 500 cells/  $\mu$ L). Samples were incubated in the dark at room temperature (19 °C) for 5 min before flow cytometric analysis using the guava Viacount assay.

#### **2.2.9.4. CD marker microarray**

In a 6 well plate, monocytic U937 cells at passage 5 and passage 25 were cultured for differentiation. Cells were differentiated at a density of  $5 \times 10^5$  cells/ mL in 100 nM PMA in complete media for 48 h followed by 24 h in fresh culture medium. After differentiation, the adherent cells were removed via gentle pipetting and pelleted by centrifugation at 250 G at 37 °C for 5 min. The supernatant was aspirated and cells resuspended in fresh culture medium. The cell density was adjusted to  $5 \times 10^6$  cells/ mL in FBS. Halt Protease Inhibitor Cocktail from ThermoFisher Scientific was used to protect the protein from degradation by endogenous proteases released during protein extraction and purification. The protease inhibitor cocktail was added to give a 1x final concentration. Samples were stored in liquid nitrogen and transported in dry ice.

The samples were analysed by microarray technology for expression of CD-markers, a selected set of cytokines and additional relevant proteins by Sciomics, Heidelberg, Germany. There, proteins were extracted with Scio-Extract buffer using the extraction SOPs. BCA assay determined the bulk protein concentration. The samples were

labelled at an adjusted protein concentration of 1 mg/ mL for one hour with Scio-Dye1 and Scio-Dye 2. After one hour, the reaction was stopped by the addition of hydroxylamine. Excess dye was removed 30 min later, and the buffer changed to PBS using Zeba Desalt columns (ThermoFisher Scientific). The arrays were blocked with Scio-Block on a Hybstation 4800 (Tecan, Austria), and the samples were incubated competitively. After incubation for 3 h, the slides were thoroughly washed with PBS detergent, rinsed with 0.1x PBS as well as water, and dried with nitrogen.

During the commercial analysis, slide scanning was conducted on a Powerscanner using identical instrument laser power. Spot segmentation was performed with GenePix Pro 6.0 (Molecular Devices, Union City, CA, USA). The resulting raw data was analysed using the linear models for microarray data (LIMMA) package following calculation of the mean signal intensities. For normalisation, a specialised invariant Lowess method was applied. In the analyses, duplicate spots were accounted for. A one-factorial linear model was fitted with LIMMA to analyse the samples, resulting in a two-sided t-test or F-test based on moderated statistics. All presented p-values were adjusted for multiple testing via the Benjamini and Hochberg procedure.

#### **2.2.9.5. In Cell Analyser**

Differentiated U937 cells were exposed to amiodarone hydrochloride for 24 h. The protocol used is as described by Hoffman and co-workers (Hoffman *et al.*, 2017). Cells were assessed for health and morphology post-exposure by incubating them with a master mix- dye-containing Hoechst 33342 10 µg/ mL, MitoTracker Red 300 nM, Image-It Dead Green 25 nM and fresh CCM for 30 min in a humidified incubator at 37 °C, 5% v/v CO<sub>2</sub>. The master mix dye was carefully aspirated as not to remove

semi adherent cells and washed with 100  $\mu$ L PBS. Cells were centrifuged at 380 g for 5 min and fixed with 3.7 % w/v PFA for 15 min. Fixed cells were stained overnight with Cell Mask Deep Red diluted 1: 1000 in PBS (according to the manufacturer's protocol) in the dark at 4 °C for up to 7 days. Before imaging, cells were washed once with 100  $\mu$ L PBS. Images were acquired using the In-Cell Analyser 6000 imaging system with a 40x objective with an exposure time of 0.1 seconds. Image analysis was performed using In-Cell Developer Toolbox v 1.9.2, Level 3 analysis (GE Healthcare, Little Chalfont, Bucks, UK).

### **2.2.10 Transepithelial electrical resistance (TEER)**

TEER values were recorded to verify cell barrier integrity for the formation of tight junctions. For TEER measurements, chopstick electrodes were connected to an epithelial voltohmmeter EVOM system and sterilised in 70 % v/v IMS before use to measure TEER. Cells cultured at the ALI had 100  $\mu$ L CCM added to the apical compartment, so the final volumes were 100  $\mu$ L apical and 500  $\mu$ L basolateral. Samples were allowed to equilibrate in an incubator for 1 h before conducting TEER measurements. Afterwards, the medium was aspirated, and the cells were cultured at ALI. An average reading from blank Transwell® insert without cells was deducted from the raw TEER value to account for the resistance (R) produced by the membrane and collagen treatment. TEER values were adjusted for area (M) of the Transwell® insert and stated in  $\Omega \cdot \text{cm}^2$  (39  $\Omega$  for 0.33  $\text{cm}^2$ ).

Where  $R_{\text{tissue}}(\Omega) = R_{\text{total}} - R_{\text{blank}}$

TEER values are reported (TEER reported) in units of  $\Omega \cdot \text{cm}^2$  and calculated as:

TEER reported = R tissue ( $\Omega$ )  $\times$  M area ( $\text{cm}^2$ ) (Srinivasan *et al.*, 2015).

### 2.2.11 Transport studies

According to previous protocols, transport experiments were conducted (Salomon *et al.*, 2014; Wirthet *et al.*, 2016) with minor modifications. Prior to starting the experiment, the epithelial cells at days 7 and 14 were washed twice in freshly prepared, pre-warmed Krebs-Ringer Buffer (KRB; 116.4 mM NaCl, 5.4 mM KCl, 15 mM HEPES, 5.55 mM D-Glucose, 0.81 mM  $\text{MgSO}_4$ , 0.78 mM  $\text{NaH}_2\text{PO}_4$  25 mM  $\text{NaHCO}_3$  1.8 mM  $\text{CaCl}_2$ ; pH 7.4) and were further incubated with KRB for 60 min at 37°C. TEER values were recorded before and after the transport study to verify cell layer integrity. To start the transport study, KRB was aspirated, and 150  $\mu\text{L}$  of 50  $\mu\text{M}$  fluorescein sodium (FluNa) in KRB  $\pm$  16 mM EDTA was added to the apical (donor) compartment, and 450  $\mu\text{L}$  KRB was put into the basolateral compartment (acceptor). Samples were directly taken from the donor (20  $\mu\text{L}$ ) at the start and end of the experiment and the acceptor compartment (200  $\mu\text{L}$ ) and subsequently transferred into a 96- well plate. Samples from the basolateral compartment were taken and replaced with 200  $\mu\text{L}$  of fresh transport buffer every 15 min for 90 min. The samples were then measured using BMG labtech CLARIOstar® at 485 nm (em) and 520 nm (ex) wavelengths. Each experiment was run in triplicate.

### 2.2.12 Proteome Profiler Human Cytokine Array

The Proteome Profiler Human Cytokine Array Kit was purchased from R&D Systems (Abingdon, Oxfordshire, UK) and used for proteome profiling of human cytokines. The kit was a membrane-based multiplex immunoassay used to detect multiple cytokines in a single sample. Samples were mixed with a cocktail of biotinylated detection

antibodies and then incubated with the array membranes, which were spotted in duplicate with capture antibodies to specific target proteins (Appendix 1). Captured proteins were visualized using chemiluminescent detection reagents where the signal produced was proportional to the amount of analyte bound.

Briefly, 500  $\mu$ L cell culture supernatants were isolated from the U937/ MØ monoculture and epithelial cell co-culture at ALI and LLC. Particulates were removed by centrifugation at 250 g for 5 min, and samples were stored at  $\leq -20$  °C.

The protocol was executed as described by the manufacturer. Briefly, 2.0 mL of blocking buffer was pipetted into each well of the 4-well multi-dish array. Each membrane was placed in a well of the 4-well multi-dish. The membranes were incubated on a rocking platform at 20 rpm for 1 h at room temperature (19 °C). Cell culture supernatant samples were thawed and added to 500  $\mu$ L of kit supplied blocking buffer and adjusted to a final volume of 1.5 mL with array buffer 5. A 15  $\mu$ L volume of reconstituted Human Cytokine Array Detection Antibody Cocktail was added to each prepared sample and incubated at room temperature (19 °C) for 1 h. Blocking buffer was aspirated from the wells, and the sample/antibody was added and incubated overnight at 2-8 °C on a 20 rpm rocking platform.

After the elapsed time, each membrane was placed into individual plastic containers with 20 mL of 1X Wash Buffer. The 4-Well Multi-dish was rinsed with dH<sub>2</sub>O and air-dried. Each membrane was washed with 1X Wash Buffer for 10 minutes on a rocking platform shaker at 20 rpm and repeated twice for a total of three washes. Streptavidin-HRP was diluted according to the manufacturer's protocol and 2.0 mL pipetted into each well of the 4-Well Multi-dish. The membranes were carefully removed from the



wash containers; excess buffer was allowed to drain from the membrane and returned to the 4-Well Multi-dish containing the Streptavidin-HRP. Samples were incubated for 30 min at room temperature on a rocking platform shaker at 20 rpm.

Membranes were again removed to individual plastic containers with 20 mL of 1X Wash Buffer, and the 4-Well Multi-dish was rinsed with dH<sub>2</sub>O and air-dried thoroughly. Membranes were blotted against a paper towel to remove excess wash buffer and placed on the plastic sheet protector. 1 mL of Chemi Reagent Mix was evenly pipetted onto each membrane. The membrane was covered with a top sheet of plastic sheet protector and incubated for 1 minute. The plastic was removed, and membranes were wrapped in cling film. Membranes were exposed for 17 min and 54 seconds and visualised with the myECL<sup>™</sup> Imager (Thermo Fisher Scientific) in Chemiluminescence mode. Digital images of the films for analysis were saved as TIFF images.

Image J software was employed to analyse the positive signals visible on developed film images. An overlay template of the array was aligned with the pairs of reference spots in three corners of each array. Each film was digitally stamped with an identification number to distinguish between test samples. Pixel densities on developed films were analysed using Image J analysis software. A circular template was placed around each spot on the film. Signal values for mean pixel density were calculated for each spot and exported to a Microsoft Excel spreadsheet file. Each visualised spot was manually identified, labelled with its corresponding cytokine, and the average signal (pixel density) of the pair of duplicate spots representing each cytokine was calculated. Using the background from the negative control spots (averaged), the difference in pixel density was calculated for each cytokine on each of the 8 films to determine the relative change in cytokine levels between samples.

### 2.2.13 General data management and statistical analysis

For data analysis, the relevant data was exported into a Microsoft Excel (version 14, 15 and 16) sheet, the mean  $\pm$  standard deviation (SD) or standard error mean (SEM) was calculated for data obtained from cell viability assays and relative median fluorescent intensity  $\pm$ SD for FC.

Quantitative high content image analysis was performed using In-Cell Developer Toolbox v 1.9.2, Level 3 analysis (GE Healthcare, Little Chalfont, Bucks, UK). For morphometric data analysis, data outputs expanding over 100,000 data points were analysed using macro programming in Microsoft Excel.

Using Incyte software version 2.7, the median data  $\pm$ SD was calculated for flow cytometric analysis. The IBM SPSS software pack version 22 was used for statistical analysis to determine normal distribution (Levene's test) and homogeneity of variance (Shapiro-Wilk test) of data. GraphPad Prism 5 software was used for detailed statistical analysis of parametric and non-parametric tests of one-way ANOVA or two-way ANOVA and Kruskal Wallis, respectively. Where significance was determined for  $p < 0.05$ , multiple comparison post-hoc tests: Tukey, Bonferroni and Dunn's test were applied depending on test group size. All graphs were generated through GraphPad Prism

ImageJ (ImageJ bundled with 64-bit Java 1.8.0\_112) was employed to view exported cell images from InCell Analyser and image overlay of fluorescent cells and analysis for human cytokine array pixel intensities.

## Validation of human monocytic lymphoma cell line-U937 as alveolar like macrophages

### 3.1. Introduction

*In vitro*, alveolar models are in demand to investigate the biological roles of alveolar macrophages (AM)s in human health and disease (Evans *et al.*, 2020; Steimer *et al.*, 2005) and for inhaled drug discovery research (Forbes *et al.*, 2014). To generate translational human *in vivo* data, cell systems must respond similarly to cells *in situ* (Steimer *et al.*, 2005). Cell culture lung models are available, but few represent alveolar physiology, and response and, additionally, most exclude macrophages (BéruBé *et al.*, 2009; Miller *et al.*, 2017).

3D alveolar model constructed from established human cell lines avoids multiple problems, including changes in phenotype, finite life span, available cell numbers and high cost, commonly encountered during work with primary blood cells. Conversely, the validity of a single myeloid-macrophage model system has yet to be fully characterised. For over 35 years, myeloid cell lines: HL-60, THP-1 and U937 have been widely used as models for investigating monocyte-macrophage differentiation and biological mechanisms of differentiated cells (Gallagher *et al.*, 1979; Sundström *et al.*, 1976; Tsuchiya *et al.*, 1982).

Cellular differentiation of the monocytes requires a stimulus (i.e. DMSO, IFN- $\gamma$ , retinoic acid, PMA, vitamin D3, granulocyte-macrophage colony-stimulating factors (GM-CSF), either alone or in combination to induce maturational changes into macrophages (Harris *et al.*, 1985). The myeloid cell lines differ morphologically and biochemically in standard culture conditions and the following differentiation via a stimulant. Phenotypically, HL-60 cells are progenitors of granulocytes, whereas THP-1 and U937 are progenitors of pro-monocytes and monocytes, respectively. HL-60 and THP-1 blood leukemic cells are less mature than U937 cells, which originate from a pleural effusion of histiocytic lymphoma and are arrested in a more advanced phase of differentiation (Chanput *et al.*, 2015; Harris *et al.*, 1985).

Upon differentiation with GM-CSF, retinoic acid or DMSO, HL-60 cells fail to develop secondary granules and have been reported to transform along the eosinophil line (Metcalf, 1983; Newburger *et al.*, 1979; Padilla *et al.*, 2000). U937 cells exposed to PMA are reported to increase in size, acquire a lobulated nucleus, and replace cytoplasmic granules by vacuoles mimicking a more mature monocyte or immature macrophage (R Hass *et al.*, 1989; Minta *et al.*, 1985). Published reports state a similar differentiation outcome when THP-1 cells are exposed to PMA (Daigneault *et al.*, 2010). Both U937 and THP-1 cells can then be further transformed to classically activated M1 and alternatively activated M2 macrophages in the presence of lipopolysaccharide (LPS) and interleukin-4 (IL-4), respectively (Genin *et al.*, 2015; Taniguchi *et al.*, 2015).

A prospective cell line used for alveolar macrophage responses to stimuli is U937. The human hematopoietic cell line U937 was derived from the pleural effusion of a 37-year-old man with histiocytic lymphoma (Sundström *et al.*, 1976). U937 cells have morphological and functional characteristics in line with those found in macrophages after chemical differentiation (Hass *et al.*, 1989; Sundström *et al.*, 1976). U937 are commonly reported to differentiate to alveolar-like macrophages in the presence of PMA or vitamin D treatment (Harris *et al.*, 1985). U937 cells and their differentiated phenotype can be found throughout the literature and are used for measuring AM cytotoxic responses to environmental and pathological stimuli (Vogel *et al.*, 2012), understanding biochemical pathways and mechanisms such as cell cycle, phagocytosis and inflammation (Ruijters *et al.*, 2014). The suitability of using differentiated U937 cells to determine macrophage responses are supported within the literature (Braydich-Stolle *et al.*, 2010; Larrick *et al.*, 1980).

However, the methodology available to differentiate and validate these cell lines is largely variable, especially for U937 cells, whereby methodology for differentiation ranges significantly in cell densities, the concentrations of various stimuli, incubation and resting times (Table 3.1). Cell densities range from  $2 \times 10^5$  to  $2 \times 10^6$  cells/mL, PMA concentrations between 1 nM to 162 nM, incubation times range between 8 h to 96 h and resting periods whereby the PMA is removed from the cells and replenished with fresh culture medium ranges from 0 h to 72 h.

To advance AM response biology, protocol standardisation is required to facilitate comparable data exchange. Furthermore, validation of differentiated U937 cells and their phenotype differ due to multiple differentiation procedures and a lack of standardised terminology of morphological and phenotypical characteristics among

other macrophage cell lines (Harris *et al.*, 1985). As a result of there not being a standardised protocol for monocyte-derived macrophages phenotype and functional data from the literature cannot be directly compared. Thus, suggesting a possible need to characterise individual cell lines to their specificity profiles. The availability of a standardised human alveolar-like macrophage cell line would provide a reproducible source for exploration of the process of the biochemistry and biology of an immune response to pharmaceutical or pathogenic stimuli and in the generation of an alveolar *in vitro* system.

To better understand the responses of an AM-like model to external stimuli, characteristics of the U937 cells in their differentiated state also need to be well understood. We hypothesise that ranges in the PMA differentiation protocol of U937 cells may give rise to a variety of macrophage progeny. Additionally, there is a need to identify the most suitable differentiation protocol to generate alveolar-like macrophages which are phenotypically and functionally closer to native humans.

Table 3.1 Current PMA differentiation protocols for U937 cells

Cell density/mL	Concentration	Incubation	Rest period	Surface marker expression	Compared to control	Reference
3x10 <sup>5</sup> cells/mL	160nM	72h	0h	CD 11a/b/c, 29, 54, 56, 59, 36, 44, 61, 41b	Y	(Prieto <i>et al.</i> , 1994)
1x10 <sup>6</sup> cells/mL	40nM	48h	0h	CD 36	Y	(Alessio <i>et al.</i> , 1996)
5x10 <sup>5</sup> cells/mL	81nM	48h	0h	n/a	N	(Ruijters <i>et al.</i> , 2014)
2x10 <sup>4</sup> cells/well	5nM	72h	72h repeated*	CD 11a/b, 14, 18	Y	(Ralf Hass <i>et al.</i> , 1991)
n/a	16nM	72h	72h	CD 14, 206	Y	(Minafra <i>et al.</i> , 2011)
5x10 <sup>5</sup> cells/mL	1-10nM	48h	0h	CD 14,13, 4, 71	Y	(Hewison <i>et al.</i> , 1992)
4x10 <sup>4</sup> - 7.5x10 <sup>5</sup> cells/mL	162nM	24, 48h	0h	n/a	Y	(Minta <i>et al.</i> , 1985)
2x10 <sup>5</sup> cells/mL	20nM <sup>+</sup>	0-24h	0h	CD 11b, 36	Y	(T. Yamamoto <i>et al.</i> , 2009)
4x10 <sup>5</sup> cells/mL	32nM	48-72h	0h	CD 11a/b/c, 15, 33, 14	Y	(García <i>et al.</i> , 1999)
5x10 <sup>5</sup> cells/mL	150nM	96h	0h	n/a	N	(Ralph <i>et al.</i> , 1982; Stoppelli <i>et al.</i> , 1985)
1x10 <sup>6</sup> cells/mL	4nM	96h (48h+48h)	24h	CD 11b	Y	(Shepherd <i>et al.</i> , 2004)
n/a	16nM	12h	72h <sup>**</sup>	CD 14	Y	(Verhoeckx <i>et al.</i> , 2004)
1x10 <sup>6</sup> cells/mL	160nM <sup>++</sup>	48h	48h	CD 11b	Y	(Sintiprungrat <i>et al.</i> , 2010)

**Table 3.1 (continued) Current PMA differentiation protocols for U937 cells**

Cell density/mL	Concentration	Incubation	Rest period	Surface marker expression	Compared to control	Reference
5x10 <sup>5</sup> cells/ mL	16nM	24h	0h	n/a	n/a	(Sordet <i>et al.</i> , 1999)
5x10 <sup>5</sup> cells/ mL	20nM	12-72h	0h	CD 11a/b, 14	Y	(Sordet <i>et al.</i> , 2002)
4x10 <sup>5</sup> cells/ mL	32nM	8h	36-46h <sup>***</sup>	n/a	N	(Sajjadi <i>et al.</i> , 1996)
5x10 <sup>5</sup> cells/ mL	16nM	72h	24h	n/a	Y	(Tenney <i>et al.</i> , 1987)
2x10 <sup>5</sup> to 10 <sup>6</sup> cells/ mL	81nM	48h	Not disclosed <sup>****</sup>	n/a	N	(Vogel <i>et al.</i> , 2012)
5x10 <sup>5</sup> cells/ mL	16nM	12, 24, 48, 72h	0h	n/a	Y	(Twomey <i>et al.</i> , 1993)
n/a	100nM	48h	0h	CD 14	N	(Kuroda <i>et al.</i> , 1997)
1x10 <sup>6</sup> cells/ mL	1.6nM <sup>+++</sup>	72h	0h	n/a	Y	(Fukunaga <i>et al.</i> , 2001)
1x10 <sup>6</sup> cells/ mL	100nM	72h	0h	n/a	N	(Matheson <i>et al.</i> , 2002)

\*fresh complete culture medium every 72 h up to 2- 3 weeks, \*\*fresh complete culture medium every 24 h up to 72 h, \*\*\*included 3 h incubation with LPS, \*\*\*\*did not disclose the length of time for a rest period. Concentrations were corrected to nM, +Concentration range: +0-200 nM, ++80-162 nM for 24 and 48 h, +++0.16 nM- 24.3 nM. Rest period: the amount of time cells were incubated in fresh culture medium following treatment. Compared to control: Differentiated U937 cells were either compared (Y- yes) or not compared (N-no) to their untreated phenotype.



### **3.2. Aims**

This chapter focuses on identifying an optimal differentiation protocol for the human lymphoma cell line (U937) to mimic an alveolar macrophage-like phenotype.

Specifically, the objectives were to:

- Identify human monocyte to alveolar-like macrophage PMA differentiation protocols within the literature
- Assess the influence of differentiation protocol (PMA concentration and exposure time) on:
  - Cell health and proliferation
  - Cell morphology
  - Cell phenotype
  - Cell functionality
- Evaluate the optimal differentiation protocol to generate cells with the closest characteristics to alveolar macrophages

### **3.3. Results**

#### **3.3.1 Biomarker Identification of PMA treated U937 cells**

The Scio-CD antibody microarray targeted 81 CD -markers as well as additional relevant cytokines, chemokines and other proteins (Table **3.2** in Appendix I) and compared their expressions for treated cells (PMA treated) and untreated controls at a passage 5 (low) and passage 25 (high). The comparison results were summarised in the respective volcano plots (Figure 3.1 A and Figure 3.1 B). All significant ( $p<0.05$ ) differential proteins were identified.

##### **3.3.1.1. Biomarker comparison of low and passage 25 for untreated and PMA treated U937 cells**

For the cell passages 5 and 25, both the untreated U937 cells were compared at a low and passage 25, PMA treated U937 cells were compared at a low and passage 25 (Figure 3.1). Only two protein markers were identified to be differentially expressed where  $p<0.05$  in the untreated U937 cells at passage 25, compared to its passage 5. These markers were CD 41 and Etoxin-1. In comparing passage 5 versus passage 25 in the treated U937 cells, multiple protein markers were identified to be significantly expressed in passage 25: CD 6, CD 17, CD 45RA, and TSLPrec.

### **3.3.1.2. Biomarker comparison of PMA treated cells versus control cells**

Surface markers for treated PMA and untreated cells were identified in both groups. At passage 5, untreated U937 cells expressed biomarkers; CD 58 and CD 20 (Figure 3.1 A). Similarly, for passage 25 untreated U937 cells, only CD 4 was significantly expressed (Figure 3.1 B). Thus, there was minimal surface marker expression in U937 cells.

U937 cells were found to significantly express multiple markers following treatment with PMA. At passage 5 treated U937 cells expressed biomarkers; CD 11a, CD 23, CD 25, CD 29, CD 33, CD 36, CD 45RA, CD 45RA, CD 54, CD 58, CD 8, FDC (Follicular dendritic cell), IL-15, TSLPrec (thymic stromal lymphopoietin protein receptor) (Figure 3.1 A). At passage 25, treated U937 cells expressed biomarkers; CD 8, CD 11a, CD 17, CD 23, CD 29, CD 33, CD 36, CD 45RA, CD 45RA, CD 45RB, CD 54, CD 54, CD 58, CD 62L, CD 147, Etoxin-1, IL-6, IL-7, IL-18, FDC, HLA I, TSLPrec (Figure 3.1 B).

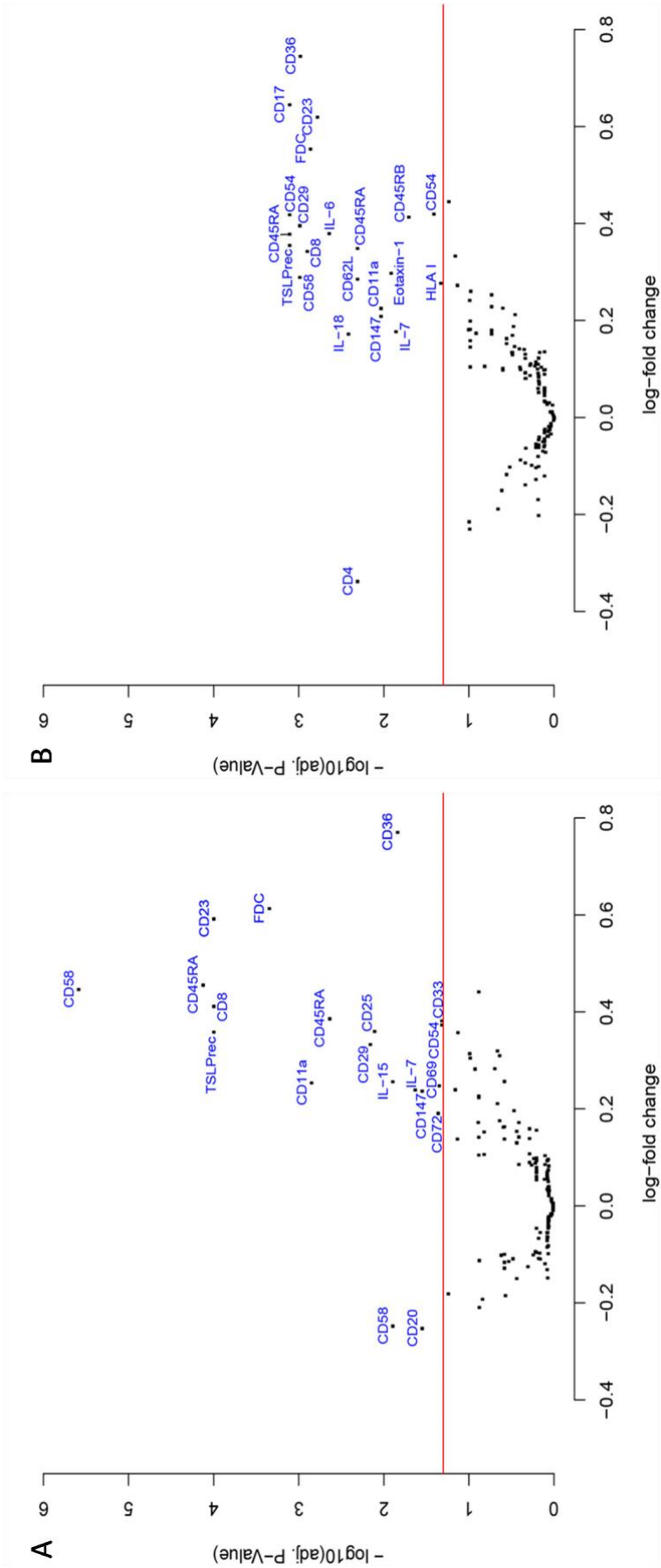


**Figure 3.1 Biomarkers identified in PMA treated U937 cells at passage 5 number (A) or a passage 25 (B).**

The Volcano plots identifying expression differences in PMA treated U937 cells at a passage 5 compared to untreated U937 cells at the same passage number was plotted on the x-axis, and false discovery rate adjusted significance was plotted on the y-axis ( $-\log_{10}$  scale). Sample size was  $n=3$  and pooled together for this experiment. Significance where  $p < 0.05$  is indicated as a red horizontal line. The positive value indicated a higher abundance of proteins in treated cells. Biomarkers identified in untreated cells were shown to the left of 0.0 log fold change on the x-axis and those biomarkers expressed due to PMA stimulation are shown to the right of 0.0 log fold change for passage 5 and passage 25.

### **3.3.2 CD Marker expression profile**

Five CD markers were selected from the CD microarray and current literature: CD 11a, CD 11b, CD 14, CD 36, and CD 206. Expressions of these markers were measured and quantitatively analysed using flow cytometry for PMA treated U937 cells and primary human alveolar macrophages.

#### **3.3.2.1. Effects of DMSO on U937 cells**

The effects of DMSO on U937 cells were determined by measuring changes in CD marker expression using flow cytometry as PMA was initially reconstituted in DMSO. The U937 cells were incubated in a 1: 5000 dilution of DMSO in CCM, the equivalent of that present in 100 nM PMA for 48 h followed by a 24 h rest period in fresh culture medium. For all markers: CD 11a, CD 11b, CD 14, CD 36 and CD 206, no expression differences were detected in the DMSO treated U937 cells when compared to untreated U937 cells, and CD marker expression was lower than the PMA treated U937 cells (Figure 3.2). Therefore, at 0.001%, DMSO did not affect the CD marker expressions on U937 cells

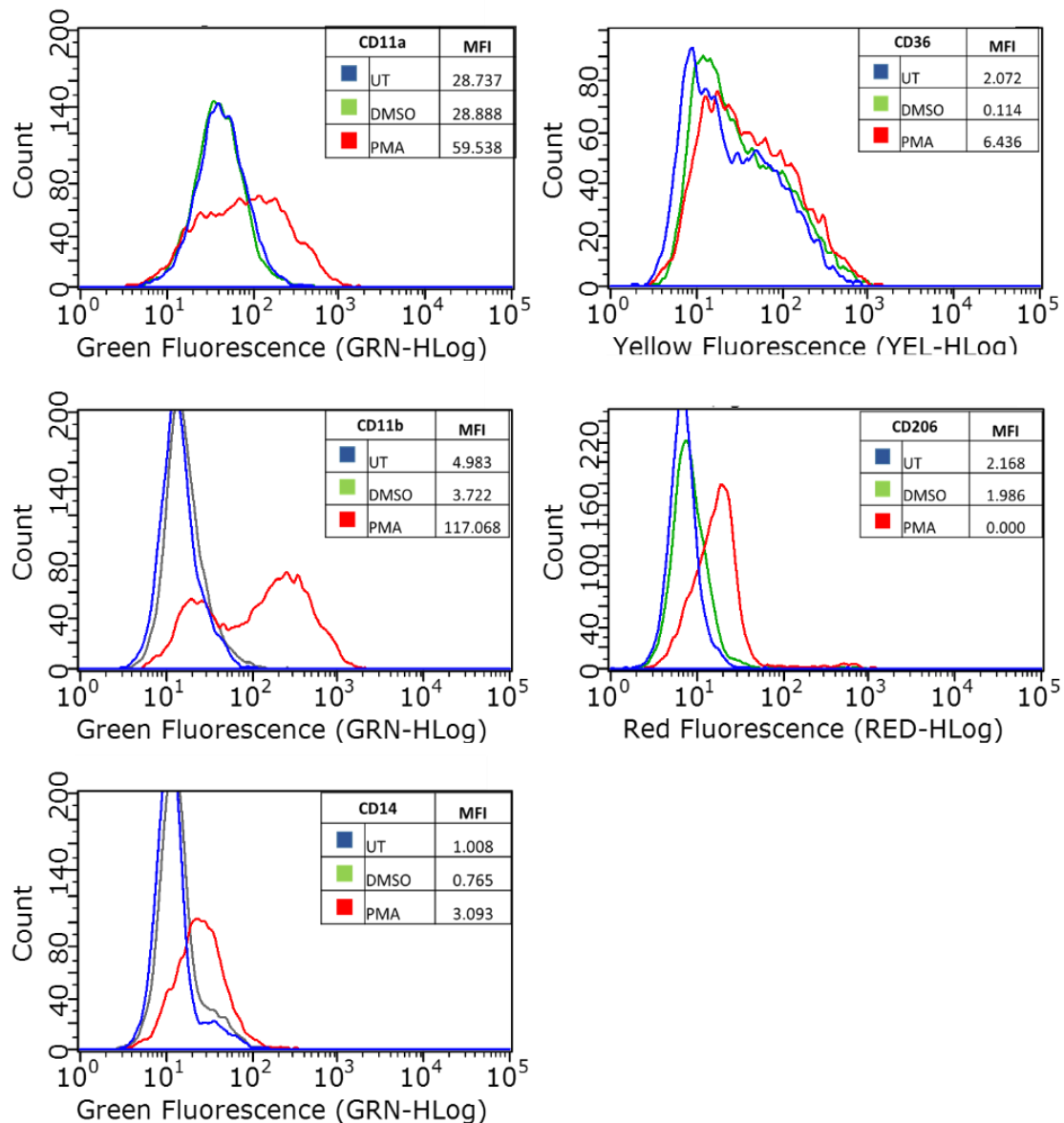


**Figure 3.2 Effects of DMSO on U937 cells and PMA treated U937 cells for surface markers.**

U937 cells were exposed to 0.001 % (v/v) DMSO, 100 nM PMA or untreated (UT) for 48 h followed by a 24 h rest period, where  $n=5$ . The effects of DMSO on U937 cells were measured by comparing its median fluorescent intensity (MFI) to each treatment group: UT and PMA. No CD marker expression changes were detected between the UT and DMSO groups. MFI for DMSO treated cells were lower than PMA treated cells for all CD markers.

### 3.3.2.2. Differentiated U937-PMA CD marker profile

U937 cells were exposed to either 0 nM (control), 5 nM and 100 nM PMA for 24 h, 48 h, 72 h and 96 h in standard culture conditions followed by a 24 h rest period in fresh culture medium. CD marker expression following treatment with PMA was measured by flow cytometry, Figure 3.3. CD 11a **(A)** expression in untreated U937 cells increased over time. No significant difference ( $p<0.05$ ) in the expression of CD 11a was observed between control and 5 nM. Treatment of 100 nM PMA significantly increased CD 11a expression compared to untreated cells, but the expression significantly decreased upon the increase of incubation time with PMA. No significant difference ( $p<0.05$ ) in the expression of CD 11b **(B)** was observed at different time points. However, the treatment of 100 nM PMA was found to significantly ( $p<0.05$ ) enhance CD 11b MFI compared to untreated cells. The presence of CD 14 **(C)** (Figure 3.3) was low for all 0 nM, 5 nM, and 100 nM PMA treatment groups and treatment of 100 nM PMA significantly ( $p<0.05$ ) increased CD 14 MFI compared to untreated cells. For CD 36 **(D)**, no significant difference ( $p<0.05$ ) was detected for samples with different incubation time points or PMA concentrations. Marker, CD 206 **(E)** was poorly expressed in the control and both treatment groups and showed no significant ( $p<0.05$ ) differences between time points of the groups.

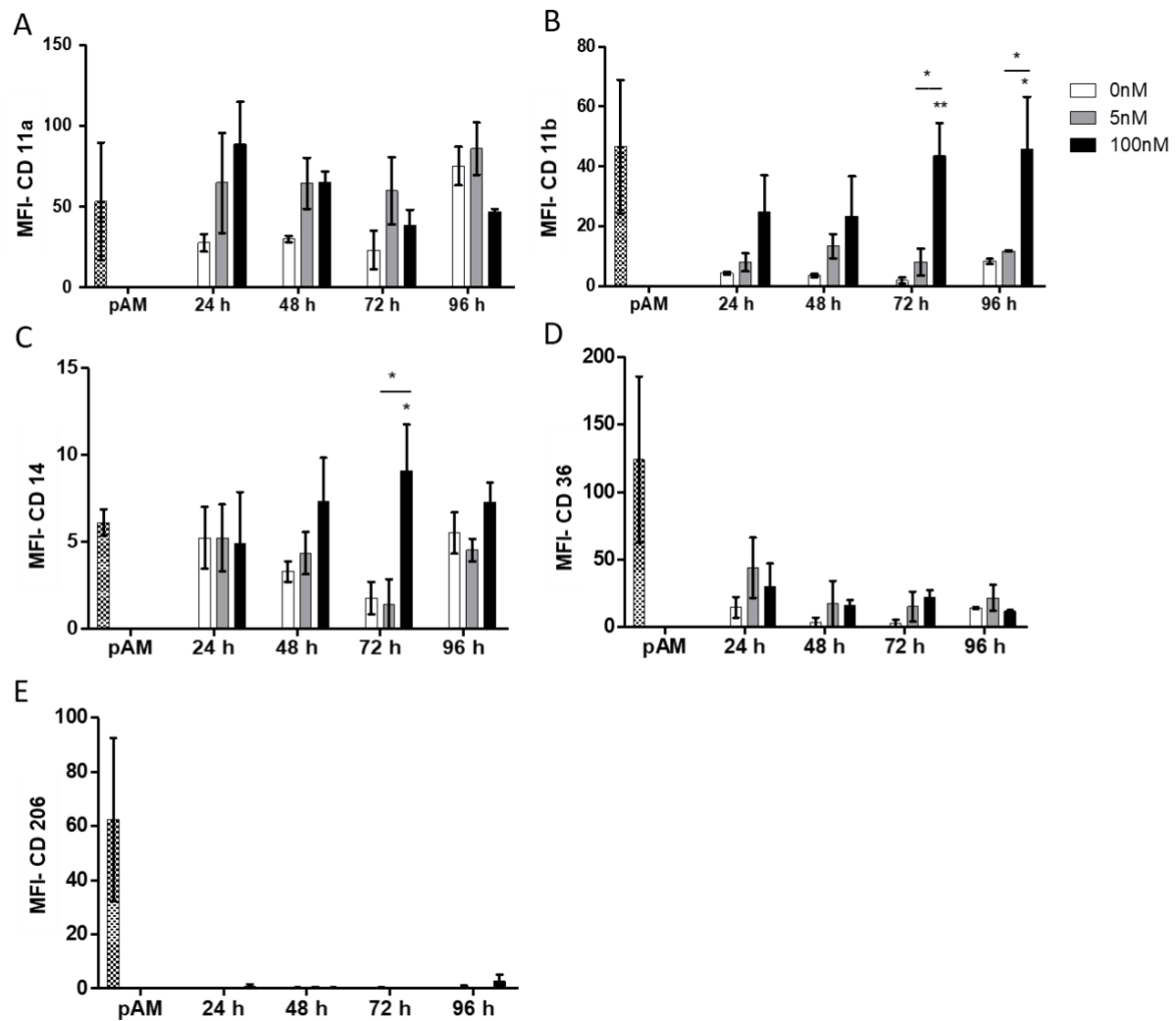


**Figure 3.3 Expression profile comparison of selected CD markers in PMA treated U937 cells and primary alveolar macrophages.**

CD markers are: (A) CD 11a, (B) CD 11b, (C) CD 14, (D) CD 36 and (E) CD 206. U937 cells were treated with (0 nM, 5 nM, and 100 nM) PMA for 24 h to 96 h followed by a 24 h rest period in fresh culture medium. Expression of CD markers was measured by flow cytometry and are presented as median fluorescent intensity (MFI  $\pm$  SEM). A two way ANOVA was used to determine significance for each treatment group, and Bonferroni post hoc test was employed when \*:  $p < 0.05$ , \*\*:  $p < 0.01$  where  $n = 12$  of four cell passages for U937 cells. Human primary AMs (pAM) were cultured, where  $n = 3$  patients.



PMA concentration and PMA incubation time did not significantly ( $p<0.05$ ) alter the expression of CD 11a (Figure 3.3 A). Cell expression of CD 11a was within the range expressed in pAMs ( $0.67 \pm 126.68$ ).

There was a significant increase ( $p<0.05$ ) in the expression of CD11b (Figure 3.3 B) when cells were exposed to all concentrations of PMA for all incubation times assessed. Exposure to 100nM PMA for above 72 hours resulted in a 4-fold higher expression of CD11b in comparison with cells exposed to 5 nM, in line with primary alveolar macrophage expression of CD11b ( $6.92 \pm 76.18$ )

A significant increase ( $p<0.05$ ) in the expression of CD 14 was determined when cells were exposed to 100 nM PMA for 72 h ( $8.96 \pm 4.64$ ) compared to untreated cells ( $2.086 \pm 1.6346$ ) (Figure 3.3 C) and were not significant. Independently, concentration had a significant effect on CD 14 expression. ( $p<0.05$ ) Expression of CD 14 in the were in line with pAMs ( $6.1644 \pm 1.52106$ ).

No significant ( $p<0.05$ ) differences were determined for CD 36 on cells in the presence of PMA (Figure 3.3 D). Expression of CD 36 was 3-fold higher in pAMs than in PMA treated cells. Exposure conditions of PMA incubation time or concentration did not alter CD 36 in cells.

CD 206 was not expressed in U937 cells. There were no significant differences ( $p<0.05$ ) in the expression of CD 206 (Figure 3.3 E) between exposure groups. Marker CD 206 was expressed in pAMs.

### **3.3.3 Phagocytic activity of PMA treated U937 cells**

The phagocytic ability of U937 cells, PMA-differentiated U937 cells, and pAMs were examined and compared (Figure 3.4, Figure 3.5). Monocytic U937 cells were naturally phagocytic without PMA stimulation suggesting the cells already possess macrophage-like characteristics. It was evident that culture conditions affected the functional profile of the cells. Culture conditions in this experiment included the length of time for cells in culture and to PMA stimulus. Variability in the phagocytic activity regarding length in culture was evident for PMA naive cells and similarly for PMA treated cells with maximum phagocytic functioning at 48 h and 72 h post-seeding or PMA stimulation.

Stimulation of U937 cells with PMA significantly increased cells ability to phagocytose 1  $\mu$ M beads compared to PMA naive cells.

Both PMA concentration and incubation time were shown to have a significant ( $p<0.05$ ) effect on the phagocytic function of cells. Additionally, 80% of the cells treated with 100 nM at 48 and 72 h had phagocytic activity in accordance with primary AMs. Cells incubated with 100 nM PMA concentration for 48 h, 72 h, and 96 h had significantly higher ( $p<0.05$ ) phagocytic activity than untreated and 5 nM PMA concentrations. Thus, 100 nM PMA achieved a significantly higher phagocytic proportion of the cell population in line with human primaries.

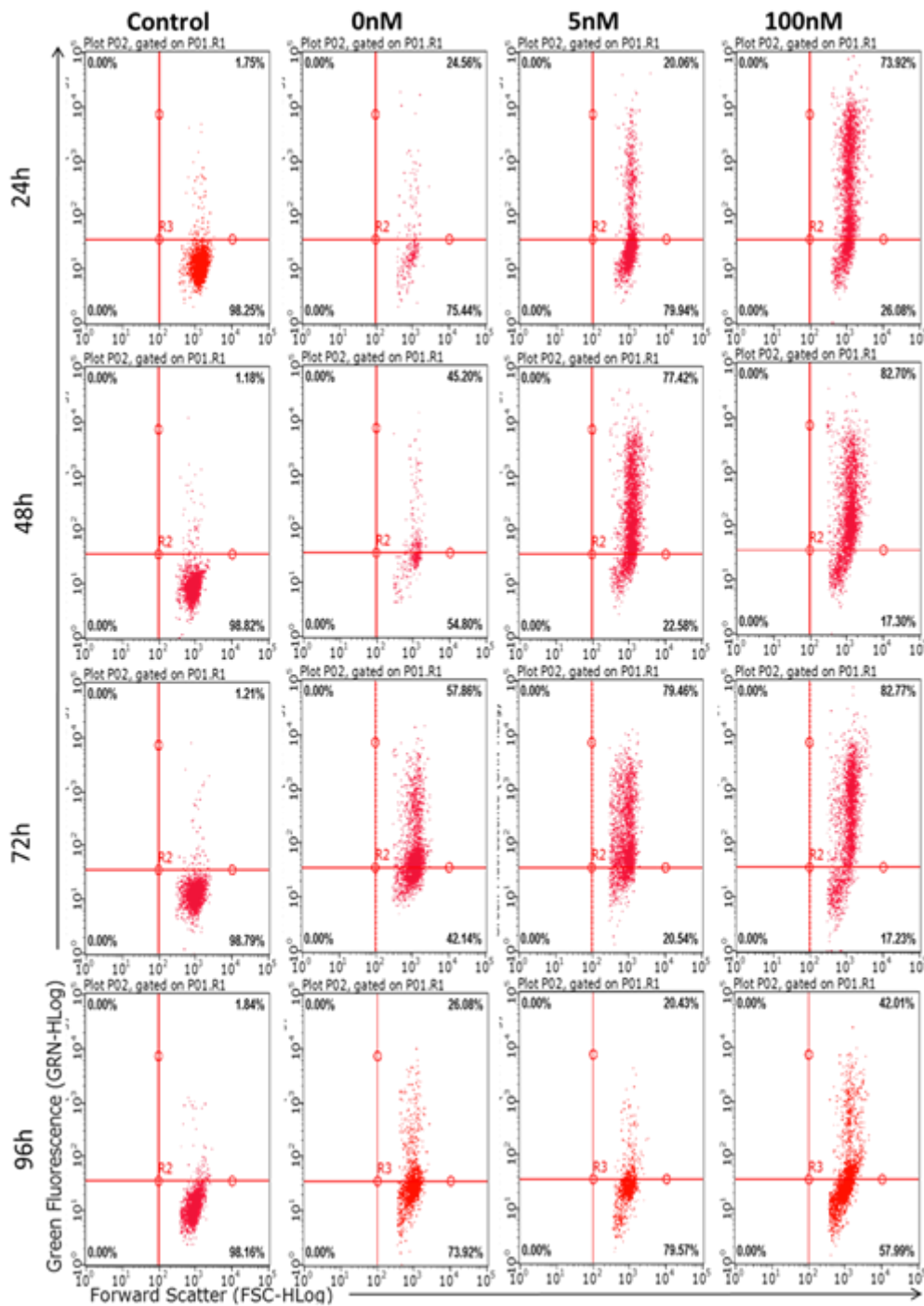


**Figure 3.4 Determining the phagocytic ability of U937 cells following incubation with PMA.**

PMA induced cells were incubated with FITC tagged beads for 2 h and read on flow cytometer excited by 488 nm laser. The gated population was analysed for fluorescence on the Y-axis and forward scatter on the x-axis. Control shows a no bead sample, n= 1 on each graph.

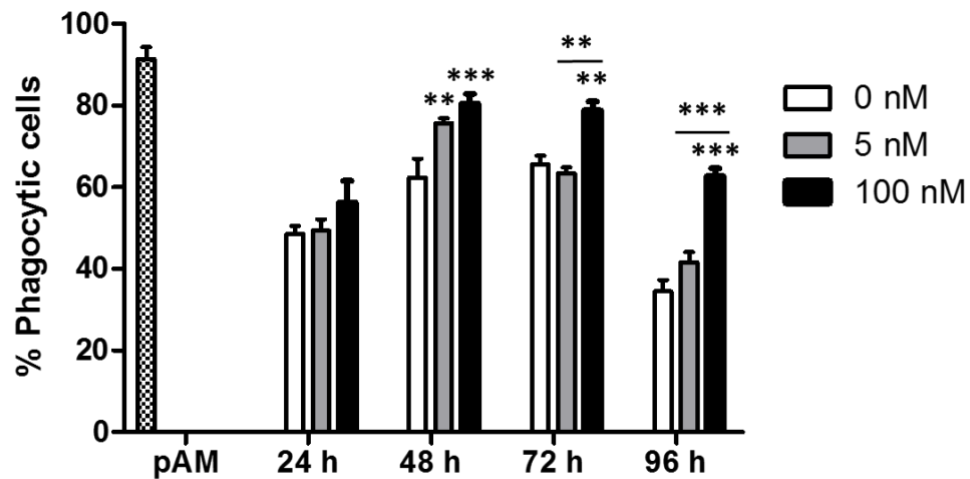


**Figure 3.5 Comparison of Phagocytic activity of PMA treated U937 cells.**

Percentage of phagocytic cells (mean  $\pm$  SEM) from PMA treated U937 cells. Cells were cultured with 5 nM or 100 nM PMA for 24 h -96 h and incubated with fluorescent 1  $\mu$ M beads. The phagocytic population was determined by flow cytometry. Data are shown for treatment groups  $n=9$  for each time point for PMA and  $n= 3$  for primary alveolar macrophage cells,  $p<0.01^{**}$  and  $p<0.001^{***}$ .

### **3.3.4 Morphology of differentiated U937 cells and primary AMs**

Monocytes, U937 cells were seeded onto 6 well chamber slides and incubated with PMA for 24 h, 48 h, 72 h or 96 h. Cells were stained with Eosin, a common dye specific for the cytoplasm and methylene blue, specific for the cell nuclei. Phenotypic plasticity of cells was evident following PMA stimulation, and cells were irregular in shape (Figure 3.6). PMA naive cells were small, round cells with densely stained nuclei irregularly shaped nuclei with a high nucleus/ cytoplasmic ratio with minimal adherence. PMA induced cells displayed some morphological characteristics of alveolar macrophages, such as larger cell area: reduced nuclei/ cytoplasmic ratio compared to PMA naive cells and rounded nuclear uniformity among cells. Some PMA induced cells had a highly vacuolated cytoplasm (foamy cells) as well as extensive pseudopodia (Figure 3.6).

The 5 nM PMA treatment group displayed increased adherence and cell clustering at 48 h (Figure 3.6). Longer incubation of cells in 5 nM PMA at 72 h and 96 h resulted in a further loss of adherence and reduction in morphological macrophage similarities (Figure 3.6). The 100 nM treatment group displayed multiple morphological changes over incubation time of increased adherence after 24 h and cell clustering at 48 h, which reduced after 72 h.

Vacuolation was evident in the treated 100 nM cells (Figure 3.6). Vacuoles were seen to increase in size over incubation time. After 96 h, cell structures became irregular, and approximately half of the cell population was reduced in size.

Healthy pAMs adhered to the chamber slides following 2 h incubation in complete culture media. Differences were observed in cellular morphology; cells lacked uniformity in that some were large and rounded, whereas others were slightly

elongated. Pseudopodia was evident in all samples, with some vacuoles present (Figure 3.6).

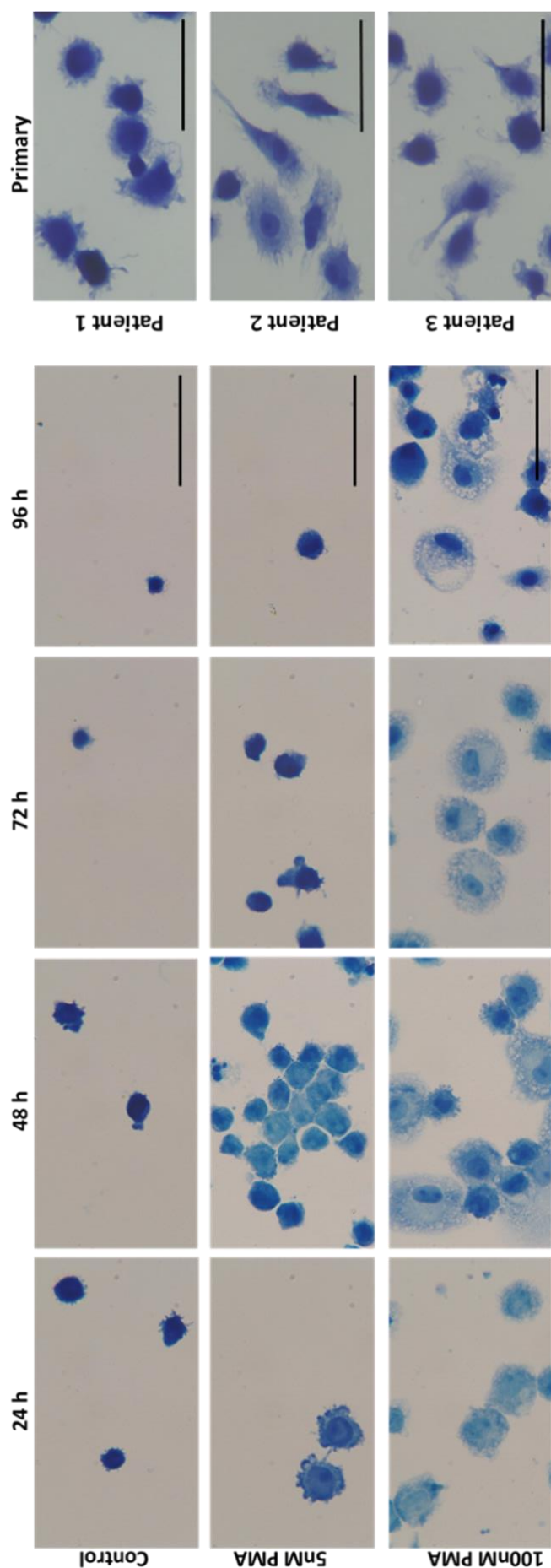


**Figure 3.6 Morphology of U937 cells with exposure to PMA.**

U937 cells were cultured on chamber slides with medium supplemented with either 0 nM, 5 nM or 100 nM PMA and incubated for 24 h, 48 h, 72 h and 96 h followed by a 24 h recovery phase in fresh medium. Non-adherent PMA naive cells required centrifuge preparation. Comparisons were made to surgically excised, primary human alveolar macrophages. The cells were photographed at x400 magnification with an inverted light microscope. 50  $\mu$ m scale bar.

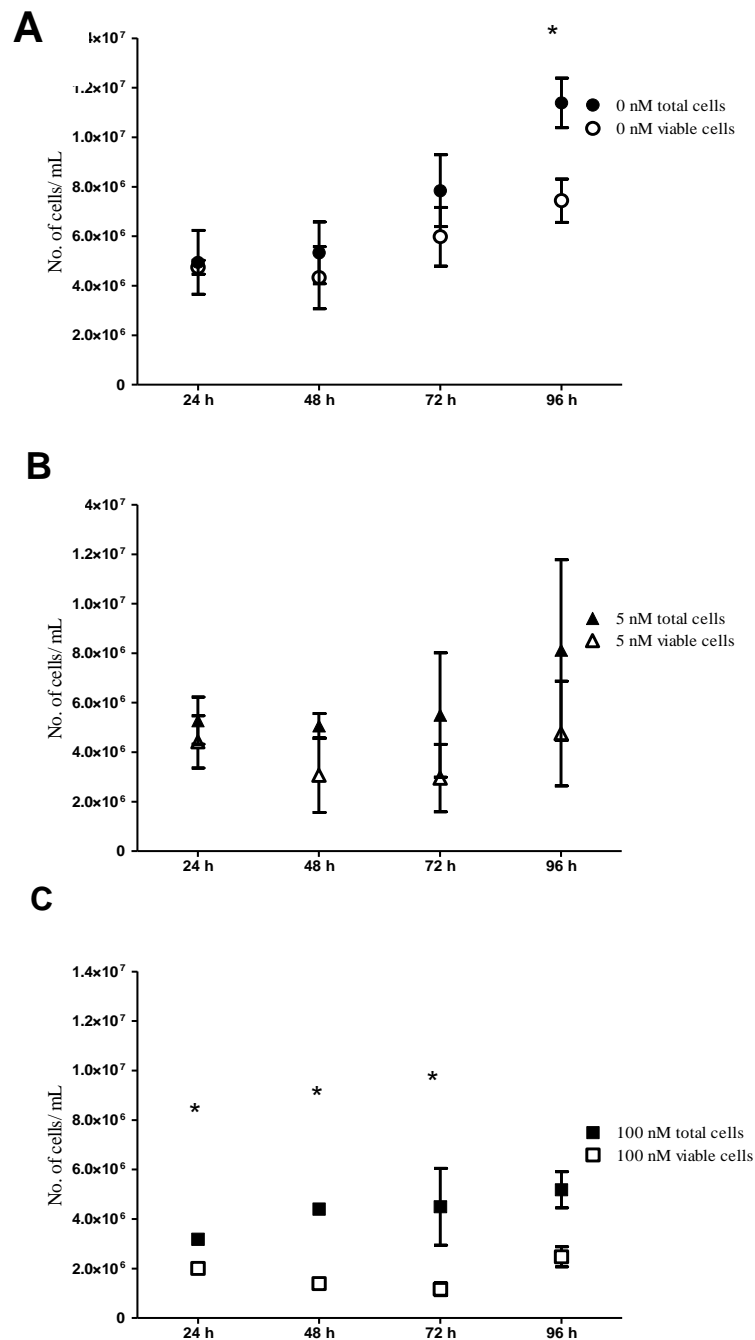
### **3.3.5 Cell Health**

The health of U937 cells following PMA treatment at 24 h, 48 h, 72 h and 96 h with a 24 h rest period in fresh culture medium was assessed by measuring: cell viability, mitochondrial activity, and cytotoxicity.

#### **3.3.5.1. Cell viability and proliferation**

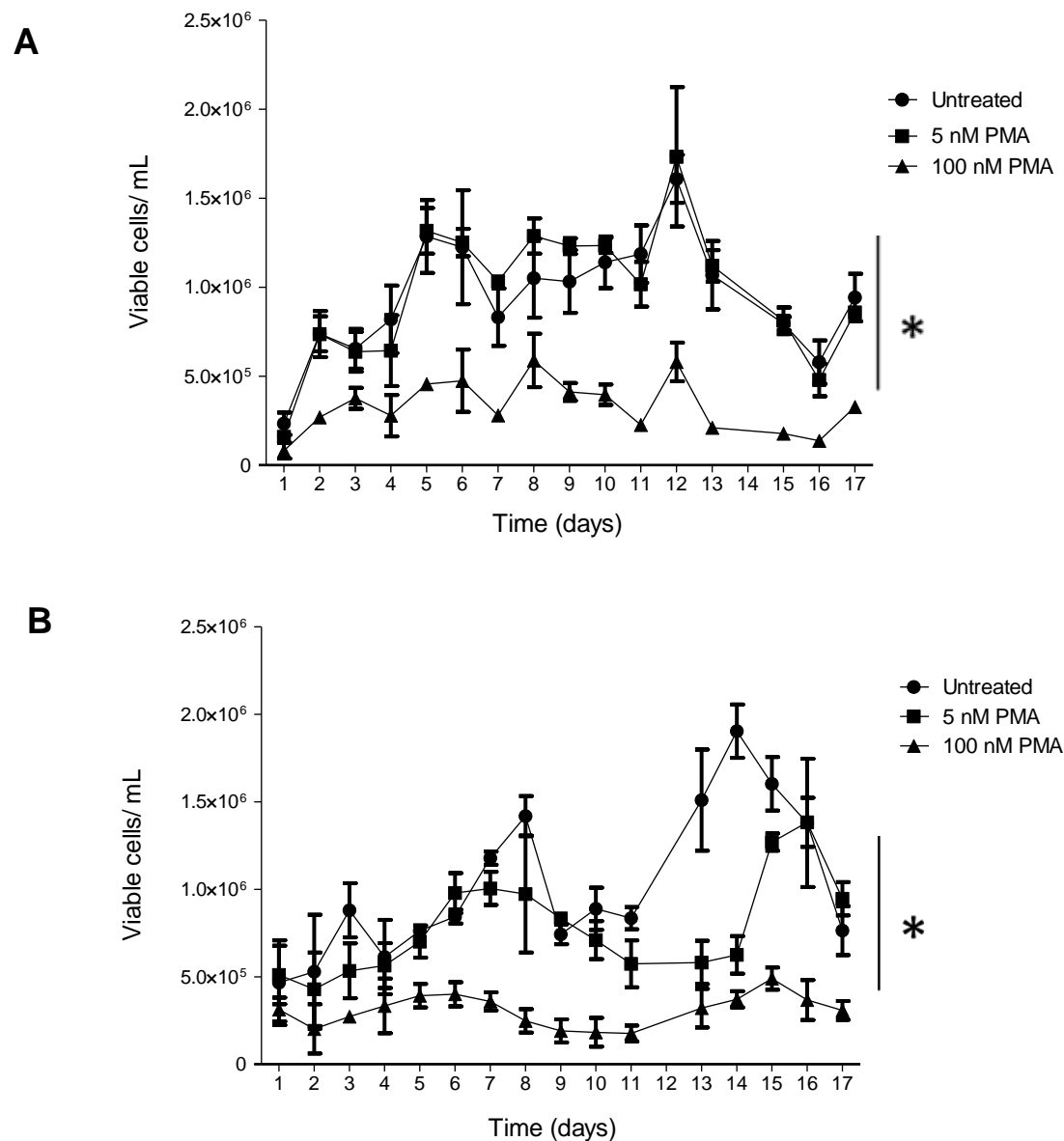
Viability of U937 cells post-incubation with PMA was assessed using ViaCount reagent to determine both cell count and cell viability by flow cytometry. PMA naive cells significantly ( $p<0.05$ ) proliferated over 96 h with more debris with increased time (Figure 3.7 A). Viability and proliferation of cells treated with 5 nM PMA remained unaffected (Figure 3.7 B). Viability was noticeably higher in the PMA naive U937 cells, which increased to  $7 \times 10^6$  cells/ mL than the 100 nM treated U937 cells, which remained unchanged at  $2 \times 10^6$  cells/ mL up to 96 h (Figure 3.7 C). Cell debris was significantly ( $p<0.05$ ) elevated against viable 100 nM treated cells at 48 h, 72 h and 96 h.





**Figure 3.7 Assessment of cell viability for U937 cells cultured in PMA.** U937 cells were incubated with 0 nM (A), 5 nM (B) and 100 nM (C) concentrations of PMA over 24 h to 96 h timepoints. Cells were resuspended, and entire well contents were assessed using Viacount reagent via flow cytometry for total and viable cells/ mL (median $\pm$  SEM) for 10,000 events, where n= 6. A two-way ANOVA was used to determine significance for each treatment group, and the Bonferroni post hoc test was employed when  $*p < 0.05$ .

In the absence of PMA, U937 cells displayed typical proliferative cell conditions increasing in total cell number and viable cell number (Figure 3.7 A), similarly for 5 nM PMA U937 cells (Figure 3.7 B). In the presence of 100 nM PMA, U937 cell proliferative conditions were inhibited at 24 h, 48 h 72 h and 96 h (Figure 3.7 C).

**Figure 3.8 Long-term proliferation profile of PMA treated U937 cells.**

Cells were seeded at  $5 \times 10^5$  cells/mL with no PMA (untreated), 5 nM or 100 nM PMA for 24 h (A) or 96 h (B) followed a 24 h rest period in fresh complete cell culture medium, which was exchanged every 48 h. Cell proliferation was assessed using Guava ViaCount assay via flow cytometry for 10,000 events. Results shown are representative for two repeated experiments performed in triplicate. Viable cells/mL shown as mean  $\pm$  SD. A one-way ANOVA was used to determine each treatment group's significance (\* $p < 0.05$ ).

Proliferation and culture characteristics were not significantly ( $p<0.05$ ) different for PMA naïve and 5nM PMA treated U937 cells. U937 cells exposed to 5 nM PMA followed similar cell culture growth characteristics as PMA naïve cells, which moved to exponential growth phase by day two for 24 h (Figure 3.8 A) and day three for 96 h (Figure 3.8 B) cell types. For the 24 h and 96 h PMA treatment groups, cell viability of PMA naïve and 5 nM treated cells ranged from 1.5- 15 x10<sup>5</sup> cells/ mL and 4.9- 13 x10<sup>5</sup> cells/ mL, respectively. Conversely, treatment of U937 cells with 100 nM PMA for 24 h and 96 h caused the cells to maintain a viability range of 1 x10<sup>5</sup> cell/ mL to 5 x10<sup>5</sup> cells/ mL without proliferating ( $p<0.05$ ) for up to 17 days.

### **3.3.5.2. Metabolic activity of PMA treated U937 cells by comparison of two mitochondrial activity assays**

Mitochondrial activity was assessed using two individual assays: MTS assay (Figure 3.9) and mitotracker dye on the flow cytometer (Figure 3.10). Mitochondrial activity was significantly ( $p<0.05$ ) increased in both 5 nM PMA and 100 nM PMA treatment groups after 24 h compared to untreated control increase in mitochondrial activity of the untreated cells. No significant differences ( $p<0.05$ ) between the treatment groups at 48h, 72 h or 96 h were detected. Additionally, there were no significant ( $p<0.05$ ) differences between 5 nM and 100 nM concentrations at each time point. Thus, U937 cells displayed a natural increase in mitochondrial activity after 24 h post-seeding, and PMA did not influence their metabolic activity.

For mitochondrial activity assessed by flow cytometry (Figure 3.10), no significant differences ( $p<0.05$ ) were found between the treatment groups compared to control. After 24 h, there was a significant difference ( $p<0.05$ ) in absorbance between cells exposed to PMA compared with untreated cells. However, after 48 h, no significant difference ( $p<0.05$ ) was observed in mitochondrial activity of cells with/without PMA exposure. Viable primary AMs were not available for comparison.

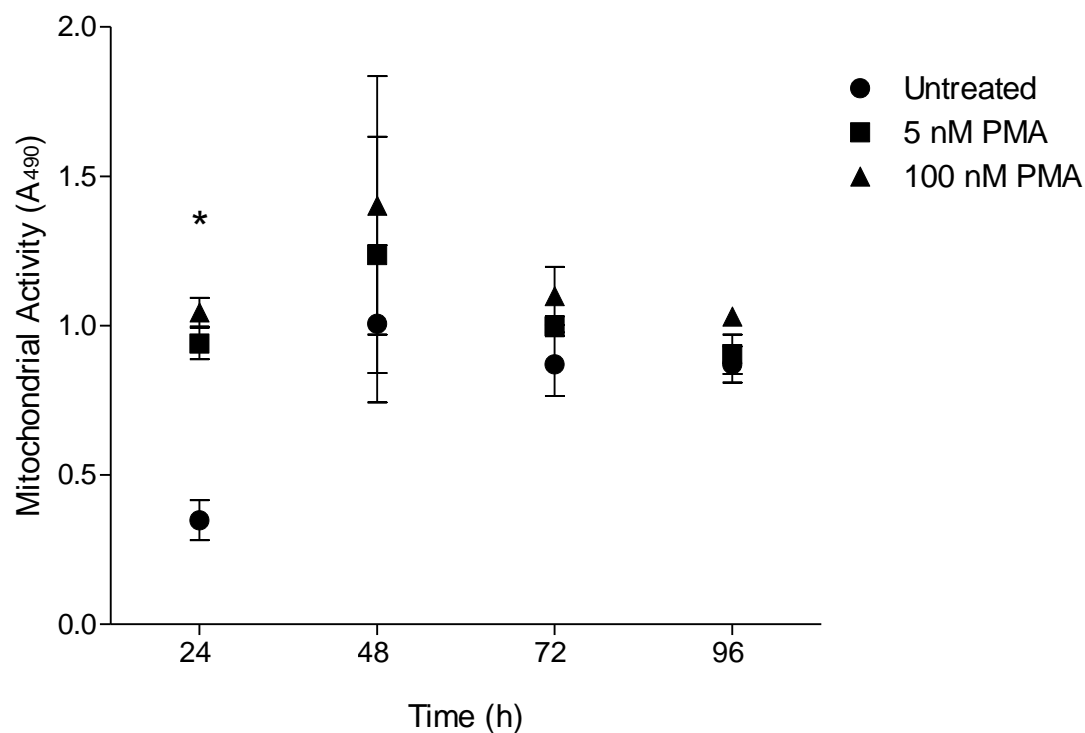


**Figure 3.9 Effect of PMA on U937 cell mitochondrial activity determined by MTS assay.**

Mitochondrial activity (MTS assay) was measured by OD 490 nm using the CellTiter 96® AQueous One Solution Cell Proliferation Assay. The results shown are median  $\pm$  SEM, where  $n=3$ . A two-way ANOVA and Bonferroni post hoc test determined confidence interval (95%) for treatment groups: untreated control, 5 nM PMA and 100 nM PMA at time points: 24 h, 48 h, 72 h and 96 h where  $p<0.05^*$ .

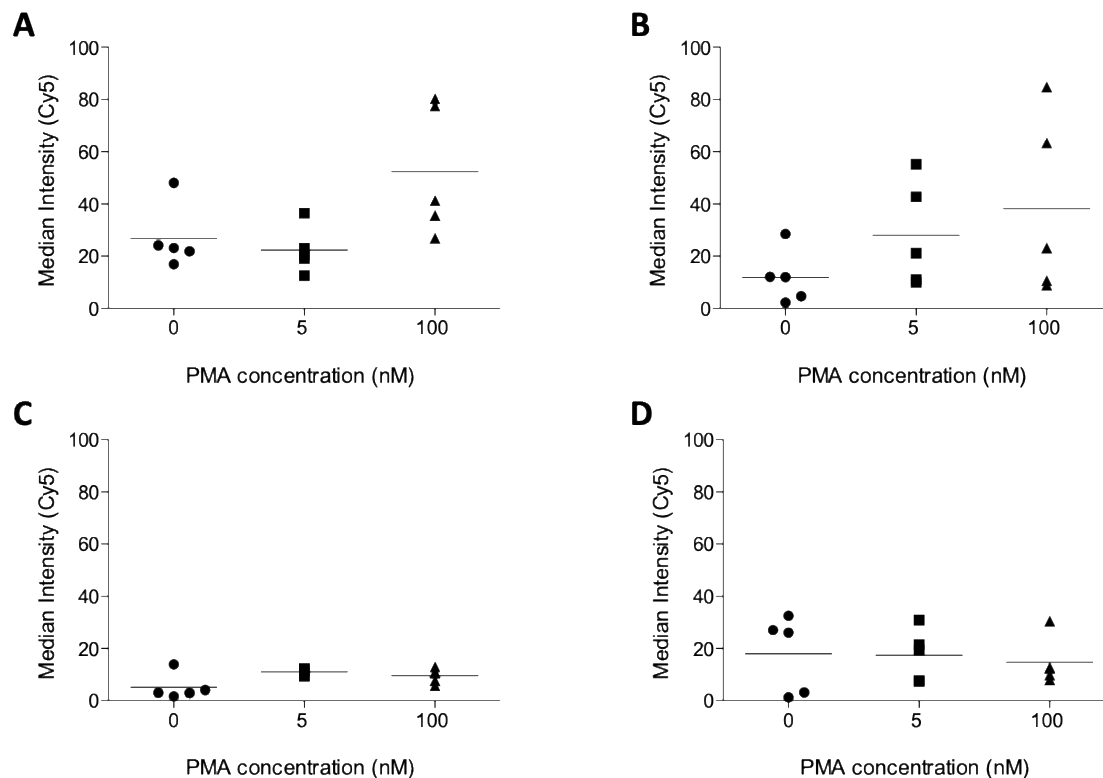


**Figure 3.10 Effect of PMA on U937 cell mitochondrial activity determined by flow cytometry.**

Mitochondrial activity was measured by flow cytometry using MitoTracker Deep Red.

The results shown are mean with MFI data points where  $n=4$ . A one-way ANOVA determined significance of  $p<0.05$  for treatment groups: 0 nM (untreated control), 5 nM PMA and 100 nM PMA) at time points: (A) 24 h, (B) 48 h, (C) 72 h and (D) 96 h.

### **3.3.5.3. Cell membrane integrity of PMA treated U937 cells by two cytotoxic assays**

Cytotoxicity of PMA exposure to U937 cells was assessed using two individual assays: Cytotox-one assay (Figure 3.11) and Image It-dead permeability dye (Figure 3.12). Extracellular concentrations of LDH were shown to significantly ( $p<0.05$ ) increase after 24 h for 100 nM PMA treated cells and after 48 h for 5 nM PMA -treated cells compared to untreated control (0 nM PMA). Increased exposure time and increased PMA concentrations up to 72 h significantly ( $p<0.05$ ) affected cells resulting in increased permeability. Thus, PMA increases cell permeability in a concentration and time-dependent manner.

For the cytometric assay with Image It dead dye, no significance ( $p<0.05$ ) was detected for adherent U937 cells exposed to 5 nM and 100 nM PMA compared to untreated control. Thus, PMA did not affect adherent U937 cell permeability.

.



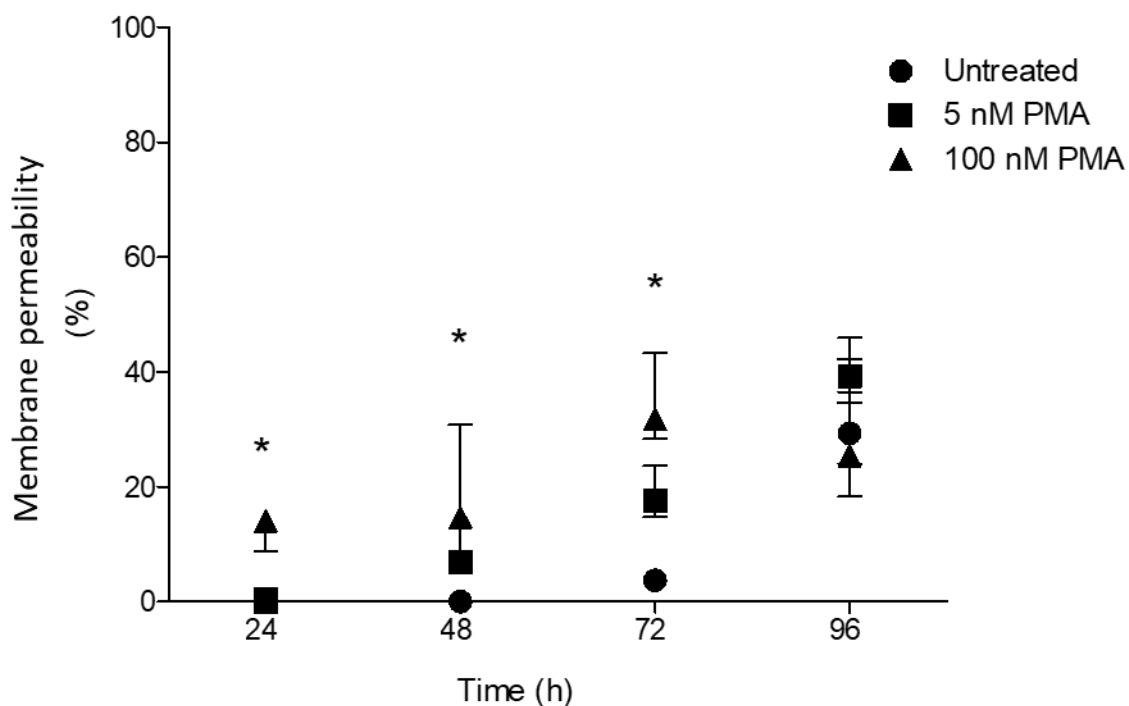


**Figure 3.11 Membrane Integrity of PMA treated U937 cells by Cytotox ONE assay.** Membrane integrity was assessed by 560 nm using the CytoTox-One homogeneous membrane permeability assay. The results shown are percentage LDH released (mean  $\pm$  SD) normalised to 0.1% Triton X-100 positive control where  $n=3$ . A two-way ANOVA determined the significance of  $p<0.05$ , and Bonferroni post hoc test showed significance for treatment groups: 0 nM (untreated control), 5 nM PMA and 100 nM PMA at time points: 24 h, 48 h, 72 h and 96 h where  $p<0.05^*$ .

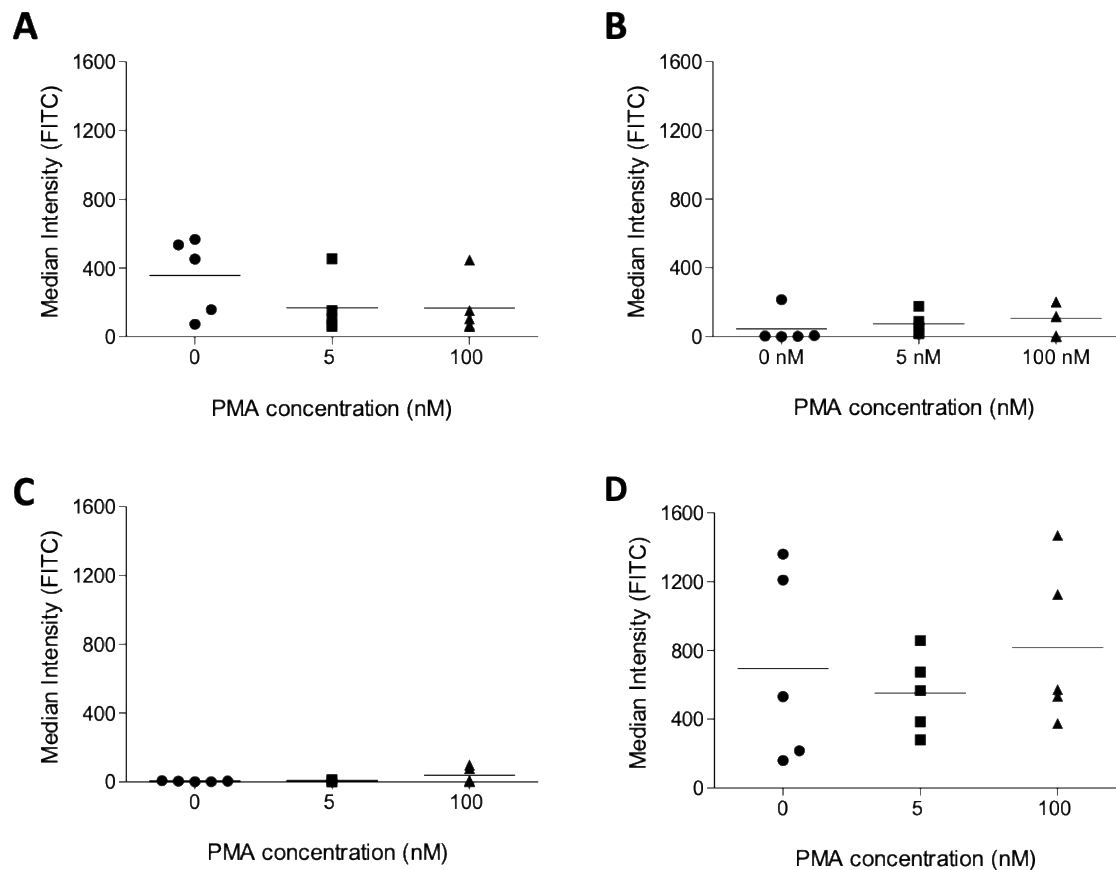


**Figure 3.12 Cytotoxic assessment of PMA treated U937 cells by Image It Dead.**

Permeabilised cells were measured by flow cytometry for Image It dead dye. The results are mean with the median fluorescent intensity of 1000 gated events where  $n=5$ . A one-way ANOVA determined significance of  $p<0.05$  and Tukey post hoc test,  $p<0.05^*$  for treatment groups: 0 nM (untreated control), 5 nM PMA and 100 nM PMA) at time points: (A) 24 h, (B) 48 h, (C) 72 h and (D) 96 h.

### 3.4. Discussion

#### 3.4.1 Differentiation of AMs

To measure and determine macrophage responses to inhaled pharmaceuticals, the development of a robust co-culture model representative of *in vivo* response is required, and therefore selection of an appropriate macrophage cell line is essential. The monocytic cell line U937 is readily available without the need to isolate them from animals or donors. U937s are established in the literature, are shown to yield reproducible results due to lack of inter-donor variability (Baek *et al.*, 2009; Sundström *et al.*, 1976) and have been documented as suitable response models to inhaled xenobiotics and pathogens.

To better understand the responses of an alveolar macrophage model to external stimuli, characteristics of the U937 cells in their differentiated state also need to be well understood. Monocyte U937 cells were differentiated to alveolar-like macrophages in the presence of PMA. Although U937 differentiation by PMA is well reported in the literature, the protocols vary considerably (e.g., cell density, PMA concentration, incubation times, and rest periods), which promote differentiation vary immensely. Cell densities range between  $2 \times 10^5$  and  $2 \times 10^6$  cells/mL, PMA concentrations are from 1nM to 162nM, incubation times range from 8h to 96 h and resting periods whereby the PMA is removed from the cells, and they are replenished with fresh culture medium ranges from 0h to 72 h. It was hypothesised that changes to the PMA differentiation protocol of U937 cells might give rise to a heterogeneous macrophage phenotype. Additionally, there is a need to identify the most suitable differentiation protocol to generate alveolar-like macrophages.

### 3.4.2 Biomarker identification in PMA naive and PMA treated U937 cells

Functional protein microarray technology is a powerful, high throughput tool for biomarker identification (Templin *et al.*, 2002) and has yet to be used for profiling cluster of differentiation (CD) markers in PMA naive and PMA treated U937 cells. The microarray permitted identification showed differentiation of PMA naive and PMA treated U937 cells positive for the CD antigens on the microarray panel and determined if differences between low and passage 25s were apparent.

In agreement with previous studies, our findings show that PMA treated U937 cells are abundant in surface markers. CD markers present on U937 exposed to PMA identified in the microarray and literature were: CD 4, CD 11a, CD 29, CD 33, CD 36, and CD 54. CD 4 is often associated with T-cells, but it is known to be expressed on parent U937 cells, and expression is reduced following PMA stimulation, confirming its suitability as a monocyte biomarker for U937 as shown in published reports (Hewison *et al.*, 1992; Pelchen-Matthews *et al.*, 1993; Vigerust *et al.*, 2012). The expression of several markers (CD 8, CD 11a, CD 23, CD 29, CD 33, CD 36, CD 45RA (i), CD 45RA (ii), CD 54, CD 58, FDC and TSLPrec) was found to be similar regardless of passage number and PMA exposure.

CD 11a, CD 23, CD 29, CD 36, CD 54 and CD 58 have been demonstrated to be expressed on AMs extracted via BAL from humans (Lofdahl *et al.*, 2006; Taylor *et al.*, 2000; C. Ward *et al.*, 2001). Marker CD 33 is involved in macrophage cell-cell interactions and signalling functions, but its expression on human AMs is unknown (Crocker, 2002). Additionally, CD 45 (lymphocyte common antigen) is expressed in humans, BAL extracted AMs, and the microarray highlighted increased expressions of

multiple epitopes compared with the untreated U937 (Altin *et al.*, 1997; Taylor *et al.*, 2000). Similarly, for CD 58, there were two antibodies against this target; these two antibodies may not necessarily recognise the same conformation of the protein. It is possible that the recognition epitope is modified and the respective antibody cannot capture the protein anymore or that the protein has lost some conformational aspects/ conformation epitopes and is therefore not recognised anymore (Sela-Culang *et al.*, 2013).

Compared to the low and high number of cell passages, our findings confirmed that multiple markers for PMA treated U937 cells were more highly expressed in passage 25 than those at passage 5. Similarly, markers Etoxin-1 and CD 41 were more highly expressed in PMA naive U937 cells at passage 25 than at passage 5. Surface markers CD 15 and CD 36 were highlighted as they were heterogeneously expressed, and the individual protein expression increased for the PMA treated cells investigated. CD 36 could be a possible candidate for further analysis of alveolar-like macrophage development.

The myeloid cell line U937 differentiates into adherent macrophage-like cells following exposure to either PMA or vitamin D3 (Harris *et al.*, 1985; Zhang *et al.*, 1994). These reports suggest that myeloid leukaemias are capable of terminal differentiation into a mature cell type. Conversely, PMA induced macrophage differentiation of U937 cells has been shown to generate a heterogeneous cell population (Minta *et al.*, 1985). To date, the evaluation of lymphocyte biomarker expression, other than that for macrophages on PMA differentiated U937 cells, varies significantly for U937 cells. One group describe the generation of a megakaryocyte following IFN $\gamma$  stimulation of a PMA differentiated U937 cell subgroup identified by biomarkers CD 41 and CD 42

(Schneider *et al.*, 2009). Another study has shown the differentiation of U937 cells to dendritic cells induced by IL-4 and identified by CD86 (Python *et al.*, 2007).

We need to consider the myeloid lineage of cells in the mononuclear phagocyte system *in vivo* and the ability of these cells to differentiate to multiple cells types. It is, then, possible to understand that PMA induced U937 cells could express markers heterogeneous to macrophages such as T- cell co-receptor CD 8, follicular dendritic cell (FDC) and other antigen-presenting cell characteristics (Rasaiyaah *et al.*, 2007; Stonehouse *et al.*, 1999). The studies described in this chapter showed that protein biomarker expression of FDC was significantly ( $p<0.05$ ) elevated in PMA treated U937 cells compared to their phenotype at 3-fold higher at both a low and passage 25. Thus, FDC could act as a suitable internal control for future AM generation and validation work.

Interleukins and other surface proteins on differentiated U937 cells varied in expression compared to their phenotype at a low (IL-15 and TSLPrec) and high (IL-6, IL-7, IL-18, FDC, Etoxin-1, HLA I and TSLPrec) passage number. These proteins are responsible for regulating the immune system, cell-cell interactions and inflammation signalling (Liles *et al.*, 1995). Our findings showed that TNF $\alpha$  was not expressed in PMA induced U937 cells. Hence, PMA exposure did not stimulate a TNF $\alpha$  inflammatory cascade but did initiate regulatory cell biomarker characteristics.

CD 11a and CD 36 were selected as suitable AM biomarkers because they are strongly supported in the literature as markers for human AM. Moreover, in the protein microarray, these markers were shown to be significantly ( $p<0.05$ ) expressed in U937 cells once induced with PMA. Multiple studies have used CD 11b and CD 14 as

markers of macrophage response in PMA differentiated U937 cells, Table 3.1. Because these markers were not found to be expressed in the microarray, their expressions might only become upregulated under specific differentiation conditions. Additionally, reports describing expressions of the mannose receptor CD 206 are contradictory (Minafra *et al.*, 2011; Taniguchi *et al.*, 2015). Therefore, CD 11a, CD 11b, CD 14, CD 36 and CD 206 were selected for profiling PMA induced U937 cells to compare to *ex vivo* human AMs.

### **3.4.3 CD biomarker differentiation profiles**

The expression of multiple surface markers during differentiation by PMA at 24 h, 48 h, 72 h and 96 h each followed by a rest period of 24 h in fresh culture medium at 0 nM, 5 nM, and 100 nM concentrations were observed with the primary aim to determine if variances in the differentiation protocol affected surface membrane expression profiles.

Heterodimeric integrins, CD 11a and CD 11b, function as adhesion molecules on macrophages (Viksman *et al.*, 2002; C. Ward *et al.*, 2001). In agreement with a previous report, the abundance of CD 11a and CD 11b in PMA induced U937 cells was significantly higher ( $p<0.05$ ) compared with control (García *et al.*, 1999). Conversely, Prieto *et al.* describe a higher abundance of CD 11a and CD 11b in untreated U937 cells (Prieto *et al.*, 1994). Our findings show CD 11a is a marker for both untreated U937 and differentiated U937, and under standard culture conditions, the expression of CD 11a increases significantly over time in untreated U937 cells. Furthermore, the expression of CD 11a on differentiated cells is affected in a dose and

time-dependent manner. Incubation of 5 nM PMA for 96 h yielded comparable expression of CD 11a to that of cells incubated with 100 nM PMA for 24 h.

Identified as a macrophage marker, expression of CD 11b increases on PMA (20 nM) induced U937 cells in a time-dependent manner (Sordet *et al.*, 2002). Although unable to compare MFI values, the results in this study showed an increase in CD 11b expression of PMA exposed U937 cells with 100 nM but not with 5 nM concentration. Furthermore, Yamamoto *et al.* describe a similar response (MFI: 20-25) of CD 11b and a dose-response to PMA after 24 h in line with our results after 24 h (T. Yamamoto *et al.*, 2009).

CD 14 serves as a pattern recognition receptor in innate immunity for a variety of ligands and is synthesised and expressed by monocytes and macrophages only (Jersmann, 2005). Overall, CD 14 is poorly expressed (R Hass *et al.*, 1989); an increased level of the antigen on the cell surface of 100 nM PMA induced U937 cells was observed in these studies in line with previous reports using western blotting and flow cytometry. Increased CD 14 expression at 5 nM PMA for 48 h was in line with the result from Hewison *et al.* (Hewison *et al.*, 1992).

CD 36 functions as a pattern recognition receptor on phagocytes (Silverstein *et al.*, 2010). It is better known as a scavenger receptor and is thought to bind oxidising lipoproteins and mediate foam cell formation (Endemann *et al.*, 1993). CD 36 is described to be abundant in U937 cells (Prieto *et al.*, 1994; Vigerust *et al.*, 2012) and markedly lower in PMA induced U937 cells at 48 h (Prieto *et al.*, 1994), unlike our findings where CD 36 is elevated at 24-96 h relative to untreated U937 cells (Alessio *et al.*, 1996; T. Yamamoto *et al.*, 2009).



Mannose receptor is a large (175kDa), complex ligand and plays a role in the clearance of endogenous molecules, regulation of cellular activation, molecule trafficking and promotion of antigen presentation (Martinez-Pomares, 2012). Previous work shows CD 206 expressed on subpopulations of macrophages *in vitro* and AMs *ex vivo* (Cai *et al.*, 2014; Chana *et al.*, 2014; Minafra *et al.*, 2011; Taniguchi *et al.*, 2015; Vigerust *et al.*, 2012; Zaynagetdinov *et al.*, 2013). The work in this chapter shows CD 206 was not expressed in U937 cells or PMA induced cells (Daigneault *et al.*, 2010; Vigerust *et al.*, 2012), but may with the addition of IL-4 (Taniguchi *et al.* 2015). Conversely, Minafra *et al.* describe the presence of CD 206 on PMA induced U937 cells (Minafra *et al.*, 2011).

The absence of surface molecules CD 11b and CD 14 in the microarray are explained by their low MFIs in CD marker profile. Thus, the protein expressions of CD 11b and CD 14 were below the designated threshold set by the internal controls for the microarray. This outcome highlights the sensitivity of flow cytometry when determining small differences between samples. CD 11b and CD 14 were expressed at lower levels than CD 11a and CD 36 as indicated by protein microarray and flow cytometry. Unaffected by DMSO, PMA induced cells were easily distinguished from their monocytic phenotype by the expression of CD 11a, CD 11b, CD 14, and CD 36. They are expressed at varying levels among differentiated U937 cells suggesting their suitability as cell maturation markers.

#### **3.4.4 Phagocytosis activity**

We assessed the phagocytic ability of U937 and PMA-treated U937 cells. In accordance with the literature, U937 cells differentiated on exposure to PMA displaying phagocytic characteristics (Daigneault *et al.*, 2010; Minta *et al.*, 1985; Taniguchi *et al.*, 2015). No significant differences ( $p < 0.05$ ) between treatment groups at each time point were observed. However, the percentage of phagocytes decreased ( $p < 0.05$ ) in a time-dependent manner where cells at 96 h showed more than a 20% decrease compared to cells at 24 h. This suggests that the phagocytic efficiency of the cells with or without PMA decreases over time.

#### **3.4.5 Cell viability and physiology**

In the present study, adherent PMA exposed U937 cells did not affect cell viability or cell membrane integrity, as also described by (Sordet *et al.*, 2002). When assessed for longevity, U937 cells did not display the ability to proliferate following differentiation at 100 nM concentrations of PMA, similar to other reports that state proliferation was inhibited following stimulation of similar PMA concentrations (Bhalla *et al.* 1989; Hass *et al.* 1989; Otte *et al.* 2011). Furthermore, few studies assess the proliferation characteristics of differentiated U937 cells. A recent study reported incubating U937 cells with PMA for 72 h followed by further incubations with compounds for up to 72 h (Meshkini *et al.*, 2009). Although the authors do not confirm the proliferation or viability profile of the cells, they at least assumed they were still viable. To follow on from this, there is little data to support that, following induced senescence, the cells either undergo cell death or survive. Our findings suggest that the survival and viability of these U937 cells were still evident 17 days after exposure, after which they died. Hence, differentiation of U937 cells using PMA may not inhibit proliferation at low

concentrations of 5 nM. In support of this argument, one research group reported a kind of 'reversal' of macrophages to monocytes following a 20-day culture of PMA induced U937 cells in PMA-free media. By day 20, the cells were no longer adherent, although 100% viable with proliferative characteristics (Minta & Pambrun 1985), suggesting that U937 differentiation via PMA results in a short-term stable perturbation in cell structure and function.

In the presence of PMA, U937 cells undergo significant morphological changes. The formation of adherent aggregates is associated with extension pseudopodia, enlarged and foamy cells (Hass *et al.* 1989; Minta & Pambrun 1985; Sundström & Nilsson 1976). Minta *et al.* report that at low concentrations (2.5- 10 nM), the induced cells do not reach maximal differentiation until 72 - 96 hours. In addition, at higher concentrations (40-162 nM), maximal differentiation is reported to be reached at 48 h.

The morphological change in differentiated U937 cells is dose and time-dependent; with increased PMA concentration, differentiation can occur faster (Minta & Pambrun 1985). The results from the study show similar morphological changes of cultured U937 cells as undifferentiated, small, dense cells to differentiated cells characterised by enlarged size, foamy/ vacuolated cytoplasm with pseudopodia, but induced with a lower concentration of PMA. This study's results suggest that 100 nM PMA may be sufficient to appropriately differentiate U937 cells to AM-like phenotype. The experiment exploits multiple time points, so PMA induced differences in morphology over time can be determined. The work examined morphological differences between PMA induced and PMA naïve groups compared to pAMs. Cells differentiated with 100 nM PMA displayed significantly more adherence and homogeneity, unlike 0 nM or 5 nM PMA induced cells. Further repetition and observation by fluorescent microscopy may clarify these observations.

### **3.5. Conclusion**

PMA promotes the differentiation of human U937 monocytic cells into macrophage-like cells. Stimulation of U937 cells changes the characteristic of the cell from its phenotype morphologically and proteome, from up-regulated surface glycoproteins to activation of intracellular signalling. Additionally, these differentiated, phagocytic cells are shown to express markers specific to alveolar macrophages, suggesting that they are suitable as an alveolar like macrophage model in their differentiated state. Moreover, finally, differences in PMA concentration and incubation time of PMA induced U937 cells significantly affect the immediate progeny of that cell.

### 3.6. Appendix I

**Table 3.2 CD Microarray table of surface biomarkers measured.**

CD Marker	Gene name	CD Marker	Gene name	Chemokine / Cytokine	Gene name	Additional proteins	Gene name
CD1a	LEU6	CD50	ICAM3	GM-CSF	CSF2	ANCA	PRTN3
CD2	SRBC	CD52	HE5	IFN alpha	IFNA1	BDNF	BDNF
CD3	T3G	CD53	TSPAN25	IFN gamma	IFNG	Cox1	PTGS1
CD4	LEU3	CD54	ICAM1	IL-1alpha	IL1A	CYTL	CYTL1
CD5	LEU1	CD55	DAF	IL-1beta	IL1B	IgE	FCER1A
CD6	TP120	CD56	NCAM1	IL-2	IL2	HLA I	
CD7	LEU9	CD57	B3GAT1	IL-4	IL4	HLA-ABC	
							HLA-
CD8	MAL	CD58	LFA3	IL-6	IL6	HLA-DP	DPB1
CD9	MIC3	CD59	MIC11	IL-7	IL7	HLA-DQ	
CD10	MME	CD61	ITGB3	IL-8	CXCL8	HLA-DR	
CD11a	ITGAL	CD62L	SELL	IL-10	IL10	MPO	MPO
CD11b	ITGAM	CD62p	SELP	IL-12B	IL12B	NT-4	NTF4
CD11c	ITGAX	CD63	TSPAN30	IL-13	IL13	NTAL	LAT2
CD13	ANPEP	CD66a	CEACAM1	IL-15	IL15	pan HLA-class II	
CD14		CD66b	CEACAM8	IL-16	IL16	p53	TP53
CD15	FUT4	CD66c	CEACAM6	IL-18	IL18	p72Syk	SYK
CD16	FCGR3A	CD66d	CEACAM3	IL-37	IL37	TRYG1	TPSG1
CD17		CD66e	CEACAM5	LIF	LIF	TSLPR	CRLF2
CD18	ITGB2	CD69	CLEC2C	TNF alpha	TNF	tTG	TGM2
CD19	LEU12	CD70	TNFSF7	TSLP	TSLP	VEGF	VEGFA
CD20	MS4A1	CD71	TFRC	Eotaxin-1	CCL11		
CD21	CR2	CD72	Lyb-2	MIP-1 alpha	CCL3		
CD22	SIGLEC2	CD79a	MB1	RANTES	CCL5		
CD23	FCER2	CD80	LAB7	MCP-2	CCL8		
CD24		CD86	LAB72	MCP-3	CCL7		
CD25	IL2RA	CD95	FAS	MIP-4	CCL18		
CD27	TNFRSF7	CD97					
CD28	TP44	CD98	SLC3A2				
CD29	ITGB1	CD99	MIC2				
CD30	TNFRSF8	CD105	ENG				
CD31	PECAM1	CD106	VCAM1				
CD33	SIGLEC3	CD116	CSF2RA				
CD34		CD117	KIT				
CD35	CR1	CD123	IL3RA				
CD36	GP3B	CD131	CSF2RB				
CD37	TSPAN26	CD137	TNFRSF9				
CD38	ADPRC 1	CD139					
CD40	TNFRSF5	CD147	BSG				
CD41	ITGA2B	CD162	SELPLG				
CD42b	GP1BA	CD177	NB1				
CD43	SPN	CD222	IGF2R				
CD44	MDU2	CD223	LAG3				
CD45	PTPRC	CD230	PRNP				
CD46	MCP	CD235a	GYPA				
CD47	MER6	CD235b	GYPB				
CD48	BCM1	CD253	TNFSF10				
CD49d	ITGA4	CD274	PDL1				
		CD279	PD1				

## Development & characterisation of human immunocompetent alveolar co-culture models

### 4.1. Introduction

In order to get new medicines to market, pharmaceutical companies are required to pass a series of regulatory approvals. Before embarking on clinical trials, pharmaceutical companies and independent investigators must conduct extensive pre-clinical *in vitro* and *in vivo* studies (C. Ehrhardt *et al.*, 2008). These studies must demonstrate the biological activity and efficacy of a drug against the targeted disease and evaluate the compound's safety (Forbes *et al.*, 2011). These studies also assist the decision-making process to determine whether a candidate drug has scientific weight to justify further development (M. Song *et al.*, 2015).

Rats are the predominant species used for *in vivo* pre-clinical inhalation assessment. However, rats fail to represent human airway physiology or cell phenotype and, as a result, are poor models to predict the safety and efficacy of inhaled compounds in humans (Stone *et al.*, 1992). Furthermore, ethical limitations, legislation, high costs and concerns over the predictive value of animal experiments are responsible for the increased surge of applications of *in vitro* model systems in recent years (Törnqvist *et al.*, 2014).

*In vitro* cell cultures comprising a single cell type cultured on flat tissue culture plastic surfaces are widely used as *in vitro* models to study cellular responses from biophysical and biochemical stimuli (Edmondson *et al.*, 2014). These well-accepted approaches have advanced the understanding of cell biochemistry (Crapo *et al.*, 1983; Edmondson *et al.*, 2014; B. Rothen-Rutishauser *et al.*, 2008). In recent years, growing evidence indicates that these simple monoculture systems can result in cell phenotypes and functionalities that deviate from those found in the *in vivo* environment, questioning their relevance for *in vivo* predictions (Nahar *et al.*, 2013). To overcome this limitation, culturing multiple cell types in a 3D orientation and incorporating suitable biochemical and physiochemical features has been created to mimic the *in vivo* environment better (see chapter 1). In many cases, these new platforms have proven more capable of inducing *in vivo*-like responses for the specific processes under study (Nahar *et al.*, 2013)

Multiple lung co-culture systems have been developed, although many of these models are poorly validated and not anatomically accurate (Crapo *et al.*, 1983). Biological responses are determined by the interaction of several cells within the tissue. Therefore, studying multiple cell types in a tissue system enables researchers to mimic better or approximate physiological conditions existing *in vivo* (Hittinger *et al.*, 2015; Takayama, 2020). There is substantial evidence to support that co-culture systems are more suitable for understanding cell/tissue functionality *in vivo* than monoculture models (Table 4.1) (BéruBé *et al.*, 2009). As a result, *in vitro* co-culture model systems are proving to be valuable tools to observe tissue responses and further evaluate the effects of compounds in specific organs for human health (Larson, 2015).

**Table 4.1 List of cell behaviours that can be examined in co-culture models**


---

1	Cell morphology (structure, phenotype)
2	Polarity (functional directionality)
3	Growth (proliferation)
4	Cell motility (migration, invasion)
5	Neurite outgrowth
6	Signal transduction (surface receptor function)
7	Gene and protein expression (organ and tissue-specific)
8	Biochemical activities (proteins, enzymes)

---

Adapted from Larson, 2015.

Currently, most pre-clinical human *in vitro* cell culture assessments is carried out on airway epithelial cells (Weibel, 2015; Whitsett *et al.*, 2015). While these models may mimic the barrier function, airway secretions, and potentially some aspects of metabolism, they oversimplify the airways. They cannot mimic the complex functionality of the airway tissues (Bhowmick *et al.*, 2016). In particular, *in vivo* safety endpoints comprised of histological slices of whole rat lung and changes to the epithelial structure is only one of many observations used to assess safety (Bell *et al.*, 2018). Over the past decade, alveolar macrophage responses to inhaled compounds visible in rodent lungs during *in vivo* studies have not been successfully studied *in vitro* due to the lack of appropriate models (Nikolić *et al.*, 2018; B. Rothen-Rutishauser *et al.*, 2008). Therefore, there is a need to develop a suitable immunocompetent model representative of the human alveolar region, which can more accurately assess airways response for inhaled safety prediction.



## 4.2. Aims

This chapter aimed to optimise and characterise two human immunocompetent *in vitro* models of the human alveolus: (i) type I alveolar epithelial cell with alveolar macrophage-like cells and; (ii) type II alveolar epithelial cell with alveolar macrophage-like cells. Specifically, the objectives were to:

- Determine the optimal culture conditions for alveolar epithelial cells (including medium composition, seeding density, culture period and culture substrate);
- Develop a methodology to construct the co-culture model;
- Assess the viability of the co-culture system;
- Assess the functionality of the epithelial component in the co-culture system;
- Assess the functionality and phenotype of the alveolar macrophage-like component in the co-culture system;
- Evaluate how the presence of different cell types in the culture system affects cellular activity

## 4.3. Results

### 4.3.1 Optimisation of co-culture conditions

#### 4.3.1.1. Selection of medium composition

The impact of media composition on the viability and proliferation of epithelial cells was assessed. Monocultures of hAELVi cells were cultured on 96 well plates in the complete cell culture medium described for U937 cells (U937 CCM). The complete cell culture medium as described for hAELVi cells (hAELVi CCM) and a 1:1 ratio of both media. Optimisation assays showed higher levels (>50 %) of hAELVi media resulted in uncharacterised morphological changes of U937 cells. This was likely due to the large quantity of added nutrients and proteins in the hAELVi media. Thus, optimum viability was determined at equal volumes. As A549 cells have been documented in the literature to be cultured in U937 CCM, only this medium was assessed for these cells.

The number of viable cells did not significantly differ until the fourth day after seeding (Figure 4.1 A). For hAELVi cells cultured in hAELVi CCM, the number of viable cells peaked at day 5 in culture and was maintained around  $2 \times 10^6$  cells/mL for the duration of the experiment. In comparison, cells cultured in U937 CCM and the 1:1 ratio of U937 CCM:hAELVi CCM followed a similar proliferative profile with cell number increasing with time in culture. After day 7, there was a significantly lower number of viable cells ( $p < 0.05$ ) in the samples where hAELVi CCM was used compared to the other two media types. The decreased number of viable cells cultured in the hAELVi CCM, particularly from day 11, suggest that media supplements inhibit proliferation. The extracellular LDH concentration from hAELVi cells cultured in the three media types was also measured over a 13-day time course (Figure 4.1B) and was normalised against a lysed cell control. On the first day, when hAELVi cultures were transferred to U937 CCM and the 1:1 U937 CCM:hAELVi CCM media, the extracellular LDH

concentration was significantly raised ( $p<0.05$ ) in comparison with hAELVi CCM. However, no significant differences ( $p<0.05$ ) in extracellular LDH concentrations were observed between days 2- 9 of culture. A comparable and gradual increase in the extracellular LDH concentration was observed for hAELVi cells cultured in all media types throughout the experiment. No significance was evident at day 11 for the 1:1 U937 CCM:hAELVi CCM media compared to other media types.

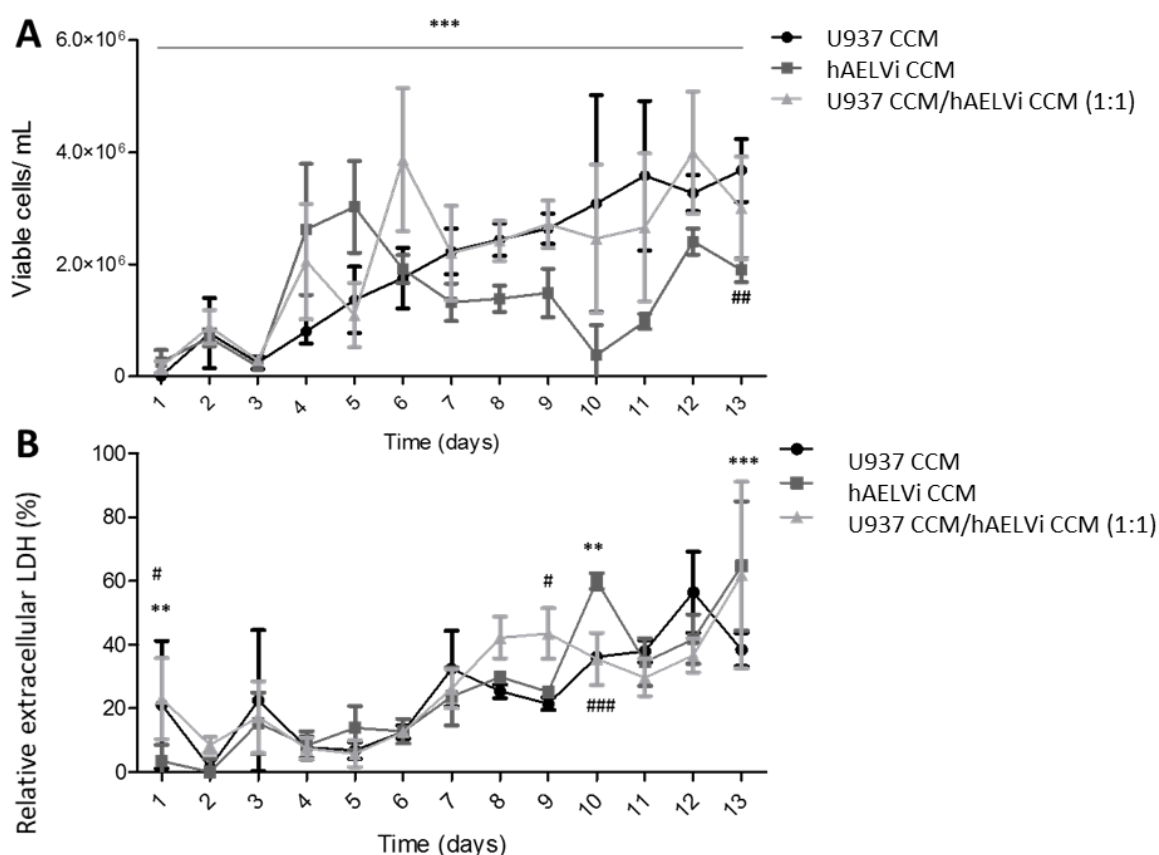


**Figure 4.1 Assessment of medium compositions the proliferation and viability of hAELVi cells.**

hAELVi cells were seeded at a density of  $1.5 \times 10^5$  cells/cm<sup>2</sup> in a 96 well plate under submerged conditions for 13 days. Cells were cultured in either hAELVi CCM, U937 CCM or a 1:1 ratio of U937 CCM: hAELVi CCM. Every 24 h, the number of viable cells was determined by counting (A), and extracellular LDH was determined (B). Viable cells were measured using a flow cytometer and the ViaCount assay. LDH release was presented as relative to a lysed cell sample (treated with 0.5%v/v TX-100) Data shown represents mean  $\pm$  SD (n= 6) from two independent experiments; \* $p<0.05$ ; \*\* $p<0.01$ ; \*\*\* $p<0.001$  vs. RPMI.

In comparison to hAELVi cells, A549 cells displayed quicker proliferation with a population doubling time of 24 -36 h (Figure 4.2 A). The cell number had not plateaued by the end of the 13-day observation period and was significantly greater than that of hAELVi cells ( $1.4 \times 10^7$  cells/mL vs  $2-4 \times 10^6$  cells/mL). The extracellular LDH concentration increased over time in culture with increased cell proliferation (Figure 4.2 B). A549 and hAELVi cell proliferation and viability were not negatively impacted when cultured in U937 CCM.

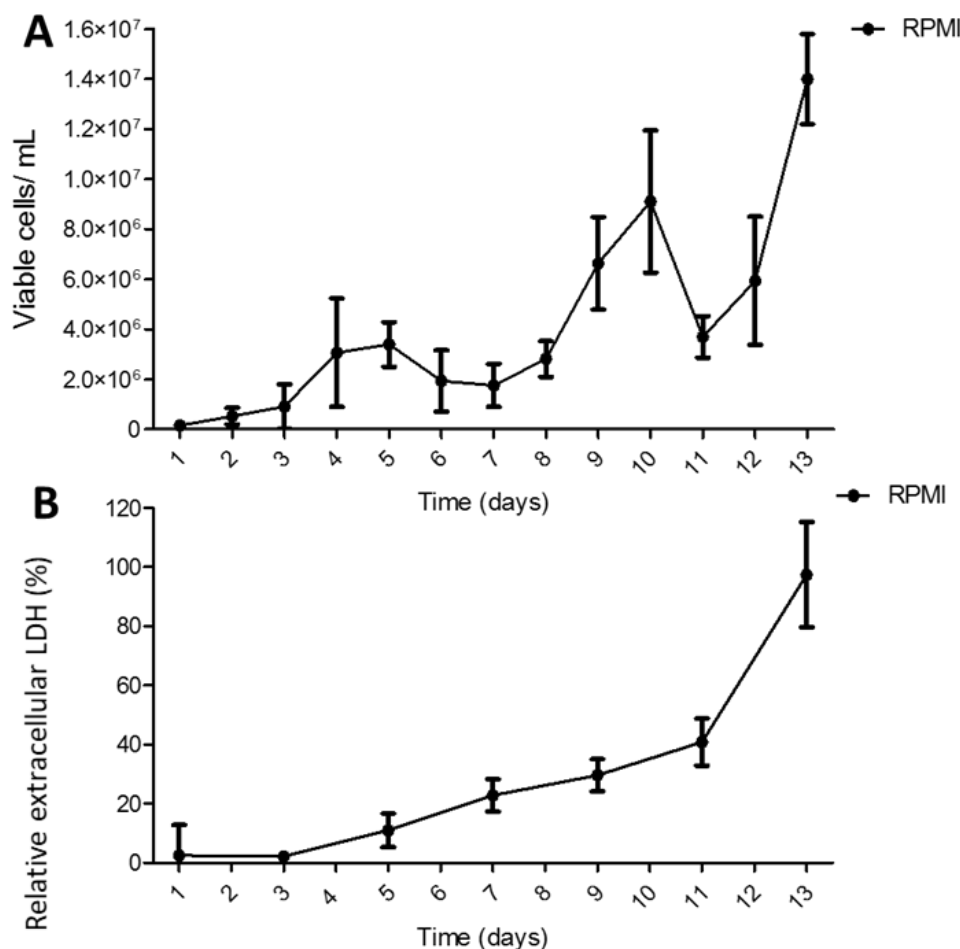


**Figure 4.2 Assessment of U937 CCM on the proliferation and viability of A549 cells.**

A549 cells were seeded at a density of  $1.5 \times 10^5$  cells/cm<sup>2</sup> in a 96 well plate under submerged conditions. Cells were cultured in U937 CCM for 13 days. Every 24 h, the number of viable cells was determined (A), and extracellular LDH was determined (B). Exponential growth was accompanied by increasing LDH release. Absolute viable cell confluency at 100% was reached at day 13, where 100 % LDH was detected. Viable cells were measured using a flow cytometer and the ViaCount assay. LDH release was presented relative to a lysed cell sample (treated with 0.5%v/v TX-100). The data shown represent mean  $\pm$  SD (n= 6) from two independent experiments.

#### **4.3.1.2. Selection of culture substratum**

The influence of pore diameter in the Transwell® insert on cell viability was assessed. No significant difference ( $p < 0.05$ ) was observed between extracellular LDH concentrations for hAELVi cells cultured in well plates or on Transwell® inserts with 0.4  $\mu\text{m}$  or 3  $\mu\text{m}$  pore sizes until 9 days in culture (Figure 4.3 A). hAELVi cells cultured on 0.4  $\mu\text{m}$  inserts released significantly less LDH after 9 and 11 days in culture than control and 3.0  $\mu\text{m}$  Transwell® inserts but was significantly elevated after 13 days. The hAELVi cell membranes were significantly less compromised when cultured on 0.4  $\mu\text{m}$  Transwell® inserts. Similarly, culture substratum had no significant impact on the LDH release from A549 cells for the first 5 days in culture (Figure 4.3 B). A549 cells cultured on 0.4  $\mu\text{m}$  Transwell® inserts produced significantly higher extracellular LDH concentrations ( $p < 0.001$ ) from day 6 onwards in comparison with cells cultured in well plates (control). From 11 days in culture, extracellular LDH concentrations from cells cultured on Transwell® inserts with 0.4  $\mu\text{m}$  and 3.0  $\mu\text{m}$  were not significantly different ( $p < 0.05$ ).

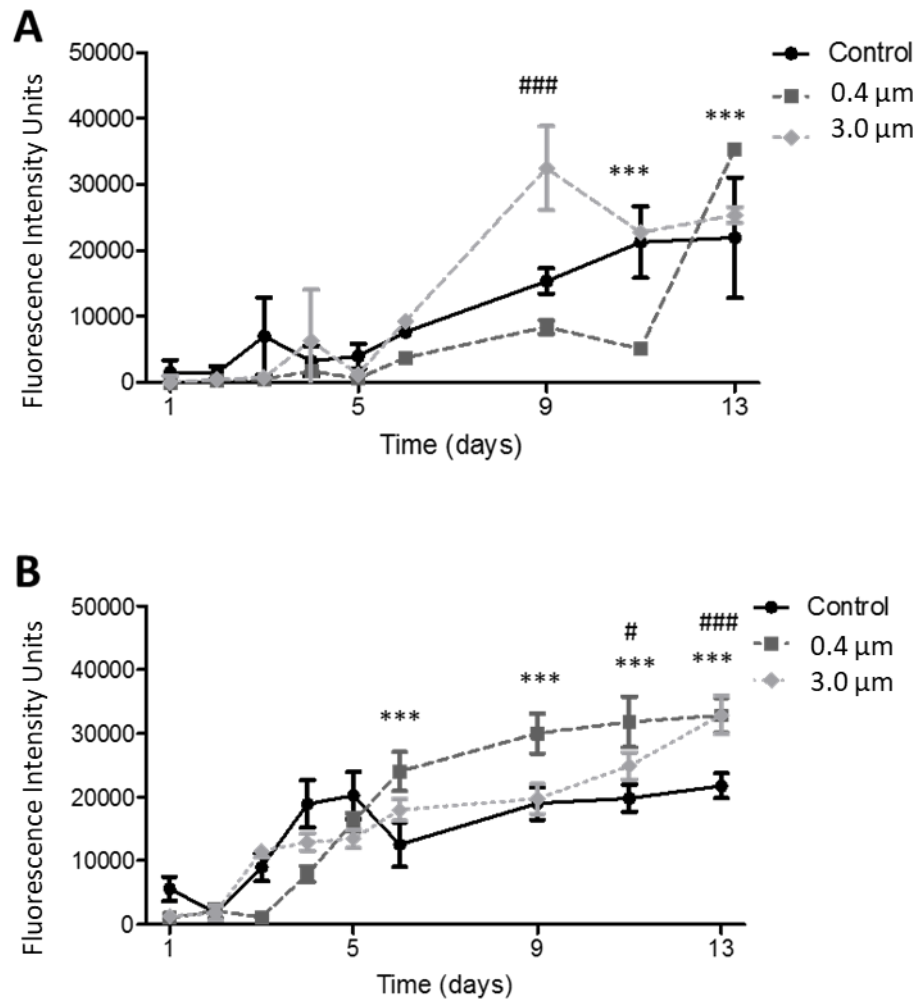


**Figure 4.3 Assessment of culture substratum on epithelial cell viability.**

hAELVi cells (A) or A549 cells (B) were seeded at a density of  $9 \times 10^4$  cells/cm<sup>2</sup> on a 96 well plate (control) or 0.33 cm<sup>2</sup> Transwell® inserts with a pore size of either 0.4 µm or 3.0 µm. Cells were cultured under submerged conditions for 13 days. The apical compartment was sampled to assess the extracellular LDH concentration at designated time points. The data shown are the mean  $\pm$  SD of three samples. Data is considered significant for 0.4 µm (\*) or 3.0 µm (#)  $p$  values where  $p < 0.0001$  (\*\*\*),  $p < 0.05$  (#) vs control.

#### **4.3.1.3. Selection of seeding density**

The effect of cell seeding density on the ability of the epithelial cells to form polarised cell layers was determined. TEER measurements were taken every 2-3 days to indicate if a functional polarised cell layer was present (Figure 4.4)



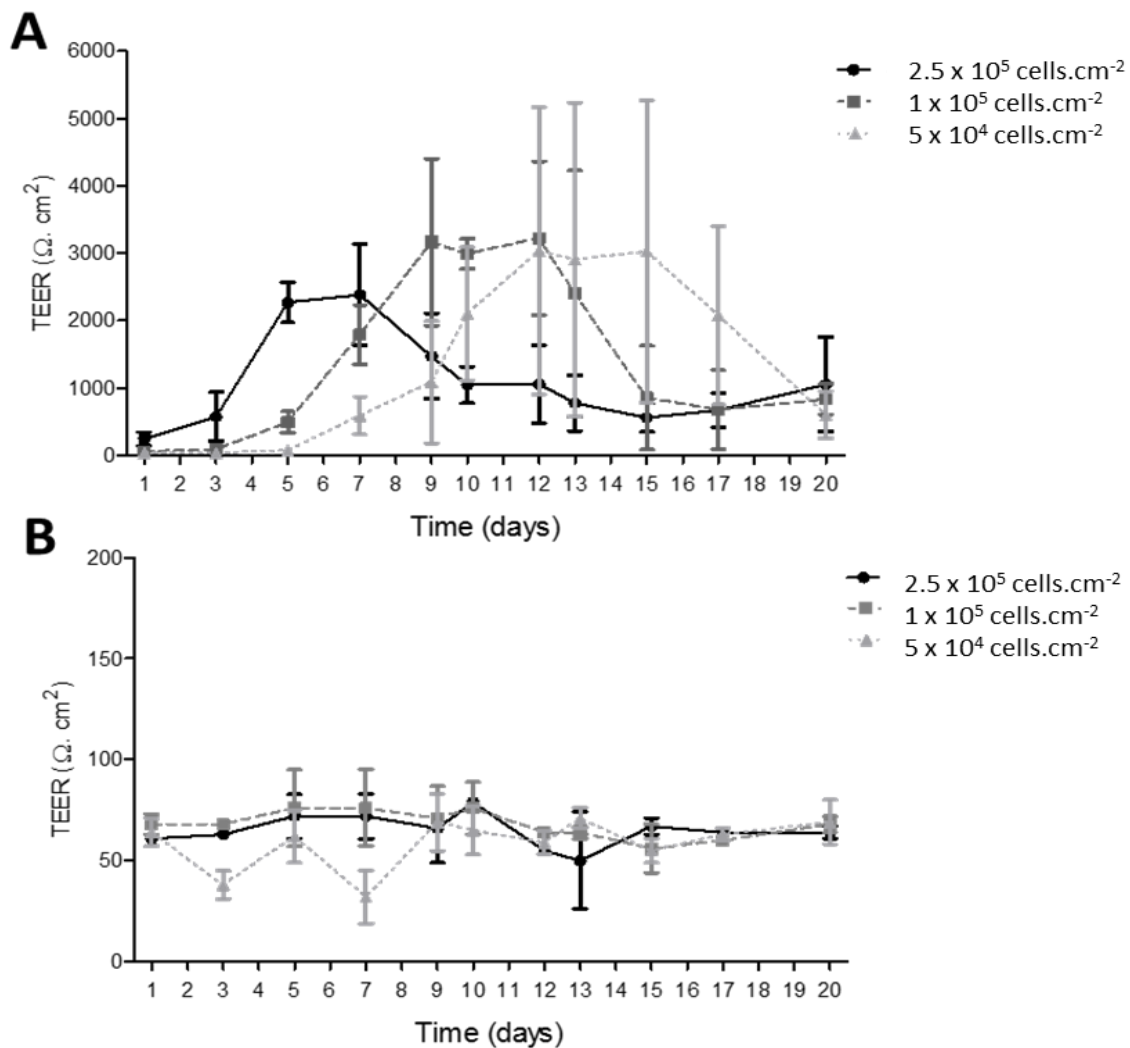


**Figure 4.4 Assessment of seeding density on epithelial cell barrier function.**

hAELVi cells (A) or A549 cells (B) were seeded at densities of  $5 \times 10^4$ ,  $1 \times 10^5$  or  $2.5 \times 10^5 \text{ cells} \cdot \text{cm}^{-2}$  on  $0.4 \mu\text{m}$  pore diameter,  $0.33 \text{ cm}^2$  Transwell® inserts. Cells were cultured under submerged conditions for 20 days, and the medium was replaced on alternate days. Every 2-3 days, TEER was recorded using EVOM2 chopstick electrodes. Results were adjusted for the resistance of the filter and normalised to the insert area. Data are represented as mean  $\pm$  SD of 4-6 inserts.

All TEER profiles for hAELVi cells followed a similar profile with increasing TEER, 3-5 days of maximum readings followed by reduced values (Figure 4.4 A). Reducing the seeding density delayed the time to reach the maximum TEER values (5-7 days for cells seeded at  $2.5 \times 10^5$  cells.cm<sup>2</sup>; 9-12 days for cells seeded at  $1 \times 10^5$  cells.cm<sup>2</sup>; 12-15 days for cells seeded at  $5 \times 10^4$  cells.cm<sup>2</sup>). Whereas TEER values were maintained above 1000  $\Omega$ .cm<sup>2</sup> for hAELVi cells once confluence was reached, TEER values for A549 cells were <100  $\Omega$ .cm<sup>2</sup> for the entire time course, indicating they did not form polarised cell layers and the absence of functional tight junctions.

The effect of cell seeding density on the viability of the epithelial cell layers was determined (Figure 4.5). For hAELVi cells, no significant difference ( $p < 0.05$ ) in extracellular LDH concentration was observed until 17 days in culture (Figure 4.5 A and B). After 17 days, extracellular LDH release increased and was comparable for hAELVi cells seeded at  $1 \times 10^5$  and  $2.5 \times 10^5$  cells.cm<sup>-2</sup> but was significantly lower ( $p < 0.05$ ) for cells seeded at the lowest density of  $5 \times 10^4$  cells.cm<sup>-2</sup>. Compared with hAELVi cells, extracellular LDH concentrations increased earlier, after day 5 in culture but were approximately 2-fold lower at the end of the study after 20 days in culture (Figure 4.5 C and D). Samples for LDH were taken from both the apical and basolateral compartment; however, in comparison with the apical compartment, LDH concentration in the basolateral compartment was negligible for the entire duration of the experiment (Figure 4.5 B and D).

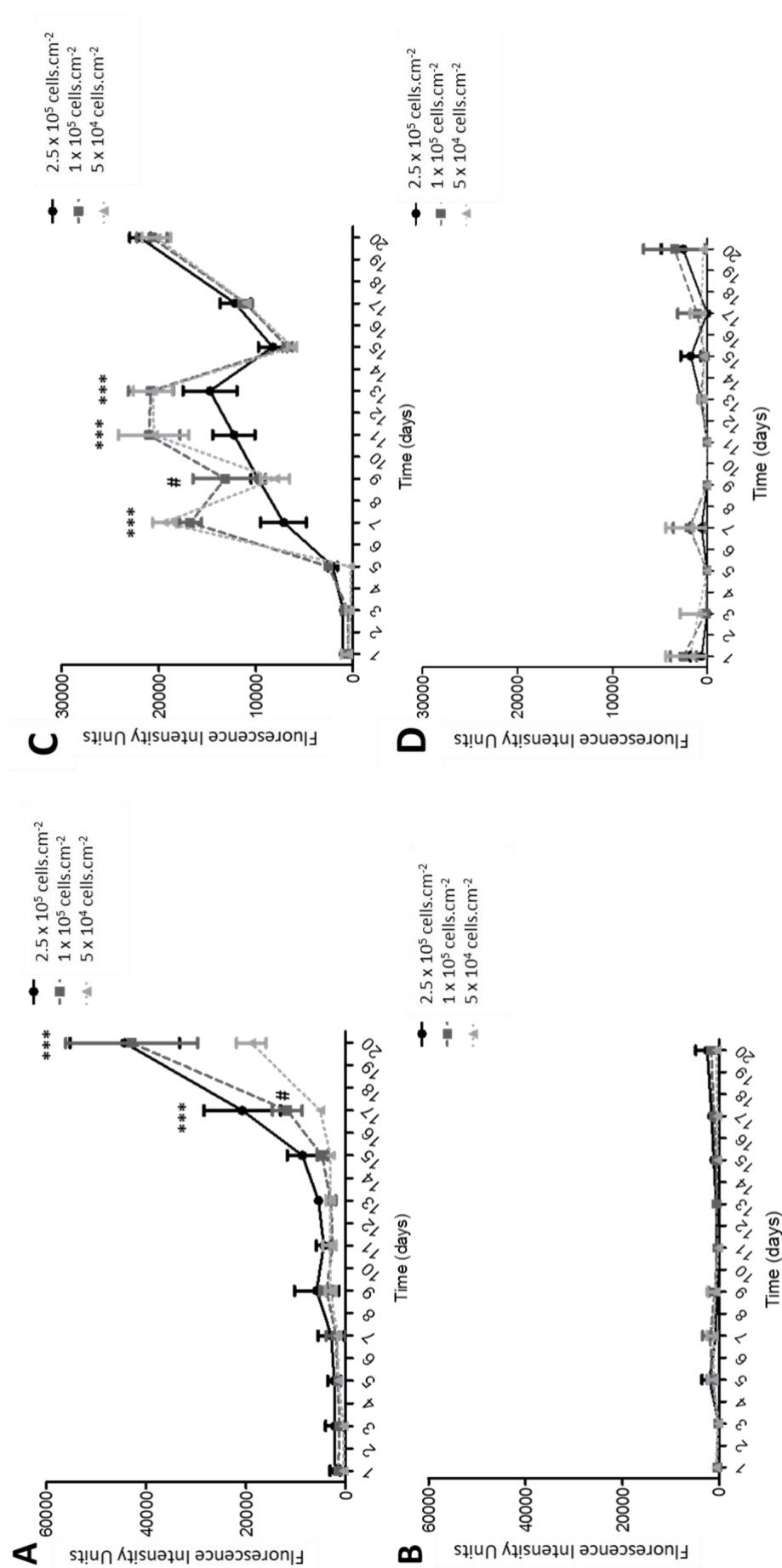


**Figure 4.5 Assessment of cell seeding density on epithelial cell viability for apical and basolateral compartments.** hAELVi cells (A, B) or A549 cells (C, D) were seeded at densities of 5 x 10<sup>4</sup>, 1 x 10<sup>5</sup> or 2.5 x 10<sup>5</sup> cells.cm<sup>-2</sup> on 0.4 µm pore diameter, 0.33 cm<sup>2</sup> Transwell® inserts. Cells were cultured under 200 µL submerged conditions up to 20 days and medium was replaced on alternate days. Every 2-3 days, medium from the apical compartment (A, C) or basolateral compartment (B, D) was sampled to assess the extracellular LDH concentration. Three supernatant samples were collected from n=4 Transwell® inserts over two passages. Data shown are the mean ± SD. Bonferroni post hoc test after two-way ANOVA where #: p<0.05, \*\*\*: p<0.0001 is shown.

#### **4.3.1.4. Suitability of epithelial culture at the air-liquid interphase (ALI)**

To evaluate the ability of epithelial cells to form polarised cell layers at the ALI, hAELVi and A549 cells were seeded onto 0.4 µm pore diameter Transwell® inserts and cultivated under either submerged liquid-liquid conditions (LLC) or at the air-liquid interphase (ALI). TEER was determined every second day for 14 days (Figure 4.6).

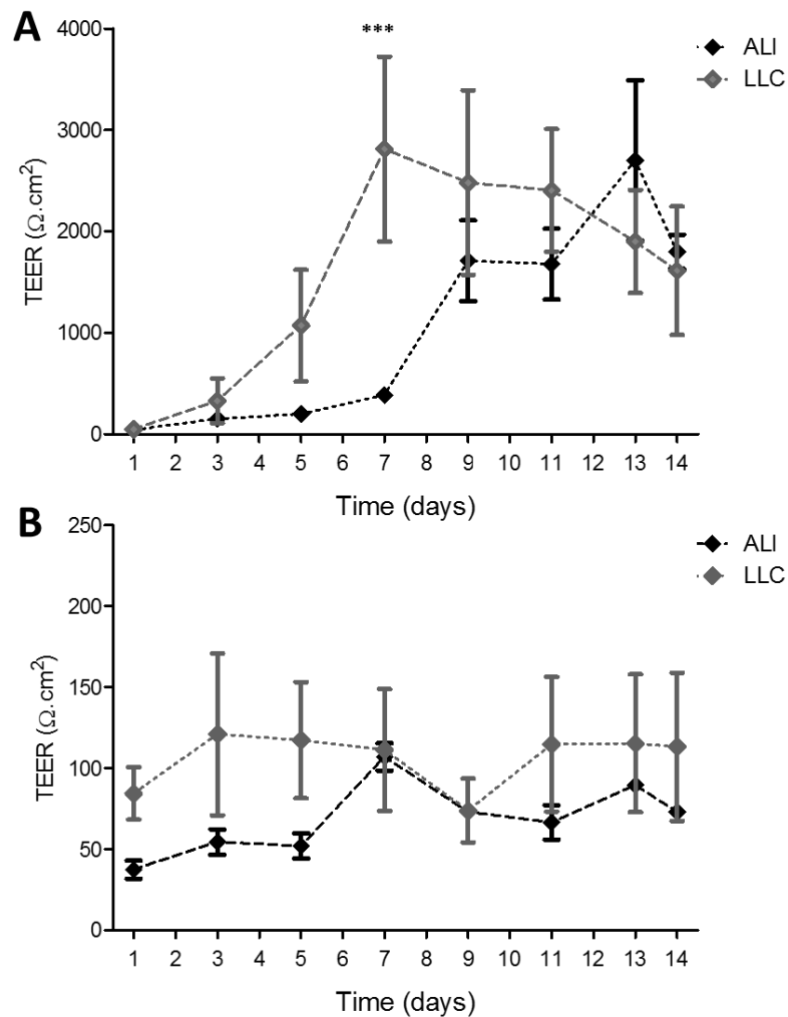


**Figure 4.6 Assessment of ALI culture on epithelial barrier function**

hAELVi cells

(A) or A549 cells (B) were seeded at  $1.5 \times 10^5$  cells.cm<sup>-2</sup> on 0.4 μm pore diameter, 0.33 cm<sup>2</sup> Transwell® inserts. Cells were cultured under either submerged conditions (LLC) or raised to the ALI for 14 days. Media was exchanged on alternate days, and TEER was recorded using EVOM2 chopstick electrodes. Results were adjusted for the resistance of the filter and normalised to the insert area. Data shown are mean ± sd (n= 5) independent Transwell® inserts; \*\*\**p*< 0.0001 vs. ALI.

hAELVi cell-cultured at the ALI took longer to reach TEER values of  $1000 \Omega \cdot \text{cm}^2$  in comparison with submerged cultures (5 days LLC vs 9 days ALI) (Figure 4.6). However, once cells reached confluency (day 9), there was no significant difference ( $p < 0.05$ ) in the TEER value. In comparison, A549 cell layers produced TEER readings  $< 150 \Omega \cdot \text{cm}^2$  for the duration of the experiment. Neither LLC nor ALI culture generated polarised cell layers with functional tight junctions.

TEER values were verified with transport studies using the paracellular marker fluorescein. Before starting the experiment, the epithelial cells at days 7 and 14 were washed twice in freshly prepared, pre-warmed Krebs-Ringer Buffer (KRB) and were further incubated with KRB for 60 min at 37 °C. To start the transport study, KRB was aspirated and 150  $\mu\text{L}$  of 50  $\mu\text{M}$  fluorescein sodium (FluNa) in KRB  $\pm$  16 mM EDTA was added to the apical (donor) compartment, and 450  $\mu\text{L}$  KRB was put into the basolateral compartment (acceptor). Samples were directly taken from the donor (20  $\mu\text{L}$ ) at the start, and the end of the experiment and from the acceptor compartment (200  $\mu\text{L}$ ) and were subsequently transferred into a 96- well plate. Samples from the basolateral compartment were taken and replaced with 200  $\mu\text{L}$  of fresh transport buffer every 15 min for 90 min. The samples were then measured using BMG labtech CLARIOstar® at 485 nm (em) and 520 nm (ex) wavelengths. Each experiment was run in triplicate.

Fluorescein  $P_{\text{app}}$  was comparable between cells cultured under LLC and ALI conditions (Figure 4.7). This was achieved by measuring the permeability of fluorescein through cell monolayers. The hydrophilic molecule is used as a marker to assess paracellular transport, alone or in combination with EDTA, where EDTA modulates cell barrier integrity called tight junctions. Generally, barrier cells

mechanically restrict the diffusion of lipids and proteins via the paracellular route. Thus, high TEER is accompanied by low paracellular transport. This effect was observed on day 7 and day 14. In the presence of EDTA, TEER dropped to zero, and the  $P_{app}$  value of fluorescein reached maximum output, resulting in the opening of the tight junctions and elevated transport of fluorescein to the basolateral compartment. In line with TEER data obtained, Fluorescein  $P_{app}$  was significantly lower ( $p<0.05$ ) for hAELVi cells cultured for 14 days compared with a 7 day culture period, indicating tight junction maturation overtime culture at both LLC and ALI.

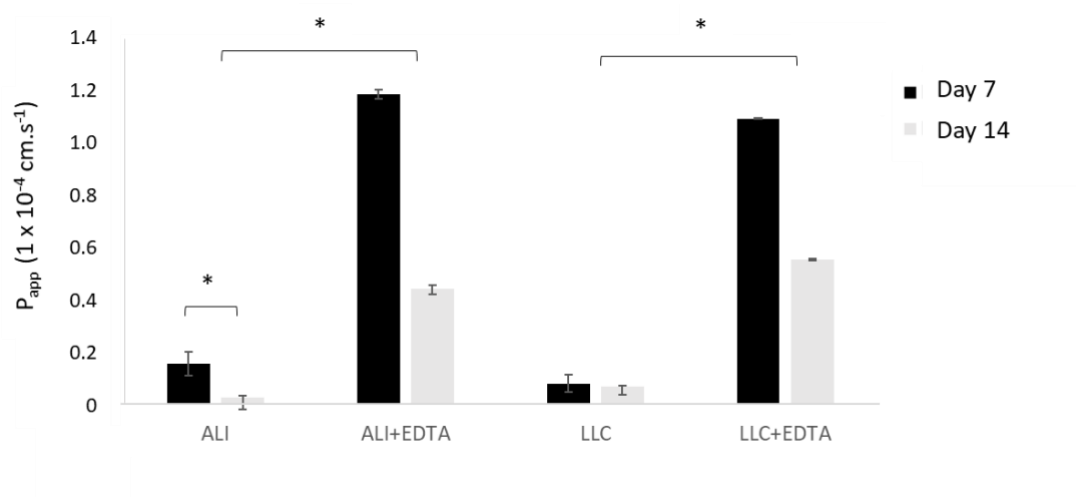


**Figure 4.7 Assessment of paracellular permeability for hAELVi cell layers using paracellular marker fluorescein.**

EDTA was used to disrupt tight functions as a negative control. hAELVi cells were seeded on 0.4  $\mu\text{m}$  pore diameter, 0.33  $\text{cm}^2$  Transwell® inserts and cultured under submerged conditions (LLC) or raised to the ALI for 7 and 14 days. Cells were assessed for apparent permeability using a paracellular marker, 50  $\mu\text{M}$  fluorescein. Data shown are mean  $\pm$  sd ( $n = 4$ ) independent Transwell® inserts; \* $p < 0.05$ .



### 4.3.2 Construction of immunocompetent alveolar co-culture systems

The resulting methodology for model construction was determined by cell viability and functionality for all cell types used in this chapter (Figure 4.8)

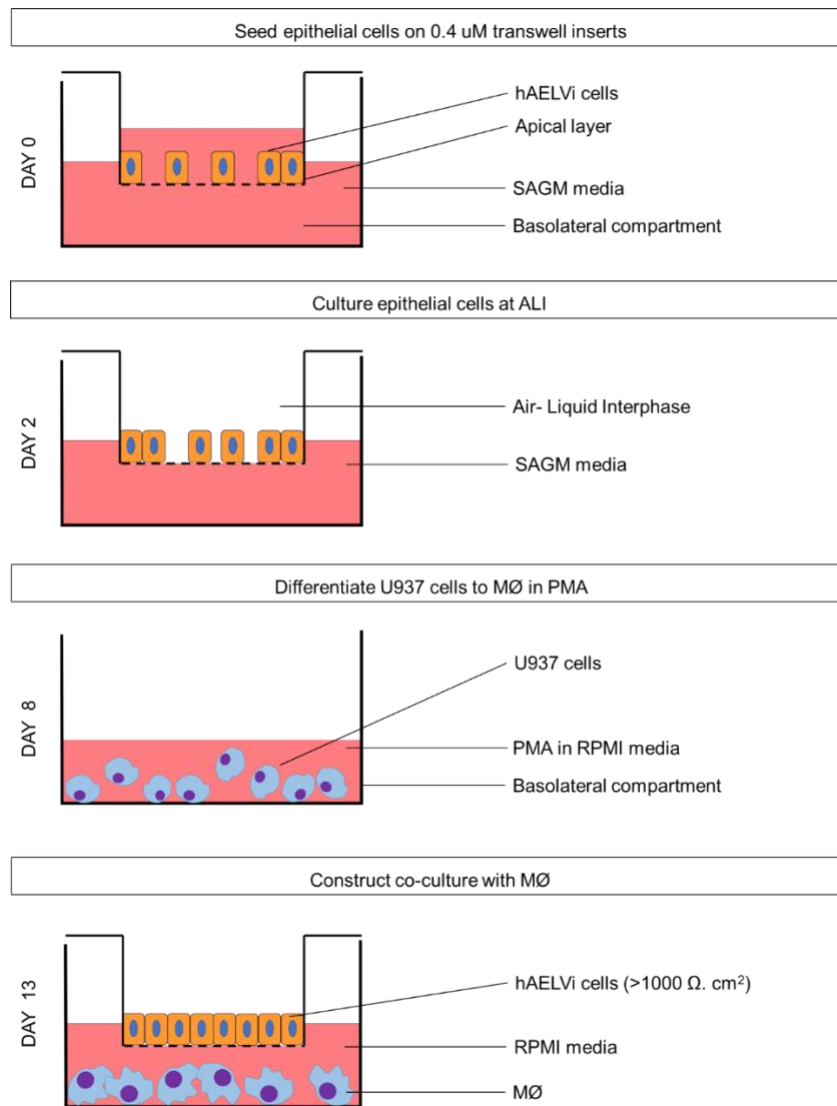


**Figure 4.8 Generation and construct methodology for T I model.**

Optimised co-culture model of human alveolar type I epithelial cells (hAELVi) and differentiated U937 cells (MØ). Models were incubated for 24 h under normal cell culture conditions following construction.

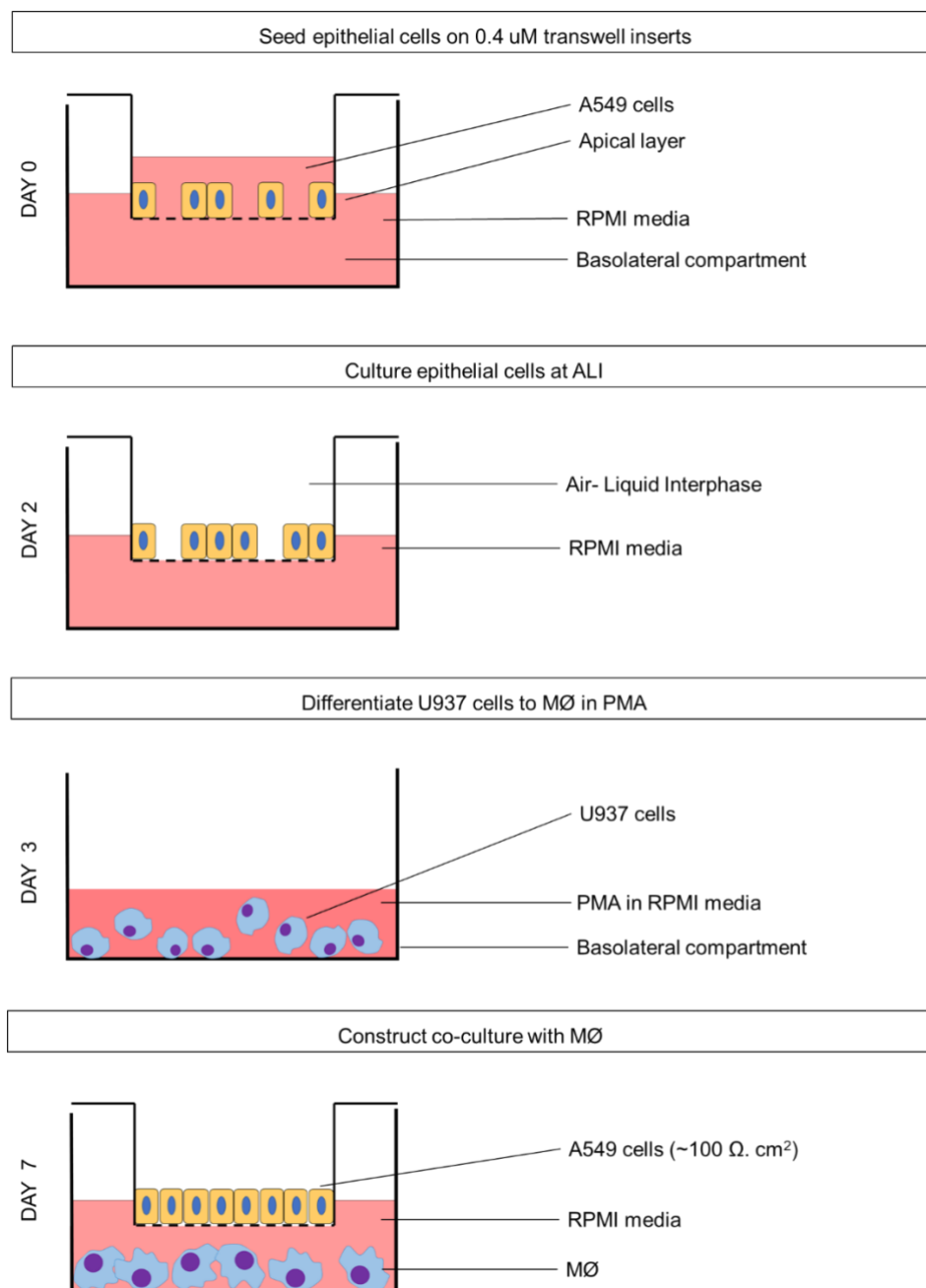


**Figure 4.9 Generation and experimental set-up for T II model.**

Optimised co-culture model of human alveolar type II epithelial cells (A549) and differentiated U937 cells (MØ). Models were incubated for 24 h under normal cell culture conditions following construction.

### **4.3.3 Characterisation of immunocompetent alveolar co-culture systems**

Two alveolar co-culture models were constructed: type I epithelial co-culture model (hAEVLI cells and PMA differentiated U937 cells) and type II epithelial co-culture model (A549 cells and PMA differentiated U937 cells). Based on earlier work, optimisation studies conditions were utilised. To sensitise the model, both co-culture models were assessed for viability and functionality of each cell type within the co-culture with and without stimulation with LPS.

#### **4.3.3.1. Characterisation of cell health**

Extracellular LDH concentration was assessed as a measure of cell health and compared for PMA differentiated U937 cells in monoculture and the type I and type II epithelial co-culture models with and without exposure to LPS (Figure 4.10). Tukey's post hoc test was adopted to compare all possible pairs of means. No significant difference ( $p < 0.05$ ) was observed in extracellular LDH concentration between PMA differentiated U937 cells in monoculture or co-culture with type I epithelial cells. However, there was a significant increase ( $p < 0.05$ ) in extracellular LDH concentration between PMA differentiated U937 cells in monoculture and the type II epithelial cell co-culture system. Treatment with LPS did not significantly ( $p < 0.05$ ) alter cell viability in any of the models tested.

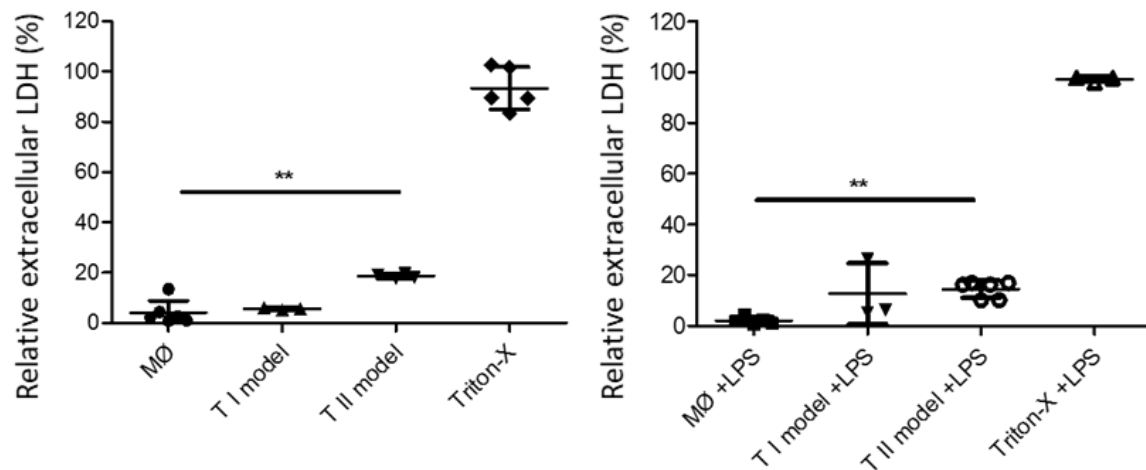
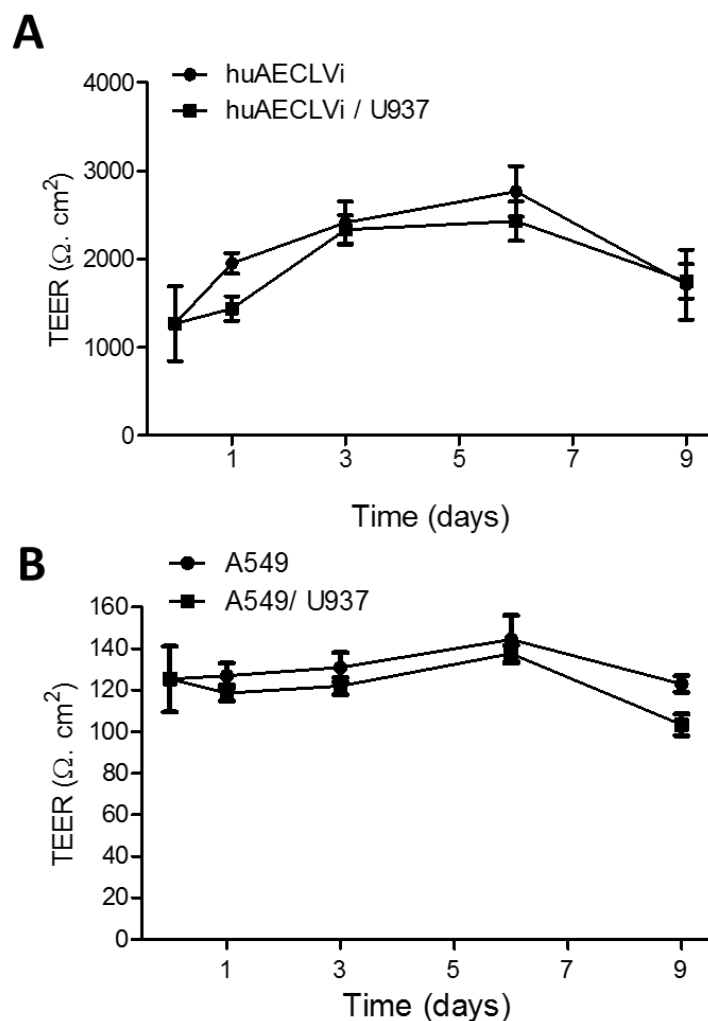


**Figure 4.10 Assessment of co-culture system on cell health.** Relative extracellular LDH release in relative to lysed control (Triton-X 100) for PMA differentiated U937 cells cultured in monoculture or co-culture with hAELVi cells (TI model) or with A549 cells (Type II model) naïve (A) and stimulated with 10 ng/mL LPS for 24 h(B). Extracellular LDH concentration was assessed 2 days after models were constructed. A one way ANOVA was used to determine significance for each treatment group, and Tukey's multiple comparison post hoc test was employed when\*  $p < 0.05$ , \*\* :  $p < 0.001$  Data shown represent  $n = 6$  data points  $\pm$  SD of three independent cell model experiments.

#### 4.3.3.2. Characterisation of co-culture barrier function

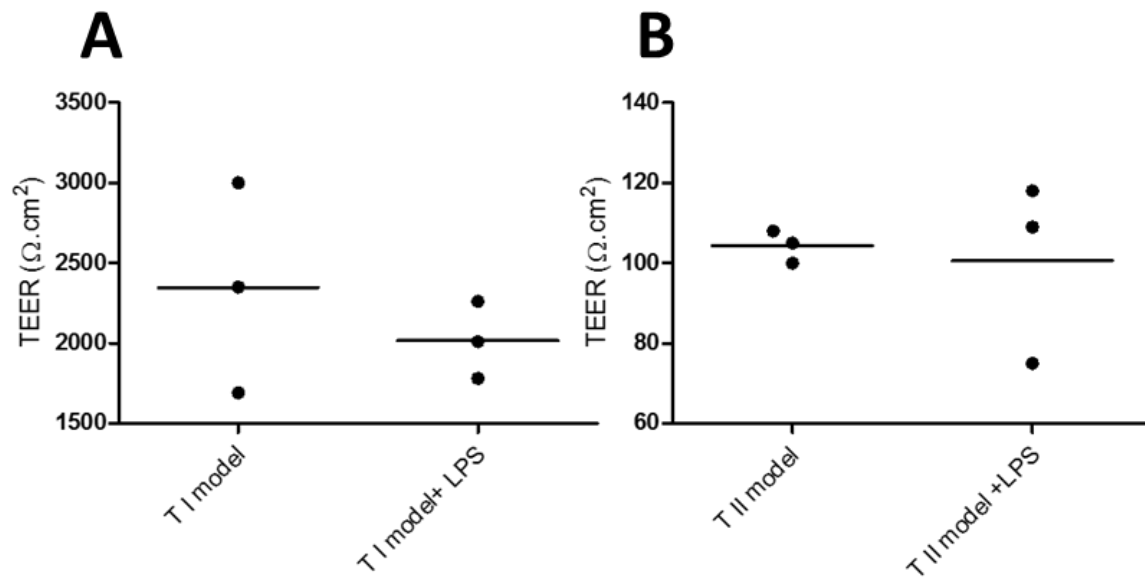
Comparison of epithelial cell TEER values in monoculture and co-culture systems with PMA-differentiated U937 cells was assessed for hAELVi and A549 cells up to 9 days after model construction (Figure 4.11). For the type I epithelial cell co-culture model (hAELVi), TEER remained above 1000  $\Omega \cdot \text{cm}^2$  for the duration of the experiment and peaked  $\sim 2500 \Omega \cdot \text{cm}^2$  at day 6. No significant difference was observed in TEER for hAELVi cells cultured alone or in the presence of PMA differentiated U937 cells (Figure 4.11 A). In contrast, A549 cells cultured alone or in co-culture with PMA differentiated U937 cells recorded TEER values  $<140 \Omega \cdot \text{cm}^2$  for the duration of the experiment indicating A549 cells did not form polarised cell layers with functional tight junctions (Figure 4.11 B).

Exposure of the model to 10 ng/mL LPS for 24 h did not significantly alter barrier function ( $p < 0.05$ ) (Figure 4.12), however, it did cause a decrease in variability for the TEER values obtained for the type I epithelial co-culture model.



**Figure 4.11 Assessment of co-culture system on epithelial barrier function.**

TEER measurements for (A) hAELVi (B) A549 cells in monoculture and co-culture with PMA differentiated U937 cells at ALI Medium was exchanged on alternate days, and TEER was recorded using EVOM2 chopstick electrodes every third day. Results were adjusted for the resistance of the filter and normalised to the area of the insert. Data shown are mean  $\pm$  sd (n= 5) independent Transwell® inserts.

**Figure 4.12 Assessment of LPS exposure on epithelial barrier function in the co-culture systems.**

TEER measurements for hAELVi cells - T I model (A) or A549 cells- T II model (B) cultured with PMA differentiated U937 cells either naïve or stimulated with 10 ng/mL LPS for 24 h. TEER measurements were recorded using EVOM2 chopstick electrodes 2 days after model construction. Results were adjusted for the resistance of the filter and normalised to the area of the insert. Data shown are mean  $\pm$  sd (n= 3) independent Transwell® inserts. A paired T-test determined no significance ( $P>0.05$ ).

#### **4.3.3.3. Characterisation of macrophage functionality**

The influence of epithelial cells in the co-culture system on the phagocytic ability of PMA differentiated U937 cells was assessed by incubating cells with 1.0µm FluoSpheres™ for 2 h. Macrophages in both monoculture and co-cultures phagocytosed microspheres confirmed by fluorescent microscopy (Figure 4.13) and a flow cytometry (Figure 4.14)



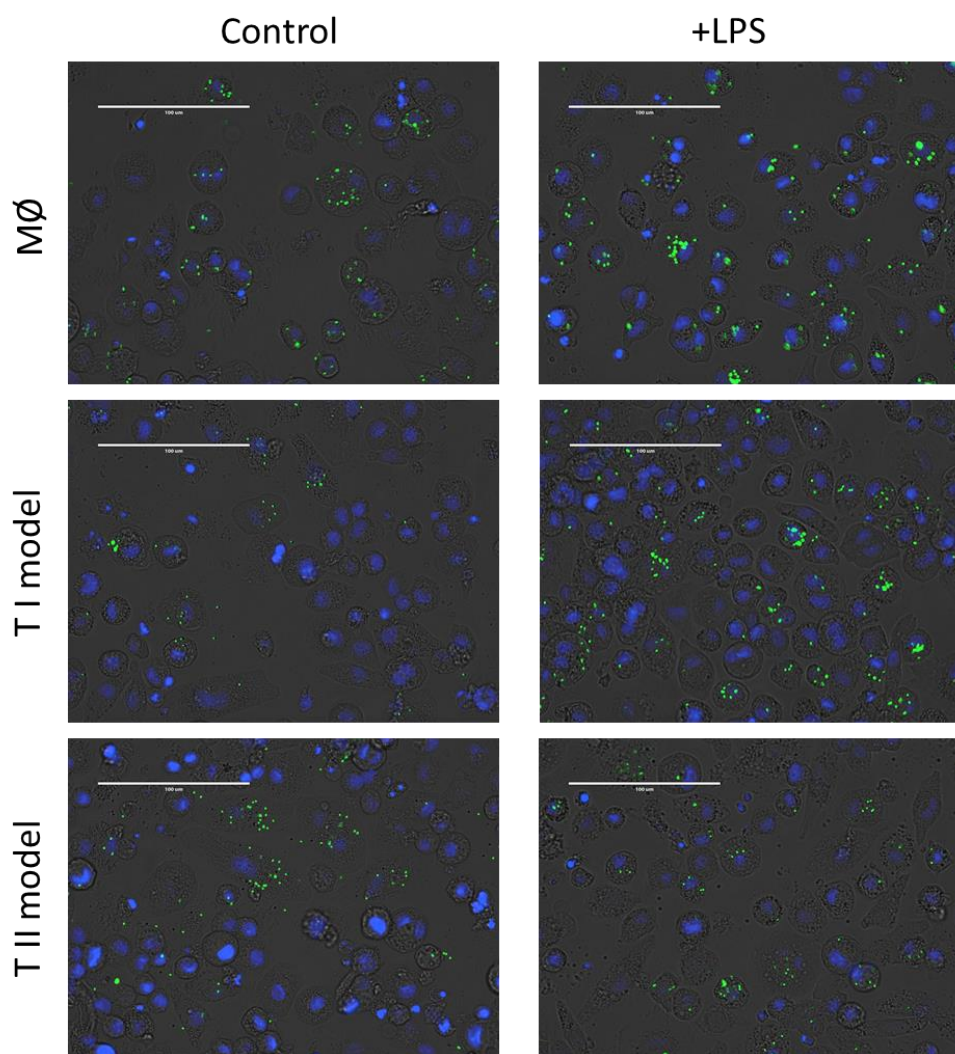


**Figure 4.13 Phagocytic observations for PMA differentiated cells in monoculture and co-culture systems.**

PMA differentiated U937 cells were cultured in monoculture or co-culture with hAELVi cells (T I model) or A549 cells (T II model). Models were either naïve or exposed to 10 ng/ mL LPS (+ LPS) for 24 h. Phagocytosis assessment was performed after 2 h incubation with 1.0 µm FluoSpheres™ Carboxylate-Modified microspheres using fluorescent microscopy. FluoSpheres were labelled with Yellow-green fluorescent and imaged using ex/em (505/515). Cell nuclear were stained with Dapi (blue) and visualised ex/em (358/461). Images were obtained at 40 x magnification. The scale bar is 100 µm. Repeats were n=3 for 3 independent models.

Flow cytometry quantitatively assessed phagocytosis for PMA differentiated U937 cells in monoculture and T I and II co-culture models. Incubation with inflammatory stimulant LPS resulted in a significant decrease ( $p < 0.0001$ ) in phagocytic functionality for PMA differentiated U937 cells in monoculture and the T II model (by 14%), whereas no significant change ( $p < 0.05$ ) in phagocytic ability was observed for the T I mode in the presence of LPS. In contrast, there was no significant influence ( $p < 0.05$ ) on phagocytic ability for PMA differentiated U937 cells co-cultured with A549 cells, the phagocytic ability of the PMA differentiated U937 cells (MØ) in the T I model was significantly reduced by ~20% ( $p < 0.001$ ).

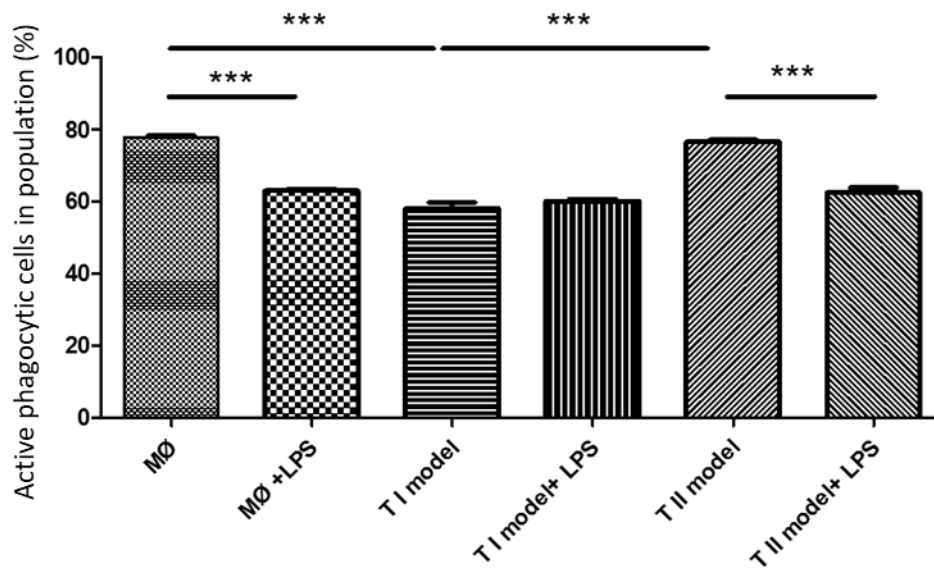


**Figure 4.14 Phagocytic activity of PMA differentiated U937 cells (MØ) in monoculture and co-culture systems.**

PMA differentiated U937 cells were cultured in monoculture or co-culture with hAELVi cells (T I model) or A549 cells (T II model). Models were either naïve or exposed to 10 ng/ mL LPS (+ LPS) for 24 h. Phagocytosis assessment was performed after 2 h incubation with 1.0 µm FluoSpheres™ Carboxylate-Modified microspheres using flow cytometry. 1000 cells were assessed for n=3 independent models. The percentage of cells taken up the FluoSpheres™ relative to the whole population was calculated. A one-way ANOVA was used to determine significance for each treatment group, and Tukey's multiple comparison post hoc test was employed when \*\*\*:  $p < 0.0001$ .

#### **4.3.3.4. Determination of inflammatory mediator synthesis**

A panel of 24 inflammatory molecules were used to investigate how the cytokine/chemokine secretion signatures may alter between monoculture and co-culture systems. Models were assessed either naïve or stimulated with 10 ng/mL LPS for 24 h (Figure 4.15) and (Figure 4.16). Significant cytokine presence between non stimulated versus LPS stimulated models shown in Table 4.2.

All cytokines expressed in PMA differentiated U937 cells and hAELVi cells were detected in the type I epithelial co-culture system except for MIF and IL-17E (Figure 4.16). However, IL-17, IL-4, IL-2 and IL-1ra, which were not expressed in either of the monoculture cell lines, were detected in the type I epithelial co-culture system.

Compared to hAELVi cells, A549 cells expressed more cytokines/chemokines (16 vs 6). All cytokines expressed in PMA differentiated U937, and A549 cells were detected in the type II epithelial co-culture system at a similar level except IP-10. IL-23 was detected in the type II co-culture system but not in either of the cell types in monoculture (Figure 4.16).

Changes in cytokines and chemokine production of the functionality of the models stimulated with 10 ng/mL LPS for 24 h were assessed (Figure 4.17). The type I epithelial co-culture model observed no difference in the cytokine/chemokine profiles. However, PMA differentiated U937 cells expressed IL-17, IL-4 and IL-2 when stimulated with LPS but not in the naïve cells. Furthermore, all 24 cytokines/chemokines were detected in the type II epithelial co-culture system after stimulation with LPS, including sTREM-1, MIP 1b, MIP1a, MIF, IP10, IL32a, IL6, and IFN  $\gamma$  (Figure 4.17 C).

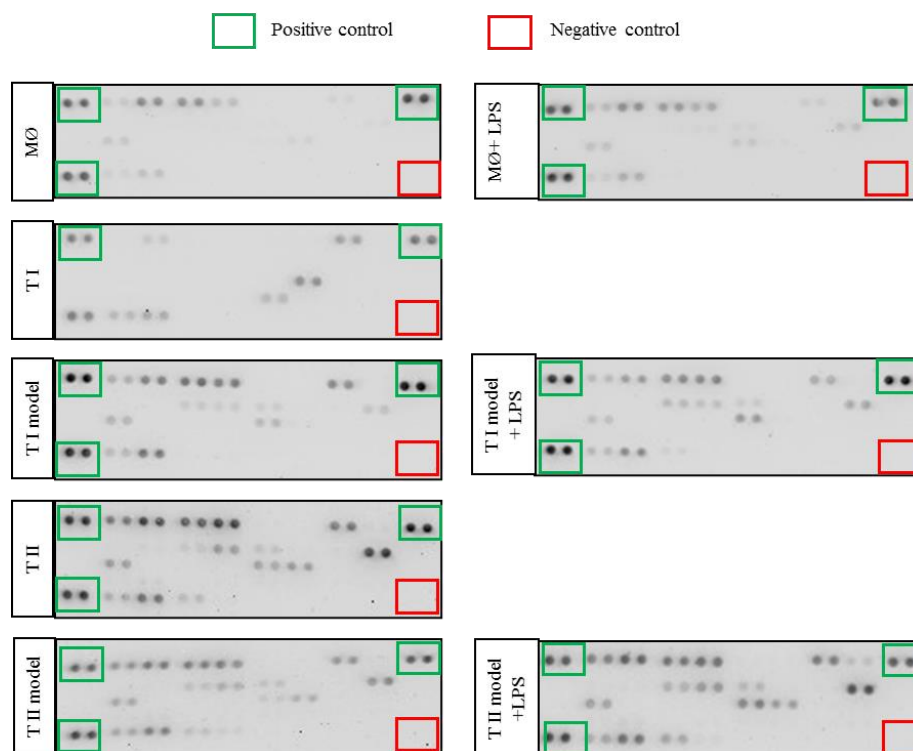


**Figure 4.15 Human cytokine profile of lower airway for ALI cell models.**

Detection of spots on array membranes from supernatant collected from monoculture and co-cultures of differentiated U937 cells (MØ) with LPS (MØ+ LPS), hAECLVi TI cells (T I), A549 TII cells (T II), type I co-culture model: hAECLVi and MØ (T I model) with LPS (T I model +LPS), type II co-culture model: A549 and MØ (T II model) with LPS (T II model +LPS). Models were untreated or stimulated with 100 ng/ mL LPS for 24 h. Controls are shown as positive (green) and negative (red). Data represents four independent Transwell® inserts.

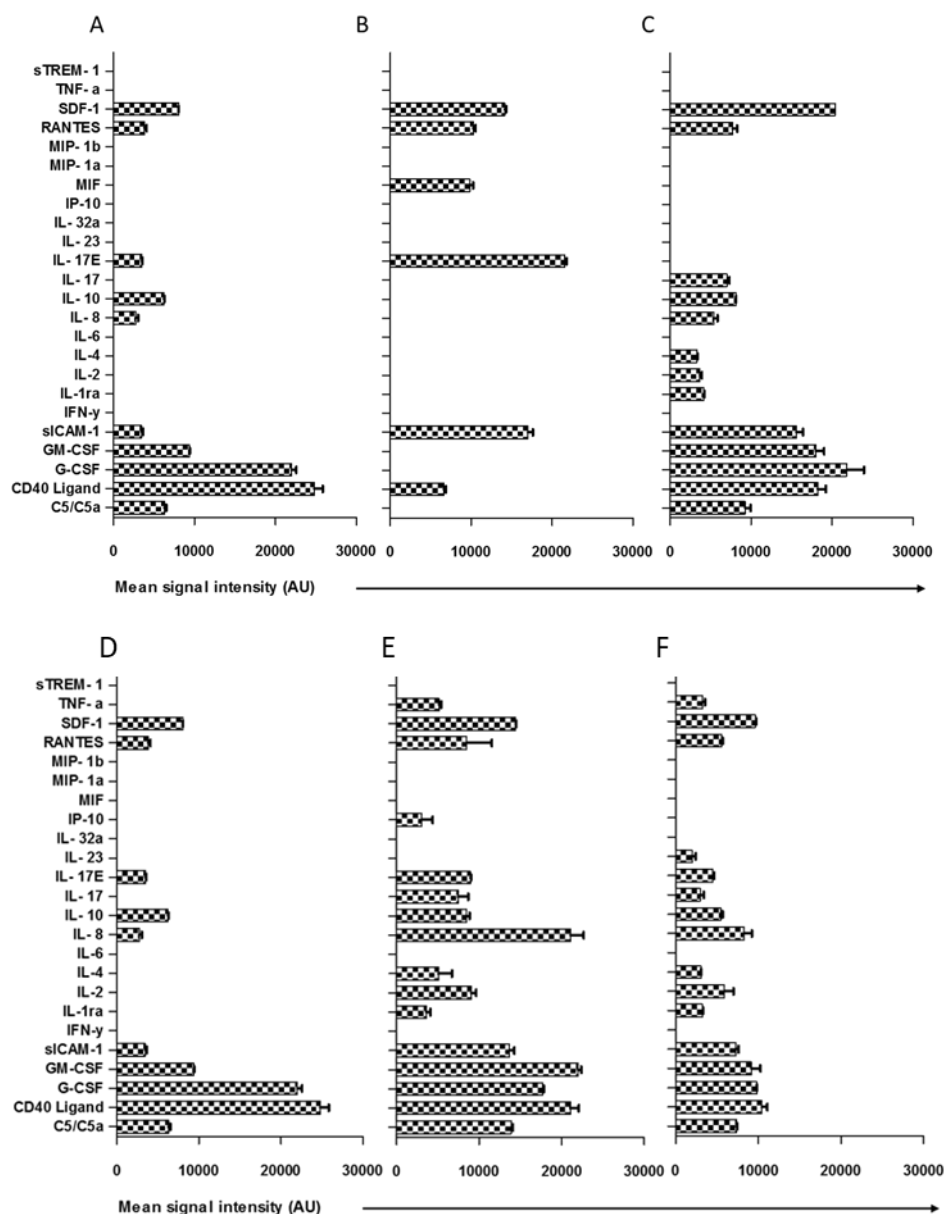


**Figure 4.16 Expression of human cytokines/chemokines panel for monoculture and co-culture type I and II systems.**

PMA differentiated U937 cells (A), and hAELVi cells (B) were cultured in monoculture or co-culture (C) (T I model). PMA differentiated U937 cells (D) and A549 cells (E) were cultured in monoculture or co-culture (F) (T II model). Supernatant was assayed for the presence of 24 cytokines/chemokines. Data represents mean signal intensity (AU) of each protein spot from the blot detected using chemiluminescence imaging and quantified using ImageJ software for four independent Transwell® inserts  $\pm$  SD.

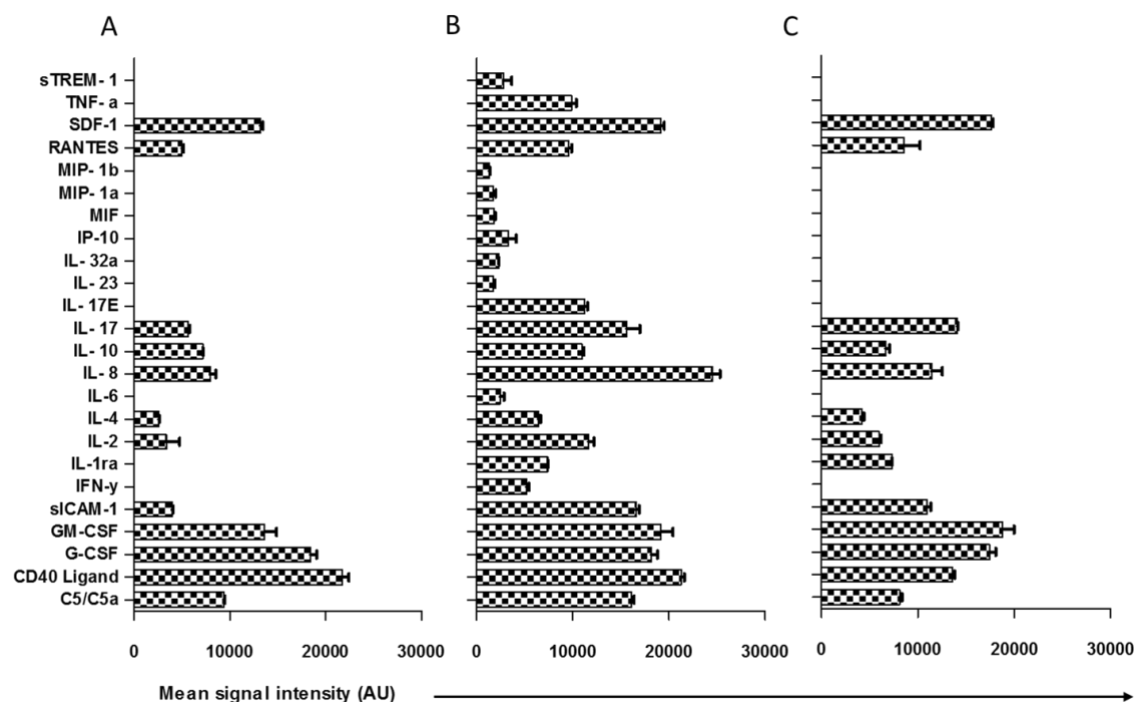


**Figure 4.17 Expression of a panel of human cytokines/chemokines for monoculture and co-culture systems stimulated with LPS.**

PMA differentiated U937 cells (A) in co-culture with hAELVi cells – type I (B) or A549 cells type II (C). Supernatant was assayed for the presence of 24 cytokines/chemokines. Data represents mean signal intensity (AU) of each protein spot from the blot detected using chemiluminescence imaging and quantified using ImageJ software for four independent Transwell® inserts  $\pm$  SD.

#### 4.3.3.5. Comparison of cell models functionalities with specific cytokine markers

**Table 4.2 Human cytokine profile of lower airway of monoculture and co-culture models in LPS.**

	MØ only		T I model		T II model	
	Non-stimulated	+ LPS	Non-stimulated	+ LPS	Non-stimulated	+ LPS
C5/C5a		***		***		
CD40 Ligand		***		***		***
G-CSF		***		***		***
GM-CSF		***		***		
sICAM-1				***		***
IFN- $\gamma$				***		
IL-1ra				***		***
IL-2		***		***		**
IL-4		***		***		
IL-6				***		
IL- 8		***		***		***
IL- 10				***		
IL- 17		***		***		***
IL- 17E		***		***		
IL- 23						
IL- 32 $\alpha$				***		
IP-10				***		
MIF				*		
MIP- 1 $\alpha$				*		
MIP- 1 $\beta$						
RANTES				***		
SDF-1		***		***		***
TNF- $\alpha$				***		
sTREM- 1				***		

**\*Significance at \*P< 0.05, \*\* P<0.01 and \*\*\*P< 0.001**

Cytokine presence in models: MØ only (differentiated U937 cells), T I model (MØ and hAELVi cells) and TII model (MØ and A549 cells) indicated in green with no detection in red. Two-way ANOVA analysed data with Bonferroni post hoc test of non-stimulated cells vs LPS stimulation.



## 4.4. Discussion

### 4.4.1 Optimising the in vitro co-culture systems

Co-culturing multiple cell types within the same culture system require extensive optimisation of the culture conditions to achieve optimal viability and functionality of all cells. It is well reported in the literature that cells in co-culture have synergistic functionality not observed in the cells in monoculture. This is likely due to cell-cell interactions (Grabowski *et al.*, 2016). Specifically for co-culture models of the airways described by Kletting (Kletting, 2016).

#### 4.4.1.1. Composition of cell culture medium

The composition of the cell culture medium can be an important factor in determining the function and viability of cells (McKee *et al.*, 2017). In a co-culture system, where different cell types may have different nutrient requirements, a compromise in the medium composition may have to be struck to sustain all cells in the co-culture system adequately. In chapter 3, PMA differentiated U937 cells were characterised in standard non-defined (FBS containing) RPMI-based medium, which is well established for the cell line (Kitamura *et al.*, 2004; Python *et al.*, 2007). Maintaining an alveolar macrophage-like functionality in co-culture was the primary goal, the suitability of alveolar epithelial cell lines with the U937 CCM was assessed. A549 cells have been characterised in the U937 CCM in the literature, and the data from (Cooper *et al.*, 2016) supports that cell viability and proliferation of the A549 cell line was adequately supported in the U937 CCM.

Whilst variability in LDH release from hAELVi cells was observed for individual days when cultured in U937 CCM, hAELVi CCM and the 1:1 mixture, the profiles over time remained similar, suggesting medium composition did not adversely affect whole population hAELVi cell health (Figure 4.1). However, hAELVi cell proliferation was lower when cultured using hAELVi CCM than the other media types. Therefore, the LDH release per cell was significantly ( $p<0.05$ ) elevated for hAELVi cells cultured in hAELVi CCM compared to the other medium types indicating the U937 CCM may be preferable for maintaining cell health.

The hAELVi CCM is a more defined culture medium (containing bovine pituitary extract, hydrocortisone, human epidermal growth factor, epinephrine, transferrin, insulin, retinoic acid, triiodothyronine and bovine serum albumin) more typically used for primary cell culture and to support the specific requirements for cell growth and proliferation (Wirth *et al.*, 2016). In contrast, the U937 medium uses the FBS to provide growth factors and hormones required for cell growth and proliferation. It was demonstrated by Wirth *et al.* that hAELVi cells cultured in FBS-containing CCM displayed low proliferation and that the defined medium was more suited for the hAELVi cells to maintain exponential growth characteristics. However, to limit this effect, the U937 CCM would only be used to maintain the cells once differentiated into polarised cell layers, whereafter nutritional requirements for proliferation would be reduced.

#### 4.4.1.2. Culture substratum

It is well established that the surface on which cells are cultured has a significant impact on their morphology and functionality (Ryan, 2008). *In vivo*, alveolar epithelial cells would be growing on basement membranes made up of collagen and laminin, which provide multiple functions, including cell anchoring, immunomodulation, and signalling (Jadad *et al.*, 1996). *In vitro*, the polycarbonate Transwell® insert can not provide these exact conditions. Pores in the Transwell® insert are essential to allow the flow of nutrients from the basolateral compartment to the epithelial cells on the apical side of the insert. Pore diameter has been shown to influence cell viability and a balance between permitting sufficient medium exchange and optimal surface properties for cell attachment (Wirth *et al.*, 2016). Figure 4.3 indicated pore diameter affected cell health of cultures only after 6 days in culture once cell layers were established, suggesting it might have less influence on cell attachment for these cell lines. Similarly, hAELVi were cultured on 0.4 or 3 µm Transwell membranes. Larger pore membranes showed cells to have significantly ( $p > 0.05$ ) reduced TEER values. Kletting *et al.* described optimal pore size for Transwell® insert to be 0.4 µm for hAELVi with functional TEER values  $< 2000 \Omega \cdot \text{cm}^2$

#### 4.4.1.3. Cell seeding density

The density at which cells are seeded on the culture substratum can directly affect the cell's functionality. High seeding densities deplete medium supplements faster, accelerating local pH concentration changes due to increased metabolic loading (Tang *et al.*, 2009). This was observed in figure 4.5, where hAELVi cells seeded at a higher density were associated with increased cell death. Furthermore, the negligible levels of LDH detected in the basolateral compartment suggest that cells attached to the

insert membrane maintain viability. In contrast, the significantly higher concentrations of LDH detected in the apical chamber are associated with cell death for cells on top of the cell layers.

Regarding epithelial cell barrier function, the cell seeding density directly affects the time to produce confluent cell layers and determines the timeframe for proliferation, differentiation and maturation of primary hAELVi and Caco-2 cell layers (Elbert *et al.*, 1999; Volpe, 2008). Extreme low or high seeding densities may even prevent the formation of functional cell layers altogether. This was observed in Figure 4.4A, where reducing the seeding density of hAELVi cells delayed the time to reach maximum TEER for the cell layers but increased variability of the polarised cell layers as small differences in cell number proliferative ability are amplified with increased population doublings.

#### **4.4.1.4. Culture at the ALI**

It is well documented that cells exposed to the same physical stimuli they would encounter *in vivo* differentiate to a more *in vivo*-like phenotype (Fatehullah *et al.*, n.d.; Finnberg *et al.*, 2017). Airway epithelial cells are exposed to air at their apical surface, and there is extensive literature for a range of airway epithelial cell types that culture at an ALI promotes cells with a closer morphology to their native tissues (C. Ehrhardt *et al.*, 2002; Grainger *et al.*, 2006). Specifically, hAELVi cells cultured at the ALI display tight junctions (C. Ehrhardt *et al.*, 2002) and differentiate to a phenotype that more closely resembles the elongated morphology typical of type I epithelial cells in the human alveoli (Elbert *et al.*, 1999). Similarly, A549 display oxidative stress levels

and release of proinflammatory mediators IL-1 $\beta$ , IL-6, IL-8 detected *in situ* (Kooter *et al.*, 2013; G. Wang *et al.*, 2020).

In line with other airway epithelial cell lines and research published on hAELVi cells, whilst culture at the ALI may enhance desired morphological features, barrier function is reduced (Figure 4.6A). However, TEER values were still suitable to model the barrier function of the alveolar epithelium and in line with other published reports (Wirth *et al.*, 2016). Paracellular permeability of the hAELVi cell layers was in line with that published in the literature ( $\sim 1 \times 10^{-6} \text{ cm.s}^{-1}$ ) and indicative of functional polarised cell layers. Additionally, the permeability of hAELVi cell layers on day 7 was less variable in LLC compared to those at ALI, which was reduced ( $p < 0.05$ ) on day 14 in line with literature and proliferation studies (Kletting, 2016). The well-documented A549 cells that are alveolar type II epithelial cells do not form polarised cell layers, which is also observed in Figure 4.6 – 4.7. Whilst barrier function is important in the co-culture model to provide barrier characteristics and assess permeability *in vitro*, A549 cells also offer the advantage of representing other features such as alveolar surfactant production and other biochemical signalling (Cooper *et al.*, 2016; Hiemstra *et al.*, 2018).

*In vitro* co-culture construction requires careful consideration for optimal alveolar conditions. Few models have been characterised to such conditions to include optimal seeding densities and medium, showing significant differences in cell morphology and biochemistry (Victoria Hutter, 2012; Kletting, 2016). Similarly, the culture of differentiated U937 cells in SAGM activates proliferation compared to the cell's proliferation profiles in RPMI, further differentiating the U937s from their known baseline and *in vivo* like representation.

#### 4.4.2 Characterisation of co-culture model

It is well documented that different cells types cultured in the same environment can alter the functionality of the other cells in culture, inhibit or enhance response synergistically, or display new functionalities not observed with each cell type alone (Haghi *et al.*, 2015). Given this, it is important to characterise the co-culture systems' functionality to understand better these synergies and how they influence our modelling and understanding of cell responses *in vitro* systems. The maturation state of AMs can typically be characterised by the expression of specific surface markers and AM functionality. At the site of insult of infection, inflamed cells are often described as being in an activation state (Mosser, 2003), which can be obtained by stimulating differentiated U937 cells with an inflammatory activator, for instance, lipopolysaccharide (LPS). Use of LPS activation for monocyte-derived macrophages, mainly U937 and THP-1 but also ML-2, HL-60 and MonoMac 6 cells, have been used in biomedical research and show no impact on cell health co-culture models in line with this chapter's findings (Qin, 2012; Sharif *et al.*, 2007; Ziegler-Heitbrock *et al.*, 1994).

Raised LDH concentrations in the TII model compared with those of the TI model or differentiated U937 cells in monoculture are most likely related to the A549 cells inability to form tight junctions. Unlike hAELVi cells, the release of LDH from A549 epithelial cells is not restricted to the apical layer and instead migrates to the medium in the basolateral layer of the well towards AMs. Increased LDH concentrations may additionally signal an inflammatory response of the AMs (Drent *et al.*, 1996) and supports the validity of the U937/ A549 alveolar models through sensitivity to stimuli and cell to cell communication as previously described (Crabbe *et al.*, 2011).

#### 4.4.2.1. Macrophage co-culture characterisation

Striz *et al.* showed that cell contacts between pulmonary epithelium (A549) and THP-1 are important for regulating the phenotype of human macrophages (Stříž *et al.*, 2001). The phagocytic functionality of alveolar like macrophages assessed in co-culture remained consistent, at 80% active phagocyte population for the TII model but significantly reduced for the TI model compared to its monoculture AM phenotype. Interestingly, only the TI model displayed phagocytic stability in the presence of LPS suggesting that interaction between the different epithelial cells in the co-culture system makes them more resistant to this insult (Luyts *et al.*, 2015).

#### 4.4.2.2. Whole model response characterisation

PMA differentiated U937 cells have been widely used as an *in vitro* model of human monocytes and macrophages in mechanistic studies of inflammatory respiratory response (Hoffman *et al.*, 2017; Larrick *et al.*, 1980). Both TI and TII cell systems displayed differences in their cytokine/ chemokine signatures in line with findings for hAELVi and A549 monocultures. In monoculture, hAELVi cells display few cytokines, which is in line with an AEC I phenotype (Weibel, 2015), although due to the novelty of the hAELVi cell line, a cytokine library is yet to be published (Wirth *et al.*, 2016). Unlike hAELVi cells, A549 cells produce a cascade of cytokines IL-4, IL-6, TNF- $\alpha$  to enhance cell to cell communication channels between barrier cells and AEC II / alveolar macrophages as reported *in vivo* (Fehrenbach, 2001). In line with the chapter's findings, additional cytokines such as IL-8 are produced or further enhanced by A549 cells following stimulant exposure (Bitterle *et al.*, 2006). When stimulated by LPS, the presence of AMs in culture with A549, cytokine responses decrease for IL-6,

IL-8 and TNF-  $\alpha$  suggesting active pro-inflammatory responses by AMs (Chanput *et al.*, 2014). Thus, representing an integrative unit within the alveolus models.

## 4.5. Conclusion

Chapter four aimed to optimise and characterise two human immunocompetent *in vitro* models of the human alveolus: (i) type I alveolar epithelial cell with alveolar macrophage-like cells and; (ii) type II alveolar epithelial cell with alveolar macrophage-like cells. Optimal culture conditions for alveolar epithelial cells (including medium composition, seeding density, culture period, and culture substrate) were determined and shown to influence cell characteristics from their phenotype significantly. Two alveolar immunocompetent cell systems were constructed and cultured with the established A549 or new hAELVi cells. Both viable systems display functional characteristics for the barrier cells and alveolar like macrophages. Different cell types in the culture system affect the cellular activity and highlight the necessity of constructing an optimised and validated model suitable for the desired assessment.

These models were designed for medium-high throughput assessments of inhaled medicines but can also be used for inhaled chemicals. The value of this model is that many different endpoints can be measured to access changes in alveolar homeostasis or alveolar toxicity, such as barrier function and inflammation.



## U937 cell phenotypes in mono- and co-culture systems using a high content image analysis approach

### 5.1. Introduction

Inhaled drug delivery offers excellent potential for fast, non-invasive delivery therapeutic molecules for both local airways diseases (e.g. asthma, COPD) and systemic therapies (e.g. diabetes) (Nikula *et al.*, 2014). Despite the fact that significant research and development budgets in the pharmaceutical industry are spent on developing new inhaled therapies, few new inhaled medicines have made it to market over the past two decades (Forbes *et al.*, 2014).

New inhaled medicines must undergo extensive pre-clinical safety assessment to evaluate their safety and efficacy before human studies (Forbes *et al.*, 2011, 2014; Jones *et al.*, 2012a; Lewis *et al.*, 2014; Nikula *et al.*, 2014; Owen, 2013). *In vivo* studies in rats are typically employed to assess pre-clinical safety, and it is not uncommon to observe alveolar macrophage responses to be observed in histological lung slices (Lewis *et al.*, 2014; Nikula *et al.*, 2014). These responses are typically characterised by a highly vacuolated appearance and larger cell size (Forbes *et al.*, 2014; Lewis *et al.*, 2014) and are often termed ‘foamy’ macrophages – a term used by pathologists to describe an alveolar macrophage with a vacuolated cytoplasm when viewed by light microscopy (Lewis *et al.*, 2014; Nikula *et al.*, 2014). These cell responses may be unaccompanied by other changes or associated with other immune cell infiltration of lung tissue remodelling (Forbes *et al.*, 2014; Lewis *et al.*, 2014).

Whilst the pathophysiology for these ‘foamy’ phenotypic responses are not well understood; they are used to set safe exposure levels. As a result, safety and efficacy are the leading reasons why inhaled medicines fail in pre-clinical studies without knowing if the responses are relevant to humans (Jones & Neef, 2012; Owen 2013; Forbes *et al.*, 2014).

Cell culture models of the upper respiratory tract have proven to shorten the development time for new drug products (Owen, 2013). As a pre-clinical application, they can be used as a screening tool and replace whole animal tests providing a less expensive and less time-consuming alternative. Subsequently, data obtained from absorption mechanisms from such *in vitro* experiments enables better judgement on the safety of new drugs and chemicals (Jones & Neef 2012; Forbes *et al.*, 2014). In contrast with the upper airways, few *in vitro* models of the alveolus are published or commercially available, and our current understanding of immunological, foamy macrophage responses after the molecule interacts with cells of the alveolus is still relatively limited (Forbes *et al.*, 2014). In this context, *in vitro* models of the lower airways will prove helpful to clarify interactions between drug compounds and biological response mechanisms.

*In vitro* strategies using human immunocompetent alveolar models to screen new drug compounds for their ability to induce macrophage vacuolation and understand the mechanism of vacuolation is one potential approach to improve pre-clinical safety assessment (Hoffman *et al.*, 2015). Discerning the different mechanisms by which the vacuolated phenotypes develop and resolve could be key to understanding the safety implications of this phenomenon.

High content imaging systems allow a high level of detail to be captured from individual cells in a high throughput screening approach (Giuliano *et al.*, 2003; O'Brien, 2014; Wink *et al.*, 2014). These cell images are quantitatively analysed to characterise morphometric and biometric parameters of cells, which can be used to capture the phenotypic cellular responses of a cell to a stimulus (Wink *et al.*, 2014). Whilst high content analysis is widely established in drug discovery, its use in toxicity assessment is less prevalent (O'Brien, 2014; Giuliano *et al.*, 2014). High content image analysis has been recently proposed for use in inhaled toxicity assessment by Hoffman and co-workers who used fluorescence imaging of untreated and drug-treated human and rat macrophages to generate morphometric, viability and functionality profiles (Hoffman *et al.*, 2015). This technique could prove advantageous in characterising detailed morphological changes in alveolar macrophages *in vitro* to predict *in vivo* responses and provide earlier go/no-go decision making for inhaled drug candidates. This technique also provides an opportunity to study how other cells present in a co-culture system may influence the morphology of alveolar macrophage-like cells providing a more in-depth understanding of the relationship between cell types in the alveolus.

## 5.2. Aims

This chapter aimed to determine if the presence of epithelial cells within the co-culture system (developed from chapter 4) affects the alveolar-like macrophage component's response and functionality. Specifically, this chapter focuses on characterising how 'foamy' alveolar macrophage phenotype responses may differ in the presence of other cells by employing detailed morphological characterisation techniques. Specifically, the objectives of this chapter were to:

- Adapt established high content imaging methodologies for the co-culture system
- Determine the viability and functionality of cells within the co-culture systems to amiodarone (inducer of phospholipidosis, a well-characterised foamy macrophage phenotype)
- Perform detailed analysis of macrophage morphology in the co-culture system in the presence and absence of amiodarone
- Establish baseline characteristics of alveolar-like macrophages and determine the influence of the co-culture environment
- Apply phenotype analysis to determine morphological and metabolic differences of alveolar-like macrophages cultured in different environments.

## 5.3. Results

### 5.3.1 Effect of amiodarone on cell viability and functionality in mono- and co-culture U937 models.

The effect of amiodarone on cell viability and functionality was assessed on PMA-differentiated U937 cells in monoculture and on the type I and type II co-culture models. Models were cultured at the ALI as previously described. Dosing of amiodarone to cells was via The extracellular concentration of LDH was less than 3% for untreated models, and no significant difference ( $p < 0.05$ ) in viability was observed for PMA-differentiated U937 cells cultured alone or in co-culture with epithelial cells (Figure 5.1). Exposure to 1  $\mu$ M and 10  $\mu$ M amiodarone in CCM to the basolateral compartment for 48 h resulted in a significant increase ( $p > 0.0001$ ) in the extracellular concentration of LDH to 37-43 % in both monoculture and co-culture models (Figure 5.1 Cytotoxicity of monoculture and co-cultured PMA-differentiated U937 cells on exposure to amiodarone. Figure 5.1). The presence of epithelial cells did not significantly affect the viability of cells within the model in the presence or absence of amiodarone.

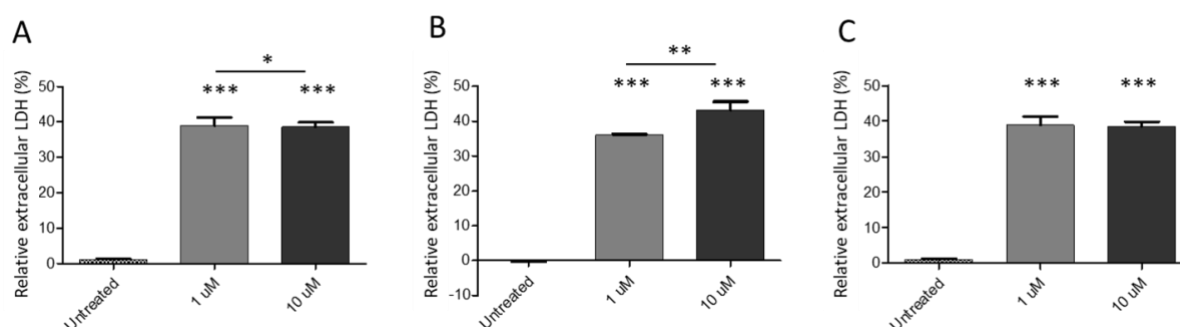


**Figure 5.1 Cytotoxicity of monoculture and co-cultured PMA-differentiated U937 cells on exposure to amiodarone.**

PMA differentiated U937 cells cultured alone (A) with hAELVi cells (B) or A549 cells (C) were either untreated or exposed to 1  $\mu$ M or 10  $\mu$ M amiodarone for 48 h. The extracellular LDH concentration was determined using the CytoToxONE assay, and relative extracellular LDH release was calculated from cells lysed with positive control 0.1% v/v Triton-X 100. A one way ANOVA was used to determine significance for each treatment group and Tukey's multiple comparison post hoc test was employed when \*\*  $p < 0.005$ , \*\*\* :  $p < 0.0001$ . Data shown represent  $n = 3$  data points  $\pm$  SEM of three independent cell model experiments.

Flow cytometry was employed to assess the influence of amiodarone exposure on the functional phagocytic ability of PMA-differentiated U937 cells in mono- and co-culture models (Figure 5.2). As demonstrated in Chapter 3, approximately 80% of cells within the population were engaged in active phagocytosis (Figure 3.4). For direct comparison of phagocytic ability in different co-culture systems, the data was normalised and readjusted to 100% for untreated (healthy) cells compared to the amiodarone treatment groups. Untreated models were expressed at 100% as a phagocytically active population.

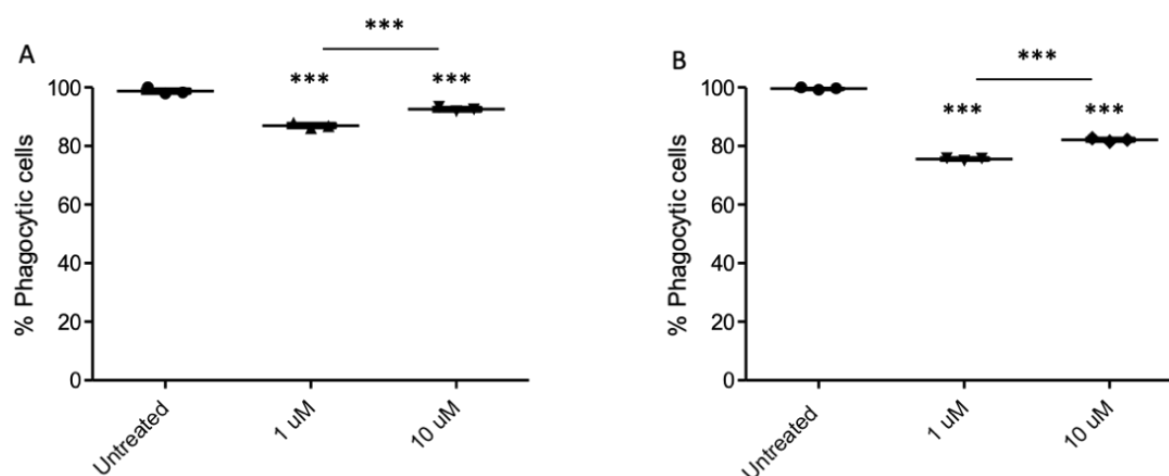


**Figure 5.2 Influence of amiodarone on the phagocytic activity of PMA differentiated U937 cells in co-culture.**

PMA differentiated U937 cells were cultured with (A) hAELVi and (B) A549 and exposed to 1  $\mu$ M or 10  $\mu$ M of amiodarone for 24 h. Phagocytosis assessment was performed after 2 h incubation with 1.0  $\mu$ m FluoSpheres™ Carboxylate-Modified microspheres using flow cytometry. 1000 cells were assessed for  $n=3$  independent models. The percentage of cells taken up the FluoSpheres™ relative to the whole population was calculated. Data are expressed as mean  $\pm$  SEM, where  $n = 9$  for 5,000 events. Bonferroni post hoc test after one-way ANOVA where \*\*\*  $p<0.0001$  is shown.

Amiodarone significantly ( $p<0.0001$ ) inhibited PMA differentiated U937 cells to phagocytose microbeads for both type I epithelial (TI) and type II (TII) epithelial co-culture models (Figure 5.2). Phagocytic function of 1  $\mu$ M and 10  $\mu$ M amiodarone treated macrophages decreased significantly ( $p<0.001$ ) by 15 % and 8 % respectively in the T I model and 25 % and 18 % respectively in the T I the T II model. The sensitivity of each model was evident through concentration dependant changes within the T I

and T II models, where 1  $\mu$ M amiodarone significantly ( $p < 0.0001$ ) reduced the phagocytic function of the macrophages.

### 5.3.2 Adaptation of high content image analysis for co-culture system

The high content image analysis methodology established by Hoffman *et al.* was successfully adapted for the co-culture system. Using the InCell Analyser 6000, images were taken of fluorescently stained PMA-differentiated macrophages in mono- or co-culture in the presence and absence of 1  $\mu$ M or 10  $\mu$ M amiodarone at 40 x magnifications (Figure 5.3, Figure 5.4, Figure 5.5) Grayscale images of fields were exported from InCell software and Image J software adopted to colour and stack images.

For morphological cell health analysis, the nucleus was oval or irregular and stained dark blue. Cytoplasm regions within cells stained red and active mitochondria presented in yellow. The qualitative assessment indicated that the untreated, PMA-differentiated U937 cell population displayed a more homogeneous morphology with minimal vacuolation. Monoculture and co-culture models exposed to amiodarone resulted in more heterogeneous cell responses, including enlarged cells with distinct vacuolation patterns (large single vacuole within the cell).



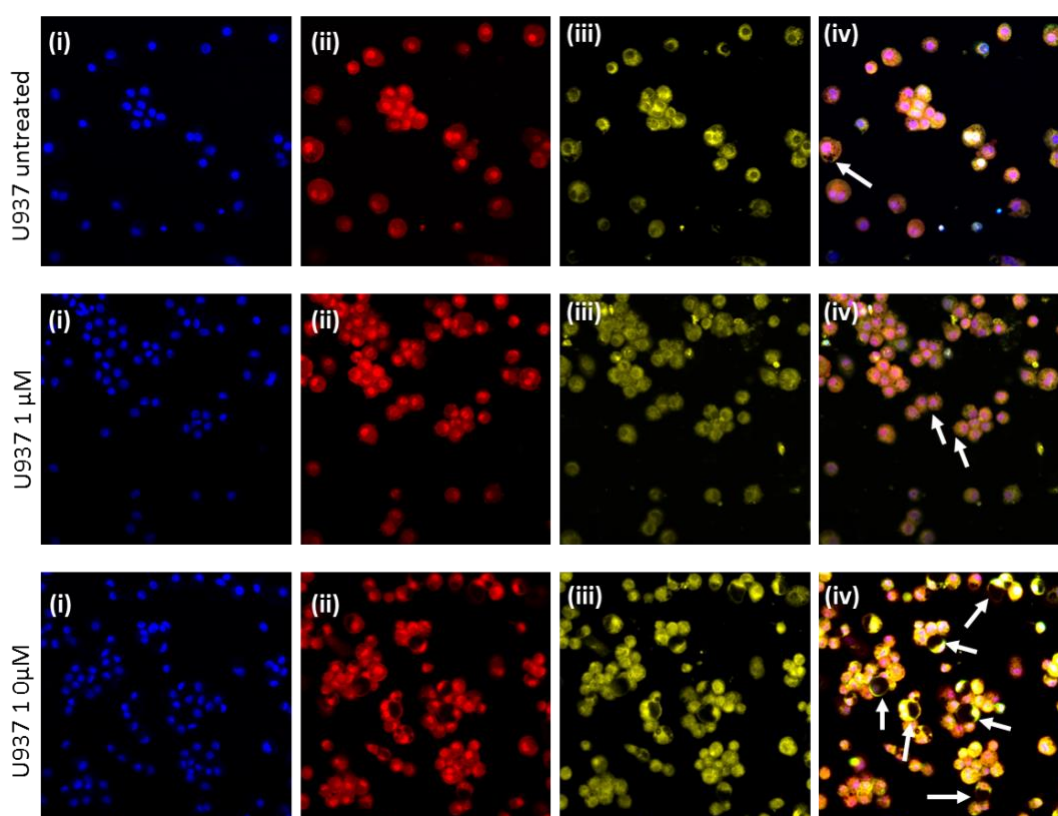


**Figure 5.3 Multi-parameter images of PMA-differentiated U937 cells in monoculture exposed to 1  $\mu$ M and 10  $\mu$ M amiodarone.**

PMA-differentiated U937 cells were cultured on 24 well plates and exposed to either 1  $\mu$ M or 10  $\mu$ M amiodarone for 48 h. Cells were fluorescently labelled (i) nuclei (blue); (ii) cytoplasm (red); (iii) mitochondrial activity (yellow); (iv) image overlay. Images were taken using the InCell Analyser 6000 with x40 objective. White arrows indicate cell responses of vacuolation. Control shown as untreated PMA-differentiated U937 cells. Data are shown for n=3 independent experiments where 72 fields per well were imaged.

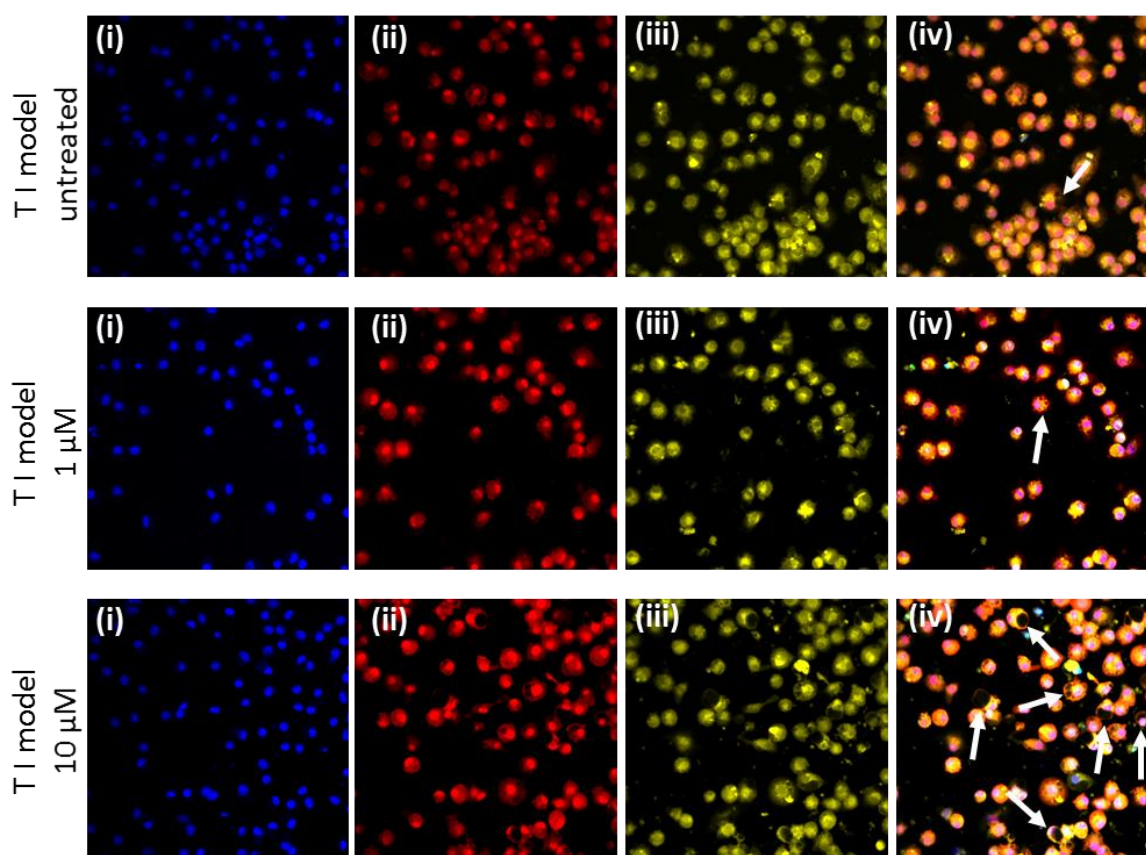


**Figure 5.4 Multi-parameter images of PMA-differentiated U937 cells in a co-culture system with type I alveolar epithelial cells exposed to 1 $\mu$ M and 10 $\mu$ M amiodarone.**

PMA-differentiated U937 cells were co-cultured on 24 well plates with hAELVi cells suspended in Transwell® inserts at the ALI. The culture system was exposed to either 1  $\mu$ M or 10  $\mu$ M amiodarone for 48 h. Cells were fluorescently labelled (i) nuclei (blue); (ii) cytoplasm (red); (iii) mitochondrial activity (yellow); (iv) image overlay. Images were taken using the InCell Analyser 6000 with x40 objective. White arrows indicate cell responses of vacuolation. Control shown as untreated PMA-differentiated U937 cells. Data are shown for n=3 independent experiments where 72 fields per well were imaged.

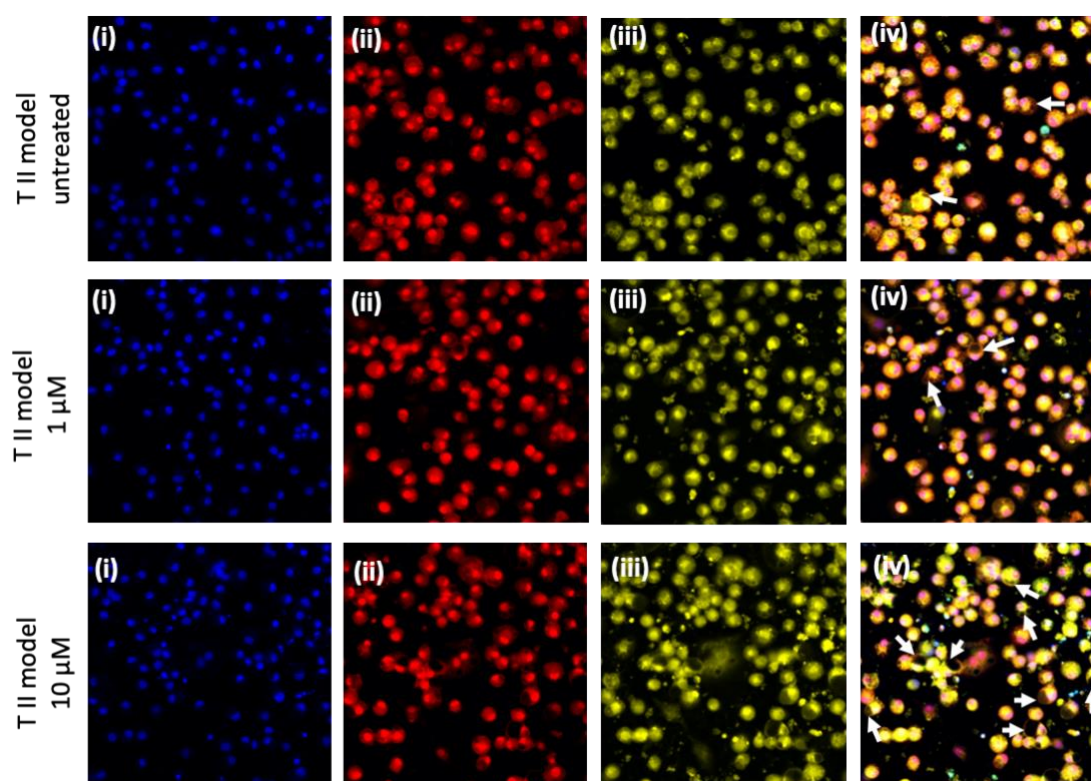


**Figure 5.5 Multi-parameter images of PMA-differentiated U937 cells in a co-culture system with type II alveolar epithelial cells exposed to 1μM and 10μM amiodarone.**

PMA-differentiated U937 cells were co-cultured on 24 well plates with A549 cells suspended in Transwell® inserts at the ALI. The culture system was exposed to either 1 μM or 10 μM amiodarone for 48 h. Cells were fluorescently labelled (i) nuclei (blue); (ii) cytoplasm (red); (iii) mitochondrial activity (yellow); (iv) image overlay. Images were taken using the InCell Analyser 6000 with x40 objective. White arrows indicate cell responses of vacuolation. Control shown as untreated PMA-differentiated U937 cells. Data are shown for n=3 independent experiments where 72 fields per well were imaged.

### 5.3.3 Quantitative High Content Analysis

For cell health and morphology analysis, Hoechst 33,342 cell nuclear staining was used to identify nucleated cells. Cell Mask Deep Red dye is an established cell delineation tool for cellular imaging and was used to highlight the cytoplasmic regions within the cells identified. Conversely, vacuoles within cells were identified based on negative staining with Cell Mask Deep Red. MitoTracker Red detects the changes in the mitochondrial membrane potential and accumulates in active mitochondria. Image-It Green Dead is an impermeant dye to healthy cells that become permeant when the plasma membrane of cells is compromised. These two cell health stains were reported as fluorescence intensity values. Eight quantitative measurements were generated from the analysis, namely cell area, nuclear area, mitochondrial activity, cell permeability, vacuole number per cell, vacuole area per cell, which characterised cell health, morphology.

Secondary Analysis Criteria was performed. Exclusion of Cells with Reduced Mitochondrial Activity Criteria to identify dead and dying cells were defined so that these cells could be excluded from the analysis to prevent morphology characterisation parameters being impacted by changes induced from cell death. Exposure conditions that reduced the total number of cells imaged to less than 50 % of the image in control (untreated) cells were excluded. In the remaining wells, cells with reduced mitochondrial activity were classified as those possessing less than two standard deviations below the mean fluorescence intensity of MitoTracker Red dye in the untreated cell population and were excluded from the analysis.

Mitochondrial activity was selected as a more sensitive marker over cell permeability as the washing steps within the assay methodology removed most cells with compromised cell membrane integrity. Cells exposed to 200  $\mu$ M FCCP (potent mitochondrial oxidative phosphorylation uncoupling agent) were used as an internal assay control to confirm the appropriate mitochondrial activity exclusion boundary set. Cell viability has been measured as the percentage of cells with mitochondrial activity above the mean fluorescent value minus the second standard deviation, out of the total number of cells per well.

#### **5.3.3.1. High content image analysis: Cell Health**

Images of individual cells captured in the fluorescent images were analysed quantitatively to define detailed cell features. Parameters describing cell health were calculated for each cell within the population and compared between PMA-differentiated alveolar-like macrophages grown in mono- and co-culture conditions (Figure 5.6).

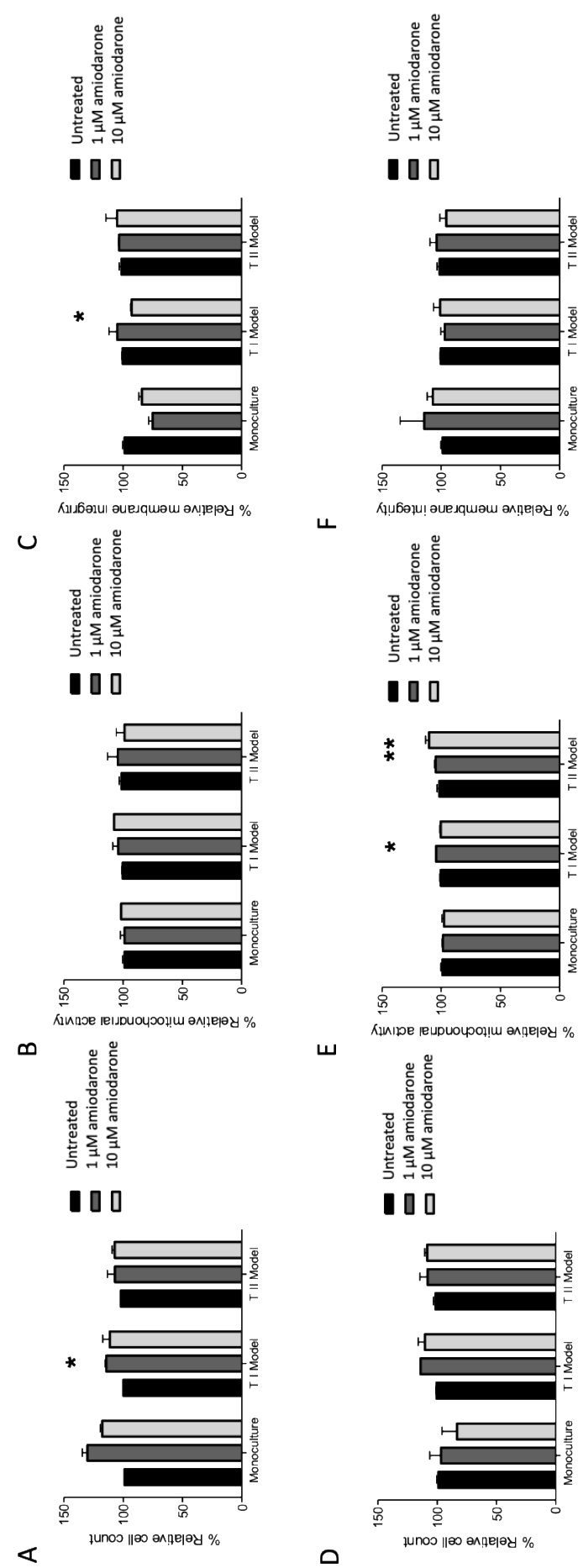


**Figure 5.6 Characterisation of PMA-differentiated U937 cell health using high content image analysis methodology.**

PMA-differentiated U937 cells were seeded on 24 well plates at a density of  $6.25 \times 10^5$  cells/ well in monoculture and coculture with either hAELVi (type I alveolar epithelial) cells (T I model) or A549 (type II alveolar epithelial) cells (T II model). Culture systems were exposed to 1 μM or 10 μM amiodarone for 24 h. Cells were fluorescently stained with Hoescht, Mitotracker, Image it Dead and imaged using the InCell Analyser 6600 followed by quantitative analysis for individual cell characteristics. Cell health parameters were characterised for the whole cell population (A-C) and subset cell population (D- F). (A, D) relative cell count based on the % of cells remaining on the plate relative to the untreated control; (B, E) relative mitochondrial activity expressed as a % relative to untreated control and (C, F) relative membrane integrity expressed as a % relative to untreated control.. Data is represented as mean  $\pm$  SD of 72 fields where  $n = 3$  wells . Significance determined by Kruskal-Wallis and Dunn's post hoc test. \* indicates  $p < 0.05$ , \*\* indicates  $p < 0.001$ .

To determine the proportion of cells that may have become detached from the well plate during the assay, the number of cells observed for each treatment was calculated relative to the untreated sample. No significant difference ( $p>0.05$ ) regarding the number of cells counted on exposure to either concentration of amiodarone was observed for either PMA-differentiated U937 cells in monoculture or either co-culture model (Figure 5.6 A). A significant reduction ( $p<0.05$ ) in cells counted was observed between the U937 cells in monoculture and within the type I co-culture but not the type II co-culture model (Figure 5.6 B). For individual cell viability assessment, no significant difference was observed in the mitochondrial activity of PMA differentiated U937 cells in each culture system or with amiodarone exposure. The only significant observation for altered cell membrane integrity was between untreated and 10  $\mu\text{M}$  amiodarone in the T I model ( $p<0.05$ ) (Figure 5.6 C).

A subset of the population with elevated mitochondrial activity was also characterised to explore if this population of more metabolically active cells had altered cell health and morphological properties. No significant difference ( $p>0.05$ ) in the total number of PMA-differentiated U937 cells with elevated mitochondrial activity was observed in the subset population in the presence of amiodarone or co-culture with epithelial cells (Figure 5.6 D). The membrane integrity of the PMA differentiated U937 cells in the population remained unchanged (Figure 5.6 F) with exposure to amiodarone in all models. A significant change in mitochondrial activity was observed for 5 nM and 10 nM in the T II model ( $p<0.01$ ) and 10 nM in the T I model ( $p<0.05$ ) compared to control (Figure 5.6 E).

### 5.3.3.2. High content image analysis: Morphology

Analysis of morphological features was divided into gross morphology (cell area, nuclear area and cell area: nuclear area ratio) and detailed intracellular morphology (number of vacuoles, percentage of the cell area occupied by vacuoles, average area of cell occupied by each vacuole). For untreated samples, the cell area of PMA differentiated U937 cells was significantly increased ( $p>0.05$ ) in both co-culture models in comparison with cells in monoculture (Figure 5.7A). No significant difference ( $p>0.05$ ) in cell area was observed with amiodarone exposure at either concentration. Nuclear area of PMA differentiated cells was not significantly different in cells in monoculture but was significantly elevated ( $p<0.0001$ ) for cells exposed to 10  $\mu\text{M}$  amiodarone in comparison with untreated cells (Figure 5.7B). The average area occupied by each vacuole was observed to be significantly greater ( $p<0.001$ ) for PMA differentiated U937 cells cultured with A549 cells after exposure to 10  $\mu\text{M}$  amiodarone in comparison with untreated cells (Figure 5.7C). No other differences in vacuole characteristics were observed to be significant ( $p<0.05$ ).

In the subset population with elevated mitochondrial activity, PMA differentiated U937 cells had significantly larger cell area (250-300  $\mu\text{m}$  vs 475-775  $\mu\text{m}$ ) than the average of the whole population; however, no significant difference ( $p>0.05$ ) was observed for cell area with exposure to amiodarone or between the different culture systems (Figure 5.7D). Similarly, no significant differences ( $p>0.05$ ) were observed for nuclear area for PMA-differentiated U937 cells between culture systems or in the presence of amiodarone for the subset population (Figure 5.7E). Furthermore, cells with elevated mitochondrial activity had a comparable nuclear area with the whole cell population.



---

In the subset population, there was no significant difference ( $p>0.05$ ) in the average area of each vacuole within PMA differentiated U937 cells on exposure to amiodarone or between culture systems; however, this value was significantly higher ( $p<0.0001$ ) for cells with elevated mitochondrial activity in comparison with the whole cell population (Figure 5.7F).

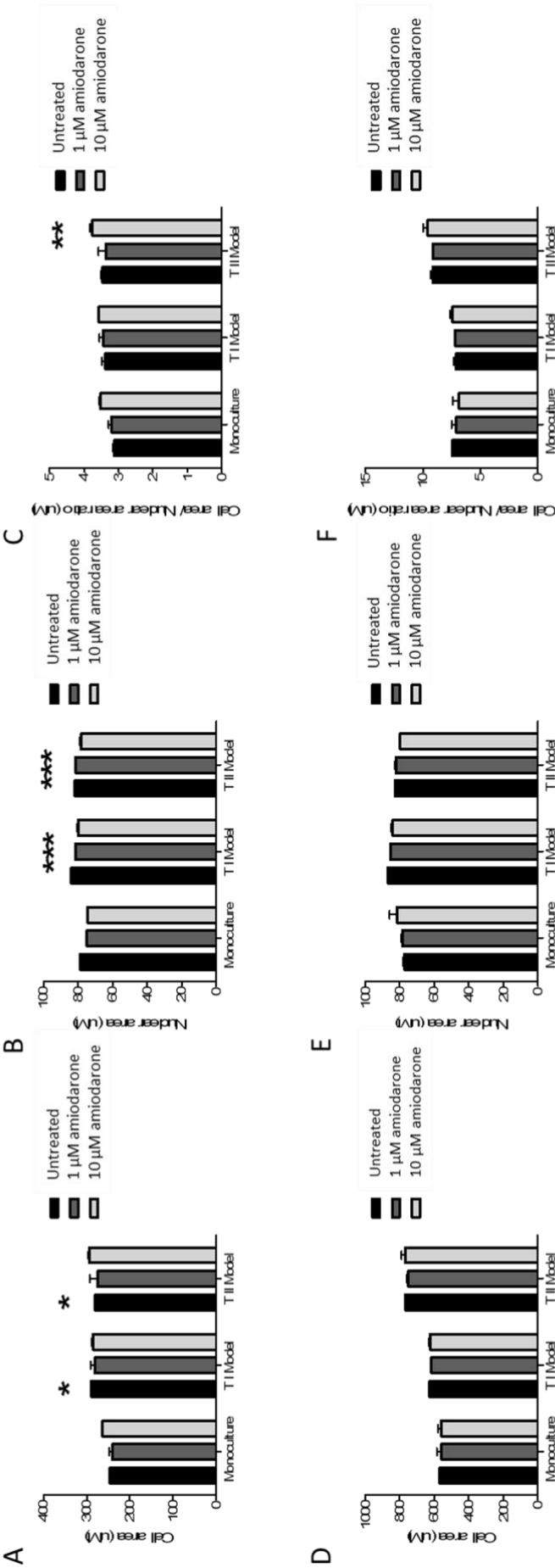


**Figure 5.7 Characterisation of PMA-differentiated U937 gross morphological features using high content image analysis methodology.**

PMA-differentiated U937 cells were seeded on 24 well plates at a density of  $6.25 \times 10^5$  cells/well in monoculture and coculture with either hAELVi (type I alveolar epithelial) cells (T I model) or A549 (type II alveolar epithelial) cells (T II model). Culture systems were exposed to 1 µM or 10 µM amiodarone for 24 h. Cells were fluorescently stained with Hoescht, Mitotracker, Image it Dead and and imaged using the InCell Analyser 6600 followed by quantitative analysis for individual cell characteristics. Gross cell morphological parameters were characterised for the whole cell population (A-C) and subset cell population (D-F). (A, D) cell area; (B, E) nuclear area (C, F) cell area:nuclear area ratio. Data is represented as mean  $\pm$  SD of 72 fields where  $n = 3$  wells. Significance determined by Kruskal-Wallis and Dunn's post hoc test. \* indicates  $p < 0.05$ , \*\* indicates  $p < 0.001$  and \*\*\* indicates  $p < 0.0001$ .

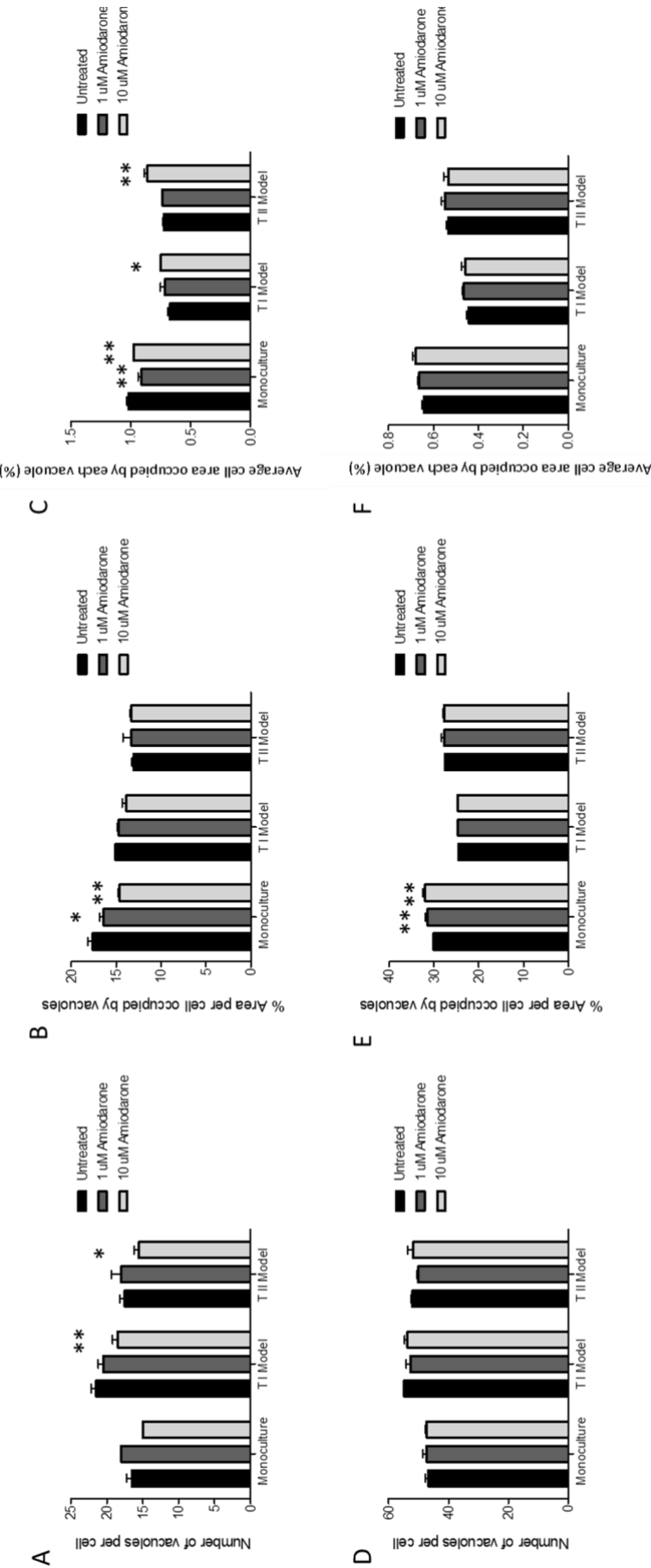


**Figure 5.8 Characterisation of PMA-differentiated U937 detailed morphological features using high content image analysis methodology.**

PMA-differentiated U937 cells were seeded on 24 well plates at a density of  $6.25 \times 10^5$  cells/ well in monoculture and coculture with either hAELVi (type I alveolar epithelial) cells (T I model) or A549 (type II alveolar epithelial) cells (T II model). Culture systems were exposed to 1  $\mu$ M or 10  $\mu$ M amiodarone for 24 h. Cells were fluorescently stained with Hoechst, Mitotracker, Image it Dead and and imaged using the InCell Analyser 6600 followed by quantitative analysis for individual cell characteristics. Detailed cell morphological parameters were characterised for the whole cell population (A-C) and subset cell population (D- F). (A, D) number of vacuoles per cell; (B, E) % area per cell occupied by vacuoles (C, F) average area of cell occupied per vacuole. Data is represented as mean  $\pm$  SD of 72 fields where n= 3 wells . Significance determined by Kruskal-Wallis and Dunn's post hoc test. \* indicates  $p < 0.05$  ,  $p < 0.001$  \*\*.

The number of vacuoles per cell was significantly increased ( $p<0.001$  and  $p<0.05$  respectively) for PMA differentiated U937 cells exposed to 10  $\mu\text{M}$  amiodarone in both TI and TII co-culture models in comparison with cells in monoculture (Figure 5.8A). The cell subset with elevated mitochondrial activity had a significantly higher number of vacuoles ( $p<0.0001$ ) than the whole population ( $>2$  fold greater) (Figure 5.8D). No significant difference ( $p>0.05$ ) was observed in the percent area per cell occupied by vacuoles on exposure to amiodarone or with regards to the culture system (Figure 5.8B). However, the percent of the cell area occupied by vacuoles was approximately 2-fold higher in cells with elevated mitochondrial activity in comparison with the whole cell population (Figure 5.8E). The average area occupied by each vacuole was significantly lower ( $p<0.001$ ) for PMA differentiated U937 cells exposed to 10  $\mu\text{M}$  amiodarone in both co-culture systems compared to the monoculture system. (Figure 5.8C). The population of cells with elevated mitochondrial activity had a significantly lower ( $p<0.05$ ) average area of each vacuole in comparison with the whole cell population (Figure 5.8F).

#### **5.3.3.3. High content image analysis: Population profiling**

Characterising the profile of multiple cell health and morphology average population parameters was conducted to ascertain if and how PMA-differentiated U937 cell morphology and health differed in the presence and absence of alveolar epithelial cells. Amiodarone was also used to generate a 'foamy' macrophage phenotype by the mechanism of phospholipidosis in order to assess if PMA-differentiated U937 cell responses differed when cultured with or without epithelial cells. A reproducible baseline was established for untreated PMA differentiated U937 cells, which was

consistent for cells cultured on both 96 and 24 well plates in the presence and absence of hAELVi type I epithelial cells and A549 type II epithelial cells in co-culture (Figure 5.9).

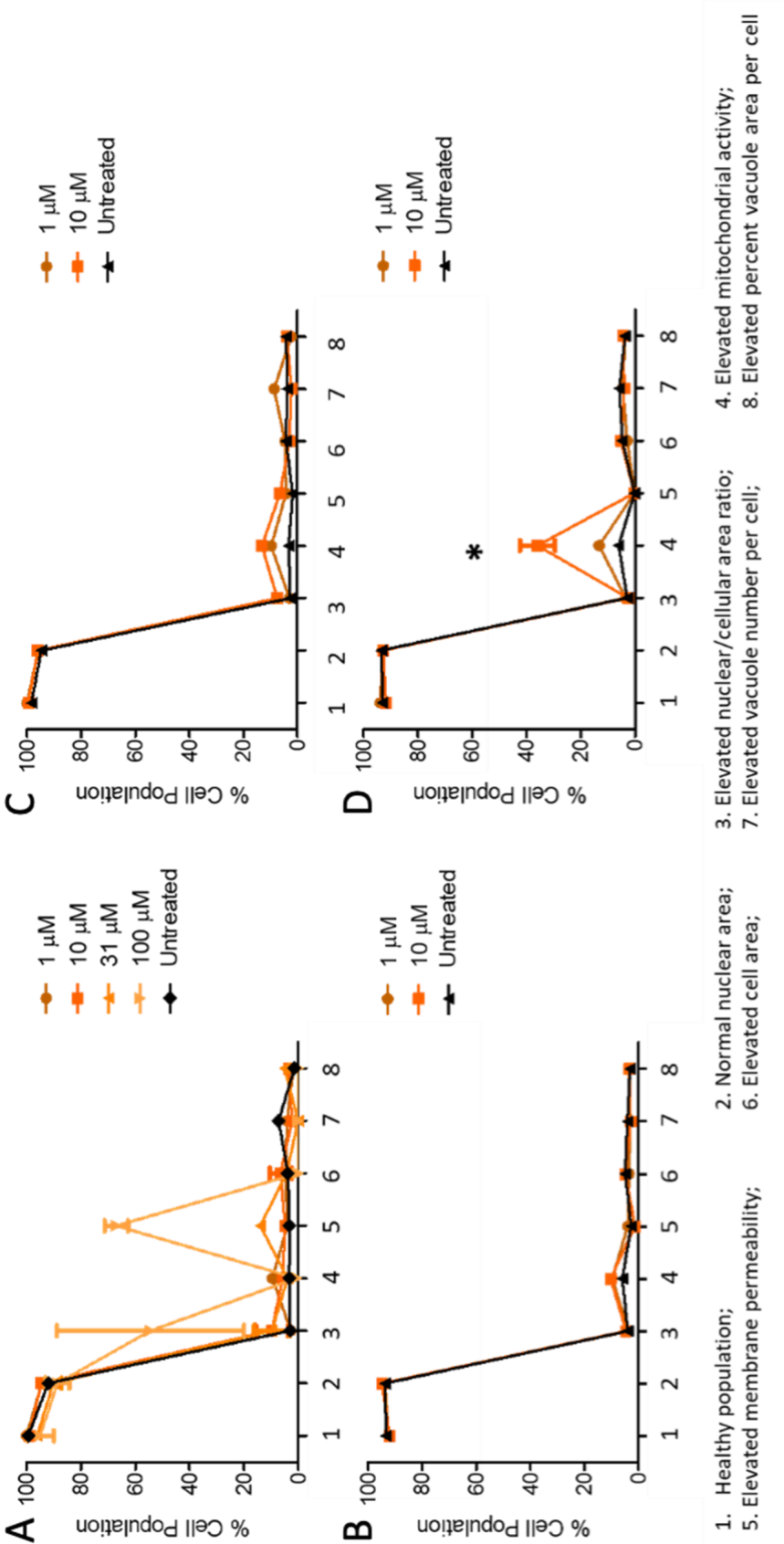


**Figure 5.9 Population profiling of PMA differentiated U937 cells exposed to amiodarone.** PMA-differentiated U937 cells were cultured in monoculture on 96 well plates (A) or 24 well plates (B) and coculture with either hAELVi type I alveolar epithelial cells (C) (T1 model) or A549 type II alveolar epithelial cells (D) (T II model). Culture systems were exposed to 1  $\mu$ M -100  $\mu$ M amiodarone for 48 h. Cells were fluorescently stained with Hoechst, Mitotracker, Image it Dead and imaged using the InCell Analyser 6600 followed by quantitative analysis for individual cell characteristics. Multiparameter profile charts for cell health and morphological features were obtained for the subset population of cells with elevated mitochondrial activity.. Data is represented as mean of 3 experiments  $\pm$  SEM, where n= 6 for each investigation. Significance determined by Kruskal-Wallis and Dunn's post hoc test. \* indicates p<0.05.

A concentration dependant response to amiodarone was observed for U937 cells cultured on 96 well plates for nuclear area:cellular area ratio ( $55 \% \pm 34 \%$  with 100  $\mu\text{M}$  amiodarone,  $10 \% \pm 7 \%$  with 31  $\mu\text{M}$  amiodarone and  $9 \% \pm 6 \%$  with 10  $\mu\text{M}$  amiodarone) and membrane permeability ( $67 \% \pm 4 \%$  with 100  $\mu\text{M}$  amiodarone and  $14 \% \pm 2 \%$  with 31  $\mu\text{M}$  amiodarone) (Figure 5.9 A). Whole population cell viability was significantly reduced ( $p < 0.05$ ) when PMA differentiated U937 cells were exposed to amiodarone at concentrations  $> 10 \mu\text{M}$ ; therefore, the 1  $\mu\text{M}$  and 10  $\mu\text{M}$  concentrations were taken forward to assess morphological changes directly induced by amiodarone rather than those linked with cell death.

No significant difference ( $p < 0.05$ ) in the profile characteristics was observed between culture conditions or exposure to amiodarone except for mitochondrial activity. Mitochondrial activity was elevated in the presence of both amiodarone concentrations tested in the monoculture and type I alveolar epithelial co-culture and was significantly increased ( $p < 0.05$ ) for PMA differentiated cells in the type II alveolar epithelial co-culture model in comparison with the other model systems (Figure 5.9D).

#### 5.3.3.4. High content image analysis: Population phenotyping

In order to assess individual cells for multiple morphological and health characteristics, a dynamic single-cell phenotyping approach was undertaken, which classified the cells into reduced, normal or elevated for four characteristics (mitochondrial activity, cell area, number of vacuoles per cell and the percent area of the cell occupied by vacuoles) (**Error! Reference source not found.**).

**Table 5.1 Phenotype classification of PMA-differentiated U937 cells exposed to amiodarone.**

Phenotype	Mitochondrial activity	↓	-	-	-	-	-	-	↑	↑
	Cell area	-	-	-	-	-	↑	↑	-	-
	Number of vacuoles	-	-	-	-	↑	-	↑	-	-
	% cell area occupied by vacuoles	-	↓	-	↑	-	-	-	↓	-
		% Population expressing phenotype								
Monoculture (U937)	Untreated	0	2	86	2	1	1	2	0	5
	Amiodarone 1 $\mu$ M	0	1	88	2	2	0	1	0	5
	Amiodarone 10 $\mu$ M	0	1	85	5	1	4	1	0	3
TI Model (U937 + hAELVi)	Untreated	1	3	88	1	1	1	1	0	3
	Amiodarone 1 $\mu$ M	1	5	80	2	1	1	1	1	8
	Amiodarone 10 $\mu$ M	1	8	74	2	1	2	1	1	8
TII Model (U937 + A549)	Untreated	1	1	86	3	2	1	2	0	3
	Amiodarone 1 $\mu$ M	0	1	83	3	2	1	1	0	8
	Amiodarone 10 $\mu$ M	0	2	65	3	1	2	2	0	24

PMA-differentiated U937 cells were seeded on 24 well plates at a density of  $6.25 \times 10^5$  cells/ well in monoculture and co-culture with either hAELVi (type I alveolar epithelial) cells (TI model) or A549 (type II alveolar epithelial) cells (T II model). Culture systems were exposed to 1  $\mu$ M or 10  $\mu$ M amiodarone for 24 h. Cells were fluorescently stained with Hoescht, Mitotracker, Image it Dead, and imaged using the InCell Analyser 6600 followed by quantitative analysis for individual cell characteristics. Cells were categorised using four characteristics (mitochondrial activity, cell area, number of vacuoles per cell and the percent area of the cell occupied by vacuoles. These categories were subdivided into reduced (two standard deviations below the population mean), normal (between two standard deviations above and below the population mean) and enhanced (two standard deviations above the population mean). The percent of the total population expressing the phenotype was calculated. Phenotypes greater than 1% of the population are displayed.

**Error! Reference source not found.**

From 72 potential phenotypes, only 9 contained >1% of the cell population and only 4 of these phenotypes represented >95% of the total cell population. The majority of cells (65-90%) were defined as possessing a 'normal' level of all four characteristics. Cell phenotypes with reduced cell area occupied by vacuoles, increased cell area occupied by vacuoles and increased mitochondrial activity were identified to contain



>2% of the population for all systems tested. The baseline of the untreated PMA-differentiated cell phenotype was similar for cells in monoculture and both co-culture systems. A greater proportion of the cells had a reduced vacuolation area within the cell in the type I epithelial co-culture system in comparison with the other models (for 10  $\mu$ M amiodarone 8% of cells in the type I model vs 2 % in the type II model and 1 % in monoculture). Cells in co-culture systems also exhibited phenotypes with elevated mitochondrial activity (for 10  $\mu$ M amiodarone 3% in monoculture vs 8% and 24% in type I and type II epithelial cell co-culture models, respectively).

## 5.4. Discussion

### 5.4.1 High content image analysis as a tool to assess macrophage responses

High content image analysis is employed in the pharmaceutical industry for screening the phenotypic changes induced by compounds for the identification of novel therapeutics based on knowledge of a distinct phenotype (Lin *et al.*, 2020). Whilst *in vitro* approaches for predicting drug safety are widely used pre-clinically in the pharmaceutical industry; they typically rely on single parameter readouts typically providing information about a cell population. Cell responses to drug challenge *in vivo* may impact only a small percentage of the total cell population (Lewis *et al.*, 2014; Nikula *et al.*, 2014), and this has also been observed *in vitro* (Hoffman *et al.*, 2017). As a result, cellular responses *in vitro* may be overlooked when considering single, average data descriptors. Morphological assessment has traditionally been carried out by low-resolution imaging, and fluorescent/confocal microscopy images provide a crude description of the phenotype with little detail regarding the cellular changes (Forbes *et al.*, 2014). The high content image analysis methodology described in this chapter captures multiple parameters for individual cells, enabling analysis of a subset of the population of cells that respond to the drug stimulus. This chapter investigated if the high content image analysis techniques employed for identifying phenotypic changes to the cells in drug discovery could be applied to identify phenotype changes associated with toxicity and provide a rapid, reliable preclinical safety assessment.

Fluorescence staining, imaging and analysis methodologies developed by Hoffman and co-workers to characterise cell morphology and cell health was adapted for the PMA differentiated U937 cells in the co-culture systems (Hoffman *et al.*, 2017).

Amiodarone is a cationic amphiphilic drug used clinically via the oral and systemic route to treat arrhythmia. It was selected as a model drug in this study as it is associated with inducing phospholipidosis in alveolar macrophages *in vivo* and *in vitro* (Hoffman *et al.*, 2017, 2020; A. Patel *et al.*, 2019). Cells undergoing phospholipidosis display distinct phenotypic changes, namely increase in cell size and distinct vacuolisation patterns within cells which have been characterised for macrophages *in vitro* (Hoffman *et al.*, 2020; Hoffman *et al.*, 2017;).

#### **5.4.1.1. Cell health determination**

One important consideration for the technique is that the multiple wash steps required as part of the staining procedure remove dead/dying cells from the sample as they detach from the surface of the well plate. Therefore, cells remaining on the plate represent the viable cells from the population, and the pronounced phenotypic changes that might be anticipated may be reduced if assessing drug concentrations that induce cell death. For this reason, amiodarone concentrations of 1  $\mu\text{M}$  and 10  $\mu\text{M}$  were selected as they induce phenotypic changes without reducing the cell population (i. e. cells remain attached to the well plate) (Hoffman *et al.*, 2017; Nioi *et al.*, 2007; Pauluhn, 2005; Reasor *et al.*, 2001; Wolkove, 2009). Whilst the cell number of PMA differentiated U937 cells was unaffected by amiodarone, the extracellular LDH concentration was significantly increased with amiodarone (Figure 5.1). This is likely to be a transient increase in cell membrane permeability rather than due to cell lysis as the proportion of LDH released relative to lysed control did not reflect the viable number of cells in the high content imaging analysis technique. LDH increase can be transient, and it is imperative that extracellular LDH concentrations should always be

considered alongside other endpoints (e.g. cell number, mitochondrial activity etc.) to validate membrane permeability (Kaja *et al.*, 2015). Membrane integrity measured by the high content image analysis technique (Figure 5.6C) confirmed this theory. Membrane integrity in this assay was assessed by the presence of an intracellular fluorescent dye that enters cells with compromised membrane permeability. Whilst membrane integrity was reduced, other markers of cell death (reduced cell count, reduced mitochondrial activity) were not observed, suggesting that these changes were likely to be transient.

The benefits of the models designed and validated in this thesis allow the culturing of barrier and PMA differentiated U937 cells in separate compartments. This model design proves favourable for cell health determination and associating responses to individual cell types. Multiple reports describe that macrophages interact weakly with epithelial cell surfaces under such LLC conditions and are easily removed and lost by aspiration of the medium (Kletting *et al.*, 2018). Macrophage cells cultured with alveolar cell types in the ALI system are too low in density to be easily harvested and detected with FC analysis (Luyts *et al.*, 2015). Other co-culture systems only compare viability or cell readout comparisons of monocultures to co-cultures where cell responses are measured as a whole tissue than separately. In the presence of LPS, the tri-culture airway model displayed increased IL-8 compared to THP-1 monoculture, whereby the origin of the cytokine could not be established due to the complex construction of the model (Costa *et al.*, 2019). The MTT assay was used to compare mono/ co-cultures of hAELVi and THP-1 cells for viability and robustness, yet the report could not discriminate between the viable cells and thus did not conclude cell health (Kletting *et al.*, 2018).

#### 5.4.1.2. Morphological characterisation

The high content image analysis methodology allows detailed analysis of cell features. Protocols for defining the nuclear area and cell area (segmentation) are well established, and the software was able to accurately identify and quantify these parameters based on greyscale images obtained for Hoechst and Cell Mask fluorescence microscopy. The morphological features of PMA-differentiated U937 cells are comparable with other studies reporting cell size (Hoffman *et al.*, 2017, 2020; Krombach *et al.*, 1997). Whilst small differences were observed for the cell area of PMA-differentiated U937 cells cultured in the presence and absence of epithelial cells in this study, these fall within the typical distribution for cell area of PMA-differentiated U937 cells (123-391  $\mu\text{m}^2$ ) as reported by Hoffman *et al.*, 2017.

Characterising the vacuolation parameters is more challenging as these are smaller and less clearly defined morphological features. Vacuoles were identified as non-stained areas within the cell area which were not stained with the Cell Mask dye. The methodology for identifying these features was optimised; however, a balance between the sensitivity of detecting all vacuoles and the accuracy of the size of the vacuole was struck. The number of vacuoles per cell and the average area occupied by a vacuole for PMA-differentiated U937 cells has been reported by Hoffman *et al.* The results from these studies were in agreement. Morphological characterisation of PMA-differentiated U937 cells in the presence or absence of amiodarone was in agreement with the findings of Hoffman *et al.*, 2017. This supports using the technique to assess the differences in baseline morphology and drug response for PMA-differentiated U937 cells in co-culture.

## **5.4.2 Impact of co-culture on PMA-differentiated U937 morphology**

### **5.4.2.1. AECI cells and PMA-differentiated U937 cells**

*In vivo*, alveolar macrophages are in close contact with both AECI and AECII cells within the alveolar sac. It has been established that the alveolar epithelium plays an important role in orchestrating immune responses of alveolar macrophages (Bhattacharya *et al.*, 2016; Müller *et al.*, 2010). For the hAELVi co-culture model, no significant differences in population profiling ( $p>0.05$ ) were observed for PMA-differentiated U937 cells in the presence or absence of amiodarone (Figure 5.9), and cell characteristics were comparable with PMA-differentiated U937 cells in monoculture. From the phenotypic analysis (Table 5.1), PMA-differentiated U937 cells in the hAELVi co-culture model had a comparable percentage of phenotypes in the absence of a stimulus. However, exposure to amiodarone indicated the presence of hAELVi cells reduced the size of vacuoles and raised mitochondrial activity in the PMA-differentiated U937 cells.

*In vivo*, AECI cells function to form the epithelial component of the thin air–blood barrier. It is possible that the presence of AEC I in co-culture increased the mitochondrial activity of the PMA differentiated U937 cells. More research into understanding the hAELVi phenotype is required to determine this outcome (Kletting *et al.*, 2018).

### **5.4.2.2. AECII cells and PMA-differentiated U937 cells**

The baseline characteristics and phenotypes for PMA-differentiated U937 cells cultured with A549 cells were comparable to cells in monoculture. However, on

exposure to amiodarone, mitochondrial activity was significantly increased ( $p < 0.05$ ) in both the population (Figure 5.9) and phenotypic analysis (Table 5.1), in comparison with PMA-differentiated U937 cells in monoculture.

*In vivo*, AECII cells function to synthesize and secrete surfactant material, initiate hyperplasia in reaction to alveolar epithelial injury and serve as the progenitor for AEC I cells (Fehrenbach, 2001). Interactions between AEC II cells and AMs are important for alveoli homeostasis. These interactions result in the clearance of alveolar surfactants to prevent phospholipid buildup in alveoli which can cause alveolar proteinosis leading to respiratory failure (Lindert *et al.*, 2007). Another unique feature of macrophage-epithelial interactions that might determine alveolar immunity is the alveolar wall liquid lining. The alveolar wall liquid lining defends against inhaled pathogens by providing an aqueous flow at the air-epithelial interphase towards the terminal bronchiolar epithelium, downstream from AMs (Suzuki *et al.*, 2014).

Increased mitochondrial activity is probably due to the AEC II (A549) cell. These secretory cells are responsible for the secretion of the protein, surfactants, and cytokine production. Chapter four describes increased cytokine production compared to AEC I cells in the presence of LPS. Thus, the mitochondrial activity could be associated with increased production of inflammatory proteins (He *et al.*, 2019)

Several A549- U937 co-culture and triculture models are established in the literature. Braydich-Stolle and colleagues constructed a co-culture system composed of PMA differentiated U937 cells with epithelial cells (A549) cultivated at LLC and exposed to aluminium nanoparticles pertaining to the biochemical interactions of the alveoli (Braydich-Stolle *et al.*, 2010). Rothen-Rutishauser and colleagues established a triple cell culture system cultivated at ALI composed of epithelial cells (A549), monocyte-

derived macrophages and dendritic cells, which could show more efficacy in predicting in vivo toxicity compared to mono-cultures (Rothen-Rutishauser *et al.*, 2005). Applications of additional models are discussed in chapter six.

### 5.4.3 Interpretation of data

The datasets produced by high content imaging are large and complex, making subsequent data analysis and interpretation challenging (Lin *et al.*, 2020). Here, four methods of data interpretation were considered. Firstly, the average morphological characteristics for all cells in the population were reported. This study findings show no changes in morphological characteristics based on average data outputs. Thus, high content imaging and analysis of average data sets may only be useful with potent and toxic concentrations of compounds. More subtle morphological changes are masked by the heterogeneous population with heterogeneous responses and will therefore go undetected.

The next approach was to consider a subset analysis. Cells with elevated mitochondrial activity were selected. Increased metabolic activity indicates change and response within the model's microenvironment and, therefore, the cells responding is more to a stimulus or drug treatment (K. Chan *et al.*, 2005).

The next approach was to profile the elevated responses of morphological profiles. A significant decrease in vacuole numbers and increasing mitochondrial activity is that only one or two elevated response characteristics are considered at a time. The advantage of this technique is the power in the datasets are individual for each cell.

The final approach used was the phenotyping approach to four main characteristics linked to foamy macrophages. These phenotypes were: mitochondrial activity, cell



area, number of vacuoles and percentage cell area occupied by number of vacuoles. This approach identified significant changes in macrophage-like cell- characteristics when exposed to amiodarone concentrations for both TI and TII co-culture systems. Until recently, understanding biological processes through phenotypic high content screening approaches have been limited to monoculture systems. The work in this chapter describes the application of an innovative high content screening assay for cellular toxicity and response to amiodarone. Plate-based assays are relatively easy to handle and can facilitate standardisation in a small laboratory setting, thus allowing the subsequent screening of compound libraries within a short time.

#### **5.4.4 Conclusion**

Morphology through high content screening can be used to identify foamy macrophages in both mono- and co-culture systems. PMA differentiated U937 cells did not appear to be affected by the presence of AEC I or AEC II cells but did show sensitivity when exposed to 10  $\mu$ M amiodarone concentrations, further supporting the appropriateness of more complex *in vitro* models. The use of co-culture models for high content screening requires particular considerations for throughput limitations, labour intensive experimental design, data-intensive computational methods. However, high data complexity leads to multiple data points for both selected populations or single cells compared with low data-complexity assays, which generate one data point for the whole population (Lin *et al.*, 2020), or a selected population could be adopted for modern drug discovery and toxicology.

# General discussion

## 6.1. Respiratory diseases

Respiratory diseases constitute a huge burden in our society. Worldwide, around 339 million people are living with asthma (*Asthma*, n.d.) and 251 million with chronic obstructive pulmonary disease (COPD) (*Chronic Obstructive Pulmonary Disease (COPD)*, n.d.). Furthermore, COVID-19 has recently become known across the globe as a respiratory disease with high mortality, particularly in high-risk categories (*Coronavirus Disease (COVID-19) Situation Reports*, n.d.). The COVID-19 pandemic highlighted what little we know about lung response biology and the valuable information learnt about the virus infection using *in vitro* science studies (Takayama, 2020). Consequently, the compound annual growth rate (CAGR) of the global respiratory drug market has grown from 17% to 42% in 2020 (*World Respiratory Diseases Drugs Market Analysis 2020 - Market Forecast to Grow to \$92.6 Billion in 2020 at a CAGR of 42.5% Due to Increased Demand as a Result of COVID-19 Outbreak*, n.d.). Subsequently, the lung has gained interest as a site for drug delivery for both local targeting of therapeutics for treating respiratory diseases and for the inhalation of systemic therapeutic outputs (Takayama, 2020).

Whilst there is an overabundance of research regarding particle size, device development and particle deposition, research regarding the morphological and functional mechanisms of cellular responses to drug molecules in the alveolar space and the site of macrophages is limited (Clippinger *et al.*, 2018; Patton *et al.*, 2010). Well characterised *in vitro* models have been established, and drug transport

mechanisms are reasonably understood for the main sites of oral drug absorption (small intestine), metabolism (liver) and secretion (kidney). In contrast, airway alveolus *in vitro* models and alveolar macrophages are less well characterised (Evans *et al.*, 2020). Establishment of standardised *in vitro* alveolar models with characterised functional properties, including morphological measurements, would provide an ideal platform for developing novel, effective treatments with high bioavailability for both airway and systemic diseases.

## **6.2. Immunocompetent alveolar *in vitro* cell culture models**

The use of *in vitro* cell culture models for screening of drug candidates and disease modelling has become widespread (C. Ehrhardt *et al.*, 2008). These studies have focused on characterising selected bronchial epithelial cell *in vitro* models to assess their morphological and functional suitability as drug molecule screening tools with no immunocompetent component. Employment of alveolar *in vitro* models has had significant implications for high throughput screening of potentially therapeutic compounds, enhancing the understanding of cell toxicity at the molecular level and reducing the use of *in vivo* testing (Clippinger *et al.*, 2018). However, unless these models represent the human alveolar region *in vivo* or a correlation to the *in vivo* situation can be deduced, these efforts may be ineffective.

## **6.3. Limitations of Current *in vitro* Inhalation Testing**

Due to low demands in advanced cell culture, a limited number of tools to develop *in vitro* models have been developed. Such tools include cell growth platforms for cell coculturing and anatomically suitable cell types representative of those in the alveolar sacs, particularly alveolar macrophage cells (Forbes *et al.*, 2014). Recent advances in tissue-engineering technologies for *in vitro* cell-based models for drug molecule

screening can be classified into (i) lung cultures grown at the Air–Liquid Interphase(ALI) or Liquid-Liquid Interphase(LLI); (ii) lung organoids; and (iii) lung-on-chip (Sedláková *et al.*, 2019).

Macrophage characteristics, particularly concerning identifying and defining macrophage response to drug molecules in the alveolar sacs, have remained relatively uncharacterised in both *in vitro* bronchial and alveolar models. The available myeloid cell lines differ morphologically and biochemically from each other in standard culture conditions and following differentiation via PMA stimulus. Phenotypically, HL-60 cells are progenitors of granulocytes, whereas THP-1 and U937 are progenitors of pro-monocytes and monocytes, respectively. HL-60 and THP-1 blood leukemic cells are less mature than U937 cells, which originate from a pleural effusion of histiocytic lymphoma and are arrested in a more advanced phase of differentiation (Chanput *et al.*, 2015; Harris *et al.*, 1985).

Finally, variation in the construction and cell set-up of the alveolar *in vitro* models prevents molecular and drug response comparisons in the literature. Monoculture models are too simplistic, falling short in recapitulating the complex interactions between different cell types and tissues occurring in humans (Movia *et al.*, 2020), tetra-culture models (Klein *et al.*, 2013) are too complex, requiring further characterisation and not commercially relevant.

Herein, the properties of the two *in vitro* co-culture models characterised in this thesis will be summarised, and their effectiveness as a model for alveolar-like macrophage response discussed in connection with the limitations named above. Additionally, the potential uses for these models in current and future *in vitro* -lung research will be considered.

#### **6.4. Overcoming limitations: Advanced tools, the immunocompetent *in vitro* model**

In the presence of PMA, human monocytic U937 cells were differentiated to alveolar-like macrophages to be morphologically and functionally like human AMs. The literature reported a plethora of PMA differentiation protocols which the findings in chapter three confirmed generated different cell phenotypes. Of these findings, the PMA differentiated U937 cells were most characteristically like AMs following incubation with 100 nM PMA for 72 hours followed by a 24-hour rest period. The reproducible findings of the cells will support immunocompetent airway studies and their AM-like characteristics suitable for further development into multi-cell culture systems.

Newly developed alveolar epithelial (hAELVi) cells challenged the current need to use primary AECs with the advantage of being a type 1 cell line with tight junction and, thus, representative of 95% of the airway epithelium without the current limitations primary cells feature (Wirth *et al.*, 2016). Culturing hAELVi cells proved challenging with regular bacterial contaminations and low cell proliferation. Formation of a monolayer and cellular tight junctions were detected after day 7, with the cells showing promise for transport studies of drug compounds. Development of the hAELVi cell was an innovative approach for type I epithelial cells.

The third cell line examined was the well-established alveolar epithelial (A549) type II cells. With the alveolar epithelium comprised of between 2 -8% of type II cells, A549 cells are over exploited in their epithelial functions *in vitro* a monolayer epithelium. Better suited for non-transport studies (e.g., metabolism of certain classes of xenobiotics) (Hiemstra *et al.*, 2018; Weber *et al.*, 2013), the A549 was used to

develop the second co-culture model to complement the study as a comparative design *in vitro* tool and determine changes in AM in the presence of difference cell types like to findings in the literature. *In vitro* co-culture models with A549 cells are established in the literature.

When grown on permeable membranes (Transwells<sup>®</sup>), alveolar epithelial cells form monolayers with high functional and morphological resemblance to type I and type II as described in the literature (Kletting, 2016; Movia *et al.*, 2019; Swain *et al.*, 2010). Additionally, long term culture of A549 was shown to promote a more differentiated AECII cell phenotype with increased numbers of up- and down-regulated genes shared with primary cells suggesting the adoption of AECII characteristics and multilamellar body (Cooper *et al.*, 2016).

Co-cultured together as an immunocompetent type I and type II AEC model, the obtained results suggest that the established alveolar co-cultures are promising models that can serve as tools to assess the lung in a healthy state and in measuring adaptive and adverse macrophage response. Furthermore the simplistic set up of these *in vitro* models allows for adaptations in applying cell culture techniques with tools to build on immunocompetent models with/ without alveolar epithelial cells for example (Felder *et al.*, 2019; Millar *et al.*, 2016): fibroblasts or endothelial cells for focus on pulmonary fibrosis disease and acute respiratory distress syndrome treatment studies respectively.

Understanding macrophage biology has improved dramatically in the past decade (Joshi *et al.*, 2018). Alveolar macrophages demonstrate remarkable plasticity to their surrounding environment, including reversibility of their foamy phenotypes when

exposed to amiodarone through assessment of morphological changes over time (Hoffman *et al.*, 2020). Thus, knowledge of the mechanisms through which inflammatory and environmental insults affect alveolar macrophage function can guide the development of novel therapies for respiratory diseases with macrophage involvement (Hoffman *et al.*, 2017). As a tool to support guided drug development, an understanding of AM polarisation *in situ* of a healthy human population which, is still in its infancy, is required (Arora *et al.*, 2018) as much of the current research reported are based on findings in mice (C. Song *et al.*, 2012; Veldhuizen *et al.*, 2019). Differentiated monocytic U937 cells, characterised under a standardised protocol, may provide a platform to take a systems biology approach to investigate the function of AMs in the context of their partnering cell types *in vitro*.

As identified in chapter 1, *in vitro* models ranging from monocultures to multiple cell co-cultures and three-dimensional (3D) lung tissue models have been developed cultured on *in vitro* cell platforms. These platforms differ with respect to the types of cells included and the format for which they are grown (e.g., submerged in liquid-liquid condition or grown at the air-liquid interface), which influences important transport and transformation mechanisms (Vogel *et al.*, 2012). More complex biomaterial scaffolds, polymer gels (Sedláková *et al.*, 2019), spheroid structures (Movia *et al.*, 2020) and new innovative scaffolds made from keratin (Bochynska-Czyz *et al.*, 2020) and plant leaves (Lacombe *et al.*, 2020) are also available. Each system has its advantages and limitations, and the choice of which system to use will depend on the specific purpose of the testing.

3D models of lung tissue have been developed cultured on transwells regularly involve epithelial layer and other cells, such as; fibroblasts and immune cells (Alfaro-Moreno

*et al.*, 2008; Braydich-Stolle *et al.*, 2010; Carterson *et al.*, 2005; Crabbé *et al.*, 2011; Klein *et al.*, 2013; Kletting, 2016; Lehmann *et al.*, 2011; Rothen-Rutishauser *et al.*, 2005). Although abundant in the literature, 3D co-culture models are presently in development to investigate the biological roles of AMs in human respiratory health and disease (Steimer *et al.*, 2005) and in inhaled drug discovery research (Forbes *et al.*, 2014). Lack of appropriateness and overcomplexity of 3D lung models results in fewer commercially available *in vitro* models. Furthermore, few represent alveolar drug delivery and response (Forbes *et al.*, 2014).

Commercially available alveolar *in vitro* models offers advantages for testing on a standardised platform which, when used and published in the literature by multiple laboratories, allows for accurate comparisons of findings. Higher quality assurance and reproducibility between models would additionally be expected. It is important to note several drawbacks to current commercial models. EpiAlveolar™ combines primary human alveolar epithelial cells (types not disclosed), endothelial and fibroblast cells and undisclosed monocyte-derived macrophages (Jackson *et al.*, 2018). The model response was assessed for cytotoxicity controversially by LDH measurements and elevated IL-8 levels (Zavala *et al.*, 2016).

Obtained from patients undergoing lung lobectomy, SmallAir™ contains primary cells from the distal lung tissue, including beating cilia, goblet cells, and clara cells (Huang *et al.*, 2017). Although this small airway model is most likely the closest human *in vitro* model of the lower airways to contain primary cells, it does not represent alveoli physiology.

As a result of respiratory diseases, lung injuries in patients are probable. The extent of the lung injury and type of disease does not appear to be a factor when allocating cells to these primary airway models (Zavala *et al.*, 2016). Although the



commercially available cells described above are of primary origin, they should not be classified as healthy. It is important to note; there may be considerable differences between each cell model due to factors such as the patient's disease, length of time with the condition, treatments received, age, sex and if they are a smoker. None of which are disclosed to the consumer. Recently bronchial and small airway cultures from different donors were found to vary functionally in thickness, cell-type composition, and transepithelial electrical resistance when exposed to stimuli (Bovard *et al.*, 2020).

## 6.5. Concluding thoughts and deliverables of this PhD

Multiple scientific benefits were achieved throughout this research degree. Further innovations will reduce the requirement to conduct multiple *in vivo* studies. Advancements in standardising differentiation protocols of immortalised cells allowed consistency of data between studies and methodologies to engineer easy cell culture set-up allowing acceleration of studies that cannot feasibly be performed in live animal models. Finally, first-line investigations of specific responses/ immune pathways *in vitro* are allowed. Hence they are suited to drug discovery screens and toxicology studies.

Another outcome of this PhD is an alternative to *in vivo* experiments on respiratory systems, negating mild-moderate invasive procedures on rodents, ruminants and primates. Up to 24% of animals used for scientific procedures per year (UK) were used in respiratory and immune system studies (Annual Statistics of Scientific Procedures on Living Animals for Great Britain, 2017).

Practical benefits of the work completed enable users to construct an immunocompetent human alveolar model with desirable physiological and structural features and function of the human alveolus within 2 weeks. Immortalised cell lines from this study facilitate reproducibility and comparisons with previously published literature. The works can facilitate a cost-effective non-animal method approach compared to performing similar experiments *in vivo*, whereby an acute inhalation study of three hundred rats' costs 1.8 million pounds. Finally, an applied biotechnology approach enables researchers without access to animal facilities to study respiratory systems but can maintain a translational focus with their work.

Current applications from work completed throughout the thesis are that immortalised cell lines are suitable for studies involving monocultures of alveolar like macrophages and alveolar epithelial type I and II cells. The co-culture may be used for inhaled pharmaceutical response studies and safety assessment studies of inhaled manufactured chemicals (consumer products), drug molecules, vaccines, and interactions.

## 6.6. Future perspectives

*In vitro*, human alveolar models provide a new powerful platform to investigate cellular behaviour and mechanism of human lung alveolar cells, cell-cell interactions, macrophage response interactions, and conduct drug screenings and toxicity assays. Despite these advances, improved model systems to recapitulate the complexity of *in vitro* human lungs are still required.

However, imitations to the models designed in this thesis remain, the cell lines are not 100% representative of AMs, and human tissue comparison work will be needed to

advance the models further. A comparison study of the models to multiple human *ex vivo* alveolar cells will determine their relevance, similarities, and differences. As mentioned earlier, access to healthy human alveolar tissue is limited in patient number and sample size of <50,000 AMs per patient.

Another limitation was that the models included either AEC I or AECII cells and have not yet been combined as seen *in situ*. From our studies, the AECII cells played a significant role in cell-cell interactions with AMs. Compared to AECI cells, their main function was maintaining an integral barrier. Further, the AECI cells proved enormously challenging to maintain in culture, particularly on Transwell inserts both at ALI and LLC, where the model failure rate, at its lowest, was 30%. Hence, cell culture skillset and knowledge is specifically required for the hAELVi cell line to reduce the failure rate from 90% to 30%.

The next research step would be to develop methods in co-culturing AECI and AECII cells together, maintaining tight junctions of >500Ωmh whilst signalling to AMs. Both epithelial cells would require viability studies in their mediums or combined mediums before this. Adapting the cells to different mediums could alter cell characteristics and ultimately affect the models' response to external stimuli.

Further research is necessary to determine the viability of the models in transit from lab to lab. Preliminary studies showed that the AMs were sensitive to environmental changes such as temperature and atmosphere and vibrations that the cells could suffer in transit. Hence, transporting the models to other labs to assess tests' continued functionality and reproducibility will be imperative. Moreover, cryopreservation of the AM cells was not feasible. Post freeze/thaw cycles were found to cause cell death and

cell differentiation. Additionally, investigative proof of concept experiments found the current cells viably sensitive when embedded in agarose gels. Research to develop novel transport systems for cell culture is required.

Finally, prolonged culture, >5 weeks of the models showed the AMs were susceptible to reverse differentiation whereby the AMs began to revert to their monocyte phenotype. Additional research is needed to determine if AMs require regular PMA stimulation to maintain cells in their mature state.

To conclude, multiple research approaches are needed to continue advancing the current immunocompetent models for the screening of new aerosolised medicines and AM response biology. The *in vitro* models designed, validated and discussed in this thesis have set a firm baseline for development and research advancements for the lungs.

Patents have been submitted for both immunocompetent *in vitro* models designed for this thesis. The application of the models into the commercial field has already expanded beyond the pharmaceutical sector. Extensive market validation confirmed the commercial value of the technologies to the chemical, agrichemical and consumer product market to assess human safety response thresholds to inhaled products from e-vapour, aerosol and make-up powders.

Co-owned and led by the author, the spin-out company ImmuONE Limited was incorporated and secured significant funding and capital in 2019. ImmuONE is currently adapting the model for commercial use and scale-up manufacture. Research and development are ongoing to assess the scales of services required to address the

inhalation industry needs. Our future aims are to provide improved *in vitro* non-animal methods and provide stronger human-relevant predictive outputs so that chemical compounds would fail earlier in their development course.

## 7. References

- Aderem, A., & Underhill, D. M. (1999). Mechanisms of phagocytosis in macrophages. In *Annual Review of Immunology* (Vol. 17, Issue 1, pp. 593–623). Annual Reviews 4139 El Camino Way, P.O. Box 10139, Palo Alto, CA 94303-0139, USA.
- Alessio, M., De Monte, L., Scirea, A., Gruarin, P., Tandon, N. N., & Sitia, R. (1996). Synthesis, processing, and intracellular transport of CD36 during monocytic differentiation. *The Journal of Biological Chemistry*, 271(3), 1770–1775.
- Alfaro-Moreno, E., Nawrot, T. S., Vanaudenaerde, B. M., Hoylaerts, M. F., Vanoirbeek, J. A., Nemery, B., & Hoet, P. H. M. (2008). Co-cultures of multiple cell types mimic pulmonary cell communication in response to urban PM10. *The European Respiratory Journal*, 32(5), 1184–1194.
- Altin, J. G., & Sloan, E. K. (1997). The role of CD45 and CD45-associated molecules in T cell activation. *Immunology and Cell Biology*, 75(5), 430–445.
- Arora, S., Dev, K., Agarwal, B., Das, P., & Syed, M. A. (2018). Macrophages: Their role, activation and polarization in pulmonary diseases. *Immunobiology*, 223(4–5), 383–396.
- Arredouani, M. S., Palecanda, A., Koziel, H., Huang, Y.-C., Imrich, A., Sulahian, T. H., Ning, Y. Y., Yang, Z., Pikkarainen, T., Sankala, M., Vargas, S. O., Takeya, M., Tryggvason, K., & Kobzik, L. (2005). MARCO Is the Major Binding Receptor for Unopsonized Particles and Bacteria on Human Alveolar Macrophages. *The Journal of Immunology*, 175(9), 6058–6064.
- Asthma*. (n.d.). Retrieved September 30, 2020, from <https://www.who.int/news-room/q-a-detail/asthma>
- ATCC. (2002). *ATTC*. [www.atcc.org/](http://www.atcc.org/)
- Aulton, M. E., & Taylor, K. M. G. (2013). *Aulton's Pharmaceuticals : The Design and Manufacture of Medicines*. Elsevier.
- Baek, Y.-S., Haas, S., Hackstein, H., Bein, G., Hernandez-Santana, M., Lehrach, H., Sauer, S., & Seitz, H. (2009). Identification of novel transcriptional regulators involved in macrophage differentiation and activation in U937 cells. *BMC Immunology*, 10(1), 18.
- Bell, S. M., Chang, X., Wambaugh, J. F., Allen, D. G., Bartels, M., Brouwer, K. L. R.,

- Casey, W. M., Choksi, N., Ferguson, S. S., Fraczekiewicz, G., Jarabek, A. M., Ke, A., Lumen, A., Lynn, S. G., Paini, A., Price, P. S., Ring, C., Simon, T. W., Sipes, N. S., ... Kleinstreuer, N. C. (2018). In vitro to in vivo extrapolation for high throughput prioritization and decision making. *Toxicology in Vitro*, 47, 213–227.
- Berger, J. T., Voynow, J. A., Peters, K. W., & Rose, M. C. (2012). Respiratory Carcinoma Cell Lines. *American Journal of Respiratory Cell and Molecular Biology*.
- BéruBé, K., Aufderheide, M., Breheny, D., Clothier, R., Combes, R., Duffin, R., Forbes, B., Gaça, M., Gray, A., Hall, I., Kelly, M., Lethem, M., Liebsch, M., Merolla, L., Morin, J.-P., Seagrave, J., Swartz, M. A., Tetley, T. D., & Umachandran, M. (2009). In vitro models of inhalation toxicity and disease. The report of a FRAME workshop. *Alternatives to Laboratory Animals : ATLA*, 37(1), 89–141.
- Bhowmick, R., & Gappa-Fahlenkamp, H. (2016). Cells and Culture Systems Used to Model the Small Airway Epithelium. *Lung*, 194(3), 419–428.
- Bitterle, E., Karg, E., Schroepel, A., Kreyling, W. G., Tippe, A., Ferron, G. A., Schmid, O., Heyder, J., Maier, K. L., & Hofer, T. (2006). Dose-controlled exposure of A549 epithelial cells at the air–liquid interphaseto airborne ultrafine carbonaceous particles. *Chemosphere*, 65(10), 1784–1790.
- Blank, F., Rothen-Rutishauser, B., & Gehr, P. (2007). Dendritic Cells and Macrophages Form a Transepithelial Network against Foreign Particulate Antigens. *American Journal of Respiratory Cell and Molecular Biology*, 36(6), 669–677.
- Bleil, J. U., Heller, A. R., Fehrenbach, A., Heintz, M., Fehrenbach, H., Klenz, G., Abreu, M. G. de, Hübler, M., Spieth, P. M., & Koch, T. (2010). Pretreatment with perfluorohexane vapor attenuates fMLP-induced lung injury in isolated perfused rabbit lungs. *Experimental Lung Research*, 36(6), 342–351.
- Bochynska-Czyz, M., Redkiewicz, P., Kozłowska, H., Matalinska, J., Konop, M., & Kosson, P. (2020). Can keratin scaffolds be used for creating three-dimensional cell cultures? *Open Medicine*, 15(1), 249–253.
- Borok, Z., Liebler, J. M., Lubman, R. L., Foster, M. J., Zhou, B., Li, X., Zabski, S. M., Kim, K.-J., & Crandall, E. D. (2002). Na transport proteins are expressed by rat alveolar epithelial type I cells. *American Journal of Physiology. Lung Cellular and Molecular Physiology*, 282(4), L599-608.
- Bovard, D., Giralt, A., Trivedi, K., Neau, L., Kanellos, P., Iskandar, A., Kondylis, A., Luettich, K., Frentzel, S., Hoeng, J., & Peitsch, M. C. (2020). Comparison of the basic morphology and function of 3D lung epithelial cultures derived from several donors. *Current Research in Toxicology*, 1, 56–69.
- Braakhuis, H. M., Giannakou, C., Peijnenburg, W. J., Vermeulen, J., van Loveren, H., & Park, M. V. (2016). Simple in vitro models can predict pulmonary toxicity of silver nanoparticles. *Nanotoxicology*, 5390(February), 1–10.
- Braydich-Stolle, L. K., Speshock, J. L., Castle, A., Smith, M., Murdock, R. C., & Hussain, S. M. (2010). Nanosized Aluminum Altered Immune Function. *Acs*

- Nano*, 4(7), 3661–3670.
- Byron, P. R., Roberts, S. R. N., & Clark, A. R. (1986). An Isolated Perfused Rat Lung Preparation for the Study of Aerosolized Drug Deposition and Absorption. *Journal of Pharmaceutical Sciences*, 75(2), 168–171.
- Cai, Y., Sugimoto, C., Arainga, M., Alvarez, X., Didier, E. S., & Kuroda, M. J. (2014). In vivo characterization of alveolar and interstitial lung macrophages in rhesus macaques: implications for understanding lung disease in humans. *Journal of Immunology (Baltimore, Md. : 1950)*, 192(6), 2821–2829.
- Campbell, L., Hollins, A. J., Al-Eid, A., Newman, G. R., von Ruhland, C., & Gumbleton, M. (1999). Caveolin-1 expression and caveolae biogenesis during cell transdifferentiation in lung alveolar epithelial primary cultures. *Biochemical and Biophysical Research Communications*, 262(3), 744–751.
- Carterson, A. J., Höner zu Bentrop, K., Ott, C. M., Clarke, M. S., Pierson, D. L., Vanderburg, C. R., Buchanan, K. L., Nickerson, C. A., & Schurr, M. J. (2005). A549 lung epithelial cells grown as three-dimensional aggregates: alternative tissue culture model for *Pseudomonas aeruginosa* pathogenesis. *Infection and Immunity*, 73(2), 1129–1140.
- Cassetta, L., Cassol, E., & Poli, G. (2011). Macrophage Polarization in Health and Disease. *The Scientific World Journal*, 11, 2391–2402.
- Chan, P. G., Kumar, A., Subramaniam, K., & Sanchez, P. G. (2020). Ex Vivo Lung Perfusion: A Review of Research and Clinical Practices. *Seminars in Cardiothoracic and Vascular Anesthesia*, 24(1), 34–44.
- Chana, K. K., Fenwick, P. S., Nicholson, A. G., Barnes, P. J., & Donnelly, L. E. (2014). Identification of a distinct glucocorticosteroid-insensitive pulmonary macrophage phenotype in patients with chronic obstructive pulmonary disease. *The Journal of Allergy and Clinical Immunology*, 133(1), 207-16.e1-11.
- Chanput, W., Mes, J. J., & Wichers, H. J. (2014). THP-1 cell line: An in vitro cell model for immune modulation approach. *International Immunopharmacology*, 23(1), 37–45.
- Chanput, W., Peters, V., & Harry, W. (2015). *The Impact of Food Bioactives on Health* (K. Verhoeckx, P. Cotter, I. López-Expósito, C. Kleiveland, T. Lea, A. Mackie, T. Requena, D. Swiatecka, & H. Wichers (Eds.)). Springer International Publishing.
- Cheek, J. M., Evans, M. J., & Crandall, E. D. (1989). Type I cell-like morphology in tight alveolar epithelial monolayers. *Experimental Cell Research*, 184(2), 375–387.
- Chen, S., Weller, M. A., & Barnhart, M. I. (1982). Species comparisons of bronchoalveolar lavages from guinea pigs and rats exposed in vivo to diesel exhaust for one year. *Scanning Electron Microscopy, Pt 4*, 1687–1698.
- Cheng, Y. S., Bowen, L., Rando, R. J., Postlethwait, E. M., Squadrito, G. L., & Matalon, S. (2010). Exposing animals to oxidant gases: nose only vs. whole body. *Proceedings of the American Thoracic Society*, 7(4), 264–268.
- Chronic obstructive pulmonary disease (COPD)*. (n.d.). Retrieved September 30,

- 2020, from [https://www.who.int/news-room/fact-sheets/detail/chronic-obstructive-pulmonary-disease-\(copd\)](https://www.who.int/news-room/fact-sheets/detail/chronic-obstructive-pulmonary-disease-(copd))
- Clancy, J., & McVicar, A. (2002). *Physiology and Anatomy, 2Ed: A Homeostatic Approach*. Taylor & Francis.
- Clippinger, A. J., Allen, D., Behrsing, H., Bérubé, K. A., Bolger, M. B., Casey, W., DeLorme, M., Gaça, M., Gehen, S. C., Glover, K., Hayden, P., Hinderliter, P., Hotchkiss, J. A., Iskandar, A., Keyser, B., Luettich, K., Ma-Hock, L., Maione, A. G., Makena, P., ... Jarabek, A. M. (2018). Pathway-based predictive approaches for non-animal assessment of acute inhalation toxicity. *Toxicology in Vitro*, 52, 131–145.
- Colbeck, I., & Lazaridis, M. (2014). *Aerosol Science: Technology and Applications*. Wiley.
- Cooper, J. R., Abdullatif, M. B., Burnett, E. C., Kempself, K. E., Conforti, F., Tolley, H., Collins, J. E., & Davies, D. E. (2016). Long Term Culture of the A549 Cancer Cell Line Promotes Multilamellar Body Formation and Differentiation towards an Alveolar Type II Pneumocyte Phenotype. *PLOS ONE*, 11(10), e0164438.
- Coronavirus Disease (COVID-19) Situation Reports*. (n.d.). Retrieved September 30, 2020, from <https://www.who.int/emergencies/diseases/novel-coronavirus-2019/situation-reports/>
- Crabbe, A., Sarker, S. F., Van Houdt, R., Ott, C. M., Leys, N., Cornelis, P., & Nickerson, C. A. (2011). Alveolar epithelium protects macrophages from quorum sensing-induced cytotoxicity in a three-dimensional co-culture model. *Cellular Microbiology*, 13(3), 469-+.
- Crabbé, A., Sarker, S. F., Van Houdt, R., Ott, C. M., Leys, N., Cornelis, P., & Nickerson, C. A. (2011). Alveolar epithelium protects macrophages from quorum sensing-induced cytotoxicity in a three-dimensional co-culture model. *Cellular Microbiology*, 13(3), 469–481.
- Crapo, J. D., Young, S. L., Fram, E. K., Pinkerton, K. E., Barry, B. E., & Crapo, R. O. (1983). Morphometric characteristics of cells in the alveolar region of mammalian lungs. *The American Review of Respiratory Disease*, 128(2 Pt 2), S42-6.
- Crocker, P. R. (2002). Siglecs: sialic-acid-binding immunoglobulin-like lectins in cell-cell interactions and signalling. *Current Opinion in Structural Biology*, 12(5), 609–615.
- Cryan, S.-A., Sivadas, N., & Garcia-Contreras, L. (2007). In vivo animal models for drug delivery across the lung mucosal barrier. *Advanced Drug Delivery Reviews*, 59(11), 1133–1151.
- Daigneault, M., Preston, J. A., Marriott, H. M., Whyte, M. K. B., & Dockrell, D. H. (2010). The identification of markers of macrophage differentiation in PMA-stimulated THP-1 cells and monocyte-derived macrophages. *PloS One*, 5(1), e8668.
- Daum, N., Kuehn, A., Hein, S., Schaefer, U. F., Huwer, H., & Lehr, C. M. (2012). Isolation, cultivation, and application of human alveolar epithelial cells. In



- Methods in Molecular Biology* (Vol. 806, pp. 31–42). Humana Press.
- Davies, A. S., & Moores, C. (2003). *The Respiratory System*. Churchill Livingstone.
- de Souza Carvalho, C., Daum, N., & Lehr, C.-M. (2014). Carrier interactions with the biological barriers of the lung: advanced in vitro models and challenges for pulmonary drug delivery. *Advanced Drug Delivery Reviews*, 75, 129–140.
- Demling, N., Ehrhardt, C., Kasper, M., Laue, M., Knels, L., & Rieber, E. P. (2006). Promotion of cell adherence and spreading: a novel function of RAGE, the highly selective differentiation marker of human alveolar epithelial type I cells. *Cell and Tissue Research*, 323(3), 475–488.
- Drent, M., Cobben, N. A. M., Henderson, R. F., Wouters, E. F. M., & Van Diejen-Visser, M. (1996). Usefulness of lactate dehydrogenase and its isoenzymes as indicators of lung damage or inflammation. In *European Respiratory Journal* (Vol. 9, Issue 8, pp. 1736–1742). European Respiratory Society.
- Driscoll, K. E., Carter, J. M., Iype, P. T., Kumari, H. L., Crosby, L. L., Aardema, M. J., Isfort, R. J., Cody, D., Chestnut, M. H., & Burns, J. L. Establishment of immortalized alveolar type II epithelial cell lines from adult rats. *In Vitro Cellular & Developmental Biology. Animal*, 31(7), 516–527.
- Edmondson, R., Broglie, J., Adcock, A., & Yang, L. (2014). Three-dimensional cell culture systems and their applications in drug discovery and cell-based biosensors. In *Assay and Drug Development Technologies* (Vol. 12, Issue 4, pp. 207–218). Mary Ann Liebert Inc.
- Ehrhardt, C., & Forbes, B. (2008). *Drug absorption studies in situ, in vitro and in sillico models* (C. (School of P. and P. S. T. C. D. Ehrhardt (Ed.)). Springer.
- Ehrhardt, C., Kneuer, C., Fiegel, J., Hanes, J., Schaefer, U., Kim, K. J., & Lehr, C. M. (2002). Influence of apical fluid volume on the development of functional intercellular junctions in the human epithelial cell line 16HBE14o-: Implications for the use of this cell line as an in vitro model for bronchial drug absorption studies. *Cell and Tissue Research*, 308(3), 391–400.
- Elbert, K. J., Schäfer, U. F., Schäfers, H.-J., Kim, K.-J., Lee, V. H. L., & Lehr, C.-M. (1999). Monolayers of Human Alveolar Epithelial Cells in Primary Culture for Pulmonary Absorption and Transport Studies. *Pharmaceutical Research*, 16(5), 601–608.
- Endemann, G., Stanton, L. W., Madden, K. S., Bryant, C. M., White, R. T., & Protter, A. A. (1993). CD36 is a receptor for oxidized low density lipoprotein. *J Biol Chem*, 268(16), 11811–11816.
- Esch, J. L., Spektor, D. M., & Lippmann, M. (1988). Effect of Lung Airway Branching Pattern and Gas Composition on Particle Deposition. II. Experimental Studies in Human and Canine Lungs. *Experimental Lung Research*, 14(3), 321–348.
- Evans, K. V., & Lee, J. (2020). Alveolar wars: The rise of in vitro models to understand human lung alveolar maintenance, regeneration, and disease. *STEM CELLS Translational Medicine*, sctm.19-0433.
- Fatehullah, A., Hui Tan, S., Barker, N., & et al, F. (n.d.). *Organoids as an in vitro model of human development and disease*.

- Fehrenbach, H. (2001). Alveolar epithelial type II cell : defender of the alveolus revisited. *Respiratory Research*, 2(1), 33–46.
- Felder, M., Trueeb, B., Stucki, A. O., Borcard, S., Stucki, J. D., Schnyder, B., Geiser, T., & Guenat, O. T. (2019). Impaired wound healing of alveolar lung epithelial cells in a breathing lung-on-a-chip. *Frontiers in Bioengineering and Biotechnology*, 7(JAN).
- Finkelstein, J. N., Maniscalco, W. M., & Shapiro, D. L. (1983). Properties of freshly isolated type II alveolar epithelial cells. *Biochimica et Biophysica Acta (BBA) - Molecular Cell Research*, 762(3), 398–404.
- Finnberg, N. K., Gokare, P., Lev, A., Grivennikov, S. I., MacFarlane, A. W., Campbell, K. S., Winters, R. M., Kaputa, K., Farma, J. M., Abbas, A. E.-S., Grasso, L., Nicolaides, N. C., & El-Deiry, W. S. (2017). Application of 3D tumoroid systems to define immune and cytotoxic therapeutic responses based on tumoroid and tissue slice culture molecular signatures. *Oncotarget*, 8(40), 66747–66757.
- Forbes, B., Asgharian, B., Dailey, L. A., Ferguson, D., Gerde, P., Gumbleton, M., Gustavsson, L., Hardy, C., Hassall, D., Jones, R., Lock, R., Maas, J., McGovern, T., Pitcairn, G. R., Somers, G., & Wolff, R. K. (2011). Challenges in inhaled product development and opportunities for open innovation. In *Advanced Drug Delivery Reviews* (Vol. 63, Issues 1–2, pp. 69–87). Adv Drug Deliv Rev.
- Forbes, B., O'Lone, R., Allen, P. P., Cahn, A., Clarke, C., Collinge, M., Dailey, L. A., Donnelly, L. E., Dybowski, J., Hassall, D., Hildebrand, D., Jones, R., Kilgour, J., Klapwijk, J., Maier, C. C., McGovern, T., Nikula, K., Parry, J. D., Reed, M. D., ... Wolfreys, A. (2014). Challenges for inhaled drug discovery and development: Induced alveolar macrophage responses. *Advanced Drug Delivery Reviews*, 71, 15–33.
- Foster, K. A., Oster, C. G., Mayer, M. M., Avery, M. L., & Audus, K. L. (1998). Characterization of the A549 cell line as a type II pulmonary epithelial cell model for drug metabolism. *Experimental Cell Research*, 243(2), 359–366.
- Fukunaga, M., & Tsuruda, K. (2001). Actinobacillus actinomycetemcomitans induces lethal effects on the macrophage-like human cell line U937. *Oral Microbiology and Immunology*, 16(5), 284–289.
- Gallagher, R., Collins, S., Trujillo, J., McCredie, K., Ahearn, M., Tsai, S., Metzgar, R., Aulakh, G., Ting, R., Ruscetti, F., & Gallo, R. (1979). Characterization of the continuous, differentiating myeloid cell line (HL-60) from a patient with acute promyelocytic leukemia. *Blood*, 54(3), 713–733.
- García, A., Serrano, A., Abril, E., Jimenez, P., Real, L. M., Cantón, J., Garrido, F., & Ruiz-cabello, F. (1999). Differential effect on U937 cell differentiation by targeting transcriptional factors implicated in tissue- or stage-specific induced integrin expression. *Experimental Hematology*, 27, 353–364.
- García, A., Serrano, A., Abril, E., Jimenez, P., Real, L. M., Cantón, J., Garrido, F., & Ruiz-Cabello, F. (1999). Differential effect on U937 cell differentiation by targeting transcriptional factors implicated in tissue- or stage-specific induced

- integrin expression. *Experimental Hematology*, 27(2), 353–364.
- Genin, M., Clement, F., Fattaccioli, A., Raes, M., & Michiels, C. (2015). M1 and M2 macrophages derived from THP-1 cells differentially modulate the response of cancer cells to etoposide. *BMC Cancer*, 15, 577.
- Giuliano, K. A., Haskins, J. R., & Taylor, D. L. (2003). Advances in high content screening for drug discovery. *Assay and Drug Development Technologies*, 1(4), 565–577.
- Gordon, S., & Taylor, P. R. (2005). Monocyte and macrophage heterogeneity. *Nature Reviews. Immunology*, 5(12), 953–964.
- Grabowski, N., Hillaireau, H., Vergnaud-Gauduchon, J., Nicolas, V., Tsapis, N., Kerdine-Römer, S., & Fattal, E. (2016). Surface-modified biodegradable nanoparticles' impact on cytotoxicity and inflammation response on a co-culture of lung epithelial cells and human-like macrophages. *Journal of Biomedical Nanotechnology*, 12(1), 135–146.
- Grainger, C. I., Greenwell, L. L., Lockley, D. J., Martin, G. P., & Forbes, B. (2006). Culture of Calu-3 cells at the air interphase provides a representative model of the airway epithelial barrier. *Pharmaceutical Research*, 23(7), 1482–1490.
- Green, F. H. Y., Vallyathan, V., & Hahn, F. F. (2007). Comparative pathology of environmental lung disease: an overview. *Toxicologic Pathology*, 35(1), 136–147.
- Greenberg, S., & Grinstein, S. (2002). Phagocytosis and innate immunity. *Current Opinion in Immunology*, 14(1), 136–145.
- Guhad, F. (2005). Introduction to the 3Rs (refinement, reduction and replacement). *Contemporary Topics in Laboratory Animal Science / American Association for Laboratory Animal Science*, 44(2), 58–59.
- Guilliams, M., De Kleer, I., Henri, S., Post, S., Vanhoutte, L., De Prijck, S., Deswarte, K., Malissen, B., Hammad, H., & Lambrecht, B. N. (2013). Alveolar macrophages develop from fetal monocytes that differentiate into long-lived cells in the first week of life via GM-CSF. *The Journal of Experimental Medicine*, 210(10), 1977–1992.
- Guillot, L., Nathan, N., Tabary, O., Thouvenin, G., Le Rouzic, P., Corvol, H., Amselem, S., & Clement, A. (2013). Alveolar epithelial cells: master regulators of lung homeostasis. *The International Journal of Biochemistry & Cell Biology*, 45(11), 2568–2573.
- Gupta, G., & Surolia, A. (2007). Collectins: sentinels of innate immunity. *BioEssays: News and Reviews in Molecular, Cellular and Developmental Biology*, 29(5), 452–464.
- Haghi, M., Hittinger, M., Zeng, Q., Oliver, B., Traini, D., Young, P. M., Huwer, H., Schneider-Daum, N., & Lehr, C. M. (2015). Mono- and Co-cultures of Bronchial and Alveolar Epithelial Cells Respond Differently to Proinflammatory Stimuli and Their Modulation by Salbutamol and Budesonide. *Molecular Pharmaceutics*, 12(8), 2625–2632.
- Halliwel, W. H. (1997). Cationic Amphiphilic Drug-Induced Phospholipidosis.

- Toxicologic Pathology*, 25(1), 53–60.
- Harris, P., Ralph, P., & Division, S. (1985). Human Leukemic Models of Myelomonocytic Development : A Review of the HL-60 and U937 Cell Lines. *Journal of Leukocyte Biology*, 42, 407–422.
- Hass, R., Bartels, H., Topley, N., Hadam, M., Köhler, L., Goppelt-Strübe, M., & Resch, K. (1989). TPA-induced differentiation and adhesion of U937 cells: changes in ultrastructure, cytoskeletal organization and expression of cell surface antigens. *European Journal of Cell Biology*, 48(2), 282–293.
- Hass, Ralf, Lonnemann, G., Mannel, D., Topley, N., Hartmann, A., Köhler, L., Resch, K., & Goppelt-Strübe, M. (1991). Regulation of TNF- $\alpha$ , IL-1 and IL-6 synthesis in differentiating human monoblastoid leukemic U937 cells. *Leukemia Research*, 15(5), 327–339.
- Heppleston, A. G., Wright, N. A., & Stewart, J. A. (1970). Experimental alveolar lipoproteinosis following the inhalation of silica. *The Journal of Pathology*, 101(4), 293–307.
- Herzog, E. L., Brody, A. R., Colby, T. V, Mason, R., & Williams, M. C. (2008). Knowns and unknowns of the alveolus. *Proceedings of the American Thoracic Society*, 5(7), 778–782.
- Hewison, M., Brennan, a, Singh-Ranger, R., Walters, J. C., Katz, D. R., & O’Riordan, J. L. (1992). The comparative role of 1,25-dihydroxycholecalciferol and phorbol esters in the differentiation of the U937 cell line. *Immunology*, 77, 304–311.
- Hiemstra, P. S., Grootaers, G., van der Does, A. M., Krul, C. A. M., & Kooter, I. M. (2018). Human lung epithelial cell cultures for analysis of inhaled toxicants: Lessons learned and future directions. In *Toxicology in Vitro* (Vol. 47).
- Hittinger, M., Juntke, J., Kletting, S., Schneider-Daum, N., de Souza Carvalho, C., & Lehr, C. M. (2015). Preclinical safety and efficacy models for pulmonary drug delivery of antimicrobials with focus on in vitro models. In *Advanced Drug Delivery Reviews* (Vol. 85, pp. 44–56).
- Hoffman, E., Kumar, A., Kanabar, V., Arno, M., Preux, L., Millar, V., Page, C., Collins, H., Mudway, I., Dailey, L. A., & Forbes, B. (2015). In Vitro Multiparameter Assay Development Strategy toward Differentiating Macrophage Responses to Inhaled Medicines. *Molecular Pharmaceutics*, 12(8), 2675–2687.
- Hoffman, E., Murnane, D., & Hutter, V. (2020). Investigating the Suitability of High Content Image Analysis as a Tool to Assess the Reversibility of Foamy Alveolar Macrophage Phenotypes In Vitro. *Pharmaceutics*, 12(3), 262.
- Hoffman, E., Patel, A., Ball, D., Klapwijk, J., Millar, V., Kumar, A., Martin, A., Mahendran, R., Dailey, L. A., Forbes, B., & Hutter, V. (2017). Morphometric Characterization of Rat and Human Alveolar Macrophage Cell Models and their Response to Amiodarone using High Content Image Analysis. *Pharmaceutical Research*, 34(12), 2466–2476.
- Huang, S., Boda, B., Vernaz, J., Ferreira, E., Wiszniewski, L., & Constant, S. (2017). Establishment and characterization of an in vitro human small airway model

- (SmallAir™). *European Journal of Pharmaceutics and Biopharmaceutics*, 118, 68–72.
- Huh, D., Hamilton, G. A., & Ingber, D. E. (2011). From 3D cell culture to organs-on-chips. *Trends in Cell Biology*, 21(12), 745–754.
- Hunninghake, G. W., & Crystal, R. G. (1983). Cigarette smoking and lung destruction. Accumulation of neutrophils in the lungs of cigarette smokers. *The American Review of Respiratory Disease*, 128(5), 833–838.
- Hussell, T., & Bell, T. J. (2014). Alveolar macrophages: plasticity in a tissue-specific context. *Nature Reviews. Immunology*, 14(2), 81–93.
- Hutter, V, Murnane, D., Reitdorf, K., Fowler, D., Walton, C., & Bootman, M. (2014). In vitro assessment of alveolar macrophage responses to inhaled particulate medicines. *Ddl-Conference.Org.Uk*.
- Hutter, Victoria. (2012). *Characterisation of ATP-Binding Cassette ( ABC ) Transporters in Bronchial Epithelial Cell Culture Models* (Issue February).
- Jackson, G. R., Maione, A. G., Klausner, M., & Hayden, P. J. (2018). Prevalidation of an Acute Inhalation Toxicity Test Using the EpiAirway in Vitro Human Airway Model. *Applied In Vitro Toxicology*, 4(2).
- Jadad, A. R., Moore, R. A., Carroll, D., Jenkinson, C., Reynolds, D. J. M., Gavaghan, D. J., & McQuay, H. J. (1996). Assessing the quality of reports of randomized clinical trials: Is blinding necessary? *Controlled Clinical Trials*, 17(1), 1–12.
- Jalava, P. I., Salonen, R. O., Pennanen, A. S., Sillanpää, M., Hälinen, A. I., Happonen, M. S., Hillamo, R., Brunekreef, B., Katsouyanni, K., Sunyer, J., & Hirvonen, M.-R. (2007). Heterogeneities in inflammatory and cytotoxic responses of RAW 264.7 macrophage cell line to urban air coarse, fine, and ultrafine particles from six European sampling campaigns. *Inhalation Toxicology*, 19(3), 213–225.
- Jersmann, H. P. A. (2005). Time to abandon dogma: CD14 is expressed by non-myeloid lineage cells. *Immunology and Cell Biology*, 83(5), 462–467.
- Jones, R. M., & Neef, N. (2012a). Interpretation and prediction of inhaled drug particle accumulation in the lung and its associated toxicity. *Xenobiotica; the Fate of Foreign Compounds in Biological Systems*, 42(1), 86–93.
- Jones, R. M., & Neef, N. (2012b). Interpretation and prediction of inhaled drug particle accumulation in the lung and its associated toxicity. *Xenobiotica; the Fate of Foreign Compounds in Biological Systems*, 42(1), 86–93.
- Joshi, N., Walter, J. M., & Misharin, A. V. (2018). Alveolar Macrophages. *Cellular Immunology*, 330, 86–90.
- Karimi, K., Sarir, H., Mortaz, E., Smit, J. J., Hosseini, H., De Kimpe, S. J., Nijkamp, F. P., & Folkerts, G. (2006). Toll-like receptor-4 mediates cigarette smoke-induced cytokine production by human macrophages. *Respiratory Research*, 7(1), 66.
- Kikkawa, Y., Yoneda, K., Smith, F., Packard, B., & Suzuki, K. (1975). The type II epithelial cells of the lung. II. Chemical composition and phospholipid synthesis. *Laboratory Investigation; a Journal of Technical Methods and Pathology*, 32(3),

295–302.

- Kitamura, H., Nakagawa, T., Takayama, M., Kimura, Y., Hijikata, A., Hijika, A., & Ohara, O. (2004). Post-transcriptional effects of phorbol 12-myristate 13-acetate on transcriptome of U937 cells. *FEBS Letters*, 578(1–2), 180–184.
- Klein, S. G., Serchi, T., Hoffmann, L., Blömeke, B., & Gutleb, A. C. (2013). An improved 3D tetraculture system mimicking the cellular organisation at the alveolar barrier to study the potential toxic effects of particles on the lung. *Particle and Fibre Toxicology*, 10, 31.
- Kletting, S. (2016). *A new cell line-based co-culture model of the human air-blood barrier to evaluate the interaction with aerosolized drug carriers*.
- Kooter, I. M., Alblas, M. J., Jedynska, A. D., Steenhof, M., Houtzager, M. M. G., & Ras, M. van. (2013). Alveolar epithelial cells (A549) exposed at the air–liquid interphaseto diesel exhaust: First study in TNO’s powertrain test center. *Toxicology in Vitro*, 27(8), 2342–2349.
- Kopf, M., Schneider, C., & Nobs, S. P. (2014). The development and function of lung resident macrophages and DCs. *Nature Immunology*, 16(1), 36–44.
- Koullapis, P., Ollson, B., Kassinos, S. C., & Sznitman, J. (2019). Multiscale in silico lung modeling strategies for aerosol inhalation therapy and drug delivery. *Current Opinion in Biomedical Engineering*, 11, 130–136.
- Krombach, F., Münzing, S., Allmeling, A.-M., Gerlach, J. T., Behr, J., & Dörger, M. (1997). Cell Size of Alveolar Macrophages: An Interspecies Comparison. *Environmental Health Perspectives*, 105(Supp. 5), 1261–1263.
- Kuroda, A., Sugiyama, E., Taki, H., Mino, T., & Kobayashi, M. (1997). Interleukin-4 Inhibits the Gene Expression and Biosynthesis of Cytosolic Phospholipase A2 in Lipopolysaccharide Stimulated U937 Macrophage Cell Line and Freshly Prepared Adherent Rheumatoid Synovial Cells. *Biochemical and Biophysical Research Communications*, 230(1), 40–43.
- Kwok, P. C. L., & Chan, H.-K. (2013). Pulmonary drug delivery. *Ther. Deliv.*, 4(8), 877–878.
- Lacombe, J., Harris, A. F., Zenhausern, R., Karsunsky, S., & Zenhausern, F. (2020). Plant-Based Scaffolds Modify Cellular Response to Drug and Radiation Exposure Compared to Standard Cell Culture Models. *Frontiers in Bioengineering and Biotechnology*, 8, 932.
- Larrick, J. W., Fischer, D. G., Anderson, S. J., & Koren, H. S. (1980). Characterization of a human macrophage-like cell line stimulated in vitro : a model of macrophage functions. *The Journal of Immunology*, 125(1), 6–12.
- Larson, B. (2015). BioTek White Paper - 3D Cell Culture: A Review of Current Techniques. In *BioTek* (pp. 1–10).
- Laskin, D. L., Weinberger, B., & Laskin, J. D. (2001). Functional heterogeneity in liver and lung macrophages. *J. Leukoc. Biol.*, 70(2), 163–170.
- Laube, B. L. (2014). The expanding role of aerosols in systemic drug delivery, gene therapy and vaccination: an update. *Translational Respiratory Medicine*, 2(1), 3.

- Lehmann, A. D., Daum, N., Bur, M., Lehr, C.-M., Gehr, P., & Rothen-Rutishauser, B. M. (2011). An in vitro triple cell co-culture model with primary cells mimicking the human alveolar epithelial barrier. *European Journal of Pharmaceutics and Biopharmaceutics*, 77(3), 398–406.
- Lewis, D. J., Williams, T. C., & Beck, S. L. (2014). Foamy macrophage responses in the rat lung following exposure to inhaled pharmaceuticals: a simple, pragmatic approach for inhaled drug development. *Journal of Applied Toxicology: JAT*, 34(4), 319–331.
- Lieber, M., Todaro, G., Smith, B., Szakal, A., & Nelson-Rees, W. (1976). A continuous tumor-cell line from a human lung carcinoma with properties of type II alveolar epithelial cells. *International Journal of Cancer*, 17(1), 62–70.
- Liles, W. C., & Van Voorhis, W. C. (1995). Review: nomenclature and biologic significance of cytokines involved in inflammation and the host immune response. *The Journal of Infectious Diseases*, 172(6), 1573–1580.
- Lofdahl, J. M., Wahlstrom, J., & Skold, C. M. (2006). Different inflammatory cell pattern and macrophage phenotype in chronic obstructive pulmonary disease patients, smokers and non-smokers. *Clinical and Experimental Immunology*, 145(3), 428–437.
- Loira-Pastoriza, C., Todoroff, J., & Vanbever, R. (2014). Delivery strategies for sustained drug release in the lungs. *Advanced Drug Delivery Reviews*, 75, 81–91.
- Luyts, K., Napierska, D., Dinsdale, D., Klein, S. G., Serchi, T., & Hoet, P. H. M. (2015). A co-culture model of the lung-blood barrier: The role of activated phagocytic cells. In *Toxicology in Vitro* (Vol. 29, Issue 1, pp. 234–241).
- Martinez-Pomares, L. (2012). The mannose receptor. *Journal of Leukocyte Biology*, 92(6), 1177–1186.
- Matheson, L. A., Labow, R. S., & Santerre, J. P. (2002). Biodegradation of polycarbonate-based polyurethanes by the human monocytes-derived macrophage and U937 cell system. *Journal of Biomedical Materials Research*, 61(4), 505.
- McKee, T. J., & Komarova, S. V. (2017). Is it time to reinvent basic cell culture medium? *American Journal of Physiology - Cell Physiology*, 312(5), C624–C626.
- Metcalf, D. (1983). Clonal analysis of the response of HL60 human myeloid leukemia cells to biological regulators. *Leukemia Research*, 7(2), 117–132.
- Millar, F. R., Summers, C., Griffiths, M. J., Toshner, M. R., & Proudfoot, A. G. (2016). The pulmonary endothelium in acute respiratory distress syndrome: Insights and therapeutic opportunities. *Thorax*, 71(5), 462–473.
- Miller, A. J., & Spence, J. R. (2017). In Vitro Models to Study Human Lung Development, Disease and Homeostasis. *Physiology*, 32(3), 246–260.
- Minafra, L., Di Cara, G., Albanese, N. N., & Cancemi, P. (2011). Proteomic differentiation pattern in the U937 cell line. *Leukemia Research*, 35(2), 226–236.

- Minta, J., & Pambrun, L. (1985). In vitro induction of cytologic and functional differentiation of the immature human monocytelike cell line U-937 with phorbol myristate acetate. *The American Journal of Pathology*, 119, 111–126.
- Mosser, D. M. (2003). The many faces of macrophage activation. *Journal of Leukocyte Biology*, 73(2), 209–212.
- Mosser, D. M., & Edwards, J. P. (2008). Exploring the full spectrum of macrophage activation. *Nature Reviews. Immunology*, 8(12), 958–969.
- Movia, D., Bazou, D., & Prina-Mello, A. (2019). ALI multilayered co-cultures mimic biochemical mechanisms of the cancer cell-fibroblast cross-talk involved in NSCLC MultiDrug Resistance. *BMC Cancer*, 19(1), 854.
- Movia, D., & Prina-Mello, A. (2020). Preclinical development of orally inhaled drugs (Oids)—are animal models predictive or shall we move towards in vitro non-animal models? *Animals*, 10(8), 1–16.
- Murray, P. J., & Wynn, T. A. (2011). Protective and pathogenic functions of macrophage subsets. *Nature Reviews. Immunology*, 11(11), 723–737.
- Nahar, K., Gupta, N., Gauvin, R., Absar, S., Patel, B., Gupta, V., Khademhosseini, A., & Ahsan, F. (2013). In vitro, in vivo and ex vivo models for studying particle deposition and drug absorption of inhaled pharmaceuticals. *European Journal of Pharmaceutical Sciences*, 49(5), 805–818.
- Newburger, P. E., Chovaniec, M. E., Greenberger, J. S., & Cohen, H. J. (1979). Functional changes in human leukemic cell line HL-60. A model for myeloid differentiation. *The Journal of Cell Biology*, 82(2), 315–322.
- Nielsen, E., Ostergaard, G., & Larsen, J. C. (2008). *Toxicological Risk Assessment of Chemicals: A Practical Guide*. CRC Press.
- Nikolić, M. Z., Sun, D., & Rawlins, E. L. (2018). Human lung development: Recent progress and new challenges. In *Development (Cambridge)* (Vol. 145, Issue 16 Special Issue). Company of Biologists Ltd.
- Nikula, K J, Avila, K. J., Griffith, W. C., & Mauderly, J. L. (1997). Lung tissue responses and sites of particle retention differ between rats and cynomolgus monkeys exposed chronically to diesel exhaust and coal dust. *Fundamental and Applied Toxicology : Official Journal of the Society of Toxicology*, 37(1), 37–53.
- Nikula, K J, Vallyathan, V., Green, F. H., & Hahn, F. F. (2001). Influence of exposure concentration or dose on the distribution of particulate material in rat and human lungs. *Environmental Health Perspectives*, 109(4), 311–318.
- Nikula, Kristen J, McCartney, J. E., McGovern, T., Miller, G. K., Odin, M., Pino, M. V, & Reed, M. D. (2014). STP position paper: interpreting the significance of increased alveolar macrophages in rodents following inhalation of pharmaceutical materials. *Toxicologic Pathology*, 42(3), 472–486.
- O'Brien, P. J. (2014). High-content analysis in toxicology: Screening substances for human toxicity potential, elucidating subcellular mechanisms and in vivo use as translational safety biomarkers. *Basic and Clinical Pharmacology and Toxicology*, 115(1), 4–17.



- Oda, K., Yumoto, R., Nagai, J., Katayama, H., & Takano, M. (2011). Mechanism underlying insulin uptake in alveolar epithelial cell line RLE-6TN. *European Journal of Pharmacology*, 672(1–3), 62–69.
- Oosting, R. S., van Golde, L. M. G., Verhoef, J., & van Bree, L. (1991). Species differences in impairment and recovery of alveolar macrophage functions following single and repeated ozone exposures. *Toxicology and Applied Pharmacology*, 110(1), 170–178.
- Owen, K. (2013). Regulatory toxicology considerations for the development of inhaled pharmaceuticals. *Drug and Chemical Toxicology*, 36(1), 109–118.
- Padilla, P. I., Wada, A., Yahiro, K., Kimura, M., Niidome, T., Aoyagi, H., Kumatori, A., Anami, M., Hayashi, T., Fujisawa, J., Saito, H., Moss, J., & Hirayama, T. (2000). Morphologic differentiation of HL-60 cells is associated with appearance of RPTPbeta and induction of Helicobacter pylori VacA sensitivity. *The Journal of Biological Chemistry*, 275(20), 15200–15206.
- Palecanda, A., Paulauskis, J., Al-Mutairi, E., Imrich, A., Qin, G., Suzuki, H., Kodama, T., Tryggvason, K., Koziel, H., & Kobzik, L. (1999). Role of the Scavenger Receptor MARCO in Alveolar Macrophage Binding of Unopsonized Environmental Particles. *Journal of Experimental Medicine*, 189(9), 1497–1506.
- Patel, B., Gupta, N., & Ahsan, F. (2015). Particle engineering to enhance or lessen particle uptake by alveolar macrophages and to influence the therapeutic outcome. *European Journal of Pharmaceutics and Biopharmaceutics*, 89C, 163–174.
- Patton, J. S., Brain, J. D., Davies, L. a, Fiegel, J., Gumbleton, M., Kim, K.-J., Sakagami, M., Vanbever, R., & Ehrhardt, C. (2010). The particle has landed--characterizing the fate of inhaled pharmaceuticals. *Journal of Aerosol Medicine and Pulmonary Drug Delivery*, 23 Suppl 2, S71-87.
- Patton, J. S., & Byron, P. R. (2007a). Inhaling medicines: delivering drugs to the body through the lungs. *Nature Reviews. Drug Discovery*, 6(January), 67–74.
- Patton, J. S., & Byron, P. R. (2007b). Inhaling medicines: delivering drugs to the body through the lungs. *Nature Reviews. Drug Discovery*, 6(1), 67–74.
- Pelchen-Matthews, A., Parsons, I. J., & Marsh, M. (1993). Phorbol ester-induced downregulation of CD4 is a multistep process involving dissociation from p56lck, increased association with clathrin-coated pits, and altered endosomal sorting. *The Journal of Experimental Medicine*, 178(4), 1209–1222.
- Phalen, R. F., & Oldham, M. J. (1983). Tracheobronchial airway structure as revealed by casting techniques. *The American Review of Respiratory Disease*, 128(2 Pt 2), S1-4.
- Prieto, J., Eklund, A., & Patarroyo, M. (1994). Regulated expression of integrins and other adhesion molecules during differentiation of monocytes into macrophages. *Cellular Immunology*, 156(1), 191–211.
- Python, F., Goebel, C., & Aeby, P. (2007). Assessment of the U937 cell line for the detection of contact allergens. *Toxicology and Applied Pharmacology*, 220(2), 113–124.

- Qin, Z. (2012). The use of THP-1 cells as a model for mimicking the function and regulation of monocytes and macrophages in the vasculature. In *Atherosclerosis* (Vol. 221, Issue 1, pp. 2–11). Elsevier.
- Rafael-Vázquez, L., García-Trejo, S., Aztatzi-Aguilar, O. G., Bazán-Perkins, B., & Quintanilla-Vega, B. (2018). Exposure to diethylhexyl phthalate (DEHP) and monoethylhexyl phthalate (MEHP) promotes the loss of alveolar epithelial phenotype of A549 cells. *Toxicology Letters*, 294, 135–144.
- Raies, A. B., & Bajic, V. B. (2016). In silico toxicology: computational methods for the prediction of chemical toxicity. *Wiley Interdisciplinary Reviews. Computational Molecular Science*, 6(2), 147.
- Ralph, P., Williams, N., Moore, M. A. S., & Litcofsky, P. B. (1982). Induction of antibody-dependent and nonspecific tumor killing in human monocytic leukemia cells by nonlymphocyte factors and phorbol ester. *Cellular Immunology*, 71(2), 215–223.
- Rasaiyaah, J., Yong, K., Katz, D. R., Kellam, P., & Chain, B. M. (2007). Dendritic cells and myeloid leukaemias: Plasticity and commitment in cell differentiation. *British Journal of Haematology*, 138(3), 281–290.
- Raschke, W. C., Baird, S., Ralph, P., & Nakoinz, I. (1978). Functional macrophage cell lines transformed by abelson leukemia virus. *Cell*, 15(1), 261–267.
- Rayner, R. E., Makena, P., Prasad, G. L., & Cormet-Boyaka, E. (2019). Optimization of Normal Human Bronchial Epithelial (NHBE) Cell 3D Cultures for in vitro Lung Model Studies. *Scientific Reports*, 9(1).
- Redente, E. F., Higgins, D. M., Dwyer-Nield, L. D., Orme, I. M., Gonzalez-Juarrero, M., & Malkinson, A. M. (2010). Differential polarization of alveolar macrophages and bone marrow-derived monocytes following chemically and pathogen-induced chronic lung inflammation. *Journal of Leukocyte Biology*, 88(1), 159–168.
- Robinson, P. C., Voelker, D. R., & Mason, R. J. (1984). Isolation and culture of human alveolar type II epithelial cells. Characterization of their phospholipid secretion. *The American Review of Respiratory Disease*, 130(6), 1156–1160.
- Rojanarat, W., Nakpheng, T., Thawithong, E., Yanyium, N., & Srichana, T. (2012). Inhaled pyrazinamide proliposome for targeting alveolar macrophages. *Drug Delivery*, 19(7), 334–345.
- Ross, J. T., Nesseler, N., Lee, J.-W., Ware, L. B., & Matthay, M. A. (2019). The ex vivo human lung: research value for translational science. *JCI Insight*, 4(11).
- Rothén-Rutishauser, B., Blank, F., Mühlfeld, C., & Gehr, P. (2008). In vitro models of the human epithelial airway barrier to study the toxic potential of particulate matter. *Expert Opinion on Drug Metabolism & Toxicology*, 4(8), 1075–1089.
- Rothén-Rutishauser, B. M., Kiama, S. G., & Gehr, P. (2005). A Three-Dimensional Cellular Model of the Human Respiratory Tract to Study the Interaction with Particles. *American Journal of Respiratory Cell and Molecular Biology*, 34(4), 281–289.
- Ruge, C. A., Schaefer, U. F., Herrmann, J., Kirch, J., Cañadas, O., Echaide, M.,

- Pérez-Gil, J., Casals, C., Müller, R., & Lehr, C.-M. (2012). The interplay of lung surfactant proteins and lipids assimilates the macrophage clearance of nanoparticles. *PloS One*, 7(7), e40775.
- Ruijters, E. J. B., Haenen, G. R. M. M., Weseler, A. R., & Bast, A. (2014). The cocoa flavanol (–)-epicatechin protects the cortisol response. *Pharmacological Research*, 79, 28–33.
- Ryan, J. A. (2008). Return to Web Version Evolution of Cell Culture Surfaces. In *Corning Life Sciences*.
- Sajjadi, F. G., Takabayashi, K., Foster, A. C., Domingo, R. C., & Firestein, G. S. (1996). Inhibition of TNF- $\alpha$  Expression by Adenosine. *The Journal of Immunology*, 156, 3435–3442.
- Sanders, M. (2007). Inhalation therapy: an historical review. *Primary Care Respiratory Journal : Journal of the General Practice Airways Group*, 16(2), 71–81.
- Saxena, R. K., Gilmour, M. I., & Hays, M. D. (2008). Isolation and quantitative estimation of diesel exhaust and carbon black particles ingested by lung epithelial cells and alveolar macrophages in vitro. *BioTechniques*, 44(6), 799–805.
- Schlesinger, R. B., Fine, J. M., & Chen, L. C. (1992). Interspecies Differences in the Phagocytic Activity of Pulmonary Macrophages Subjected to Acidic Challenge. *Toxicological Sciences*, 19(4), 584–589.
- Schneider, D. J., & Taatjes-Sommer, H. S. (2009). Augmentation of megakaryocyte expression of Fc $\gamma$ R1a by interferon gamma. *Arteriosclerosis, Thrombosis, and Vascular Biology*, 29(7), 1138–1143.
- Sedláková, V., Kloučková, M., Garlíková, Z., Vašíčková, K., Jaroš, J., Kandra, M., Kotasová, H., & Hampl, A. (2019). Options for modeling the respiratory system: inserts, scaffolds and microfluidic chips. *Drug Discovery Today*, 24(4), 971–982.
- Sela-Culang, I., Kunik, V., & Ofan, Y. (2013). The structural basis of antibody-antigen recognition. *Frontiers in Immunology*, 4, 302.
- Sharif, O., Bolshakov, V. N., Raines, S., Newham, P., & Perkins, N. D. (2007). Transcriptional profiling of the LPS induced NF- $\kappa$ B response in macrophages. *BMC Immunology*, 8(1), 1–17.
- Shepherd, M. C., Baillie, G. S., Stirling, D. I., & Houslay, M. D. (2004). Remodelling of the PDE4 cAMP phosphodiesterase isoform profile upon monocyte-macrophage differentiation of human U937 cells. *British Journal of Pharmacology*, 142(2), 339–351.
- Shlyonsky, V., Goolaerts, A., Van Beneden, R., & Sariban-Sohraby, S. (2005). Differentiation of Epithelial Na<sup>+</sup> Channel Function: An in vitro model. *Journal of Biological Chemistry*, 280(25), 24181–24187.
- Siekmeier, R., & Scheuch, G. (2008). Systemic treatment by inhalation of macromolecules--principles, problems, and examples. *Journal of Physiology and Pharmacology : An Official Journal of the Polish Physiological Society*, 59 Suppl 6, 53–79.

- Silverstein, R. L., & Febbraio, M. (2010). CD36, a Scavenger Receptor Involved in Immunity, Metabolism, Angiogenesis, and Behavior. *Sci Signal*, 2(72), 1–16.
- Sintiprungrat, K., Singhto, N., Sinchaikul, S., Chen, S.-T., & Thongboonkerd, V. (2010). Alterations in cellular proteome and secretome upon differentiation from monocyte to macrophage by treatment with phorbol myristate acetate: insights into biological processes. *Journal of Proteomics*, 73(3), 602–618.
- Smyth, H. D. C., & Hickey, A. J. (2011). *Controlled Pulmonary Drug Delivery*. Springer Science & Business Media.
- Song, C., Ma, H., Yao, C., Tao, X., & Gan, H. (2012). Alveolar Macrophage-Derived Vascular Endothelial Growth Factor Contributes to Allergic Airway Inflammation in a Mouse Asthma Model. *Scandinavian Journal of Immunology*, 75(6), 599–605.
- Song, M., Ryoo, I., Choi, H., Choi, B., Kim, S.-T., Heo, T.-H., Lee, J. Y., Park, P.-H., Kwak, M.-K., Geissmann, F., Manz, M., Jung, S., Sieweke, M., Merad, M., Ley, K., Ingersoll, M., Platt, A., Potteaux, S., Randolph, G., ... Pickett, C. (2015). NRF2 Signaling Negatively Regulates Phorbol-12-Myristate-13-Acetate (PMA)-Induced Differentiation of Human Monocytic U937 Cells into Pro-Inflammatory Macrophages. *PLOS ONE*, 10(7), e0134235.
- Sordet, O., Bettaieb, A., Bruey, J. M., Eymin, B., Droin, N., Ivarsson, M., Garrido, C., & Solary, E. (1999). Selective inhibition of apoptosis by TPA-induced differentiation of U937 leukemic cells. *Cell Death and Differentiation*, 6(4), 351–361.
- Sordet, O., Hermine, O., Vainchenker, W., Garrido, C., Solary, E., & Dubrez-daloz, L. (2002). Specific involvement of caspases in the differentiation of monocytes into macrophages. *Hematopoiesis*, 100(13), 4446–4453.
- St-Laurent, J., Turmel, V., Boulet, L.-P., & Bissonnette, E. (2009). Alveolar macrophage subpopulations in bronchoalveolar lavage and induced sputum of asthmatic and control subjects. *The Journal of Asthma : Official Journal of the Association for the Care of Asthma*, 46(1), 1–8.
- Steimer, A., Haltner, E., & Lehr, C. M. (2005). Cell culture models of the respiratory tract relevant to pulmonary drug delivery. *Journal of Aerosol Medicine: Deposition, Clearance, and Effects in the Lung*, 18(2), 137–182.
- Stone, K. C., Mercer, R. R., Gehr, P., Stockstill, B., & Crapo, J. D. (1992). Allometric relationships of cell numbers and size in the mammalian lung. *American Journal of Respiratory Cell and Molecular Biology*, 6(2), 235–243.
- Stonehouse, T. J., Woodhead, V. E., Herridge, P. S., Ashrafian, H., George, M., Chain, B. M., & Katz, D. R. (1999). Molecular characterization of U937-dependent T-cell co-stimulation. *Immunology*, 96(1), 35–47.
- Stoppelli, M. P., Cortit, A., Soffientinit, A., Blasit, F., & Assoian, R. K. (1985). Differentiation-enhanced binding of the amino-terminal fragment of human urokinase plasminogen activator to a specific receptor on U937 monocytes. *Biochemistry*, 82(August), 4939–4943.
- Stříž, I., Slavčev, A., Kalanin, J., Jarešová, M., & Rennard, S. I. (2001). Cell-cell

- contacts with epithelial cells modulate the phenotype of human macrophages. *Inflammation*, 25(4), 241–246.
- Sundström, C., & Nilsson, K. (1976). Establishment and characterization of a human histiocytic lymphoma cell line (U-937). *International Journal of Cancer*, 17(5), 565–577.
- Swain, R. J., Kemp, S. J., Goldstraw, P., Tetley, T. D., & Stevens, M. M. (2010). Assessment of Cell Line Models of Primary Human Cells by Raman Spectral Phenotyping. *Biophysical Journal*, 98(8), 1703–1711.
- Takayama, K. (2020). In Vitro and Animal Models for SARS-CoV-2 research. In *Trends in Pharmacological Sciences* (Vol. 41, Issue 8, pp. 513–517). Elsevier Ltd.
- Tang, Y. J., Li, H. M., & Hamel, J. F. P. (2009). Significances of pH and temperature on the production of heat-shock protein glycoprotein 96 by MethA tumor cell suspension culture in stirred-tank bioreactors. *Bioprocess and Biosystems Engineering*, 32(2), 267–276.
- Taniguchi, K., Hikiji, H., Okinaga, T., Hashidate-Yoshida, T., Shindou, H., Ariyoshi, W., Shimizu, T., Tominaga, K., & Nishihara, T. (2015). Essential Role of Lysophosphatidylcholine Acyltransferase 3 in the Induction of Macrophage Polarization in PMA-Treated U937 Cells. *Journal of Cellular Biochemistry*, 116(12), 2840–2848.
- Tanjore, H., Cheng, D.-S., Degryse, A. L., Zoz, D. F., Abdolrasulnia, R., Lawson, W. E., & Blackwell, T. S. (2011). Alveolar Epithelial Cells Undergo Epithelial-to-Mesenchymal Transition in Response to Endoplasmic Reticulum Stress. *The Journal of Biological Chemistry*, 286(35), 30972–30980.
- Tao, F., & Kobzik, L. (2002). Lung macrophage-epithelial cell interactions amplify particle-mediated cytokine release. *American Journal of Respiratory Cell and Molecular Biology*, 26(4), 499–505.
- Taylor, M. L., Noble, P. W., White, B., Wise, R., Liu, M. C., & Bochner, B. S. (2000). Extensive surface phenotyping of alveolar macrophages in interstitial lung disease. *Clinical Immunology*, 94(1), 33–41.
- Templin, M. F., Stoll, D., Schrenk, M., Traub, P. C., Vöhringer, C. F., & Joos, T. O. (2002). Protein microarray technology. *Drug Discovery Today*, 7(15), 815–822.
- Tenney, D. J., & Morahan, P. S. (1987). Effects of differentiation of human macrophage-like u937 cells on intrinsic resistance to herpes simplex virus type 1. *The American Journal of Pathology*, 139(9), 3076–3083.
- Tomlinson, G. S., Booth, H., Petit, S. J., Potton, E., Towers, G. J., Miller, R. F., Chain, B. M., & Noursadeghi, M. (2012). Adherent Human Alveolar Macrophages Exhibit a Transient Pro-Inflammatory Profile That Confounds Responses to Innate Immune Stimulation. *PLoS ONE*, 7(6), e40348.
- Törnqvist, E., Annas, A., Granath, B., Jalkestén, E., Cotgreave, I., & Öberg, M. (2014). Strategic Focus on 3R Principles Reveals Major Reductions in the Use of Animals in Pharmaceutical Toxicity Testing. *PLoS ONE*, 9(7), e101638.
- Trapnell, B. C., & Whitsett, J. A. (2002). Gm-CSF regulates pulmonary surfactant

- homeostasis and alveolar macrophage-mediated innate host defense. *Annual Review of Physiology*, 64, 775–802.
- Tsuchiya, S., Kobayashi, Y., Goto, Y., Okumura, H., Nakae, S., Konno, T., & Tada, K. (1982). Induction of maturation in cultured human monocytic leukemia cells by a phorbol diester. *Cancer Research*, 42(4), 1530–1536.
- Twomey, B., McCallum, S., Isenberg, D., & Latchman, D. S. (1993). Elevation of heat shock protein synthesis and hsp gene transcription during monocyte to macrophage differentiation of U937 cells. In *Clinical and Experimental Immunology* (Vol. 93, Issue 2, p. 178). Wiley-Blackwell.
- Veldhuizen, R. A. W., McCaig, L. A., Pape, C., & Gill, S. E. (2019). The effects of aging and exercise on lung mechanics, surfactant and alveolar macrophages. *Experimental Lung Research*, 45(5–6), 113–122.
- Verhoeckx, K. C. M., Bijlsma, S., de Groene, E. M., Witkamp, R. F., van der Greef, J., & Rodenburg, R. J. T. (2004). A combination of proteomics, principal component analysis and transcriptomics is a powerful tool for the identification of biomarkers for macrophage maturation in the U937 cell line. *Proteomics*, 4(4), 1014–1028.
- Vigerust, D. J., Vick, S., & Shepherd, V. L. (2012). Characterization of functional mannose receptor in a continuous hybridoma cell line. *BMC Immunology*, 13(1), 51.
- Viksman, M. Y., Bochner, B. S., Peebles, R. S., Schleimer, R. P., & Liu, M. C. (2002). Expression of activation markers on alveolar macrophages in allergic asthmatics after endobronchial or whole-lung allergen challenge. *Clinical Immunology (Orlando, Fla.)*, 104(1), 77–85.
- Vogel, C. F. a, Garcia, J., Wu, D., Mitchell, D. C., Zhang, Y., Kado, N. Y., Wong, P., Trujillo, D. A., Lollies, A., Bennet, D., Schenker, M. B., & Mitloehner, F. M. (2012). Activation of inflammatory responses in human U937 macrophages by particulate matter collected from dairy farms: an in vitro expression analysis of pro-inflammatory markers. *Environmental Health : A Global Access Science Source*, 11(1), 17.
- Volpe, D. A. (2008). Variability in caco-2 and MDCK cell-based intestinal permeability assays. In *Journal of Pharmaceutical Sciences* (Vol. 97, Issue 2, pp. 712–725). John Wiley and Sons Inc.
- Wang, G., Zhang, X., Liu, X., & Zheng, J. (2020). Co-culture of human alveolar epithelial (A549) and macrophage (THP-1) cells to study the potential toxicity of ambient PM2.5: a comparison of growth under ALI and submerged conditions. *Toxicology Research*, 9(5), 636–651.
- Wang, S. J., Young, R. S., Sun, N. N., & Witten, M. L. (2002). In vitro cytokine release from rat type II pneumocytes and alveolar macrophages following exposure to JP-8 jet fuel in co-culture. *Toxicology*, 173(3), 211–219.
- Ward, C., Whitford, H., Snell, G., Bao, H., Zheng, L., Reid, D., Williams, T. J., & Walters, E. H. (2001). Bronchoalveolar lavage macrophage and lymphocyte phenotypes in lung transplant recipients. *The Journal of Heart and Lung Transplantation : The Official Publication of the International Society for Heart*

- Transplantation*, 20(10), 1064–1074.
- Ward, J. P. T., Ward, J., & Leach, R. M. (2011). *The Respiratory System at a Glance*. Wiley.
- Weber, S., Hebestreit, M., Wilms, T., Conroy, L. L., & Rodrigo, G. (2013). Comet assay and air–liquid interphase exposure system: A new combination to evaluate genotoxic effects of cigarette whole smoke in human lung cell lines. In *Toxicology in Vitro* (Vol. 27, Issue 6).
- Weibel, E. R. (1963). *Morphometry of the Human Lung*. Springer Berlin Heidelberg.
- Weibel, E. R. (2015). On the tricks alveolar epithelial cells play to make a good lung. In *American Journal of Respiratory and Critical Care Medicine* (Vol. 191, Issue 5, pp. 504–513).
- Westphalen, K., Gusarova, G. a, Islam, M. N., Subramanian, M., Cohen, T. S., Prince, A. S., & Bhattacharya, J. (2014). Sessile alveolar macrophages communicate with alveolar epithelium to modulate immunity. *Nature*, 506(7489), 503–506.
- Whitsett, J., & Alenghat, T. (2015). Respiratory epithelial cells orchestrate pulmonary innate immunity. *Nature Immunology*.
- Whittemore, S. (2003). *The Respiratory System*. Infobase Publishing.
- Wink, S., Hiemstra, S., Huppelschoten, S., Danen, E., Niemeijer, M., Hendriks, G., Vrieling, H., Herpers, B., & Van De Water, B. (2014). Quantitative high content imaging of cellular adaptive stress response pathways in toxicity for chemical safety assessment. In *Chemical Research in Toxicology* (Vol. 27, Issue 3, pp. 338–355). American Chemical Society.
- Wirth, D., Kuehn, A., Kletting, S., Carvalho-wodarz, C. D. S., & Repnik, U. (2016). Human alveolar epithelial cells expressing tight junctions to model the air-blood barrier Research Article Human alveolar epithelial cells expressing tight junctions to model the air-blood barrier 1. *Alternatives to Animal Experimentation*, 33(March), 251–260.
- World Respiratory Diseases Drugs Market Analysis 2020 - Market Forecast to Grow to \$92.6 Billion in 2020 at a CAGR of 42.5% Due to Increased Demand as a Result of COVID-19 Outbreak*. (n.d.). Retrieved September 30, 2020, from <https://www.globenewswire.com/news-release/2020/06/11/2046856/0/en/World-Respiratory-Diseases-Drugs-Market-Analysis-2020-Market-Forecast-to-Grow-to-92-6-Billion-in-2020-at-a-CAGR-of-42-5-Due-to-Increased-Demand-as-a-Result-of-COVID-19-Outbreak.html>
- Yamamoto, K., Ferrari, J. D., Cao, Y., Ramirez, M. I., Jones, M. R., Quinton, L. J., & Mizgerd, J. P. (2012). Type I alveolar epithelial cells mount innate immune responses during pneumococcal pneumonia. *Journal of Immunology (Baltimore, Md. : 1950)*, 189(5), 2450–2459.
- Yamamoto, T., Sakaguchi, N., Hachiya, M., Nakayama, F., Yamakawa, M., & Akashi, M. (2009). Role of catalase in monocytic differentiation of U937 cells by TPA: hydrogen peroxide as a second messenger. *Leukemia*, 23(4), 761–769.
- Zavala, J., Obrien, B., Lichtveld, K., Sexton, K. G., Rusyn, I., Jaspers, I., & Vizuite,

- W. (2016). Assessment of biological responses of EpiAirway 3-D cell constructs versus A549 cells for determining toxicity of ambient air pollution. *Inhalation Toxicology*, 28(6), 251–259.
- Zaynagetdinov, R., Sherrill, T. P., Kendall, P. L., Segal, B. H., Weller, K. P., Tighe, R. M., & Blackwell, T. S. (2013). Identification of myeloid cell subsets in murine lungs using flow cytometry. *American Journal of Respiratory Cell and Molecular Biology*, 49(2), 180–189.
- Zhang, D. E., Hetherington, C. J., Gonzalez, D. A., Chen, H. M., & Tenen, D. G. (1994). Regulation of CD14 expression during monocytic differentiation induced with 1 alpha,25-dihydroxyvitamin D3. *Journal of Immunology (Baltimore, Md. : 1950)*, 153(7), 3276–3284.
- Ziegler-Heitbrock, H. W. L., Schraut, W., Wendelgass, P., Strobel, M., Sternsdorf, T., Weber, C., Aepfelbacher, M., Ehlers, M., Schutt, C., & Haas, J. G. (1994). Distinct patterns of differentiation induced in the monocytic cell line Mono Mac 6. *Journal of Leukocyte Biology*, 55(1), 73–80.